

**DEVELOPMENT OF NEW SYNTHESISED
MULTILAYERED BIOCERAMICS FOR DENTAL CROWN
RESTORATIONS**

ALI ABDULLAH ALWAN AL-MAQTARI

**DEPARTMENT OF RESTORATIVE DENTISTRY
FACULTY OF DENTISTRY
UNIVERSITY OF MALAYA
KUALA LUMPUR**

2017

**DEVELOPMENT OF NEW SYNTHESISED
MULTILAYERED BIOCERAMICS FOR DENTAL
CROWN RESTORATIONS**

ALI ABDULLAH ALWAN AL-MAQTARI

**THESIS SUBMITTED IN FULFILMENT OF THE
REQUIREMENTS FOR THE DEGREE OF DOCTOR OF
PHILOSOPHY**

**DEPARTMENT OF RESTORATIVE DENTISTRY
FACULTY OF DENTISTRY
UNIVERSITY OF MALAYA
KUALA LUMPUR**

2017

UNIVERSITY OF MALAYA
ORIGINAL LITERARY WORK DECLARATION

Name of Candidate: ALI ABDULLAH ALWAN AL-MAQTARI

Registration/Matric No: DHA080003

Name of Degree: DOCTOR OF PHILOSOPHY

Title of Project Paper/Research Report/Dissertation/Thesis ("this Work"):

Development of New Synthesised Multilayered Bioceramics for Dental Crown Restorations.

Field of Study: Dental All-Ceramic Restoration.

RESTORATIVE DENTISTRY

I do solemnly and sincerely declare that:

- (1) I am the sole author/writer of this Work;
- (2) This Work is original;
- (3) Any use of any work in which copyright exists was done by way of fair dealing and for permitted purposes and any excerpt or extract from, or reference to or reproduction of any copyright work has been disclosed expressly and sufficiently and the title of the Work and its authorship have been acknowledged in this Work;
- (4) I do not have any actual knowledge nor do I ought reasonably to know that the making of this work constitutes an infringement of any copyright work;
- (5) I hereby assign all and every rights in the copyright to this Work to the University of Malaya ("UM"), who henceforth shall be owner of the copyright in this Work and that any reproduction or use in any form or by any means whatsoever is prohibited without the written consent of UM having been first had and obtained;
- (6) I am fully aware that if in the course of making this Work I have infringed any copyright whether intentionally or otherwise, I may be subject to legal action or any other action as may be determined by UM.

Candidate's Signature

Date:

Subscribed and solemnly declared before,

Witness's Signature

Date:

Name: Prof. Dato' Dr. Abdul Aziz Bin Abdul Razak

Designation:

UNIVERSITI MALAYA
PERAKUAN KEASLIAN PENULISAN

Nama: ALI ABDULLAH ALWAN AL-MAQTARI

No. Pendaftaran/Matrik: DHA080003

Nama Ijazah: DOKTOR FALSFAH

Tajuk Kertas Projek/Laporan Penyelidikan/Disertasi/Tesis (“Hasil Kerja ini”):
Development of New Synthesised Multilayered Bioceramics for Dental Crown Restorations.

Bidang Penyelidikan: Dental All-Ceramic Restoration.

Saya dengan sesungguhnya dan sebenarnya mengaku bahawa:

- (1) Saya adalah satu-satunya pengarang/penulis Hasil Kerja ini;
- (2) Hasil Kerja ini adalah asli;
- (3) Apa-apa penggunaan mana-mana hasil kerja yang mengandungi hakcipta telah dilakukan secara urusan yang wajar dan bagi maksud yang dibenarkan dan apa-apa petikan, ekstrak, rujukan atau pengeluaran semula daripada atau kepada mana-mana hasil kerja yang mengandungi hakcipta telah dinyatakan dengan sejelasnya dan secukupnya dan satu pengiktirafan tajuk hasil kerja tersebut dan pengarang/penulisnya telah dilakukan di dalam Hasil Kerja ini;
- (4) Saya tidak mempunyai apa-apa pengetahuan sebenar atau patut semunasabahnya tahu bahawa penghasilan Hasil Kerja ini melanggar suatu hakcipta hasil kerja yang lain;
- (5) Saya dengan ini menyerahkan kesemua dan tiap-tiap hak yang terkandung di dalam hakcipta Hasil Kerja ini kepada Universiti Malaya (“UM”) yang seterusnya mula dari sekarang adalah tuan punya kepada hakcipta di dalam Hasil Kerja ini dan apa-apa pengeluaran semula atau penggunaan dalam apa jua bentuk atau dengan apa juga cara sekalipun adalah dilarang tanpa terlebih dahulu mendapat kebenaran bertulis dari UM;
- (6) Saya sedar sepenuhnya sekiranya dalam masa penghasilan Hasil Kerja ini saya telah melanggar suatu hakcipta hasil kerja yang lain sama ada dengan niat atau sebaliknya, saya boleh dikenakan tindakan undang-undang atau apa-apa tindakan lain sebagaimana yang diputuskan oleh UM.

Tandatangan Calon

Tarikh:

Diperbuat dan sesungguhnya diakui di hadapan,

Tandatangan Saksi

Tarikh:

Nama: Prof. Dato' Dr. Abdul Aziz Bin Abdul Razak

Jawatan:

ABSTRACT

Objectives. This study aimed to investigate and establish the biomechanical behaviour of functionally graded dental ceramic cores in simulated models of a maxillary second premolar using 3D finite element analysis. It also aimed to synthesise and evaluate the microstructural, physical, thermal, and mechanical properties of a new multilayered bioceramic cores. The shear bond strength of the synthesised zirconia and alumina ceramic core with/without infiltrated graded silica with their corresponding veneering porcelains were also evaluated. Finally, cytotoxicity effects of the new synthesised dental bioceramic core (powders and discs) were evaluated using human gingival fibroblast (HGF-1) cells.

Materials and Methods. An intact maxillary premolar was digitized with a CT scanner. Eight different models (Models A-H) were developed. A total of 243 images were obtained, and the image data was saved as files in DICOM format. Mimics software was used for reconstruction of the data converted to the DICOM file in the 3D FE model on the computer. The 3D FE models were constructed meshed. The models were constrained at the bottom boundaries. A static load (200 N) was applied in three different directions (oblique, horizontal, and vertical) at three different areas on all models. All materials were assumed to be isotropic and homogeneous. The von Mises stress distributions along the veneer-core-cement-dentin interfaces and interface stresses between the crown and its surrounding structures were investigated under oblique, vertical, and horizontal loadings. Also, strain distribution at the veneer-core-cement-dentine interfaces was also investigated. Samples containing 0, 20, 40, and 50 wt.% of Al_2O_3 particles in the Y-ZrO₂ matrix were prepared by uniaxial pressing (200 MPa) and sintered in air at 1500 °C for 2h. The microstructure (FESEM, EDX, XRD), physical (density, porosity, shrinkage), thermal (TMA), and mechanical (Vickers hardness, compressives strength, elastic

modulus, and strain) were characterized and analyzed. The shear bond strength was carried out. Subsequently, all specimens were subjected to a shear load in a universal testing machine. Fractured specimens were evaluated microscopically (SEM, EDX) to determine the failure mode. *In vitro* biocompatibility evaluation of synthesised ceramic powders and discs were tested and to determine the cytotoxic level of the synthesised $ZrO_2-Al_2O_3$ ceramic composites by using the resazurin proliferation assay with HGF-1 cells lines after 72 h. For ceramic discs, ANOVA was used to determine statistical significant differences among the synthesised ceramic disc groups, and also Dunnett's test was used for multiple comparisons. For powders ceramics, two-way ANOVA was employed to determine the interaction influence between synthesised ceramic powders with five different concentrations. t-test was used to compare the mean between non-sintered and sintered synthesised ceramics. The significant level was set at 0.05.

Results and conclusions. The results showed that functionally graded structured dental ceramic cores models, B, C, D, E, F, and G, demonstrated desirable advantages in terms of stress distribution compared to homogenous zirconia (model A) cores. Dental ceramic crowns with bilayered structure cores dissipated the localized and interfacial stress and strain efficiently. Functionally graded material approach can be used to design new dental cores in order to reduce stress concentrations and interfacial stresses successfully in the dental crown. Fully dense ceramic materials were obtained with a Vickers hardness test ranging between 1292.8 VH and 1711.9 VH, depending on the amount of Al_2O_3 in the ZrO_2 matrix. There was no significant influence from the infiltrated of graded silica addition to the shear bond strength. The results indicated that the shear bond strength between zirconia/alumina cores and veneering ceramics was not affected by infiltrated graded silica. Also, the results indicated that powder form ceramic was cytotoxic to HGF-1 cells at higher concentrations. However, at lower concentrations powder ceramics showed minimal toxicity. Disc ceramics showed minimal toxicity on HGF-1 cells.

ABSTRAK

Objektif. Kajian ini bertujuan untuk menyiasat dan mewujudkan tingkah laku biomekanik teras seramik pergigian fungsi digred berstruktur dalam model simulasi gigi premolar kedua dgn rahang menggunakan analisis 3D unsur. Ia juga adalah untuk mensintesis, menilai pencirian mikrostruktur, fizikal, haba, dan mekanik teras bioceramic berbilang lapisan yang baru. Ia juga adalah untuk menilai kekuatan ikatan ricih zirkonia dan alumina teras seramik disintesis dengan / tanpa silika bergred menyusup dengan porselin veneering. Dan akhirnya, untuk menyiasat dan menentukan kesan sitotoksik disintesis gigi teras bioceramic yang baru (serbuk dan cakera) menggunakan sel fibroblast gingival manusia (HGF-1).

Bahan dan Kaedah. Gigi premolar dengan rahang utuh telah didigitalkan dengan pengimbas CT. Lapan model yang berbeza (Model A-H) telah dibuat. Sebanyak 243 imej yang telah diperolehi, dan data imej telah disimpan sebagai fail dalam format DICOM. Perisian meniru telah digunakan untuk pembinaan semula data ditukar ke fail DICOM dalam model 3D FE pada komputer. Model-model 3D FE yang dihancurkan telah dibina. Model-model yang telah dikekang pada sempadan bawah. Satu beban statik (200 N) telah digunakan dalam tiga arah yang berbeza (serong, mendatar, dan menegak) di tiga kawasan yang berbeza untuk semua model dan diedarkan pada satu kawasan. Semua bahan telah diandaikan sebagai isotropik dan seragam. von Mises taburan tekanan di sepanjang muka venir-core-simen-dentin dan tekanan antara muka antara mahkota dan struktur sekitarnya disiasat mengikut hala serong, menegak, dan beban mendatar. Juga, agihan terikan antara muka venir-core-simen-dentin juga disiasat. Sampel yang mengandungi 0, 20, 40, dan 50 wt.% zarah Al_2O_3 dalam matriks Y-ZrO₂ telah disediakan oleh ekapaksi menekan (200 MPa) dan disinter di udara pada 1500 ° C untuk 2h. Mikrostruktur (FESEM, EDX, XRD), fizikal (ketumpatan, keliangan, pengecutan), haba (TMA), dan mekanikal (kekerasan Vickers, compressives kekuatan, modulus elastik,

tekanan, ricih kekuatan ikatan) telah dikaji dan dianalisis. Kekuatan ikatan ricih telah dijalankan. Selepas itu, semua spesimen tertakluk kepada beban ricih dalam mesin ujian universal. spesimen patah dinilai secara mikroskopik (SEM, EDX) untuk menentukan mod kegagalan. Dalam penilaian biocompatibility vitro, serbuk seramik disintesis dan cakera telah diuji dan untuk menentukan tahap sitotoksik bagi komposit seramik $ZrO_2-Al_2O_3$ disintesis dengan menggunakan percambahan assay resazurin dengan HGF-1 sel garisan selepas 72 jam.

Keputusan dan kepentingan. Hasil kajian menunjukkan bahawa fungsi digred berstruktur gigi teras seramik model, B, C, D, E, F dan G, menunjukkan kelebihan wajar dari segi agihan tegasan berbanding zirkonia homogen (model A) teras mahkota seramik pergigian dengan bilayered teras struktur lesap tekanan dan ketegangan setempat dan antara muka cekap. pendekatan bahan berfungsi digredkan boleh digunakan untuk merekabentuk teras gigi baru untuk mengurangkan kepekatan tekanan dan tekanan antara muka dengan jayanya dalam mahkota gigi. bahan-bahan seramik sepenuhnya padat diperoleh dengan kekerasan Vickers yang terdiri antara 1292,8 VH dan 1711,9 VH, bergantung kepada jumlah Al_2O_3 dalam matriks ZrO_2 itu. Tidak terdapat pengaruh penting penambahan silika bergred pada kekuatan ikatan ricih. Keputusan menunjukkan bahawa kekuatan ikatan ricih antara teras zirkonia / alumina dan seramik veneering tidak terjejas oleh silika bergred menyusup. Juga, keputusan menunjukkan bahawa bentuk serbuk seramik adalah sitotoksik kepada HGF-1 sel-sel pada kepekatan yang lebih tinggi. Walau bagaimanapun, pada kepekatan yang lebih rendah, seramik serbuk menunjukkan ketoksikan minimum. seramik cakera menunjukkan ketoksikan minimum ke atas HGF-1 sel-sel.

ACKNOWLEDGEMENTS

First of all, I would like to express my sincerest gratitude and thanks to Allah for his help and support.

I would also like to express my sincere gratitude to my supervisors Prof. Dato' Dr. Abdul Aziz Bin Abdul Razak and Prof. Dr. Mohd Hamdi Bin Abdul Shokur, for their continuous guidance, patience, help, and support during my whole PhD period. Also, their profound and intuition have gradually led me towards becoming a creative researcher and an innovative thinker. Their vast knowledge in materials and mechanics always made difficult problems seemed simple. They are true scholars and excellent mentors.

I am indebted to my friends who have provided me with stimulating encouragement for the last few years.

I would like to express my appreciation to the University of Malaya Grant Program for funding this research through Grant IPPP (PV020-2011B (IPPP) and RG512-13HTM (UMR). Also, I would like to express my appreciation to the University of Thamar (Yemen) for supporting me during my PhD study.

Finally, I would like to express my gratitude to my family (my lovely wife Arwa, my sweet son Haitham and my sweet daughter Raghd). Without their support and love, I would never have succeeded. Also, I want to express my sincerest thanks and deepest gratitude to my parents and my sisters and my brothers, for their endless support and motivation. I greatly appreciate their numerous sacrifices that they have made to provide me with a good education. I dedicate this dissertation to them for all their love and support.

TABLE OF CONTENTS

Abstract	iv
Abstrak	vi
Acknowledgements	viii
Table of Contents	ix
List of Figures	xvi
List of Symbols and Abbreviations	xxvii
List of Appendices	xxix
CHAPTER 1: INTRODUCTION	1
1.1 Introduction.....	1
1.2 Rationale of Study	6
1.3 Statement of Problem	7
1.4 Thesis Layout.....	7
CHAPTER 2: LITERATURE REVIEW	9
2.1 Bioceramic in Dentistry.....	9
2.1.1 Zirconia (zirconium oxide) (ZrO ₂)	10
2.1.1.1 Yttrium-Tetragonal Zirconia Polycrystalline (Y-TZP).....	12
2.1.1.2 Partially Stabilized Zirconia (Mg-PSZ).....	14
2.1.1.3 Zirconia Toughened Alumina (ZTA)	15
2.1.2 Alumina (aluminum oxide) (Al ₂ O ₃)	19
2.1.3 Glass Ceramics	22
2.2 Modern Dental All-Ceramics	23
2.2.1 Classification of Modern Dental All-Ceramics Restorations	23
2.2.1.1 Fusion Temperature.....	24
2.2.1.2 Applications.....	24
2.2.1.3 Fabrication Techniques	24

2.2.1.4 Crystalline Phases.....	24
2.2.2 Indication of All-Ceramic Restorations.....	25
2.2.2.1 Advantages of All-Ceramics over Metal Ceramic Crown Systems	25
2.2.2.2 Disadvantages of All-Ceramics over Metal Ceramic Crown Systems.....	26
2.2.3 Mechanical Properties of Dental All-Ceramics.....	27
2.3 Bonding Veneering Ceramic to Zirconia- and Alumina-Based Dental Ceramics.	28
2.4 Biocompatibility of Dental All-Ceramic	31
2.5 Survival Rate of All-Ceramic Crowns.....	33
2.6 Several Factors Affecting the Fracture Strength of All-Ceramic Crowns.....	
in Vivo:	35
2.6.1.1 Factors Related to the Restoration.....	35
2.6.1.2 Factors Related to the Supporting Structure (Natural Teeth or Core Materials) of the Restoration.....	36
2.6.1.3 Factors Related to the Oral Environment Surrounding the Restoration...	37
2.6.1.4 Factors Related to the Cementation of the Restorations	38
2.7 Dental Multilayered Structures.....	40
2.7.1 Biomechanical System with Layer Structures of Teeth and Dental Crowns	41
2.7.2 Influence of Crown Design Parameter on Dental All-Ceramic Crowns	43
2.7.3 Thickness of the Multilayers Ceramics	45
2.7.4 Dental Adhesives as an Interlayer	46
2.8 CAD/CAM Technology in Restorative Dentistry	47
2.9 Functionally Graded Materials (FGM) in Dentistry.....	49
2.9.1 Thin Film Technologies.....	55
2.9.2 Nanomaterials in Dentistry	55
2.10 Finite Element Analysis in Dentistry.....	57
2.10.1 Application of FEM in Dentistry.....	57

2.10.2	Advantages of FEM.....	60
2.10.3	Disadvantages of FEM	61
CHAPTER 3: 3D-FE ANALYSIS OF FUNCTIONALLY GRADED.....		
MULTILAYERED DENTAL CERAMIC CORES.....		62
3.1	Introduction.....	62
3.2	Aim of this Chapter	63
3.3	Objectives of this Study.....	63
3.4	Null Hypothesis of this Chapter	64
3.5	MATERIALS AND METHODS	64
3.5.1	Computerized Tomography (CT) Scan	64
3.5.2	Geometry Model Reconstruction and Remeshing.....	65
3.5.3	Generation of the Mesh	69
3.5.4	Boundary Conditions and Loading.....	70
3.5.5	Natural Tooth and Restorative Materials and Material Properties	72
3.5.6	Finite Element Analysis (FEA)	74
3.6	Results	75
3.6.1	Oblique Load	76
3.6.2	Horizontal Load	86
3.6.3	Vertical Load	97
3.7	DISCUSSION.....	108
3.8	CONCLUSIONS	117
CHAPTER 4: SYNTHESIS AND CHARACTERIZATION OF BIOCERAMIC...		
POWDERS FOR DENTAL CROWN RESTORATIONS.....		118
4.1	Introduction.....	118
4.2	Aim of this Chapter	121
4.3	Objectives of this Chapter	121

4.3.1	Synthesis of bioceramic powders for dental crown restorations	121
4.3.1.1	To synthesise a ceramic core of 3Y-TZP with/without alumina.....	121
4.3.1.2	To synthesise graded glass $\text{SiO}_2\text{-Al}_2\text{O}_3\text{-K}_2\text{O-Na}_2\text{O-CaO-Tb}_4\text{O}_7$	
	system.....	121
4.3.2	Characterization of microstructure and chemical compositions of synthesised.....	
	ceramics	121
4.3.3	Physical, mechanical and thermal properties evaluation.....	121
4.3.3.1	Physical and mechanical properties: namely,.....	122
4.3.3.2	Thermal properties	122
4.4	Null Hypothesis of this Chapter	122
4.5	MATERIALS AND METHODS	122
4.5.1	Materials	122
4.5.2	Methodology.....	129
4.5.2.1	Metallurgy of Powders for Fabrication of the Graded Multilayered.....	
	Ceramic Cores	129
(a)	Drying of Powder	129
(b)	Blending of Pure Powder	129
4.5.2.2	Powders Mixing and Milling.....	131
4.5.2.3	Compaction of the Specimens Using Uni-Axial Hydraulic Press.....	131
4.5.2.4	Sintering of Specimens by Using Pressureless Furnace.....	133
4.5.2.5	Characterization and Optimization of the Multilayered Graded.....	
	Ceramics	137
4.5.2.6	Microstructure Characterization Analysis.....	137
(a)	FESEM Analysis	137
(b)	Element Analysis (EDX).....	138
(c)	X-Ray Diffraction (XRD) Phase Analysis.....	138

4.5.2.7	Physical Characterization	139
4.5.2.8	Mechanical Characterization	141
4.2.2.8.1.	Vickers Hardness Test (VH)	141
4.2.2.8.2.	Compressive Strength Test.....	142
4.2.2.8.3.	Thermomechanical Analysis (TMA) Test.....	144
4.6	Results	146
4.6.1	Characterization of Synthesised Graded Ceramic Cores.....	146
4.6.1.1	Morphology and Microstructures Analysed by FESEM.....	146
4.6.1.2	Composition Mapping Analyses by EDX.....	161
4.6.1.3	Phase Analysis by XRD	165
4.6.2	Results of Experimental, Relative density, and Porosity.....	169
4.6.3	Results of the Volume Shrinkage, Vickers Hardness, and CTE	172
4.6.4	Results of the Compressive Strength, Elastic Young's Modulus, and Strain.....	179
4.7	Discussion.....	185
4.8	Conclusions	197
CHAPTER 5: SHEAR BOND STRENGTH BETWEEN SYNTHESISED.....		
BIOCERAMIC CORES INFILTRATED WITH GRADED SILICA AND.....		
VENEER.....		198
5.1	Introduction.....	198
5.2	Objective of this Chapter	200
5.3	Null Hypothesis of this Chapter	201
5.4	MATERIALS AND METHODS	201
5.4.1	Materials	201
5.4.2	Methods	202
5.4.2.1	Preparation of Synthesized Zirconia and Alumina Ceramic Cores.....	202
5.4.2.2	Preparation Veneer-Core Ceramic Specimens	205

5.4.2.3	Surface Analysis	207
5.4.2.4	Shear Bond Strength (SBS) Test	209
5.4.2.5	Fracture Surface Analysis	211
5.5	Results	213
5.5.1	Results of the Shear Bond Strength	213
5.5.2	Results of the Fracture Failure.....	215
5.6	Discussion.....	222
5.7	Conclusions	232
CHAPTER 6: CYTOTOXICITY EVALUATION OF NEW SYNTHESISED.....		
DENTAL BIOCERAMIC CORES BY USING HUMAN GINGIVAL.....		
FIBROBLAST CELLS – AN IN VITRO STUDY		233
6.1	Introduction.....	233
6.2	Aim of this Chapter	234
6.3	Objectives of this Chapter	234
6.4	Null Hypothesis of this Chapter	235
6.5	MATERIALS AND METHODS	235
6.5.1	Materials	235
6.5.2	Methods	236
6.5.2.1	Maintenance of Cell Lines.....	237
6.5.2.2	Seeding HGF-1 Cells in a 24- and 96-Wells.....	237
6.5.2.3	Synthesised Bioceramic Powders and Discs Addition.....	238
6.5.2.4	Preparation of Resazurin Reagent for Proliferation Assay.....	240
6.5.2.5	HGF-1 Cell Proliferation Assay	240
6.5.2.6	Raw Data Definition, Processing and Data Compiling	242
6.6	Results:	243
6.6.1	Survival Cell Rate of HGF-1 (Cytotoxicity) of Ceramic Discs Groups.....	243

6.6.1.1	Mean of Survival Cell Rate of HGF-1 for Different Ceramic Discs.....	
	Groups	243
6.6.1.2	Effect of Different Synthesised Ceramic Discs on Survival Cell of.....	
	HGF-1.....	244
6.6.2	Survival Cell Rate of HGF-1 (Cytotoxicity) of Powders Ceramics Groups	245
6.6.2.1	Mean of Survival Cell Rate of HGF-1 of Different Ceramic.....	
	Powders Groups	245
6.6.2.2	Effect of Different Ceramic Powders on Survival Cell Rate of HGC-1.	247
6.6.3	Comparison between the Effect of the Sintered and Non-Sintered Ceramic.....	
	Groups on the Mean Survival Cell Rate of HGF-1.	249
6.7	Discussion.....	252
6.8	Conclusions	259
	CHAPTER 7: CONCLUSIONS AND FUTURE STUDIES	261
7.1	Conclusions	261
7.2	Recommendations for Future Studies.....	262
	REFERENCES.....	264
	List of Publications and Papers Presented	299
	APPENDIX A	300
	APPENDIX B	307
	APPENDIX C	314
	APPENDIX D	317

LIST OF FIGURES

Figure 2.1: A cross section of typical layers of the dental all-ceramic crown design..... and components of the crown-adhesive-tooth system.	44
Figure 2.2: The proposed CAD/CAM dental crown design with independently..... fabricated veneers and cores that would have to be joined and placed in the mouth..... On the right, is the relevant flat layered structure for mechanical testing..	44
Figure 2.3: Typical posterior all-ceramic dental crown fracture. A failure of an..... all-ceramic crown presented in a patient from Ken Malament DDS.....	44
Figure 3.1: a- CT scan of maxillary second premolar tooth. b-Different views..... of the scanned tooth in MIMICS Software. c- Remeshing of tooth. d- Tooth..... after remeshing and smoothening	65
Figure 3.2: Schematic illustration of the geometric models and load directions.....	67
Figure 3.3: Tetrahedral mesh structure of the geometric model by FEA.	69
Figure 3.4: Boundary condition of the model.....	71
Figure 3.5: A static load in three different directions.	72
Figure 3.6: Measurements of stress on the model occlusal surface of the veneer,..... the ceramic core, and the cement	74
Figure 3.7: Measurements of stress on the model dentine.....	75
Figure 3.8: Contour plot of the von Mises stress distribution within the tooth and..... veneer-core-cement of all models when loaded obliquely.....	78
Figure 3.9: The von Mises stress of the veneer-core-cement-dentine in all models.....	79
Figure 3.10: The tensile stresses of the veneer-core-cement-dentine in all models.....	80
Figure 3.11: Contour plot of the tensile stresses of the veneer-core-cement-dentine..... in all models when loaded obliquely.....	81
Figure 3.12: The compressive stress of the veneer-core-cement-dentine in all..... models when loaded obliquely.....	82
Figure 3.13: Contour plot of the compressive stress of the veneer-core-cement-dentine..... in all models when loaded obliquely.....	83
Figure 3.14: Contour plot of the shear stress distribution interface between..... Veneer core-cement-dentine-S12 (X-Y direction) when loaded obliquely.	83

Figure 3.15: The shear stress distribution between the veneer-core-cement-dentine interfaces in all models. S12 (X-Y direction) when loaded obliquely.	84
Figure 3.16: Contour plot of the strain maximum distribution within the tooth and veneer-core-cement of all models when loaded obliquely.	85
Figure 3.17: Contour plot of the strain minimum distribution within the tooth and veneer-core-cement of all models when loaded obliquely.	85
Figure 3.18: The strain maximum distribution within the tooth and veneer-core-cement of all models when loaded obliquely.	86
Figure 3.19: Contour plot of the von Mises stress distribution within the tooth and veneer-core-cement of all models when loaded horizontally.	88
Figure 3.20: The von Mises stress distribution within the tooth and veneer-core-cement of all models when loaded horizontally.	89
Figure 3.21: Contour plot of the maximum principal stress distribution within the tooth and veneer-core-cement of all models when loaded horizontally.	90
Figure 3.22: Contour plot of the minimum principal stress distribution within the tooth and veneer-core-cement of all models when loaded horizontally.	90
Figure 3.23: The tensile stress distributions within the tooth and veneer-core-cement of all models when loaded horizontally.	91
Figure 3.24: The compressive stress distributions within the tooth and veneer-core-cement of all models when loaded horizontally.	92
Figure 3.25: Contour plot of the shear stress distributions within the tooth and veneer-core-cement of all models (S12:X-Y direction) when loaded horizontally.	93
Figure 3.26: The shear stress distributions within the tooth and veneer-core-cement of all models (S12: X-Y direction) when loaded horizontally.	94
Figure 3.27: Contour plot of the strain maximum distribution within the tooth and veneer-core-cement of all models when loaded horizontally.	95
Figure 3.28: The tensile strain distribution within the tooth and veneer-core-cement of all models when loaded horizontally.	96
Figure 3.29: Contour plot of the strain minimum distribution within the tooth and veneer-core-cement of all models when loaded horizontally.	97
Figure 3.30: Contour plot of the von Mises stress distribution within the tooth and veneer-core-cement of all models when loaded vertically.	98

Figure 3.31: The von Mises stress distribution within the tooth and veneer-core-cement of all models when loaded vertically.....	99
Figure 3.32: Contour plot of the maximum principal stress distribution within the tooth and veneer-core-cement of all models when loaded vertically.....	100
Figure 3.33: Contour plot of the minimum principal stress distribution within the tooth and veneer-core-cement of all models when loaded vertically.....	100
Figure 3.34: The tensile stress distribution within the tooth and veneer-core-cement of all models when loaded vertically.....	101
Figure 3.35: The compressive stress distribution within the tooth and veneer-core-cement of all models when loaded vertically.....	102
Figure 3.36: Contour plot of the shear stress distribution within the tooth and veneer-core-cement of all models (S12: X-Y direction) when loaded vertically.	103
Figure 3.37: The shear stress distribution within the tooth and veneer-core-cement of all models (S12: X-Y direction) when loaded vertically.....	104
Figure 3.38: Contour plot of the strain maximum distribution within the tooth and veneer-core-cement of all models when loaded vertically.....	105
Figure 3.39: Contour plot of the strain minimum distribution within the tooth and veneer-core-cement of all models when loaded vertically.....	105
Figure 3.40: The tensile strain distribution within the tooth and veneer-core-cement of all models when loaded vertically.	106
Figure 4.1: A flow chart of the experimental methodology.....	123
Figure 4.2: Zirconium oxide (micro-size).....	124
Figure 4.3: Zirconium oxide (nano-size).	124
Figure 4.4: Aluminum oxide (micro-size).....	124
Figure 4.5: Aluminum oxide (nano-size).....	124
Figure 4.6: Yttrium (III) oxide (nano-size).....	125
Figure 4.7: Magnesium oxide (nano-size).	125
Figure 4.8: Silicon (IV) oxide (nano-size).....	125
Figure 4.9: Potassium oxide (micro- size).	125
Figure 4.10: Calcium oxide (micro-size).....	126
Figure 4.11: Barium Sodium oxide (micro-size)	126

Figure 4.12: Terbium (III, IV) oxide (micro powder).....	126
Figure 4.13: Drying of the substrate powders.....	130
Figure 4.14: Zirconium jar and balls.....	130
Figure 4.15: A planetary ball mill machine used.	130
Figure 4.16: A custom made stainless steel compaction die used.	134
Figure 4.17: Schematic of die compaction mould.	134
Figure 4.18: Uni-axial hydraulic pressing machine used.....	135
Figure 4.19: The graded ceramic green specimen.	135
Figure 4.20: The furnace used.....	135
Figure 4.21: Sintering schedule and densification of the graded multilayered ceramic	136
Figure 4.22: The graded ceramic green specimens before sintering.....	136
Figure 4.23: The graded ceramic green specimens after sintering.....	136
Figure 4.24: FESEM used.....	139
Figure 4.25: XRD machine used.....	139
Figure 4.26: Electronic densitometer used.....	141
Figure 4.27: Vacuum desiccators used.....	141
Figure 4.28: MicroVickers hardness testing machine used.	143
Figure 4.29: A universal testing machine used.	143
Figure 4.30: Specimens of ceramic cores fabricated for TMA.....	145
Figure 4.31: TMA machine used to measure the CTE.....	145
Figure 4.32: FESEM for zirconia powder 100%. (a) mag x25000, (b) mag x50000,..... (c) mag x100000, and (d) mag x200000.	148
Figure 4.33: FESEM for sintered zirconia 100%. (a) mag x800, (b) mag x50000,..... (c) mag x100000, and (d) mag x200000.	149
Figure 4.34: FESEM for zirconia 80% (white grain)-alumina 20% (dark grain)..... powder (a) mag x25000, (b) mag x50000, (c) mag x100000, and (d) mag x200000. ...	150

Figure 4.35: FESEM for sintered zirconia 80% (white grain)-alumina 20% (dark grain) (a) mag x800, (b) mag 10000, (c) mag x100000, and (d) mag x200000. .	151
Figure 4.36: FESEM for sintered zirconia 60% (white grain)-alumina 40% (dark grain) (a) mag x800, (b) mag 10000, (c) mag x100000, and (d) mag x200000. .	152
Figure 4.37: FESEM for sintered zirconia 50% (white grain)-alumina 50% (dark grain) (a) mag x800, (b) mag 10000, (c) mag x100000, and (d) mag x200000. .	153
Figure 4.38: FESEM for alumina 100% after sintering. (a) mag x10000, (b) mag x25000, (c) mag x500000, and (d) mag x100000. .	154
Figure 4.39: FESEM for sintered graded silica. (a) mag x800, (b) mag 10000, (c) mag x100000, and (d) mag x200000. .	155
Figure 4.40: FESEM for sintered two-layers zirconia 100% (white layer)-zirconia 80%-Alumina 20% (dark layer). (a) mag x400, (b) mag x1000, (c) mag x1000, and (d) mag x4000. .	156
Figure 4.41: FESEM for sintered two-layers zirconia 100% (white layer)-zirconia 60%-alumina 40% (dark layer). (a) mag x400, (b) mag x1000, (c) mag x10000, and (d) mag x40000. .	157
Figure 4.42: FESEM for sintered two-layers zirconia 100% (white layer)-zirconia 50%-alumina 50% (dark layer). (a) mag x400, (b) mag x1000, (c) mag x10000, and (d) mag x40000. .	158
Figure 4.43: FESEM of interface between two-layers zirconia 100% (white layer)-zirconia80%-alumina 20% (dark layer). (a) mag x1000, (b) mag 2000, (c) mag x4000, and (d) mag x10000. .	159
Figure 4.44: FESEM of interface between two-layers zirconia 100% (white layer)-Zirconia 60%-alumina 40% (dark layer). (a) mag x200, (b) mag x1000, (c) mag x2000, and (d) mag x10000. .	160
Figure 4.45: FESEM of interface between two-layers zirconia 100% (white layer)- zirconia 50%-alumina 50% (dark layer). (a) mag x200, (b) mag x1000, (c) mag x2000, and (d) mag x10000. .	161
Figure 4.46: EDX of YZrO 100% powder. .	162
Figure 4.47: EDX of YZrO 100% layer after sintering. .	162
Figure 4.48: EDX of Zr80%-Al20% powder. .	162
Figure 4.49: EDX of Zr80%-Al20% layer after sintering. .	1622

Figure 4.50: EDX of Zr60%-Al40% powder.....	1633
Figure 4.51: EDX of Zr60%-Al40% layer after sintering.....	1633
Figure 4.52: EDX of Zr50%-Al50% powder.....	1633
Figure 4.53: EDX of Zr50%-Al50% layer after sintering.....	163
Figure 4.54: EDX of MgAlO100% powder.....	164
Figure 4.55: EDX of MgAlO 100% layer after sintering.....	164
Figure 4.56: EDX of graded silica powder.	164
Figure 4.57: EDX of graded silica layer after sintering.	164
Figure 4.58: XRD pattern of ZrO 100 powder (a) and solid (b).....	167
Figure 4.59: XRD pattern of Al 100 powder (a) and solid (b).....	167
Figure 4.60: XRD pattern of silica powder (a) and solid (b).	168
Figure 4.61: XRD pattern of ZrO80Al20% powder (a) and solid (b).....	168
Figure 4.62: XRD pattern of ZrO60Al40% powder (a) and solid (b).....	168
Figure 4.63: XRD of Zr50%-Al50% powder (a) and solid (b).....	169
Figure 4.64: XRD of interface layers between two layers (a) Zr100%-Zr80%-Al20%, (b) Zr 100%-Zr60%-Al40%, and (c) Zr 100%-Zr50%-Al50%.	169
Figure 4.65: Experimental density of all synthesised ceramic cores.	171
Figure 4.66: Relative density of all synthesised ceramic cores.	171
Figure 4.67: Porosities of all synthesised ceramic cores.	172
Figure 4.68: Volume shrinkage of all synthesised ceramic cores.....	173
Figure 4.69: Vickers Hardness of all synthesised ceramic cores.....	174
Figure 4.70: Vickers indentation of YZr 100% layer.....	174
Figure 4.71: Vickers indentation of Zr80%-Al20% layer.....	174
Figure 4.72: Vickers indentation of Zr60%-Al40% layer.....	174
Figure 4.73: Vikers indentation of Zr50%-Al50% layer	174

Figure 4.74: Vickers indentation of graded silica.....	175
Figure 4.75: Vickers indentation of Zr100%-Zr80%-Al20% two layer.....	175
Figure 4.76: Vickers indentation of Zr100%-Zr60%-Al50% two layer.....	175
Figure 4.77: Vickers indentation of Zr100%-Zr50%-Al50% two layer.....	175
Figure 4.78: CTE of all synthesised ceramic cores.....	176
Figure 4.79: CTE of zirconia 100% ceramic core layer.....	176
Figure 4.80: CTE of alumina 100% ceramic core layer.....	177
Figure 4.81: CTE of graded silica layer.....	177
Figure 4.82: CTE of Zr80%-Al20% ceramic core layer.....	177
Figure 4.83: CTE of Zr60%-Al40% ceramic core layer.....	178
Figure 4.84: CTE of Zr50%-Al50% ceramic core layer.....	178
Figure 4.85: CTE of Zr100%-Zr80%-Al20% ceramic two layers.....	178
Figure 4.86: CTE of Zr100%-Zr60%-Al40% ceramic two layers.....	179
Figure 4.87: CTE of Zr100%-Zr50%-Al50% ceramic two layers.....	179
Figure 4.88: Compressive strength of all synthesised ceramic cores.....	181
Figure 4.89: Elastic modulus of all synthesised ceramic cores.....	181
Figure 4.90: Strains of all synthesised ceramic cores.....	182
Figure 5.1: Silica infiltrated to synthesised ceramic cores.....	203
Figure 5.2: Infiltrated core with silica before sintering.....	203
Figure 5.3: Infiltrated core with silica after sintering.....	204
Figure 5.4: Ceramic cores samples abraded.....	204
Figure 5.5: Materials used to build up veneer.....	205
Figure 5.6: Silicone mould used to build up the veneer.....	205
Figure 5.7: Samples before sintering.....	207
Figure 5.8: Samples after sintering.....	207
Figure 5.9: Vacuum furnace used.....	207

Figure 5.10: Atomic force microscope used.	208
Figure 5.11: Surface roughness of synthesised ceramic cores measured by AFM.	208
Figure 5.12: Mould of specimens.	209
Figure 5.13: Specimens embedded into epoxy.	209
Figure 5.14: Instron universal machine used.	210
Figure 5.15: Specimens mounted into jig mould for SBS testing.	211
Figure 5.16: Schematic of specimens mounted into jig mould for SBS testing.	211
Figure 5.17: Stereomicroscope used.	212
Figure 5.18: The mean shear bond strength of synthesised ceramic cores coated..... with silica bonded to veneering ceramic.	214
Figure 5.19: SEM of YZrO_2 100%-veneer. (a) mag x10, (b) mag x1000, (c) mag..... x5000, and (d) mag x10000	216
Figure 5.20: SEM of YZrO_2 100%-silica-veneer. (a) mag x10, (b) mag x1000, (c) mag..... x5000, and (d) mag x10000	217
Figure 5.21: SEM of $\text{Zr}80\text{-Al}20\text{-silica-veneer}$. (a) mag x10, (b) mag x1000, (c)..... mag x5000, and (d) mag x10000.....	217
Figure 5.22: SEM of $\text{Zr}60\text{-Al}40\text{-silica-veneer}$. (a) mag x10, (b) mag x1000, (c)..... mag x5000, and (d) mag x10000.....	218
Figure 5.23: SEM of $\text{Zr}50\text{-Al}50\text{-silica-veneer}$. (a) mag x10, (b) mag x1000, (c)..... mag x5000, and (d) mag x10000.....	218
Figure 5.24: SEM of Al_2O_3 100%-veneer. (a) mag x10, (b) mag x1000, (c) mag..... x5000, and (d) mag x10000	219
Figure 5.25: SEM of Al_2O_3 100-silica-veneer. (a) mag x10, (b) mag x1000, (c)..... mag x5000, and (d) mag x10000.....	219
Figure 5.26: EDX of interface surface between $\text{Zr}100$ and veneering.	220
Figure 5.27: EDX of interface surface between $\text{Zr}100$, graded silica, and veneering ..	220
Figure 5.28: EDX of interface surface between $\text{Al}100$ and veneering.	220
Figure 5.29: EDX of interface surface between $\text{Al}100$, graded silica, and veneering ..	220

Figure 5.30: EDX of interface surface between Zr80-Al20%, graded silica, and..... veneering.....	221
Figure 5.31: EDX of interface surface between Zr60-Al40%, graded silica, and..... veneering.....	221
Figure 5.32: EDX of interface surface between Zr50-Al50%, graded silica, and..... veneering.....	221
Figure 6.1: The well plate used.....	238
Figure 6.2: Incubator used.....	238
Figure 6.3: The falcon tubes used.	239
Figure 6.4: Ceramic powders with HGF-1 cell in 96 well plates.....	239
Figure 6.5: Ceramic discs with HGF-1cells in 24 well plates.....	240
Figure 6.6: Resazurin reagent added into well plates.	241
Figure 6.7: Inverted light microscope used.....	241
Figure 6.8: Spectrophotometer used.	241
Figure 6.9: Mean of survival cell rate of different synthesised ceramic cores discs. ...	244
Figure 6.10: Mean of survival cell rate of different synthesised ceramic powders.	247
Figure 6.11: Mean survival cell rate of HGF-1 of non-sinetered and sintered..... ceramic groups.	250

List of Tables

Table 2.1: Physical and mechanical characteristics of alumina and partially stabilized	17
Table 2.2: Ceramic toughening mechanisms.	17
Table 2.3: Forms of transformation-toughened zirconia.....	20
Table 2.4: Mechanical properties of different ceramics.....	20
Table 3.1: Models with different designs and materials.	66
Table 3.2: Elastic properties of the tooth and restorative material properties.	73
Table 3.3: The von Mises stress value on tooth restored with various types of..... ceramic core loaded under different loading directions.....	107
Table 4.1: Specification of materials used in the study.	127
Table 4.2: Specification of materials used in the study.	128
Table 4.3: Grouping of compactions of specimens.....	132
Table 4.4: Mean of experimental, relative density, and porosity of synthesised..... bioceramic cores.....	170
Table 4.5: Mean of volume shrinkage, Vickers Hardness, and CTE of..... synthesised bioceramic cores.	173
Table 4.6: Mean of compressive strength, elastic modulus, and strain of..... synthesised bioceramic cores.	180
Table 4.7: Compressive stresses of synthesised ceramic cores.	182
Table 4.8: Effect of the elastic modulus of all synthesised ceramic cores.....	183
Table 4.9: Effect of the strains on all synthesised ceramic cores.....	184
Table 5.1: Properties of veneering material as provided by the manufacturer.	201
Table 5.2: Groups of synthesized ceramic cores.....	202
Table 5.3: Fracture surface criteria.	212
Table 5.4: Mean of shear bond strength of synthesised bioceramic cores and veneer..	213
Table 5.5: Shear bond strength of synthesised bioceramic cores and veneer (MPa)..	214

Table 5.6: Failed bonded surfaces by percentage (%).	215
Table 6.1: The cell line and materials used for testing biocompatibility of..... synthesised bioceramic.....	235
Table 6.2: The synthesised bioceramic materials (powders and discs).	236
Table 6.3: Mean of survival cell rate of different synthesised ceramic cores discs.....	243
Table 6.4: The effect of different ceramic discs core on survival cell rate of HGF-1. .	245
Table 6.5: Multiple comparisons of different ceramic discs Dunnett t (2-sided) ^a	245
Table 6.6: Mean of survival cell rate of different ceramic powders with..... different concentrations (%).	246
Table 6.7: The effect of different ceramic powders and different concentrations..... on survival cell rate of HGF-1.	248
Table 6.8: The effect of different ceramic powders and different concentrations..... on survival cell of HGF-1.	248
Table 6.9: Mean survival cell rate of HGF-1 of non-sintered and sintered..... synthesised ceramic groups.....	249
Table 6.10: The effect of sintering and non-sintering ceramic on survival cell rate of..... HGF-1.	250
Table 6.11: The comparisons effect between sintering and non-sintering in each..... same ceramic material on survival cell rate of HGF-1.	251

LIST OF SYMBOLS AND ABBREVIATIONS

AFM	:	Atomic Force Microscope
ASTM	:	American Society for Testing and Materials
ATZ	:	Alumina-Toughened-Zirconia
c	:	Cubic Phase
°C	:	Centigrade
CAD/CAM	:	Computer-Aided Design/Computer Aided Manufacturing
Ce-TZP	:	Cerium-Tetragonal Zirconia Polycrystalline
CT	:	Computerized Tomography
CTE	:	Coefficient of Thermal Expansion
CVD	:	Chemical Vapour Deposition
EDX	:	Energy Dispersive X-ray
FEA	:	Finite Element Analysis
FEM	:	Finite Element Method
1D	:	One Dimensional
2D	:	Two Dimensional
3D	:	Three Dimensional
FESEM	:	Field Emission Scanning Electron Microscope
FGM	:	Functionally Graded Material
FGMDC	:	Functionally Graded Material Dental Ceramic
FPD	:	Fixed Partial Denture
h	:	Hour
HMDS	:	Hemaethylsiloxane
HF	:	Hydrofluoric Acid
HGF	:	Human Gingival Fibroblast
ICCD	:	International Center for Diffraction Data
ISO	:	International Organization for Standardization
JCPDS	:	Joint Committee of Powder Diffraction Standard
K_{IC}	:	Fracture Toughness
LTD	:	Low Temperature Degradation
m	:	Monoclinic Phase
Mg-PSZ	:	Magnesium Partially Stabilized Zirconia
MPa	:	Megapascal
MVD	:	Molecular Vapor Deposition

N	:	Newton
PFM	:	Porcelain-Fused-to-Metal
PM	:	Powder Metallurgy
PVD	:	Physical Vapour Deposition
PSZ	:	Partially Stabilized Zirconia
MTT	:	5-diphenyltetrazolium bromide
ROM	:	Rule of Mixture
s	:	Second
SBS	:	Shear Bond Strength
SD	:	Standard Deviation
SE	:	Standard Error Mean
SEM	:	Scanning Electron Microscope
SHS	:	Self-Propagation High Temperature Synthesis
t	:	Tetragonal Phase
t—m	:	Transformation from Tetragonal Phase to Monoclinic Phase
TMA	:	Thermo-Mechanical Analysis
Vol%	:	By Volume
VH	:	Vickers Hardness
XRD	:	X-Ray Diffraction
wt%	:	By weight
3Y-TZP	:	Three mole% Y_2O_3 Tetragonal Zirconia Polycrystalline
YSZ	:	Yttrium Partially Stabilized Zirconia
Y-TZP	:	Yttrium Tetragonal Zirconia Polycrystalline
ZTA	:	Zirconia-Toughened-Alumina

LIST OF APPENDICES

Appendix A.....	300
Appendix B.....	307
Appendix C.....	314
Appendix D.....	317

University of Malaya

CHAPTER 1: INTRODUCTION

1.1 Introduction

All-ceramics are very attractive biomaterials for use as dental crown restorations because of their inertness, aesthetics, and biocompatibility (Mallinen et al., 2013). However, they are brittle, to a lesser or greater extent, and tend to fail beyond a lifetime or critical load (Lawn et al., 2002a). However, the failure rate of posterior all-ceramic crowns is reported as 3 % to 4% each year (Conrad et al., 2007; Rekow and Thompson, 2007; Denry and Kelly, 2008; Chevalier and Gremillard, 2009; Ho and Matinlinna, 2011; Silva et al., 2012; Anusavice, 2012; Miyazaki et al., 2013; Zhang, 2014; Babu et al., 2015; Tang et al., 2015; Cattani-Lorente et al., 2016; Hamza et al., 2016), despite recent significant improvement in dental ceramic strength (i.e. high strength zirconia and alumina cores). The main clinical failure mode is the subsurface radial crack in the ceramic, at the interface between the cement and dental ceramic crown (Kelly, 1997; Kelly & Denry, 2008). This failure rate is caused largely by the tensile stress concentration in the dental ceramic at that interface (Lawn et al., 2002a; Huang et al., 2007a). It is, therefore, advantageous to find out efficient techniques for the stress reduction at this interface.

Using bioceramics as a biomaterial is traced back to the 1970's, and since then, a constant improvement these biomaterials, in many applications, had been observed (Diego et al., 2007). Bioceramics materials have rapidly been utilized in the dental restorations for composites, bridges, onlays/inlays, all-ceramic crowns, and implants. This is due to their excellent aesthetics and biocompatibility as well as their mechanical, and corrosive resistances, and the ability to fabricate complex shapes. Structurally, dental bioceramics cover a broad spectrum of reinforced porcelains, glass–ceramics, fibre

reinforced ceramic composites, zirconia, alumina, and multi-layered ceramic structures (Rosenblum and Schulman, 1997; Ironside and Swain, 1998; Yin et al., 2006; Yi and Kelly, 2008; Best et al., 2008; Miyazaki et al., 2013; Al-Amleh et l., 2014; Soares et al., 2016; Özcan and Bernasconi, 2016 Zhang et al., 2016a, 2016b).

Restorations made of the dental bioceramics have also resulted in increased survival rates (Hankinson and Cappetta, 1994; Hansen, 2000; Bindl and Mormann, 2002; Otto and De Nisco, 2002; Lohbauer et al., 2002; Soares et al., 2016; Özcan and Bernasconi, 2016 Zhang et al., 2016a, 2016b). Regardless of the attractiveness of dental bioceramics, failure in the multilayer bioceramic restorations, particularly in external veneer porcelains have been observed due to their inherent brittleness (Lawan et al., 2002a, 2002b; Hsueh et al., 2008; Reich et al., 2008; Yi and Kelly, 2008; Marchack et al., 2008; Beuer et al., 2009; Ho and Matinlinna, 2011; Miyazaki et al., 2013; Al-Amleh et l., 2014; Özcan and Bernasconi, 2016 Zhang et al., 2016a, 2016b).

The persistent patient demand for aesthetic treatment and the clinical success of all-ceramic restorations have resulted in the development and introduction of several bioceramic systems such as zirconia and alumina. The ongoing development in technology and ceramic materials has sustained an advanced research benefit in dental all-ceramic restorations. This stable improvement is based on the superior properties of all-ceramics, fundamentally their chemical stability, biocompatibility, and a great amplitude to mimics dental tissues (Della Bona et al., 2008). The reduction of disorders had been the target of all-ceramic frameworks to improve fracture toughness and strength. It has been reported that the composition, microstructure and processing are the controlling parameters in the evolution of coveted mechanical properties of dental all-ceramic crown restorations (Della Bona and Anusavice, 2002; Della Bona et al., 2007, 2008; Zhang et al., 2008; Özcan and Bernasconi, 2016 Zhang et al., 2016a, 2016b).

Pure zirconia (ZrO_2) cannot be utilized in the production of compounds, without the addition of stabilisers (Diego et al., 2007). Zirconia, in tetragonal phase, can be stabilised by either cerium oxide (CeO), magnesium oxide (MgO), calcium oxide (CaO), or yttrium oxide (Y_2O_3). The interest in ZrO_2 is from its tensile strength and high fracture toughness (Hench, 1998; Sundah and Göran, 2006; Lazar et al., 2008; Sundah and Göran, 2008; Reich et al., 2008; Al-Amleh et al., 2010; Miyazaki et al., 2013; Zhang, 2014; Srikanth et al., 2015; Özcan and Bernasconi, 2016; Zhang et al., 2016a, 2016b).

Zirconia and alumina bioceramics have preferable mechanical properties compared to leucite ceramics due to their chemical composition, microstructure, and increased crystalline content (Tinschert et al., 2000; Guazzato et al., 2004a, 2004b; Lazar et al., 2008; Srikanth et al., 2015; Kaizer et al., 2016; Kohal et al., 2016). In addition, with the evolution of modern technology, like CAD/CAM, permits the production of zirconia-based restorations for all-ceramic dental crowns and FPDs to be a more practical method (Piconi and Maccauro, 1999; Tinschert et al., 2000; Giordano, 2002; Vult von Steyern et al., 2005; Sailer et al., 2006; Sundah and Göran, 2006; Chaiyabutr et al., 2008; Sonza et al., 2014; Tsukada et al., 2014; Li et al., 2014; Wendler et al., 2015; Basso et al., 2015; Duan and Griggs, 2015; Seker et al., 2016; Kaizer et al., 2016; Kohal et al., 2016).

Three mol% Y_2O_3 tetragonal zirconia polycrystalline (3Y-TZP) has become a common alternative to alumina as a structural bioceramic, because it presents greater flexural strength and fracture toughness with a low Young's modulus and is also inert in a physiological media (Stevens, 1981; Sundah and Göran, 2006; Thompson et al., 2007; Diego et al., 2007; Sundah and Göran, 2008; Teixeira et al., 2008; Lazar et al., 2008; Miyazaki et al., 2013; Tang et al., 2015; Hamza et al., 2016; Harada et al., 2016).

There are considerable relationships between atomic structure, chemical composition, properties of polycrystalline, microstructure, and the fabrication process (Della Bona et

al., 2005). Evaluation of microstructure is usually related to the information and material properties is used to portend properties and develop the design of modern materials (Della Bona and Anusavice, 2002). Consequently, the microstructure, that refers to size, nature, quantity, shape, and distribution of the phases or structural elements in the ceramics, has a deep influence on physical properties. As well, recent on research ceramics has intensified on developing an essential understanding of bioceramic failure/damage modes as effected by microstructure (Rahaman, 1995; Della Bona and Anusavice, 2002; Anusavice, 2012; Miyazaki et al., 2013; Zhang, 2014).

Quantitative information on the clinical achievements have not been widely published, however, some existent studies have indicated an inclination for all-ceramic dental crowns restorations to fail due to the fatigue failure (Yin et al., 2006). Similarly, the evolution of new testing processes is required to complete the existent knowledge of chemical stability of the dental all-ceramics restorations (Jakovac et al., 2006; Al-Amleh et al., 2010).

Y-TZP had been used as a ceramic biomaterial in medical applications since the late 1960s', its use in dentistry is relatively recent (Piconi and Maccauro, 1999; Lüthy et al., 2005; Cavalcanti et al., 2009, Tang et al., 2015) and occurred following advances in CAD/CAM technology. These high strength materials offer a wide variety of clinical application, such as orthodontic brackets, posts, implant abutments and frameworks for crowns and bridges (Wolfart et al., 2007; Özcan et al., 2008; Cavalcanti et al., 2009; Abduo and Lyons, 2013; Miyazaki et al., 2013; Abduo et al., 2014; Ender et al., 2016).

In contrast to traditional dental bioceramics, 3Y-TZP consists of several small particles without any glassy phase at the crystallite boundary (Luthardt et al., 2002). The absence of a glassy phase and silica damages the effectiveness of traditional adhesive luting steps, which include etching surfaces of ceramic with hydrofluoric acid and using

silanes before the use of a resin luting cement (Kern and Wegner, 1998; Blatz et al., 2003; Yoshida et al., 2004; Derand et al., 2005; Yoshida et al., 2006; Atsu et al., 2006; Matinlinna and Vallittu, 2007; Özcan et al., 2008). Recent studies have suggested specific luting techniques for Y-TZP ceramics. These include surface treatment and the use of materials with a chemical affinity for zirconium dioxide (Kern and Wegner, 1998; Kosmac et al., 1999; Blatz et al., 2003; Yoshida et al., 2004; Ernst et al., 2005; Derand et al., 2005; Lüthy et al., 2006; Yoshida et al., 2006; Wolfart et al., 2007; Özcan et al., 2008; Cavalcanti et al., 2009, Inokoshi et al., 2014; Tzanakakis et al., 2016; Xie et al., 2016).

Although the abrasion and grinding behaviours of zirconia ceramics (particularly their influences on strength) have been studied (Zhang et al., 2004a, 2006b), the Y-TZP CAD/CAM with/without infiltration by graded silica subject to grit-blasting, abrasive machining, and bonding has not been systemically evaluated. In addition, little attention has been paid to the low temperature degradation (LTD) behaviours of CAD/CAM Y-TZP machined with/without infiltration by graded silica (Zhang and Kim, 2010; Canneto et al., 2016; Pereira et al., 2016).

The longevity of an indirect restoration is closely related to the integrity of the luting cement at the margin (Valandro et al., 2005). Although the use of zirconia ceramics for dental applications is still in progress, the best technique to raise a durable bond between the tooth and ceramic is still unknown (Kern and Wegner, 1998; Luthra and Kaur, 2016). But, the only unanimity found in the literature is that the hydrofluoric acid etching and popular silane agents are efficient for zirconia bioceramics (Kern and Wegner, 1998; Yoshida et al., 2006; Atsu et al., 2006; Al-Harbi et al., 2016; Luthra and Kaur, 2016).

Dental multilayer ceramics are an engineering idealization of dental crowns. This method mimics the layered structure of the crown on a real tooth. Medical and dental researchers have focused on applying finite element analysis (FEA), one of the most

successful engineering computational methods, to predict stress distributions and the mechanical behaviour of the restorations, fixed partial denture and dental crowns (Toparli et al., 1999; Ausiello et al., 2001; Fischer et al., 2003; Dittmer et al., 2009; Zheng et al., 2012; Dejak et al., 2012; Ha et al., 2013; Della Bona et al., 2013; Ha et al., 2016; Hondo et al., 2016; Jalali et al., 2016). Few studies have reported the optimum design of all-ceramic crowns based on the geometry of a real tooth, which is obtained through a computerized tomography (CT) scan, and analysed by FEA.

The concept of functionally graded materials (FGMs) is a new approach for the improvement of dental ceramic core material performance. Compared with traditional homogeneous and uniform materials, FGM allows the production of materials with different characteristics within the same material at various interfaces (Suresh, 2001; Hedia and Mahmoud, 2004; Hvizdos et al., 2007; Yanga and Xianga, 2007; Wang et al., 2007; Zhang and Ma, 2009; Zhang et al., 2010; Zhang and Kim, 2010; Zhang et al., 2012; Tsukada et al., 2014; Srikanth et al., 2015). The use of accurately graded finite elements for FGM modeling has been recently developed (Watari et al., 2004).

1.2 Rationale of Study

The main goal of the bioceramic researches is to produce tougher, stronger ceramics which are structurally dependable in the dental application. The key challenges for further improved dental ceramic frameworks appears to be low cost, crack-tolerance, excellent aesthetic characterization, and bondability. These goals involve materials design more than fabrication limitations. Microstructural control and novel ceramic textures can be produced by stereolithography, rapid prototyping, and printing techniques. Their potential has not yet been recognised.

1.3 Statement of Problem

Multilayered all-ceramic dental crowns have become excessively used since the introduction of strong zirconia and alumina cores, but problems related to the flaws in bioceramics, that arises from its essential brittleness have resulted in the inaccuracy in strength. This has led to the evolution of methods to inhibit these cracks or flaws to expand, and, as a result, a raise in strength. FGM and thin film technologies are possible solution to problems associated with use of all-ceramic systems for restorative dental applications. To extend the longevity of a bioceramic restoration, it is important to address the question of how to perform microstructural refined dental ceramic to avoid or preferably to reduce the number and size of flaws and cracks. Hence, it is fundamental to optimize the fabrication techniques and thereby improve control of the quantity and quality of the all-ceramic dental crown restorations.

1.4 Thesis Layout

The thesis layout was followed the following route:

Chapter one will outline all seven chapters in this study. Chapter two will outline the relevant literature related to this study. Chapter three will outline the methodologies using CT scan with 3D FE model to predicate the strategies developed to serve as guidelines throughout the rule of mixture (ROM) and FEM which were utilized to portend the mechanical properties of synthesised ceramics and assist in achieving the main objectives. The outlines of the methodology are presented using a CT scan, Mimics software, and Abaqus software for FEA, followed by a detailed discussion regarding the procedures and techniques used.

Chapter four will outline the experimentally synthesised bioceramic single layer and multilayered core include ceramic synthesis powders, characterization, and experiment tests which are relative density, volume of shrinkage, porosities, Vickers hardness, CTE, compressive strength, elastic of Young's modulus, and strain.

Chapter five will outline how suitably graded silica is chosen to match veneering porcelains and ceramic cores. For this, matching of thermal expansion coefficients is vital, to avoid residual stresses in the finished product. Also, chapter 5 will describe how synthesised glasses are tested to meet this need, and then rejected because of incompatibility concerns. Then describe how new glass compositions are designed and fabricated to overcome these incompatibility issues. Infiltrated graded silica processing will form the underlying processing route, with the prospective advantage of low-temperature manufacture. Various tests for assessing the glass properties will then be described, including the degree of wetting, crazing and pore formation. Chapter six will describe the cytotoxicity effects of new synthesised dental bioceramic core (powders and discs) using human gingival fibroblast (HGF-1) cells lines by using proliferation cell assay. Chapter seven will summarise for all chapters and recommendation studies.

CHAPTER 2: LITERATURE REVIEW

2.1 Bioceramic in Dentistry

A biomaterial is defined as a non-viable material utilized in a medical device, which is intended to interact with biological systems (Williams, 1990; Park and Bronzino, 2003). Among the three major classes of biomaterials: polymers, metals, and ceramics, the last is an attractive preference for prostheses, mainly because of superior biocompatibility and, in dental uses, such as restorative of dental prosthetics, the esthetics (Rekow and Thompson, 2007). Most biomaterials require excellent long-term clinical performance to be considered viable commercial alternatives (Bayne, 2005). The development of new technologies for manufacturing biomaterials has been motivated by the request for materials, qualified for bearing new applications and specifications (Bayne, 2005; Diego et al., 2007). Bioceramics have quickly emerged as one of the main dental biomaterials in prosthodontics due to their biocompatibility and aesthetics. However, studies have shown higher clinical failure rates due to brittleness, which has to a specific extent prohibited the ceramics from fully substituting metals in such major dental restorations as multi-unit bridges (Kelly, 2004; Li et al., 2006). In order to increase the performance of these materials, the application of thin film coatings has been suggested (Thompson et al., 2007; Teixeira et al., 2008).

Several millennia ago, advanced ceramics found unique applications in the biomedical industry besides their potential and current uses in various other high technology related fields. Ceramics engineered for biomedical applications are called bioceramics (Hench, 1991). Bioceramics are fabricated in a variety of phases and forms and serve several different applications in repair of the body (Hench, 1998). Depending on the properties or functions required, bioceramics could be fabricated in several various phases.

Bioceramics can be polycrystalline (zirconia, alumina or hydroxyapatite), single crystals (sapphire), glass (Bioactive glass), or composites (polyethylene- hydroxyapatite) (Hench and Wilson, 1993).

Dental bioceramics are widely utilized as veneers, onlays/inlays, anterior and posterior crowns, and partial crowns in prosthetic restorations. This is because of their aesthetic comparable wear resistance to natural translucency, natural tooth structures, and biocompatibility (Kelly, 1997; Rosenblum and Schulman, 1997; Ironside and Swain, 1998; Van Noort, 2002). Restorations made of the dental bioceramics have also resulted in increasing survival rates (Hankinson and Cappetta, 1994; Hansen, 2000; Bindl and Mormann, 2002; Otto and De Nisco, 2002; Lohbauer et al., 2002). Regardless of the attractiveness of dental bioceramics, failure in the multilayer bioceramic restorations, particularly in external veneer porcelains have been observed due to their inherent brittleness (Jung et al., 1999; Lawan et al., 2002a, 2002b). Quantitative information on the clinical achievements have not been widely published, however, some existent studies have indicated an inclination for all-ceramic dental crowns restorations to failure after years in the mouth due to the fatigue fail (Jung et al., 2000; Yin et al., 2006; Tang et al., 2015; Pereira et al., 2016; Cattani-Lorente et al., 2016; Luthra and Kaur, 2016).

2.1.1 Zirconia (zirconium oxide) (ZrO_2)

The name “zirconium” comes from Arabic word “*Zargon*” which means “golden in colour”. Zirconium oxide (ZrO_2) was fortuitously recognized by German chemist Martin Heinrich Klaproth in 1789 while he was working with certain steps that involved the heating of some gems. Subsequently, zirconium dioxide was utilized as a rare pigment for a long time. It was the impure zirconium that was used as a pigment (Piconi and Maccauro, 1999).

In the 1990s, zirconia ceramics were utilized as root canal posts and as implant abutments. The use of zirconia bioceramics for dental restorations has increased in popularity due to its excellent physical properties, white colour, superior fracture strength (Tinschert et al., 2000), toughness as compared to other systems of dental ceramic (Guazzato et al., 2005) and excellent biocompatibility. It is being investigated as an alternative system for FPDs and full coverage all-ceramic crowns (Kelly and Denry, 2008; Denry and Kelly, 2008).

Pure zirconia (ZrO_2) cannot be utilized in the fabrication of components, without the addition of stabilizers (Diego et al., 2007). It has three polymorphic phases at atmospheric pressure: monoclinic from room temperature to 1170 °C, tetragonal (1170–2370 °C), and cubic (2370–2680 °C). During cooling, the tetragonal-to-monoclinic transformation occurs at the temperature range of about 100 °C below 1070 °C. The phase transformation, which occurs in creating cracks during cooling from sintering temperature, is associated with volume expansion of approximately 3–4%. This means that components made of pure zirconium oxide would burst due to a tension and volume increase of grains (Garvie et al., 1975; Piconi and Maccauro, 1999; Kosmac et al., 1999; Conrad et al., 2007; Lazar et al., 2008). To prevent these phase transformations, the addition of stabilizing oxides such as Y_2O_3 , MgO, CaO, and CeO to pure zirconia is recommended because it permits retention of the tetragonal structure at room temperature, thus controlling the volume expansion stress-induced t→m transformation, effectively inhibiting crack propagation and leading to high toughness (Garvie and Nicholson, 1972; Garvie et al., 1975; Heuer et al., 1986; Luthardt et al., 1999; Denry and Kelly, 2008; Al-Amleh et al., 2010). The t/m phase transformation can also be induced at the surface of Y-TZP *in vivo*, which leading to the so-called aging phenomena (Lawson, 1995). The aging degradation categorized by particle release, microcracking at the surface of the material, or surface roughening, limits the development of yttria stabilized zirconia as a biomaterial

(Chevalier et al., 2004). Therefore, there is a requirement for ceramic biomaterials with enhanced mechanical properties compared to alumina, and improved *in vivo* stability compared to Y-TZP (Benzaid et al., 2008). Although several kinds of zirconia-containing ceramic systems now exist (Hannink et al., 2000), only three classes of zirconia materials have been utilized till now in dentistry. These are magnesium cation-doped partially stabilized zirconia (Mg-PSZ), yttrium cation-doped tetragonal zirconia polycrystalline (Y-TZP), and zirconia-toughened alumina (ZTA) (Piconi and Maccauro, 1999; Kosmac et al., 1999; Denry and Kelly, 2008; Chevalier and Gremillard, 2009).

2.1.1.1 Yttrium-Tetragonal Zirconia Polycrystalline (Y-TZP)

Biomedical grade zirconia commonly contains 3 mol% yttria (Y_2O_3) as a stabilizer (3Y-TZP) (Piconi and Maccauro, 1999). While the stabilizing Y^{+3} cations and Zr^{+4} are randomly distributed over the cationic places, electrical neutrality is reached by the formation of oxygen vacancies (Eichler, 2001; Fabris et al., 2002). 3Y-TZP is used in dentistry for the construction of crowns and FPDs. The restorations are managed either by hard machining of fully sintered blocks, or by soft machining of presintered blanks followed by sintering at high temperature (Filser et al., 2003).

Y-TZP has mechanical properties which are attractive for prosthodontics, including its dimensional and chemical stability, fracture-toughness, and high mechanical strength (Aboushelib et al., 2005). The cores have a radiopacity comparable to metal which enhances radiographic assessment of recurrent decay as well as excess cement removal and marginal integrity (Tinschert et al., 2000; Filser et al., 2003; Raigrodski, 2004; Conrad et al., 2007; Miyazaki et al., 2013; Zhang, 2014; Wendler et al., 2015).

The mechanical properties of 3Y-TZP strongly rely on its grain size (Ozawa and Hasegawa, 1991; Ruiz and Readey, 1996; Burger et al., 1997; Tinschert et al., 2000;

White et al., 2005). However, below a certain grain size ($<0.2 \mu\text{m}$), the transformation is not possible, thus leading to reducing fracture toughness (Cottom and Mayo, 1996). Furthermore, above a critical grain size, 3Y-TZP is less stable and more susceptible to spontaneous $t \rightarrow m$ transformation, whereas smaller grain sizes ($<1 \mu\text{m}$) are associated with a lower transformation rate (Heuer et al., 1982). Thus, the sintering environment has a powerful influence on both the stability and mechanical properties of the final product as they dictate the grain size, sintering times and sintering temperatures leading to larger grain sizes (Scott, 1975; Chevalier et al., 2004) (Table 2.1).

Chevalier et al., (2004) confirmed that the presence of cubic zirconia is not desirable in 3Y-TZP for biomedical uses and is caused by irregular distribution of the yttrium stabilizer ions. The cubic grains are enriched in yttrium whereas the surrounding tetragonal grains are depleted and therefore less stable.

Zhang et al., (2004a, 2004b) and Zhang and Lawn (2005) evaluated the influence of sharp indentation damage on the long-term achievement of 3Y-TZP. It was revealed that both sharp indentations and sandblasting even at very low forces are detrimental to the long-term achievement of 3Y-TZP when examined in cyclic loading. These studies indicated the significance of controlling the final surface state of 3Y-TZP for biomedical applications.

Many researches have indicated that fracture toughness values in the range of 6-9 MPa $\text{m}^{1/2}$ range and flexural strength values of 800-1200 MPa (Kosmac et al., 1999; Kosmac et al., 2000), are possible with zirconia and substantially higher than for other all-ceramics which makes this material beneficial for highly loaded, all-ceramic restorations. Hence, recommendations have been made that zirconia could also be a feasible substitute to metal in prosthodontics, particularly for crowns in the FPDs and molar areas (Filser et al., 2003; Miyazaki et al., 2013; Tang et al., 2015; Zhang et al., 2016a; Hamza et al., 2016).

Nano-scale ZrO₂ transformation toughening appears in limited commercialization and in the literature. In a study by Bravo-Leon et al., (2002), it was reported that the trend towards increased phase stability with decreasing particle-size of t-ZrO₂ could be overcome by regulating the concentration of yttria dopant. While 3 mol% Y₂O₃ was found to optimize toughness in micrometer and sub-micrometer t-ZrO₂, critical grain size and dopant concentrations for nano-scale material were identified as 1.0 mol% for 90 nm and 1.5 mol% for 110 nm; both combinations reached fracture toughness of around 16 MPa m^{1/2} (Bravo-Leon et al., 2002). As with micro-scale zirconia, robust grain size influences (decreasing toughness with decreasing grain size) were revealed in these nano-scale ceramics as well (Bravo-Leon et al., 2002). At least one commercial nano-scale Ce-TZP containing 20% Al₂O₃ is being studied as a dental all-ceramic (Fischer et al., 2010) was reported to have a fracture toughness of approximately 20 MPa m^{1/2} (Kelly and Denry, 2008). It is possible that nano-scale t-ZrO₂ will primarily be seen in the polycrystalline form due to the difficulties for intra-granular precipitation and tertiary phase development essential in partially stabilized zirconia (PSZ) materials (Thompson et al., 2011).

2.1.1.2 Partially Stabilized Zirconia (Mg-PSZ)

Full stabilization is purposefully not performed in these materials. Hence, historical derivation of the term “partially stabilized zirconia” or PSZ, to which the relevant dopant is frequently attached: Y-PSZ, Mg-PSZ, Ca-PSZ, etc. (Heuer, 1987).

According to Denry and Kelly (2008), although a substantial amount of study has been dedicated to Mg-PSZ for possible biomedical uses, this material has not been successful, mostly due to the presence of porosity associated with its large grain size (30–60 μm), thus inducing wear to opposing teeth (Piconi and Macauro, 1999). The microstructure contains tetragonal precipitates within a cubic stabilized zirconia matrix. The amount of

MgO in the composition of commercial materials usually ranges among 8 and 10 mol%. In addition to a high sintering temperature (between 1680 °C and 1800 °C). The cooling cycle has to be accurately controlled, especially in the aging step with a preferred temperature of 1100 °C. Precipitation of the transformable t-phase happens during this step where volume fraction is regarded a critical factor in controlling the fracture toughness of the material (Heuer et al., 1986; Heuer, 1987; Hannink et al., 1994). Due to the difficulty in obtaining Mg-PSZ precursors free of SiO₂, magnesium silicates can lower the Mg content in the grains and encourage the t→m transformation (Leach, 1987). This can result in less stable material and lower mechanical properties (Denry and Kelly, 2008; Thompson et al., 2011).

This Mg-PSZ has high initial fracture toughness and flexural strength (Luthardt et al., 1999). Tensile stresses at a crack tip will cause the tetragonal phase to transform into the monoclinic phase with an associated 3-5% localized expansion (Kosmac et al., 1999). The volume increase produces compressive stresses at the crack tip that counteract the external tensile stresses and delays crack propagation. This phenomenon is recognized as transformation toughening. However, the presence of higher stress, a crack can still propagate. The toughening mechanism does not stop the development from a crack, but it just makes it harder for the crack to propagate (Piconi and Maccauro, 1999; Luthardt et al., 1999; Kosmac et al., 1999; Raigrodski, 2004; Conrad et al., 2007). This unique characteristic may make zirconia a superior material to other dental all-ceramics (Conrad et al., 2007; Teixeira et al., 2008) (Table 2.2).

2.1.1.3 Zirconia Toughened Alumina (ZTA)

Y-TZP and alumina ceramics are suitable for biomedical applications due to their robust mechanical and tribological properties and proved biocompatibility (Piconi and

Maccauro, 1999). Addition of zirconia in the alumina as a sintering additive have been utilized for a long time with the objective of alumina-based ceramics densification. However, the concept of toughening zirconia ceramics with a dispersion of alumina particles in a matrix has only been available in the last 20 years. The introduction of small amounts of alumina in zirconia as a sintering additive causes the formation of a solid solution which encourages the densification process by introducing defects (Wang and Stevens, 1989). On the other hand, the microstructure of a ceramic composite material is formed by the addition of one second phase. A composite material is recognized as a means of improving lifetime and reliability of ceramic abutments by providing higher mechanical strength and fracture toughness. Material scientists are previously familiar with ceramic composites like zirconia-alumina (Claussen, 1976; Lange, 1982; Hori et al., 1986; Casellas et al., 1999; Gregori et al, 1999).

Since both biomaterials zirconia and alumina are biocompatible, this could be proved as a new method to dental abutments. Despite the familiarity of the community of materials with zirconia and alumina separately by being both biocompatible, little has been published in the literature on the utilization of zirconia-alumina composites as biomaterial in dentistry (Piconi and Maccauro, 1999).

Two kinds of composites can be produced from this system: a matrix of alumina strengthened and stabilized with particles of zirconia (Y-ZTA) or a matrix of zirconia strengthened and stabilized with particles of alumina (Y-ATZ) (Table 2.3) (Karihaloo, 1991; Becher et al., 1993; Gregori et al., 1999; De Aza et al., 2002). With both types of material, higher toughness values when compared with the monophase ceramics can be achieved (Fantozzi and Orange, 1986; Gregori et al., 1999; De Aza et al., 2002; Nevarez-Rascon et al., 2009, 2010, 2011).

Table 2.1: Physical and mechanical characteristics of alumina and partially stabilized zirconia bioceramics (Hench, 1998; Piconi and Maccauro, 1999).

Physical characteristic	Alumina	Zirconia
Content (wt%)	Al ₂ O ₃ > 99.8	ZrO ₂ > 97
Density (g/cm ³)	>3.93	6.05
Average grain size (μm)	3-6	0.2.04
Surface roughness, R _a (μm)	0.02	0.008
Vickers hardness (HV)	2300	1300
Flexural Strength (MPa)	400	1000
Compressive strength (MPa)	4500	2000
Young's modulus (MPa)	380-434	150-205
Fracture toughness, K _{IC} (MPa·m ^{-1/2})	5-6	15
Slow crack growth	30-52	65
Bending strength (in Ringer's solution) (MPa)	595	1000
Linear CTE (x10 ⁻⁶ K ⁻¹)	7.2-8.6	8.9-10.6
Thermal Conductivity [W/(m·K)]	5.8 at 1127 °C	-2 at 1127 °C
Oxygen Diffusivity at 1000 °C (m ² /s)	10 ⁻²¹	10 ⁻¹¹

Table 2.2: Ceramic toughening mechanisms (Evans, 1990; Kelly and Denry, 2008).

Mechanism	Highest toughness (MPa m ^{1/2})	Example materials
Transformation	≈20	ZrO ₂ (MgO) HfO ₂
Microcracking	≈10	Al ₂ O ₃ /ZrO ₂ Si ₃ N ₄ /SiC SiC/TiB ₂
Metal dispersion	≈25	Al ₂ O ₃ /Al Al ₂ O ₃ /Ni
Whiskers/platelets	≈15	Si ₃ N ₄ /SiC Al ₂ O ₃ /SiC
Fibers	≥30	CAS ^a /SiC LAS ^b /SiC SiC/SiC Al ₂ O ₃ /Al ₂ O ₃
^a Calcium aluminum silicate glass ceramic. ^b Lithium aluminum silicate glass ceramic.		

In previous evaluations, mechanical properties of ceramic composites have been enhanced by adding of ceramic oxides to the matrix (Guazzato et al., 2004a, 2004b; Gutknecht et al., 2007). By the suitable combination of shape grain and particle size,

densification of these composites has been reported to be increased (Moraes et al., 2004). This, in turn, effects mechanical properties of the ceramic (Guazzato et al., 2004a). As well, the processing of starting powders, sintering temperature and time are also factors that should be considered in order to get a ceramic free of imperfections (Guazzato et al., 2004b; Nevarez-Rascon et al., 2009).

ZTA is a combination of zirconia with an alumina matrix, which subjects stress-induced transformation to attain superior mechanical properties (Denry and Kelly, 2008). However, ZTA has a large number of pores, between 8% and 11% (Guazzato et al., 2004b). ZTA is obtained by adding alumina up to 20% wt into a zirconia matrix. Alumina matrix exerts a constraint on the metastable tetragonal zirconia particles maintaining them in the tetragonal state. This allows obtaining a category of ceramic materials with improved toughness and strength. These materials which were developed in the second half of the seventies are characterized by bending strength up to 700 MPa and toughness (KIC) up to 12 MPa (Table 2.4) (Guazzato et al., 2004a).

According to Chevalier and Gremillard (2009), two approaches are now explored: (1) zirconia rich nano-composites in which both phases are below 500 nm (mentioned to as 'nano-nano-composites'), and (2) alumina rich nano-composites in which zirconia nanoparticles are equally dispersed in micron alumina grains (mentioned to as 'micro-nano-composites'). The purpose of both approaches purpose is to increase tensile strength, materials stability and crack propagation threshold as compared to the micro-scale ceramics and composites:

Micro-nano-alumina–zirconia composites increase the crack propagation threshold of alumina. In micron size alumina–zirconia composites, the increase in crack resistance is mostly due to phase transformation toughening and to a lower extent to crack bridging. Therefore, the major challenge lies in the difficulty confining zirconia nano-particles

inside alumina grains. This may be achieved by modified colloidal ways (Schehl et al., 2002; Chevalier and Gremillard, 2009).

Nano-nano-ceria doped zirconia–alumina composites increase the strength of Ce-TZP. In this regard, the standard Ce-TZP shows the largest crack resistance of ceramic oxides but moderate hardness and strength compared to Y-TZP. This is mostly a result of larger grain coarsening during sintering. The mobility of grain boundaries is actually much lower in Y-TZP than in Ce-TZP. It is, therefore, hard to attain a fully dense, fine-grained Ce-TZP. With the aim of developing ultrafine Ce-TZP based ceramics, Nawa (2005) developed a 10 mol% Ce-TZP–alumina nano-composite. In this composite, the Ce-TZP is additionally doped with a small amount of yttria. The sintered material shows a grain size around 250 nm for both phases. Table 2.3 summarizes the mechanical properties existing for the two nano-composites, as compared to Y-TZP and alumina (Chevalier and Gremillard, 2009; Thompson et al., 2011).

2.1.2 Alumina (aluminum oxide) (Al_2O_3)

The most common source of high purity alumina is the native corundum and bauxite. The usually existing alumina (alpha, α) can be made by calcining alumina trihydrate. The density and chemical composition of commercially existing “pure” calcined alumina is specified in Table 2.1. The American Society for Testing and Materials (ASTM) specifies that alumina for implant utilize should contain 99.5% pure alumina and less than 0.1% combined alkali oxides (mostly Na_2O) and SiO_2 (Park and Bronzino, 2003).

Alpha alumina has a rhombohedral crystal phase ($a= 4.758 \text{ \AA}$ and $c= 12.991 \text{ \AA}$). Natural alumina is recognized as ruby or sapphire, reliant on the kinds of impurities which give rise to its colour. The single crystal phase of alumina has been utilized successfully to make implants. The strength of alumina polycrystalline depends on its porosity and

grain size. Commonly, the smaller the grains, the higher the strength and the lower the porosity. The ASTM standard (F603-78) needs an elastic modulus of 380 GPa and a flexural strength greater than 400 MPa (Table 2.1. and Table 2.2) (Hench, 1998; Park and Bronzino, 2003).

Table 2.3: Forms of transformation-toughened zirconia.

1	Tetragonal zirconia polycrystals (TZP; e.g. Y-TZP, Ce-TZP) Nominally 98% tetragonal, fine grain size. Dental examples: DC Zirkon (DCS Precident, Schreuder & Co) Cercon (Dentsply Prosthetics) Lava (3M ESPE) In-Ceram YZ (Vita Zahnfabrik)
2	Partially stabilized zirconia (PSZ; e.g. Ca-PSZ, Mg-PSZ, Y-PSZ) Lenticular (lens shaped) tetragonal precipitates in a cubic matrix Dental example: Denzir-M (Dentronic AB)
3	Zirconia (dispersed phase) toughened ceramics; e.g., ZTA (alumina), ZTM (mullite) Dental example: In-Ceram zirconia (Vita Zahnfabrik)

Table 2.4: Mechanical properties of different ceramics (Chevalier and Gremillard, 2009).

Material	Toughness (K_{IC} , MPa m ^{1/2})	Strength (MPa)	Vickers hardness
Alumina	4.2	400-600	1800-2000
Zirconia	5.4	1000	1200-1300
A10Z0Y	5.8	700-900	1800
Mg-PSZ	8	600	1000
12Ce-TZP	7.8	700	1000-1100
Micro-nano-alumina-zirconia	6	600	1800
Nano-nano-Ce-TZP-alumina	8.4	900	1300
Hydroxyapatite	0.9	50-60	500
Silicon nitride	10	1000	2500

High-density, high-purity (>99.5%) Al₂O₃ (α -alumina) was the first bioceramic widely utilized clinically. It is utilized in dental implants and total hip prostheses because of its combination of good biocompatibility, excellent corrosion resistance, high wear

resistance, high strength, and low friction. A very small amount of MgO (<0.5%) is utilized as a sintering assistance and to limit grain growth during sintering. Fracture toughness, fatigue resistance, and strength of α -Al₂O₃ polycrystalline are a function of grain size and concentration of sintering assistance, i.e., purity. Al₂O₃ (>99.7%) with an average grain size of < 4 μ m exhibits excellent compressive strength and good flexural strength (Hench, 1998).

In-Ceram Alumina (VITA Zahnfabrik), introduced in 1989, was the first all-ceramic framework existing for single-unit restorations and 3-unit anterior FPDs. It has a high strength ceramic core made originally through the slip-casting method. A slurry of densely packed (70-80 wt%) Al₂O₃ is applied and sintered to a refractory die at 1120 °C for 10 h (Chai et al., 2000). This produces a porous skeleton of alumina particles which is infiltrated with lanthanum glass in a second firing at 1100 °C for 4 h to increase strength, remove porosity, and limit potential sites for crack propagation (Xiao-ping et al., 2002). Compressive stresses which additionally improve the strength are introduced, due to the differences in the CTE of the glass and alumina (Chai et al., 2000; Bindl and Mormann, 2002; Conrad et al., 2007). Alumina-based core ceramics consisting of a partially sintered porous alumina structure infiltrated by the molten glass are making in two methods:

- 1- As a slip powder, dispersed in water to construct FPD cores and crown copings.
- 2- As a dry pressed material processed for milling crown copings and FPD frameworks. This form can be utilized with many milling techniques Valandro et al., 2005). Another all-ceramic system based on alumina employs a method where high purity alumina FPD cores or crown copings are made-up using CAD/CAM technique. Subsequent to CAM, the alumina frameworks are densely sintered and veneered with porcelain (Miyazaki et al., 2013).

2.1.3 Glass Ceramics

Glass-ceramics are micro- or nano-polycrystalline materials made by the controlled crystallization and nucleation of a glass precursor. The dental glass-ceramic materials could be categorized as follows: the leucite-based glass-ceramics, the mica-based glass-ceramics, the fluoroapatite-based glass-ceramics, the lithia-based glass ceramics and the hydroxyapatite-based glass-ceramics (Anusavice et al., 1994). The properties of glass-ceramics rely on phase assemblage, microstructure and composition. The heat treatment and composition also define the potential phase assemblage, which in turn, governs a lot of chemical and physical characteristics such as density, thermal expansion and hardness. The microstructure that develops in the glass–ceramic is equally important, as it plays a main role in controlling the properties of glass–ceramic materials too. The temperature and time of the ceraming heat treatment regulate the number of crystals, their size and thus their growth rate (Pinckney and Beall, 2008).

The formation of the crystalline phase has two important aspects, which are crystal nucleation and crystal growth. The ceraming process consequently involves a two-step heat treatment. The first heat treatment is performed at the temperature for maximum nucleation of crystals, to maximize the number of crystals formed. After an appropriate period of time, the material temperature is increased to the higher temperature in order to facilitate crystal growth. The higher temperature is maintained until the optimum crystal size is formed. It is very important for the crystal to be numerous and uniformly distributed throughout the glassy phase to ensure a high strength for the glass ceramic. The crystalline phase will grow during ceraming, and can eventually occupy from 50% to closely 100% of the material (Pinckney and Beall, 2008).

Ceramic substrates can be coated by glasses without difficulty (Ferraris et al., 2000; Vitale Brovarone et al., 2001). However, there are some challenging issues that need to

be dealt with. For example, most of the bioactive glasses for biomedical uses, such as small bone substitution, have a CTE much higher than that of alumina. Consequently, a significant residual tensile stress is induced in the glass coating, causing the crack formation and the improper adhesion at the interface. Alumina could be coated by glasses of a lower CTE obtained through a higher content of silica. However, an increased content of silica would need a higher processing temperature that will generate reaction between the glass and the substrate. Such a reaction would in turn lead to detrimental changes in the glass composition, which would adversely affect its bioactivity. The presence of alumina in a glass even in a small amount (1.5 wt%) can noticeably affect its bioactivity resulting in a bioinert behaviour (Vitale Brovarone et al., 2001).

2.2 Modern Dental All-Ceramics

2.2.1 Classification of Modern Dental All-Ceramics Restorations

Dental all-ceramics can be classified by the processing method (machining, casting, sintering, pressure-moulding), by utilizing (crowns, bridges, inlays, onlays, veneers, denture teeth), by type (leucite-reinforced porcelain, feldspathic porcelain, aluminous porcelain, zirconia, alumina, glass-ceramic, glass-infiltrated alumina, glass-infiltrated-zirconia, glass-infiltrated spinel, and all-ceramic), by substructure material (cast glass-ceramic, cast metal, ceramic core, CAD-CAM porcelain). Dental porcelains may be classified on the basis of their firing temperatures (low fusing, medium fusing, high fusing, and ultra-low fusing) (Anusavice, 2003; Thompson et al., 2007; Miyazaki et al., 2013; Babu et al., 2015). Dental all-ceramics can be classified according to the following:

2.2.1.1 Fusion Temperature

- High-fusing (1315°C-1370°C).
- Medium-fusing (1090°C-1290°C).
- Low-fusing (870°C-1065°C).
- Ultra-low-fusing (<870°C).

2.2.1.2 Applications

- Ceramics for PFM restorations.
- Ceramics for all-ceramic restorations.
- Ceramics for denture teeth.

2.2.1.3 Fabrication Techniques

- Sintered. (e.g., Vitadur Alpha).
- Slip-Cast. (e.g., In-Ceram).
- Heat-Pressed. (e.g., IPS Empress and IPS Empress 2).
- Machined. (e.g., Vita Mark II and ProCad).

2.2.1.4 Crystalline Phases

Ceramic can be classified by the amount and nature of the crystalline form. Different crystalline phases had been used in previous studies for the fabrication of ceramics. These, include, for example:

- Feldspar (KAlSi_3O_8) (e.g., Vita Mark II).

- Leucite (KAlSi_2O_6) (e.g., IPS Empress).
- Mica ($\text{KMg}_{2.8}\text{Si}_4\text{O}_{10}\text{F}_2$) (e.g., Dicor).
- Alumina (Al_2O_3) (e.g., In-Ceram Alumina).
- Spinel (MgAl_2O_4) (e.g., In-Ceram Spinell).
- Lithium disilicate ($\text{Li}_2\text{Si}_2\text{O}_5$) (e.g., IPS Empress 2).
- Yttrium stabilized zirconium oxide (ZrO_2) (e.g., YZ Cubes).

2.2.2 Indication of All-Ceramic Restorations

All-ceramic dental restorations are indicated in areas where maximum aesthetics is required and the occlusal forces are favorably distributed (Kelly, 2004; Babu et al., 2015). They are also indicated in individuals with allergy to dental metal alloys.

2.2.2.1 Advantages of All-Ceramics over Metal Ceramic Crown Systems

The request for metal-free restorations has increased because of two factors; (1) metallic hypersensitivity and, (2) aesthetic request from patients. There are many advantages (Anusavice, 2003; Pilathadka et al., 2007; Babu et al., 2015):

1. Colour, finish line should be at gingival margin or 0.5 mm subgingival without compromising aesthetics.
2. Minimum accumulation of bacteria on the surfaces of ceramic, it can be utilized over implants in the subgingival region.
3. Aesthetic advantages of all-ceramic frameworks are demonstrated by substituting the light blocking metal substructure by extra opaque high strength ceramic.
4. All-ceramic frameworks have decreased thermal conductivity, resulting in less pulpal irritation and thermal sensitivity.

5. It is also excellent biocompatibility.

2.2.2.2 Disadvantages of All-Ceramics over Metal Ceramic Crown Systems

1. Tendency to fracture: The capability of the all-ceramic materials to support the applied loads is compromised by the presence of defects and flaws (Drummond, 2003). Two types of defects can be found in ceramics: fabrication defects (that arise during processing or as microstructural features) and surface cracks (due to machining and grinding processes) (Rosenstiel et al., 2001). Failure begins with microscopic damage that results from the interaction of preexisting flaws with subjected load (Drummond, 2003). Failure can happen due to subcritical crack growth or affect loads (Evans, 1974), which is increased in the aqueous conditions (Wiederho, 1968). Water is available for the external surface of the restoration from the saliva while both saliva and dentinal fluid can reach the internal surface of the restoration through the cement (Kelly, 2004).
2. Inadequate marginal fit and microleakage: However, development in ceramic formulation and fabrication techniques combined with improvement in bonding systems and the utilizing of computer technology have introduced new all-ceramic systems with improved marginal adaptation. The use of resin cement has improved the marginal integrity and reduced the microleakage of all-ceramic restorations (Rosentritt et al., 2004).
3. Excessive wear of the opposing teeth: Wear has been observed in the natural dentition opposing ceramic restorations (Rosenstiel et al., 2001). This observation has received considerable attention in the literature. However, many of these studies appear contradictory and there is no universal agreement in relation to the interpretation of laboratory wear tests and their clinical significance (Kelly et al., 1995). The clinical aspect (preparation, impression and cementation as well as the

laboratory part) for making all-ceramic restorations needs special attention (Blatz et al., 2003).

4. All-ceramic biomaterials are similar the appearance of natural teeth; however, the following two obstacles limit the utilize of all-ceramics in the construction of dental prostheses:

- Brittleness that results into a lack of mechanical reliability;
- Time required and greater attempt for procedures in comparison with dental composites and metal alloys (Griggs, 2007).

2.2.3 Mechanical Properties of Dental All-Ceramics

Despite the improvements in the biomaterials and widespread employment, all-ceramic prostheses are not permanently achieved as desired or predicted. Even though new all-ceramic materials have shown a considerable increase in mechanical properties, dental all-ceramic restorations fail at a rate of roughly 3% each year (Kelly, 2004) with highest fracture rates on bridges and posterior crowns where stresses are greatest. The mechanical properties are confirmed to be effected by: (1) volume fraction of the crystalline form; (2) particle size of the crystalline form; (3) differences in elastic moduli; (4) interfacial bond strength between phases; and (5) differences in thermal expansion. Because of the mechanical behavior of ceramics, different methods have been proposed for the strengthening of these materials, including the application of different surface treatments and techniques (Kelly, 2004).

Tinschert et al., (2000) showed that the mean value significantly underestimates the strength of specimens associated with the lower failure load range, which has the greatest risk of failure. In contrast to the mean value, the Weibull modulus compensates for this

lower range of values whose asymmetry is typical for all-ceramic materials. Most dental ceramic show Weibull values in the range of 5-15.

All-ceramics with high crystalline content (zirconium and/or aluminum oxides) have demonstrated preferable clinical outcomes than leucite-, lithium disilicate-, and feldspar-based ceramics (Scott, 1975; Tinschert et al., 2000; Valandro et al., 2005). In fact, increasing the mechanical strength, by decreasing the glass content and increasing the crystalline content, results in an acid-resistant ceramic whereby any kind of acid treatment generates inadequate surface changes for sufficient bonding to resin (Derand and Derand, 2000; Della Bona et al., 2002; Valandro et al., 2005; Miyazaki et al., 2013).

2.3 Bonding Veneering Ceramic to Zirconia- and Alumina-Based Dental Ceramics

In recent years, the bonding to ZrO_2 and Al_2O_3 has become increasingly significant for dental studies. It had been stated that the conventional adhesive bonding chemistry is useless on ZrO_2 surfaces, since they are basically inert and non-polar. In addition, acid etchants such as hydrofluoric acid (HF) is unable to roughen the surface for easy micromechanical retention. Using a tribochemical silica coating and surface abrasion with Al_2O_3 particles permits for chemical bonding to a resin cement and to a silane coupling agent. This procedure fails to create bond strengths as high as those reported for silane bonded veneer ceramic. Using phosphate-modified resin cements or phosphoric acid primers has been observed to create silane-like adhesion, through an equivalent kind of hydroxylation-driven chemistry. Nevertheless, the literature shows that, in general, lower values of bond strength have been reported through the use of these agents than those reported for tribochemical silica coating, coupled with resin cement and silane. It is also imperative to note that the existing methods for adhesive bonding of ZrO_2 bio-

ceramics are inadequate for all clinical applications. In addition, long-term durability is still unidentified (Blatz et al., 2004). However, other hydroxylation methods are under development, but they would often use profoundly strong basic or acidic chemistries, and their practicality for biomedical application in particular has also not been thoroughly investigated (Uchida et al., 2002; Galoppini, 2004; Fischer et al., 2005; Touzi et al., 2006; Xie et al., 2016).

Furthermore, as a result of the lack of silica in ZrO_2 , several techniques for silica-coating have been explored to exploit the chemical bonding supplied by silanization. The application of a tribochemical silica coating for metal alloys and zirconia- and alumina-based dental all-ceramics with silica is a common practice (Kern and Thompson, 1998; Sun et al., 2000; Bottino et al., 2005; Piwowarczyk et al., 2005; Ernst et al., 2005; Atsu et al., 2006; Akgungor et al., 2008). The outcome here is not only the preparation of a surface for silanization, but also the production of micromechanical attachment. It has been shown through considerable research that the application of a tribochemical coating, prior to silanization, improves bond strength among a resin cement and treated substrate significantly (Fischer et al., 2005; Touzi et al., 2006). However, extensive loss in bond strength over the long-term could occur in case of conventional resin cements utilized for silica-based ceramics. This could be a consequence of a low silica concentration on the surface, which is related to the difficulty in particle abrasion due to the high hardness of ZrO_2 (Xie et al., 2016).

Moreover, silicoating is another alternative technique that has been utilized to apply a silica layer to ZrO_2 -based ceramics (Musil and Tiller, 1984). The process of silicoating, which includes the application of a silica coating pyrolytically on a substrate surface that is followed by silane application prior to bonding by utilizing a resin cement (Mazurat and Pesun, 1998). However, the practice turned out to be highly costly and complicated, and thus

commercially unfeasible for typical dental uses (Thompson et al., 2011; Luthra and Kaur, 2016; Tzanakakis et al., 2016).

The plasma spray method is another procedure for silicoating where a siloxane coating is deposited on ZrO_2 (Derand et al., 2005). A high-frequency generator was used by Derand et al., (2005) to deposit hexamethyldisiloxane (HMDS) on the surface of ZrO_2 . When polymerized, HMDS acts like a silane, resulting in a siloxane bond among resin cement and ZrO_2 . A bond strength is significantly greater than silanized or untreated ZrO_2 , but still significantly less than ZrO_2 coated with a film of veneer micropearls. The bond strength of plasma coated ZrO_2 could be increased by enhancing the mechanical retention through the application of surface grinding or air-abrasion (Thompson et al., 2011; Tzanakakis et al., 2016).

Lately, another technique has been suggested to apply a silica layer to the ZrO_2 ceramic surface. Piascik et al., (2009), have studied the use of a unique vapor-phase deposition method. This involved combining water vapor with a chloro-silane gas ($SiCl_4$) to compose a Si_xO_y -functionalized surface on a ZrO_2 substrate. Molecular vapor deposition (MVD), an enhancement on traditional vapor deposition, is used in this process to deposit ultra-thin uniform coatings on substrates utilizing an in-situ surface plasma treatment (Thompson et al., 2011; Luthra and Kaur, 2016).

The bond strength of veneer ceramics to all-ceramic cores has been tested utilizing microtensile and shear bond strength tests (Al-Dohan et al., 2004; Comlekoglu et al., 2008; Aboushelib et al., 2008b; Chaiyabutr et al., 2008). It has been determined that the bond strength of ceramic veneer to ZrO_2 is comparable to that of veneer to metal (Al-Dohan et al., 2004). Variances in testing condition and materials could cause to variances in the bond strengths of the veneer when comparing ZrO_2 to metal (Ashkanani et al.,

2008), however, bond strength of ZrO₂ to veneers is believed to be adequate for dental uses.

2.4 Biocompatibility of Dental All-Ceramic

Biocompatibility has been defined as “the ability of a material to perform with an appropriate host response in a specific application” (Williams, 1990; Gatti and Knowles, 2002).

The biocompatibility of dental all-ceramics has been broadly assessed on the basis of research of the low rate of corrosion of traditional feldspathic porcelains and feldspathic materials (Cobb et al., 1988; Li et al., 1993; Messer et al., 2003). Most modern all-ceramic biomaterials have not been examined for biologic reaction with the similar inspection as has been applied to dental casting alloys (Messer et al., 2003). Recent *in vitro* tests with aging techniques have been utilized to calculate long-term biologic responses to ceramics (Kilic et al., 2013).

Many *in vitro* and *in vivo* cytotoxicity studies were performed in order to demonstrate that zirconia, alumina, and more recently zirconia toughened alumina are suitable for dental applications (Hanks et al., 1996). The *in vitro* test utilizing cell cultures were carried out on all-ceramic biomaterials in various physical phases (dense and powders ceramics) (Li et al., 1993). Most of the published papers on zirconia and/or alumina have reported the lack of acute toxic influences in form powders and discs on the various cell lines utilized in test, e.g. lymphocytes, macrophages, osteoblast, and fibroblast (Dion et al., 1994; Torricelli et al., 2001; Kokoti et al., 2001; Manicone et al., 2007; Brackett et al., 2008; Santos et al., 2009b). However, the effect of the physical phase of the ceramic biomaterials on the *in vitro* biocompatibility was analyzed by Li et al., (1993) who

confirmed that the dense were lower toxic than the powders ceramic, using MTT test and direct contact test with human gingival fibroblasts (HGF).

Catelas et al., (1999) observed that the ceramic powder induced apoptosis in macrophages based on the concentration of materials. Nkamgueu et al., (2000) stated that for the first time a various toxicity influence among zirconia and alumina; especially, a lower cytotoxicity of the zirconia particles in comparison to the of alumina particles was estimated as human monocytes differentiation. Also, Lohmann et al., (2002) observed a higher reduction in osteoblasts proliferation in the presence of alumina particles than in the presence of zirconia. They found that the influence occurred because of the higher reactive surface of the alumina particles, that were significantly smaller than the zirconia particles. Further, it was proven through *in vitro* investigation of the carcinogenic and mutagenic ability of the high purity zirconia ceramic that it did not induce such influences on the cells (Covacci et al., 1999).

Messer et al., (2003) evaluated the toxicity of two lithium disilicate all-ceramics (Stylepress and IPS Empress 2), two feldspathic ceramics (Vita Omega and Duceragold), and one leucite all-ceramic (IPS Empress 1) in a cell culture generated using the mouse fibroblast Balb/c 3T3 via the MTT method. In this study, they reported that IPS Empress 1, Stylepress, and IPS Empress 2 groups inhibited cell proliferation significantly, and that lithium disilicate-based ceramic was the most toxic ceramic material.

Carinci (2004) studied gene expression induced by zirconia oxide on osteoblast-like cells. He reported that affinity of zirconia for bone tissue without influences on DNA proliferation or synthesis. ZrO_2 appear to down or up-regulate expression of some genes: it influences inflammatory response resulting as a “self” material; moreover, bone growth is modified because turnover of the extracellular matrix is improved.

Brackett et al., (2008) investigated the influence of aging on cytotoxic properties of all-ceramics, including five different lithium disilicates. Three lithium silicates were produced by pressing while the others were produced with the CAD/CAM system, using MTT analysis *in vitro*. According to their results, 50-70% of cellular mitochondrial activity was suppressed at the first stage by all lithium silicate materials. Researchers preserved the samples in sterile artificial saliva to allow the release of components from the materials and to imitate clinical practice conditions. This aging process decreased the cytotoxicity of the lithium silicate. These materials suppressed mitochondrial activity, but nonetheless, after a few weeks of the aging process, the initial cytotoxicity of these materials decreased, showing that they were clinically suitable over the long-term.

Raffaelli et al., (2008) showed that the zirconia oxide showed less cytotoxicity and less ability to induce apoptosis. Cell adhesion on zirconia was higher than on felspathic ceramic; this was confirmed both by SEM observation and by fibronectin immunocytochemistry evaluation (Raffaelli et al., 2008).

2.5 Survival Rate of All-Ceramic Crowns

Dental crown restorations are utilized to restore the damaged tooth structures. However, the failure rate of ceramic restorations is still high, with 20% of these restorations have been reported to fail within the first 5 years of function in the oral cavity (Rekow and Thompson, 2007; Huang et al., 2007a; Conrad et al., 2007). The main clinical failure mode is the subsurface radial crack in the ceramic, at the interface among the cement and dental ceramic crown (Kelly, 1997; Thompson et al., 2011). This failure is caused largely by the tensile stress concentration in the dental ceramic at that interface (Lawn et al., 2002a; Huang et al., 2007b; Miyazaki et al., 2013). It is, therefore, advantageous to find out efficient techniques for the stress reduction at this interface.

Twenty-two clinical studies were included in a systematic review of clinical complications in fixed prosthodontics (Goodacre et al., 2003). All-ceramic dental crowns observed the lowest incidence of complication (8%). However, most of these studied were of short-term duration. In 18 of them, the study duration ranged between 1-4 years while four were for more than 5 years. The most popular complications encountered were loss of retention (2%), crown fracture (7%), and the requirement for endodontic treatment (1%). The incidence of crown fracture increased with the length of the study. The relationship between the fracture incidence and location in the arch was discussed in ten articles (Thompson et al., 2011; Luthra and Kaur, 2016). The molars showed higher fracture rate (21%) compared to premolar (7%) and anterior teeth (3%) (Goodacre et al., 2003).

According to Conrad et al., (2007), they reported that the survival rates for all-ceramic dental crown restorations after 2–5 years in function ranged from 88% to 100% and after 5–14 years ranged from 84% to 97%. When categorizing complications, they found that fractures of the all-ceramic material were the main frequently reported complications resulting in such failure (Anusavice, 2012; Miyazaki et al., 2013).

Al-Amleh et al., (2014), reported that the chipping of the veneering ceramic in zirconia-based crown restorations to be higher than that for metal-ceramics and all-ceramic crown restorations (Al-Amleh et al., 2010, 2014). Molin and Karlsson (2008) found that the incidence of the chipping fractures to be 35% in zirconia-based FPDs over 5 years, while Larsson et al., (2006) reported that an incidence of 54% in 1 year. Previous study by Reuter and Brose (1984) reported a chipping rate of 2.5% for metal-ceramic FPDs after 5 years, whereas the chipping of the veneering porcelain was not observed for glass infiltrated ceramic-based frameworks after 5 years in the previous studies by Olsson et al., (2003) and Vult von Steyern et al., (2001). The veneering porcelain chipping has

been identified as a major failure for zirconia-based restorations, instigating an increase of studies investigating the causes and its prevention (Al-Amleh et al., 2014).

2.6 Several Factors Affecting the Fracture Strength of All-Ceramic Crowns *in vivo*:

2.6.1.1 Factors Related to the Restoration

- 1- The composition of ceramic materials: The mechanical properties of the material are affected by the nature, distribution, size and amount of the crystalline phase as well as the mechanical properties of the glassy matrix (Guess et al., 2008; Daou, 2014).
- 2- Processing: Microstructural flaws and defects (e.g. porosity, microcracks and impurities) can develop in the ceramics restorations as a result of inaccurate or suboptimal processing (Della Bona et al., 2007, 2008; Denry, 2013).
- 3- Finishing and glazing effect in the ceramic texture and roughness (Albakry et al., 2004; Guazzato et al., 2004c).
- 4- Crown dimensions and geometry: The fracture resistance of an all-ceramic crown will increase if the crown thickness is increased (Hojjatie and Anusavice, 1990).
- 5- Core/veneer thickness ratio (in multilayer restoration): Increasing the thickness ratio of core/veneer increases the flexural strength and shifts the crack starting site from veneer to the core (Wakabayashi and Anusavice, 2000; Dunder et al., 2007; Al-Amleh et al., 2014). White et al., (2005) reported that increasing the thickness ratio of veneer/core increases the modulus of rupture of beams that were composed of zirconia core and matchable veneering porcelain materials.
- 6- Differences in ceramic mechanical and physical properties (modulus of elasticity and thermal contraction coefficients) in multilayer restorations (Kelly, 2004).

- Differences in the CTE among the materials: Mismatch in the CTE can induce residual stresses that can cause immediate or delayed failure. The veneering porcelain should always be under slight compression. This can be slightly higher than that of the veneering ceramic (Mackert et al., 1986; Aboushelib et al., 2005; De Kler et al., 2007; Al-Amleh et al., 2014; Daou, 2014).
 - Differences in modulus of elasticity of the different layers: Increasing the modulus of elasticity ratio ($E_{\text{veneer}} / E_{\text{core}}$) will increase the critical load needed to cause radial cracks on the core. This will be beneficial up to a certain limit after which using a too stiff veneering material will increase the susceptibility of radial cracking of the veneering layer (Daou, 2014).
- 7- The internal fit of the restoration: To prevent crown fracture, the crown must be fabricated with the best possible fit (Thompson et al., 2011; Daou, 2014).

2.6.1.2 Factors Related to the Supporting Structure (Natural Teeth or Core Materials) of the Restoration

1. Modulus of elasticity: The fracture strength of all-ceramic crowns will increase if the elastic modulus of the supporting structures is increased (Scherrer and de Rijk, 1993; Al-Amleh et al., 2014).
2. Preparation characteristics (preparation shape, dimension, and geometry):
 - Increasing the preparation size will increase the fracture strength of the crowns. This influence is obvious in comparing the fracture strength of molars with premolars and anterior crowns (Thompson et al., 2007; 2011; Al-Amleh et al., 2014).
 - Increasing the occlusal thickness of the crown as decreasing the preparation height will increase the fracture strength of the crown. On the

other hand, this approach is not conservative and tends to affect the retention form of the preparation (Rekow and Thompson, 2007).

- A total occlusal convergence of 10° provides the best combination of fracture strength and conservation of tooth structure. A convergence angle of five degrees is associated with the lowest fracture strength, and a 15° or 20° convergence angle require greater tooth reduction (Doyle et al., 1990).
- Doyle et al., (1990) found that an increase in the fracture strength of crowns prepared with a sharp axiokingival line angle and shoulder finish line compared to a shoulder with round axiokingival line angle and a chamfer (Doyle et al., 1990). In contrast, Burke et al., (1996) reported that preparing a 1 mm shoulder line rather than a knife edged margin did not have a significant influence on the strength of all-ceramic crowns.

2.6.1.3 Factors Related to the Oral Environment Surrounding the Restoration

1. Oral fluid: An aqueous medium will enhance crack growth and decrease ceramic restoration strength in a phenomenon called “static fatigue” (Wiederho, 1968). Oral fluids are recognised to assist stress corrosion of all-ceramic materials, resulting in slow crack growth and lastly leading to failure of all-ceramic restorations in the complex condition of the oral cavity (Peterson et al., 1998; Zhang et al., 2005; Deville et al., 2006; Guess et al., 2008; Daou, 2014).
2. Changes in temperature: Restorations in the oral cavity are subjected to thermal changes which may cause stress concentration at the restoration cement interface due to a mismatch in the CTE of the cement, ceramic and supporting structure (Al-Amleh et al., 2014; Daou, 2014).
3. Occlusal force: Clinically, dental restorations are subjected to cyclic loads. These cyclic forces have both vertical and lateral components (Julien et al., 1996), range

between 60 and 250 N during function and could reach 500 to 800 N for short periods of time (Drummond, 2003). The range of forces in maximum biting is 222-445 N in the premolar area, 400-890 N in the molar region, 133-334 N on the canines and 89-111 on incisors (Anusavice, 2003). In the posterior teeth, these forces are distributed on an average contact area of 52 and 64 mm² for females and males, respectively (Julien et al., 1996). In an average individual, the number of cycles of mastication per day ranges between 800-1400 cycles (Drummond, 2003) and can reach up to 2700 cycles/day (Wiskott et al., 1995). This number should be decreased by a factor ranging from 5 to 20 because not all the chewing cycles are active (i.e. representing maximum load in the chewing cycle) (Wiskott et al., 1995).

2.6.1.4 Factors Related to the Cementation of the Restorations

1. Adhesion mechanism: An increase in fracture strength has been reported with the use of adhesive cement compared with non-adhesive ones (Sobrinho et al., 1998; Thompson et al., 2011; Luthra and Kaur, 2016).
2. Cement thickness: Increasing the thickness of cement reduces the fracture strength of all-ceramic crowns (Proos et al., 2003; Thompson et al., 2011).
3. Mechanical properties of the cement (mainly modulus of elasticity): As increases the elastic modulus of the cement, the crown-cement-supporting structure framework becomes rigid. This decreases stresses in the crown (Rekow et al., 2006). An exception to this, however, occurs when resin cement (low modulus) are compared to zinc phosphate cement (high modulus) for the cementation of all-ceramic crowns (Sobrinho et al., 1998). This conflict can be explained by the beneficial effect of the adhesive cement on the fracture strength of all-ceramic crowns.

4. Efficacy of the bond between the cement and porcelain: This is affected by the treatment of the internal surface of the crown.
5. Efficacy of the bond between the cement and supporting structure.

It has been observed that grinding of alumina can lead to greater strength decrease when the samples are examined with the tensile axis directed perpendicular to the grinding direction (Thompson, 2000). Nevertheless, the influence of grinding orientation on the flexural strength of transformation-toughened zirconia ceramics has not yet been evaluated. According to Guazzotto et al., (2004a), generally, the flexural strength of Y-TZP ceramics can be increased by wet grinding and sandblasting, while lower mean values of strength are calculated when the same steps are followed by heat treatment.

Curtis et al., (2006) concluded that the investigation modification techniques of the pre-cementation surface were recognised to modify the surface defect population and the toughening mechanism due to the phase transformation mechanism, which engendered a transformation compressive stress that opposes the externally applied, crack propagating tensile stress and an increase in the surface hardness of the sample. Additionally, the existence of moisture was not found to have a detrimental influence on the biaxial flexural strength of the Y-TZP samples. In contrast to the grinding with a fine grit diamond bur and gentler alumina abrasion systems, the application of surface grinding with a coarse bur caused a significant reduction in the reliability and biaxial flexural strength data of the Y-TZP samples. The reduction of strength and reliability was an effect brought about by the generation of a toughening mechanism, due to the phase transformation mechanism that generated a transformation compressive stress, which opposes the externally applied, crack-propagating tensile stress and the increased surface roughness as highlighted by profilometry (Curits et al., 2006; Canneto et al., 2016; Pereira et al., 2016).

2.7 Dental Multilayered Structures

The concept of a multilayered structure has been researched for years, not only in the form of bulk substrate materials, but also as complex thin film coatings. However, even though laminate structures of thin films have been researched since the 1970s, no research has centred on the use of a ductile/brittle film on the mechanical properties of a ceramic substrate, which can possibly be utilized for biomedical uses. It is supposed that the deposition of a multilayered film of this kind will improve the strength, and hopefully the fatigue resistance, of a ceramic substrate (Thompson et al., 2007).

Multilayered biomaterials, such as zirconia-alumina composites evolved by introducing fine zirconia particles in a polycrystalline alumina matrix which had wide structural employment due to their robust mechanical properties (Tomaszewski, 1999). Koehler (1970) showed that a laminate structure composed of two metal thin-layers has higher strength than the individual metals alone).

Dental multilayer is an engineering idealization of dental crowns. This method mimics the layered structure of the crown on a real tooth. It simplifies the complexity of curvatures and loading environments into flat layers applied to ordinary compressive Hertzian loading (Kelly, 1997; Lee et al., 2002; Shrotriya et al., 2003; Rekow and Thompson, 2007). To comprehend the essential mechanics of failure in dental all-ceramics on soft dentine-like underlayers under environments that simulate basic occlusal function, a suitable basis can be laid for rational materials design of future multilayered crown frameworks (Lawn et al., 2002a, 2002b; Liu et al., 2012).

Previous studies have noted that the mechanical properties of dental all-ceramics can be enhanced by the deposition of a thin film of zirconia, gold, and aluminum utilizing a sputtering method. Flaw modification and residual stresses may be possible strengthening

mechanisms when single-layer coatings are applied. Multilayer or laminate structures can also be utilized to integrate the best forms of the ingredient layers in order to achieve a more beneficial modified material with even better mechanical properties (Ruddell et al., 2000; Thompson et al., 2007; Teixeira et al., 2008).

For the brittle layers in the multilayered thin film proposed, YSZ is still used as the material of choice, since the conditions for deposition and its effect on a single layer have been investigated previously (Hannink et al., 2000). However, one of the main disadvantage of ceramic thin films, just like for bulk ceramic materials, is their brittleness. A ductile layer is developed to overcome the brittleness of a pure film ceramic (Thompson et al., 2007).

2.7.1 Biomechanical System with Layer Structures of Teeth and Dental Crowns

Ceramics have unique biocompatibility, bioactivity/bioinertness and mechanical wear resistance, desirable attributes for a protective function. Many of these prostheses biological structures form naturally in layers, especially in teeth, to achieve combined strength, hardness and toughness that are unattainable by monolithic materials. The idea of layered or laminated structures comes from the fact that this special configuration usually can provide the joint advantages of their components or even much better performance than each of the monolithic materials (Jackson, 1988; Cuy et al., 2002).

Teeth have complex structures with hard and aesthetic inorganic enamel shielding soft and sensitive organic tissue, to achieve combined physical and biological function. The main part of the interior is a bone-like substance known as dentine. Embedded in dentine is the pulp, a filament of soft tissue containing cells and also nerves and blood vessels. Dentine and pulp are covered by a layer of enamel. Enamel has a very high mineral (97%) and low in organic (1%) content. It plays a vital role in protection and support for inner

tissue and the function of bearing biting forces. The mechanical properties of enamel are not uniform. They vary from site to site to accommodate physical biting function. The detailed mechanical properties of natural enamel have been investigated using a nanoindentation mapping method (Cuy et al., 2002), which measures the hardness and elastic modulus point by point. The average values of hardness and elastic modulus decreases from the enamel surface to the enamel-dentine junction. Elastic modulus decreases from 91.1 to 66.2 GPa and hardness decrease from 4.6 to 3.4 GPa. The variability of hardness and elastic modulus reveals a hierarchy of microstructures and graded mechanical properties. High elastic modulus and hardness at the outer surface can effectively bear the high chewing stresses. Decreased elastic modulus inside provides a cushion for impact force and distributed stresses. Such well graded mechanical properties offer natural clues for restorative dental crown design (Suresh, 2001; Cuy et al., 2002; Lawn et al., 2002a). Teeth are lost or damaged due to disease or trauma. Replacement of damaged to the structure is needed for continuing normal tooth function (Xu et al., 1998). Restorative ceramic crowns with a porcelain veneer and all-ceramic crowns exhibit excellent aesthetics from translucency that are similar to natural teeth and excellent biocompatibility due to their intrinsic inertness.

Nevertheless, their failure rates exceed the more common PFM crowns (Rekow and Thompson, 2007). Also, aesthetic ceramics are usually not strong enough to survive and high-strength ceramics usually lack aesthetics. There are no single materials that are both aesthetic and sufficiently strong, to be compatible with natural enamel. It is even more difficult to fabricate graded materials to mimic enamels, even though some researchers have shown that mechanical response for spatial gradients in the composition is more-damage-resistant than their homogenous counterparts (Suresh, 2001). The challenges to improving the all-ceramic crown design, including performance and fabrication techniques are the core subjects around dental restoration study (Lawn et al., 2002b).

2.7.2 Influence of Crown Design Parameter on Dental All-Ceramic Crowns

The basic geometry of dental crowns is restricted by the requirement to fit into the physical space dictated by a patient's tooth. It is mostly believed that dental crowns must have a 1.5 mm minimum thickness in total, with veneers taking up 1 mm and the stronger core 0.5 mm with inconstant cement thickness of 20 – 200 μm (Thompson et al., 2011), as seen in Figure 2.1 and Figure 2.2. The crown is then cemented onto a prepared tooth surface done by the clinician with a dental adhesive that has a relatively low elastic modulus (Rekow and Thompson, 2007). Dental crowns utilized in posterior locations occasionally have smaller thicknesses than the 1.5 mm minimum prescribed by most clinicians due to complexity of geometries. In fact, this can be problematic because of the higher forces shown in posterior locations during chewing and other physiologic environments. All-ceramic dental crown fails at a rate up to 3% (Burke et al., 2002; Rekow and Thompson, 2007). It has been stated that so-called bottom surface radial cracks are present in tests done by pressing rigid spheres into curved laminates (Qasim et al., 2007). Such failures are shown in clinically failed all-ceramic dental crowns as seen in Figure 2.3 (Rekow and Thompson, 2007).

The strong interest in improving the performance of posterior all-ceramic crowns has stimulated considerable research on the contact damage of dental multilayered ceramics (Huang et al., 2003, 2007b; Kelly, 1997; Lawn et al., 2000a; Lee et al., 2002; Zhang et al., 2004b; Rekow and Thompson, 2007; Zhou et al., 2007). Dental multilayer is a widely-recognized engineering idealization of dental crowns. It simplifies the curved complex structures of dental crowns into flat multilayered structures with circular cross sections and similar sizes to real human teeth (Huang et al., 2003, 2007a, 2007b; Niu et al., 2008; Zhang et al., 2004a; Zhou et al., 2007; Thompson et al., 2011).

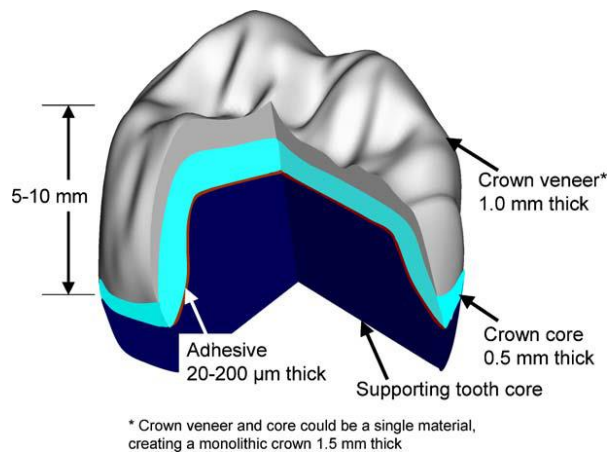


Figure 2.1: A cross section of typical layers of the dental all-ceramic crown design and components of the crown-adhesive-tooth system.

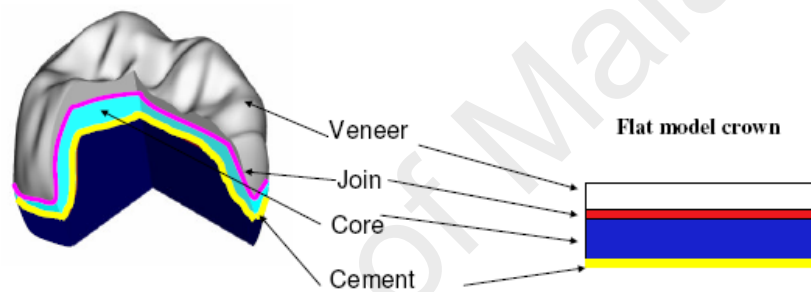


Figure 2.2: The proposed CAD/CAM dental crown design with independently fabricated veneers and cores that would have to be joined and placed in the mouth. On the right, is the relevant flat layered structure for mechanical testing. (Figure from Dr. Guangming Zhang, 2007).



Figure 2.3: Typical posterior all-ceramic dental crown fracture. A failure of an all-ceramic crown presented in a patient from Ken Malament DDS (Rekow and Thompson, 2007).

2.7.3 Thickness of the Multilayers Ceramics

Generally, a dental crown is roughly 1.5 to 2 mm thick at the top surface, 5–10 mm high and the sides become increasingly thin at the bottom surface (away from the biting surface) (Rekow and Thompson, 2007) as shown in Figure 2.1.

According to Rekow and Thomposon (2007), not much attention has been paid to the influence of surface geometry complexity on crack origination and propagation of dental all-ceramic crowns. Samples with concave, convex, and flat surfaces were subjected to a single cycle force applied with a 4-mm radius tungsten carbide sphere. The expected traditional damage happened in the flat specimens. In concave surfaces, the radial crack arms seemed to be surrounded by outer ring cracks at the top surface. In convex surfaces, radial cracks were more excessive than those in the flat specimens. Generally, to initiate radial cracks in curved surfaces, high contact loads were required, especially in concave surfaces. Consequently, strength and onset of damage is influenced by geometry. In order to identify the impacts of the complexity of real dental crowns, these should be subjected to the similar systematic investigation (Rekow and Thompson, 2007).

A ceramic crown, ideally 1.5 to 2 mm thick, can be constructed from a monolithic material or a layered ceramic structure (Rekow and Thompson, 2007). The brittle crown is held to the tooth by a layer (20–200 μm) of adhesive material with a relatively low elastic modulus. In function, the crown-cement-tooth system is subjected to cyclic loading with the magnitude of approximately 100–700 N (DeLong and Douglas, 1983; Gibbs et al., 2002; Rekow and Thompson, 2007) at the rate of about 1.5 Hz in a wet condition (Rekow and Thompson, 2007). The damage on flat specimens is the main focus of most investigations. However, a dental crown has complex geometry. Due to the complex structure of real dental restorations, flat multilayered structures (with comparable elastic properties) are often utilized to investigate contact-induced damage in

dental multilayers (Kelly, 1997; Lawn et al., 2002a; Huang et al., 2007b). For dental crowns and posterior crowns in particular, the occlusal surface geometry is complex and must contact the opposing tooth in a prescribed method throughout the entire range of motion during chewing functions (Rekow and Thompson, 2007).

2.7.4 Dental Adhesives as an Interlayer

It has been shown through previous investigations of the critical loads for under surface radial crack formation of brittle laminates that there is an adhesive thickness and modulus dependency (Kim et al., 2003). Kim and colleagues examined nine various luting and adhesives agents frequently utilized in restorative dentistry (Kim et al., 2003). The purpose for the application of various materials is to bond a flat brittle veneer layer to a supportive core, mimicking the framework of a dental crown. Hertzian contact tests are utilized to load the top surface of the veneer, thereby subjecting the bottom surface to tension and leaving it susceptible to radial crack initiation (Kim et al., 2003). The biaxial flexure of the veneer under point loading is caused by the elastic mismatch among the top stiff layer and the interlayer. In their investigations, 1 mm thick mono-crystalline silicon plates, utilized as the veneer layer, are bonded to a soda lime substrate, acting as a support core, with the various dental adhesives.

To control its strength, the bottom surface of the silicon veneer is abraded with 600 grit SiC silicon carbide. This multilayered structures has the top surface veneer layer subjected to Hertzian contact loading and simultaneously monitored for the onset of radial cracks (Chai et al., 1999; Jung et al., 1999; Chai and Lawn, 2002; Deng et al., 2002a, 2002b; Lawn et al., 2002a, 2002b). The thicknesses of the assorted interlayers are varied to characterize the effect of critical forces for radial crack initiation (Kim et al., 2003; Rekow and Thompson, 2007). Thus, there is an apparent necessity to develop a high

elastic modulus resin based adhesive that provides chemical bonding and helps in preventing radial fracture in the veneer (Zhang et al., 2009; Al-Amleh et al., 2014).

More, the use of composite interlayers to adhere veneers to cores may have advantages over current dental crown production methods. Connecting independently fabricated brittle ceramic layers with an adhesive allows for the separate processing of layers and can overcome the requirement of matching CTE of core and veneer materials (Wang et al., 2007). However, new failure modes could be introduced due to the elastic mismatch between the adhesive and veneer such as the bottom surface radial cracking of the veneer. The lack of substrate support found in current dental adhesives could be mitigated through the promising recent development of high elastic modulus composites (Wang et al., 2007; Al-Amleh et al., 2014).

Contemporary adhesive cements utilized in dentistry are insufficient to join independently freeform made-up layers (Chai and Lawn, 2002; Kim et al., 2003; Kim et al., 2007b). There is a requirement to construct a joining adhesive with good bonding and high elastic modulus that can join brittle laminates without decreasing the overall framework integrity of the dental all-ceramic crown. Any newly made-up join must be examined for achievement in order to affirm the fundamental rules for crown design (Thompson et al., 2011; Luthra and Kaur, 2016; Özcan and Bernasconi, 2016).

2.8 CAD/CAM Technology in Restorative Dentistry

Computer-assisted design and Computer-assisted manufacturing (CAD/CAM) technology was introduced in Europe in the 1980s for chaiside production of the prostheses made of machinable ceramics. With the CAD/CAM techniques, restorations can be fabricated much more efficiently and quickly, which assists in removing the requirement for temporary restorations. Furthermore, with the computer controlled design

and manufacturing, making prostheses with consistent quality become conceivable (Rekow et al., 1991; Yin et al., 2006). Dental CAD/CAM technology consists of data acquisition and digital image generation, and tooling systems and computer-assisted milling systems (Liu, 2005; Yin et al., 2006; Li et al., 2014; Ender et al., 2016).

Now, there are two main CAD/CAM techniques, one for machinable bioceramics and the other one for the difficult to-machine materials (Yin et al., 2006; Abduo and Lyons, 2013; Abduo et al., 2014; Li et al., 2014; Duan and Griggs, 2015; Basso et al., 2015; Seker et al., 2016; Ender et al., 2016). In the first technique, the computer assisted milling process can be utilized to machine the machinable ceramics directly from their blanks. In the second technique, the milling process is firstly conducted from the presintered blanks of the difficult-to-machine ceramics, and then the sintering is followed to harden the ceramic prostheses while at the same time taking into account the compensation for shrinkage during sintering in a special high-temperature furnace (Yin et al., 2006; Abduo and Lyons, 2013; Abduo et al., 2014; Li et al., 2014; Duan and Griggs, 2015; Basso et al., 2015; Seker et al., 2016; Ender et al., 2016).

Two advantages are supplied by the availability of CAD/CAM or other machining routes to all-ceramic restorations. Firstly, these systems eliminate the processing of ceramics, and hence microstructural control, from the dental laboratory and place it within the authority of the manufacturer. Secondly, the manufacturer simply supplies a few sizes of simple blocks; complex shaping is controlled by the machining method (Yin et al., 2006). Moreover, in spite of increased machinability and optimized physical properties, most of the bioceramics for dental CAD/CAM restorations suffer from microcracking and chipping at machined edges (Kunzelmann and Hickel, 1993; Sindel et al., 1998; Yin et al., 2006; Abduo et al., 2014; Basso et al., 2015; Seker et al., 2016; Ender et al., 2016).

2.9 Functionally Graded Materials (FGM) in Dentistry

The concept of functionally graded materials (FGM) is a new approach for the improvement of dental ceramic core material performance compared to conventional homogeneous and uniform materials. This technique permits the fabrication of materials with various characteristics within the similar material at different interfaces. FGM is an innovative novel technology that has developed in terms of the processing of materials and the computational modelling (Watanabe et al., 2002). It has been found that the development of FGM for implants in dental and medical applications permits the integration of unlike materials, without severe internal stress, by combining diverse properties into a single material (Hedia and Mahmoud, 2004; Watari et al., 2004; Yanga and Xianga, 2007; Wang et al., 2007). Material gradation offers a way of preserving the high thermal resistance of an outer layer and high strength of an inner core, while removing the deleterious effects of the sharp interface.

Numerous researches have revealed that radial cracking is a main failure mode that can happen in the top ceramic layer of ceramic crowns that are utilized in dental restorations (Kelly, 1997). These cracks generate in the proximity of the dental cement, that attaches the dental restoration to the dentine/dentine-like ceramic filled polymers. These ceramic filled polymers are often used as basis layers in simplified tri-layer models (Lawn et al., 2002a). Under such situations, the radial cracks happen largely as a result of the relatively high principal stresses that are induced as a result of the elastic mismatch among the cement and the ceramic layer in flat layered frameworks (Lawn et al., 2002b).

Functionally graded interfaces offer a substitute method that can be utilized to engineer reductions in the interfacial/layer stresses (Huang et al., 2007b). Unlike the sharp transitions that give rise to high elastic mismatch stresses, graded transitions may be used

to engineer reductions in the overall stresses within the individual layers, and interfaces in dental restorations.

In the computational study by Huang et al., (2007b), they added a FGM layer with its Young's modulus varying gradually from dental cement layer to enamel-like dental ceramic layer. Finite element simulations of the structure showed that adding an FGM adhesive layer can significantly reduce the stress concentrations in the sub-surface of the top ceramic layer. This increases the resistance of the structure to radial cracking. Moreover, the assessed critical crack lengths were much greater than those assessed in both existing the natural tooth enamel-dentine complex and dental crowns (Huang et al., 2007b). This suggests the possibility of building synthetic, bio-inspired, functionally graded dental multilayers that have better durability or comparable than those of natural teeth. However, the study of Huang et al., (2007b) did not provide experimental validation of the concept.

The bio-inspired functionally graded dental multilayers was also developed and evaluated in a study by Park et al., (2008). It is also important to know that FGMs may improve the current single layer dental materials, especially dental ceramics (Park et al., 2008), characterized the hardness, elastic modulus and apparent fracture toughness as a function of distance from the dentino-enamel junction (DEJ) using indentation approaches. Their results showed that the mechanical properties increased with distance from the DEJ (Park et al., 2008). Huang et al., (2007b) also suggested that the idea of FGM requirements to be extended to 2D and 3D geometries, instead of only along the thickness direction.

FGMs represent a concept in component production. Such materials are characterized by non-linear three-dimensional properties (density, thermal conductivity, hardness, modulus of elasticity) and distribution of composition over the volume, which

distinguishes them from traditional isotropic materials (Shevchenko et al., 2003). FGMs are hetero phase materials with a high concentration of interfaces. Therefore, when they are used at high temperatures (coatings, individual components and assemblies), the characteristic problems of inter phase reaction arise, which to a large extent determine the reliability and lifetime of these materials (Shevchenko et al., 2003; Dudnik et al., 2011).

Various crystalline modification of ZrO_2 (monoclinic, tetragonal, cubic) and Al_2O_3 are used in FGM. Their high melting points, free energy of formation, chemical inertness, high mechanical and thermal properties make it possible to develop FGM for different applications (Shevchenko et al., 2003).

Three types of FGM can be conditionally distinguished: graded, layer-graded, and layer material. The FGM type depends on the level of properties which must be attained for its use. In order to solve the problem of forming microstructures which provide the required properties in such materials, various methods for the production of FGM based on ZrO_2 and Al_2O_3 have been developed: dry pressing followed by heat treatment (She et al., 1998; Haijiang, et al., 1999), diffusion welding (Takayuki and Fumihitro, 1993), chemical infiltration (Marple and Green, 1993), electrophoretic deposition (Sarkar et al., 1993), centrifugal deposition (Zhang et al., 1998), sedimentation (Haijiang et al., 1999), tape casting (Chartier and Rouxel, 1997), and slip casting (Requena et al., 1989).

It was used to obtain graded Al_2O_3 /mullite material (Marple and Green, 1993). Performs of Al_2O_3 were impregnated with a sol containing SiO_2 , dried, and heated in air to 1200 °C. After the formation of mullite, the performs were sintered at 1650 °C in air. As a result, material graded in composition and microstructure was obtained. In a study by Marple and Green, (1993) it was shown that composite ceramic materials of different compositions can be obtained by this method (Shevchenko et al., 2003; Dudnik et al., 2011).

The slip casting method for the production of layered composite ceramic materials was used for the first time in study by Requena et al., (1989). The initial material chosen was a submicron sized Al_2O_3 powder (particle size $0.5 \mu\text{m}$) and monoclinic zirconium dioxide M-ZrO_2 (particle size $0.5 \mu\text{m}$). Performs were obtained by the sequential casting of slurries; their density was 60% of theoretical. After sintering at $1625 \text{ }^\circ\text{C}$ for 2 h, the density of the specimens was 99%. Approximately 50% of the tetragonal modification of ZrO_2 was retained in these. Thanks to the use of slip casting to assemble performs, and the following sintering, it was possible to fabricate multilayered composite materials with distinct and well resolved ($\sim 1\mu\text{m}$) interfaces. The thickness of the layers was within the limits of $100 \mu\text{m}$, a clear difference in the microstructures of individual layers was noted (Requena et al., 1989). The grain size in the Al_2O_3 layer was approximately $5.54 \mu\text{m}$. In the $\text{Al}_2\text{O}_3/\text{ZrO}_2$ layer, the grain size of Al_2O_3 was $\sim 3.5 \mu\text{m}$ and of ZrO_2 less than $1 \mu\text{m}$, which agrees with the amount of retained T- ZrO_2 . It was determined that a change of layer thickness in the multilayered composite material obeys the same parabolic law as a change in thickness of specimen walls of the individual slurries. The results obtained indicated that it is possible to design multilayer composite materials with thin distinct layers of controlled thickness (Requena et al., 1989; Shevchenko et al., 2003; Dudnik et al., 2011; Katayama et al., 2011).

Materials of the composition $\text{Al}_2\text{O}_3/\text{Al}_2\text{O}_3\text{-ZrO}_2$ have been obtained by sequential slip casting, in which layers possessing high strength and ductility coexist with layers possessing high creep resistance. The chosen initial powders were Al_2O_3 (average particle size $0.5 \mu\text{m}$), M-ZrO_2 (average particle size $1 \mu\text{m}$) and T-ZrO_2 (average particle size $0.4 \mu\text{m}$). Sequential slip casting produced layered materials with two grain size scales ($3/40 \mu\text{m}$) and high strength ($\sim 600 \text{ MPa}$). These materials are promising for high-temperature applications (Shevchenko et al., 2003; Dudnik et al., 2011).

Multilayered composite materials with alternating layers of Ce-TZP and a mixture of 20 mass % Al_2O_3 + 80 mass % Ce-TZP were produced by sequential slip. The authors determined that the strengthening mechanism of this material is crack reorientation and stratification (Shevchenko et al., 2003; Dudnik et al., 2011).

One method that would permit more conservative teeth reduction, while taking advantage of the useful characteristics of available dental all-ceramic materials would be the development of a controlled process to modify existing low strength materials to produce very thin (<1 mm) all-ceramic restorations. The deposition of surface modifying thin films or coatings can possibly be utilized to achieve this. Thin film coatings and surface modification procedures are usually utilized to enhance the fracture strength or wear resistance of ceramics. Thin films deposited via sol-gel processes, chemical vapor deposition, ion beam and plasma spray or sputter deposition have been used for this purpose. Moreover, surface abrasion methods have been established as a technique to decrease the mean flaw size present on a cast, machined or fired surfaces. Furthermore, of these methods report some enhancement in fracture behaviour. However, few researches have centred exclusively on the matters surrounding restorative dentistry (Thompson et al., 2007).

There are various types of production processes for producing FGMs. FGMs can be divided into two major groups namely: bulk and thin FGM. The bulk FGMs are the volume of materials which require more labour intensive processes, while thin FGMs are a relatively thin surface coating. Thin surface coating FGMs are fabricated by self-propagating high temperature synthesis (SHS), plasma spraying and chemical or physical vapour deposition (CVD/PVD) (Ivosevic et al., 2005). Bulk FGM is produced utilizing powder metallurgy technique, solid freeform technology, and a centrifugal casting method (Mahamood et al., 2012).

Powder metallurgy (PM) method is utilized to produce FGMs (Watari et al., 2001; Mishina et al., 2008) through three main stages namely: weighing and mixing of powder according to the pre-designed spatial distribution as dictated by the functional requirement, stacking and ramming of the premixed-powders, and finally sintering. PM method gives rise to a stepwise structure. If the continuous structure is desired, then the centrifugal casting technique is applied (Kieback et al., 2003; EL-Wazery and EL-Desouky, 2015).

Die compaction of the layers' technique is an easy and well developed technique. A gradient is fabricated by the deposition of powder layers with altering compositions in the compacting die. The disadvantages of the process are very clear: discrete changes, limited thickness of individual layers (normally not less than 1 mm), limited number of layers (up to 10 in laboratory scale, but not more than two or three in potential production), limited size of the part ($<100 \text{ cm}^2$) due to the limits of compaction forces, discontinuous manufacturing with low productivity. Nonetheless, this technique permits efficient laboratory researches of functionally graded structures (Kieback et al., 2003).

Individual strengthening mechanisms have been suggested for the different methods listed above; however, no one has been able to completely differentiate the influences of flaw passivation, surface modification (Thompson et al., 2007) and the mechanical effects of the thin film. Moreover, such aesthetic matters as film colour, reflectivity and transmittance, and practical considerations such as the ability to bond to the modified surface are functions of impurity concentrations, differences in stoichiometry and surface termination (Thompson et al., 2007; EL-Wazery and EL-Desouky, 2015; Cattani-Lorente et al., 2016; Al-Harbi et al., 2016; Ender et al., 2016; Luthra and Kaur, 2016; Zhang et al., 2016b;).

2.9.1 Thin Film Technologies

Thin film technologies propose one potential solution to complications associated with the utilization of dental all-ceramic structures for restorative dental uses (Thompson et al., 2007). A better understanding of the behaviour of PSZ thin films and their manageable features could produce meaningful technology that might improve the selections offered to clinicians (Thompson et al., 2007; Teixeira et al., 2008).

Earlier researches have revealed that the application of alumina thin films may increase the fracture strength of porcelain and borosilicate glass (Hoshida et al., 1996; Ruddell et al., 2000). It was proposed that the application of YSZ thin films to all-ceramic dental restorations will enhance reliability and longevity of dental restorations (Teixeira et al., 2008). PSZ seems to have a great possibilities as an applicant material for thin film alteration of available commercial dental ceramic materials such as veneer ceramics. Zirconia exhibits high toughness and flexural strength, observing promising properties not only in its bulk form but also as sputtered, thin-film coatings (Thompson et al., 2007; Teixeira et al., 2008).

2.9.2 Nanomaterials in Dentistry

Nanomaterials can be categorized into nanoparticles and nanocrystalline materials. The former are ultrafine dispersive particles with diameters below 100 nm, while the latter refers to nanocrystalline bulk materials with grain sizes in the nanometer range (from 1 nm to 100 nm). Studies in nanomaterials is a multi-disciplinary attempt that includes interaction among scientists in the field of chemistry, physics, materials science, and mechanics, or even medicine and biology. Nanocrystalline coatings with grain sizes in

the nanometer scale can exhibit novel and improved properties, which opens up chances for new technological applications (Tjong and Chen, 2004).

Different methods involving electrodeposition, ion beam assisted deposition, thermal spraying, physical vapor deposition and plasma chemical vapor deposition have been utilized to produce nano-crystalline coatings for dental restorative applications (Tjong and Chen, 2004). Nano-structured bioceramics commonly possess improved mechanical properties, such as a better resistance to crack propagation (De Aza et al., 2002) and an enhanced fracture toughness and Vickers hardness (Uno et al., 2013). Consequently, the applications of nanomaterials have the possible to efficiently enhance the comprehensive properties, involving the biological, chemical and mechanical properties, of various kinds of traditional dental biomaterials (Feng et al., 2015). Yet, the utilization of nanocrystalline coatings is still restricted because applications necessitate a large-scale control of the synthesis of nanoparticles (Tjong and Chen, 2004; Feng et al., 2015).

In recent years, nanomaterials have been extensively utilized for the purpose of producing dental materials, including bonding systems, coating materials for dental implants (Memarzadeh et al., 2015) and light polymerization composite resins (Niu et al., 2010; Kasraei et al., 2014), bioceramics, endodontic sealers (Javidi et al., 2014), and mouthwashes (Frohlich and Roblegg, 2012). However, in addition to producing important improvements in clinical treatments, the applications of dental nanomaterials have also created growing concerns regarding their biosecurity. Because the nanomaterials are similar in size to biological molecules, DNA molecules, viruses, and proteins, some of their biological influences may be derived from the interaction mechanisms among the environment and living things, which has not yet been definitely understood. Indeed, nanoparticles are a kind of mesoscopic system that owns a small size impact, a macroscopic quantum tunneling impact, and a special surface impact. When decreased to

the nanoscale, several benign materials may manifest significant cellular toxicity (Feng et al., 2015).

2.10 Finite Element Analysis in Dentistry

Finite element analysis (FEA) is a computer predictive simulation method utilized in engineering analysis. It utilizes a computational approach called the finite element method (FEM). The FEM is a computerized computational iteration method utilized to determine the displacements and stresses through a constructed model. It is recognized as an effective method principally developed for the computational solution of complex issues in structural mechanics, and it remains the technique of preference for complex frameworks. In the FEM, the structural system is modelled by a set of suitable FE interconnected at points called nodes. Elements may have physical properties such as density, thickness, Young's modulus, the CTE, Poisson's ratio and shear modulus (Geng et al., 2001; Dittmer et al., 2011; Dejak et al., 2012; Jalali et al., 2016; Jin et al., 2016).

2.10.1 Application of FEM in Dentistry

FEA has attracted the interests of dental and medical researches and is nowadays one of the furthestmost successful engineering numerical techniques. It has been also utilized to predict the mechanical behaviour and stress distributions of the dental crowns, restorations and FPDs (Toparli et al., 1999; Ausiello et al., 2001; Aykul et al., 2002; Fischer et al., 2003; Proos et al., 2003; Rekow et al., 2006; Coelho et al., 2009b; Dittmer et al., 2011; Dejak et al., 2012).

Recently, few researches have been stated on the optimum design of all-ceramic crowns based on the geometry of a natural tooth got from Computerized Tomography

(CT) scan and analyzed by FEA. FEA enables simulation of any case, but the validation and accuracy of the results depends on the build-up of a suitable model (Magen, 2007; Uddanwadiker, 2012; Ha et al., 2016; Hondo et al., 2016; Jalali et al., 2016).

Rekow et al., (2006) used FEA to conduct a factorial analysis of some variables effecting stresses in all-ceramic crowns. They studied the effect of seven factors (crown thickness, crown material, cuspal inclination, cement thickness, cement elastic modulus, supporting tooth core, and location of occlusion load). Crown material and thickness accounted for 58.2% and 24.7% of the variability in the principal stresses in the crown respectively. The elastic modulus of the supporting tooth core, cement, and location position accounted for 2.1%, 0.5% and 1% of the variability in the stresses respectively. Sensitive to these factors may not be the same for crowns made with different materials.

In the dental restorative field, a bone and a tooth are mostly important topics and have extreme complex structure. Commonly, for 3D FE modelling, many approaches involving those depended on measurement of dry skulls (Tanne et al., 1989), anatomical morphological means (Jeon et al., 1999) and the coordinate transformation of data obtained by CT and 3D coordinate measuring machine (Watanabe et al., 2002; Hedia and Mahmoud, 2004) are utilized. However, it is hard to develop valid and an accurate 3D FE model utilizing traditional modelling methods. Efficient and accurate modelling can assist to understand the sophisticated nature of a tooth that is surrounded by the jawbone. The success of modelling based on the precision in simulating the surface structure and geometry of the tooth, the material properties of the jawbone and tooth, the support and loading environments as well as the biomechanical jawbone-tooth interface. Consequently, 3D FE modelling from CT images is of great importance in understanding the individual simulations of stress values and stress distribution (Magen, 2007; Hasegawa et al., 2010; Ha et al., 2016; Hondo et al., 2016; Jalali et al., 2016).

FEM enables analyses of both sound and restored teeth. The restorations may be direct, when inserted directly by the dentist, or indirect, when the restoration itself is made in a laboratory and later cemented to the patient's tooth. For each kind of restoration, different types of materials are employed. For indirect restorations, metals and ceramics, and all-ceramic are used (Motta et al., 2006). In an effort to well comprehend the stresses in the tooth, a variety of techniques have been utilized to predict tissue response to load (Khera et al., 1988; Darendeliler et al., 1992). These include theoretical mathematical techniques (Hillam, 1973), laser holographic interferometry (Burstome and Pryputniewicz, 1980) and photoelastic systems (Mehta et al., 1996). However, these methods have the disadvantage of only determining surface stress, whilst having the added problem of often being supported by poor validation systems as judged by the present standards (Geramy and Sharafoddin, 2003). FEM does not only offer solutions for the engineering problems, but its used in biomechanical utilizations is widely accepted (Er et al., 2007). FEM is considered to be an accurate, reliable and a fast substitute to researches *in vitro* and *in vivo* (Darendeliler et al., 1992; Yaman et al., 1995; Yaman et al., 1998; Toparli et al., 2003; Yaman et al., 2004). FEM is also advantageous because of its very sophisticated structures, in which experiments can easily be modelled that would reasonable very expensive or very hard to conduct, can easily be modelled. Although the use of FEM can supply very precise outcomes, the outcomes are still only estimates for specific situations. Therefore, one should not expect FEM to produce accurate answers to real environments but rather provide reliable calculations (Er et al., 2007; Ha et al., 2016; Hondo et al., 2016; Jalali et al., 2016).

The two-dimensional axisymmetric FEM has been used in much of the previous research (Farah et al., 1989; Zheng et al., 2012). Although mathematical outcomes can be simply found with 2D modelling, it has some significant limitations. The human teeth are highly asymmetrical in shape, such that it cannot be represented in the 2D space and the

real loading cannot be simulated without taking the third dimension into consideration. The distribution of different materials of the tooth structure does not exhibit any uniformity. Thus, 3D modelling with the exact dimension must be selected for a reliable analysis (Rubin et al., 1983).

Several previous studies have applied comparative FEA in an isolated manner (Lin et al., 2001; Ausiello et al., 2001; Lee et al., 2002; Magne and Belser, 2003; Couegnat et al., 2006; Ha et al., 2013), nondestructive tests, such as strain gauge tests (Palamara et al., 2002; Soares et al., 2008b) or associated with destructive tests (Fennis et al., 2005).

2.10.2 Advantages of FEM

- It has been applied to the description of shape variations in biological structures, particularly in the region of development and growth.
- The knowledge of physiological values of alveolar stresses is important for the understanding of stress related bone remodeling and also supplies a guideline reference for the design of dental crown restorations and dental implants.
- It is also beneficial for frameworks with inherent material homogeneity and potentially sophisticated shapes such as dental crown restorations and dental implants.
- To study stresses distributions in the tooth in relation to various designs.
- To optimize the design of dental crown restorations.
- To determine stresses distributions in the teeth with cavities preparations.

2.10.3 Disadvantages of FEM

There are certain limitations and disadvantages of FEM which should be addressed:

(1) Every FE is depended on an assumed shape function expressing internal displacements as functions of nodal displacements. A certain element may give precise answers for a particular location and type of support and loading, but in accurate answers for another type and location; (2) Even with "well-behaved" elements, the solution is heavily dependent on the mesh, not only on the number of elements into which the area is divided, but also in their arrangement and shape; (3) Precision of the output to a large number of significant digits is not a guarantee of the accuracy of the solution. Even convergence with the refinement of the mesh is not an absolute proof of the correctness of solution; and (4) Finite elements become essential only when other techniques are economically viable or not existing (Geng et al., 2001; Er et al., 2007; Jin et al., 2016).

CHAPTER 3: 3D-FE ANALYSIS OF FUNCTIONALLY GRADED MULTILAYERED DENTAL CERAMIC CORES

3.1 Introduction

Ceramics are attractive materials for dental crown restorations because of advantages such as aesthetic value, inertness and biocompatibility. However, ceramics are brittle and tend to fail beyond a critical load or lifetime (Lawn et al., 2002a, 2002b). The failure rate of posterior all-ceramic crowns is around 3% to 4% each year (Conrad et al., 2007; Rekow and Thompson, 2007; Chevalier and Gremillard, 2009), despite recent significant improvements in dental ceramic strength (i.e., high-strength alumina and zirconia cores). The main clinical failure mode is the subsurface radial crack in the ceramic at the interface between the crown (dental ceramic) and cement. This failure rate is largely caused by the tensile stress concentration in the dental ceramic at that interface (Lawn et al., 2002a; Huang et al., 2007a). Therefore, efficient methods for the reduction of stress at this interface should be explored.

Dental multilayer ceramics is a widely-recognized engineering idealization of dental crowns. This method mimics the layered structure of the crown on a real tooth. Medical and dental researchers have focused on applying FEA, one of the most successful engineering computational methods, to predict stress distributions and the mechanical behavior of the restorations, dental crowns and fixed partial denture (Toparli et al., 1999; Ausiello et al., 2001; Fischer et al., 2003; Dittmer et al., 2009; Dejaka et al., 2012; Della Bona et al., 2013; Ha et al., 2013; Ha et al., 2016; Hondo et al., 2016; Jalali et al., 2016). Few studies have reported the optimum design of all-ceramic crowns based on the geometry of a real tooth, which is obtained through a computerized tomography (CT) scan, and analyzed by FEA.

The use of accurately graded finite elements for FGM modelling has been recently developed (Wang et al., 2007; Ha et al., 2016; Hondo et al., 2016; Jalali et al., 2016).

3.2 Aim of this Chapter

The purpose of this chapter was to investigate and establish the biomechanical behaviour of newly synthesized functionally graded multilayered zirconia with/without alumina ceramic cores using FEA to facilitate the formulation of ceramic cores through computer modelling when subjected to various directions of loading.

3.3 Objectives of this Study

1. To determine the von Mises stress distribution at the veneer-ceramic cores-cement-dentine interfaces.
2. To determine the tensile stress distribution at veneer-ceramic cores-cement-dentine interfaces.
3. To determine the compressive stress distribution at veneer-ceramic cores-cement-dentine interfaces.
4. To analyse the shear stress distribution at veneer-ceramic cores-cement-dentine interfaces.
5. To analyse the strain distribution at veneer-ceramic cores-cement-dentine interfaces.
6. To establish 3D FEA model of a single and multilayered graded ceramic dental cores.

3.4 Null Hypothesis of this Chapter

There is no improvement in the biomechanical behaviour of newly synthesised functionally graded multilayered zirconia with/without alumina ceramic cores using FEA to facilitate the formulation of ceramic cores through computer modelling when subjected to various directions of loading.

3.5 Materials and Methods

The geometrical model (tooth with dental ceramic crown) was obtained by 3D reconstruction from CT images of an intact extracted human maxillary second premolar. This process required reconstructing the 3D FE model of the natural tooth and tooth restored with dental ceramic crown comprising the following steps: 1) data acquisition by CT scan, 2) geometry model reconstruction and remeshing, 3) solid modelling, and 4) FE meshing.

3.5.1 Computerized Tomography (CT) Scan

For image acquisition, an intact extracted human maxillary premolar tooth was scanned with computerized tomography scanner (Siemens, Somatom®, Erlangen, Germany) (Ethics No.: DF RD1201/1007(P), Dental Committee, Faculty of Dentistry, University of Malaya) (see Appendix A) as shown in Figure 3.1a. In order to achieve real results with perfect image quality, the parameters of imaging condition were as follows: tube voltage, 120kV; exposure dose, 150 mA; image matrix, 512 x 512 points; field of view, 22.80 mm; pixel size, 0.4453; slice thickness, 0.6 mm, and exposure time, 20s. A total of 243 images of the maxillary premolar in different axis directions were taken and

these CT data were saved in Digital Imaging Communications in Medicine (DICOM) format whose length was 20 mm.

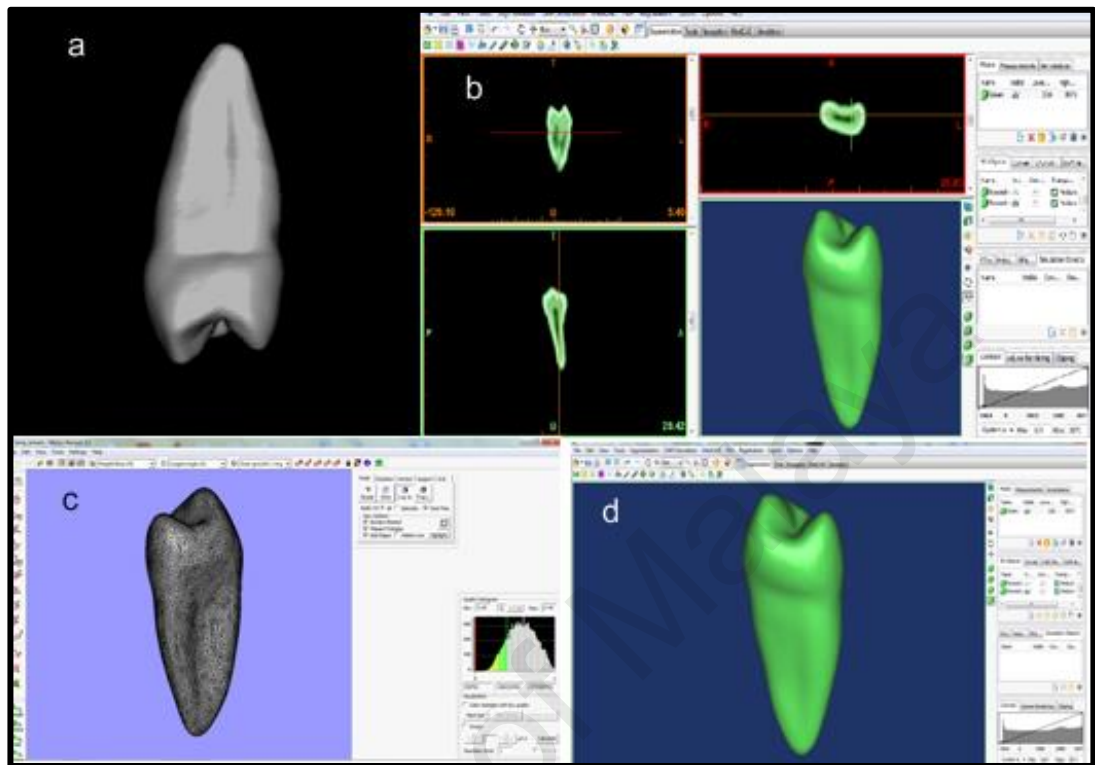


Figure 3.1: a- CT scan of maxillary second premolar tooth. b-Different views of the scanned tooth in MIMICS Software. c- Remeshing of tooth. d- Tooth after remeshing and smoothing.

3.5.2 Geometry Model Reconstruction and Remeshing

For geometry model reconstruction, the program Mimics®/MedCAD (Version 13.1, Materialise, Leuven, Belgium) was utilized to reconstruct of the converted data to the DICOM format file in the three-dimensional structures models as shown in Figure 3.1a. About 243 images were taken of the maxillary second premolar in different axis directions and then imported into the program Mimics/MedCAD as shown in Figure 3.1b.

The different hard tissues visible on the scans were identified using Mimics® based on image density thresholding as shown in Figure 3.1b. This tool gives effective

information in the non-invasive mapping of the anatomy of various subjects. Hence, the maxillary second premolar and its supporting structures were reconstructed by cropping the selected areas as shown in Figure 3.1b. Once the tooth and its supporting structures were isolated, segmentation process was commenced. Segmentation is a process that consists of separating an object of interest from other adjacent anatomical structures in different masks, such as a tooth, as illustrated in Figure 3.1c. The 3D image was automatically generated into the masks forms by increasing a region of threshold on the whole stacks of scans.

After that, smoothening, triangle reduction and remeshing (Figure 3.1c) were carried out on the model in Mimics 13.1 to create a suitable model for FEA. The remesh module connected to Mimics was utilized to automatically decrease the triangles number and jointly enhance the triangles quality while preserving the geometry. During the remeshing, the tolerance difference from main data was fixed. The quality is specified as a gauge of a triangle's base/height ratio so that the model could be imported into the FEA software. After creating the external volume of the 3D model which are tooth and tooth components in Mimics, the model was saved as a (*.INP) file prior to importing into ABAQUS/CAE software, Professional Version (Simulia, Valley St., Providence, USA) (Abaqus, 2010) (Figure 3.1d).

Table 3.1: Models with different designs and materials.

Model	Designs	Materials and percentage (%)
A	First layer ceramic core	Zirconia (100%)
B	First layer ceramic core	Zirconia (80%) + Alumina (20%)
C	First layer ceramic core	Zirconia (60%) + Alumina (40%)
D	First layer ceramic core	Zirconia (50%) + Alumina (50%)
E	Two layers ceramic core	First layer: Zirconia (100%) Second layer: Zirconia (80%) + Alumina (20%)
F	Two layers ceramic core	First layer: Zirconia (100%) Second layer: Zirconia (60%) + Alumina (40%)
G	Two layers ceramic core	First layer: Zirconia (100%) Second layer: Zirconia (50%) + Alumina (50%)
H	Natural Tooth	Enamel + dentine

Eight models focused on the ceramic core (zirconia with/without alumina) were developed in this study as shown in Table 3.1. Models A, B, C, and D represent teeth restored with veneer, one-layer core (zirconia with/without alumina), cement, and dentine (Figure 3.2a). Model E, F, and G represent a tooth restored with veneer, two-layer core, cement, and dentine (Figure 3.2b). Finally, Model H represents a naturally intact tooth. This model was used to study the effects of stress distribution on other models under oblique loading (Figure 3.2c).

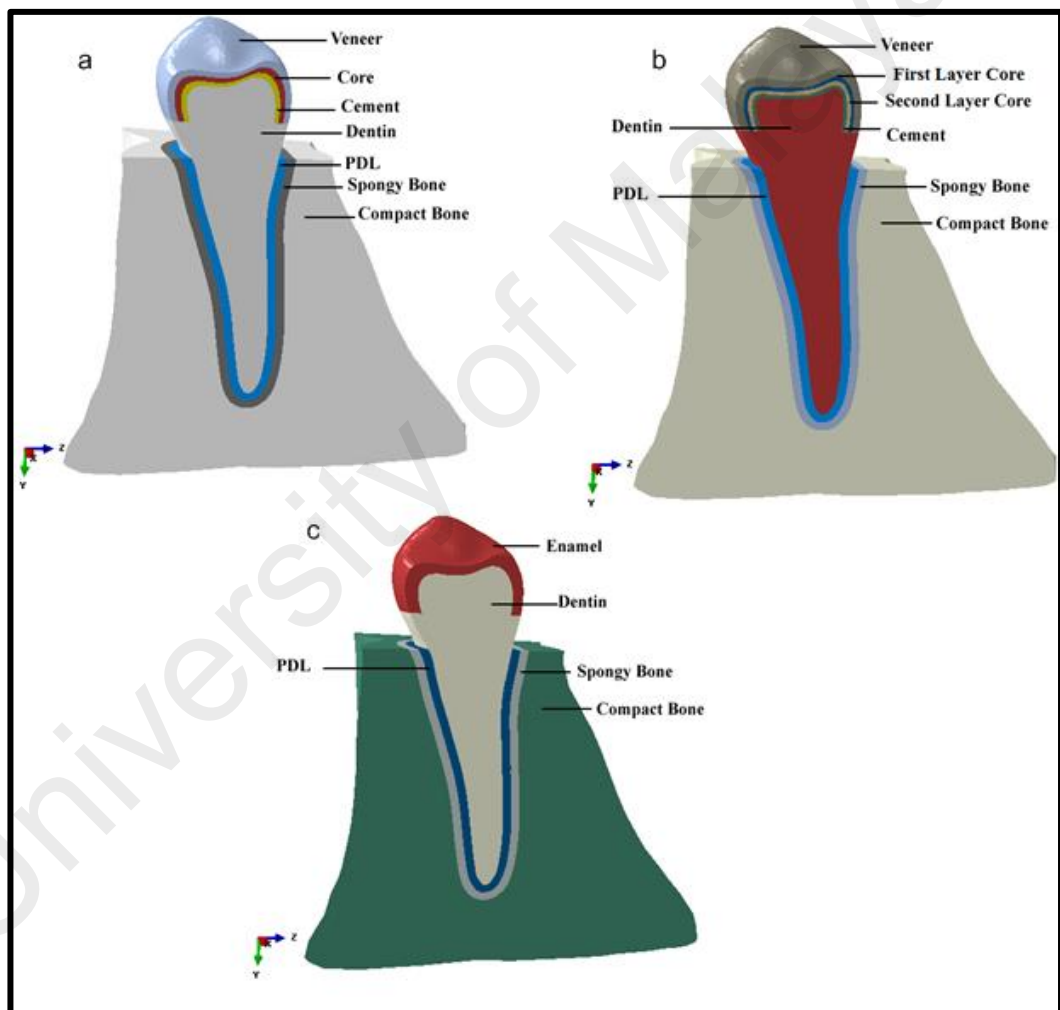


Figure 3.2: Schematic illustration of the geometric models and load directions. a- Restored tooth model with single layer ceramic core. b- Restored tooth model with multilayer ceramic core. c- Natural tooth model with supporting structures.

To simplify the creation of the 3D models for FEA, some assumptions have been made regarding the material properties of each part and its geometry.

The cementum layer that covers the surface of the root was included in the dentine portion of the tooth due to its very thin structure. As for the influence of the pulp chamber in the preparation on the stresses in the crown, it was deemed neglected according to Hojjatie and Anusavice (1990).

The time-dependent setting process of the luting cement was mimicked by a time-independent elastic-plastic material property (De Jager et al., 2006). However, these models only defined the properties for regular thickness of the cement layer, and the cement layer thickness for various models different from 25 μm to 140 μm (Proos et al., 2003).

The influence of the periodontal ligament on the stresses in the crown is negligible, although Rees (2001) found that the ligament and alveolar bone is of importance for the stress distribution. Therefore, the alveolar bone and periodontal ligament were included in all the models (De Jager et al., 2006). The temperature distribution during ceramic crown processing was uniform (DeHoff et al., 1998).

Defining the periodontal ligament from CT scan images is difficult due to its thin structure and the pixel size of 0.4453 mm. Thus, periodontal ligament of 0.18 mm thick was generated based on the isocurve of the dentine in ABAQUS (Rees and Jacobsen, 1997). The isocurves of the compact and spongy bone were also exported; their thickness was 10 mm, and their extremities corresponded to the positioning of the maxillary second premolar, respectively. The internal volume of the 3D model was then generated by adding enamel, dentine and restorative dental crown (veneer, core and cement) components.

3.5.3 Generation of the Mesh

The constructed 3D FE model from CT data was meshed. In this study, in order to obtain real results; the proper meshing was determined based on the convergence test and the mesh sizes of each component of all models were set to 0.5 mm as shown in Figure 3.3. The finest meshing was beneficial in improving of the accuracy model, because the mesh was generated in the smallest possible size. A convergence test is helpful in determining whether the number of the elements was sufficient to reflect results accurately. According to the decreased size mesh, a larger capacity of Center Processing Unit (CPU) was wanted to correspond to the arised load on the CPU with 8.0 GB RAM memory.



Figure 3.3: Tetrahedral mesh structure of the geometric model by FEA.

In this current study, the linear tetrahedral solid elements (C3D3) with four nodes were used for the stress analysis. The C3D3 was used with fine meshes 0.5 mm to obtain

accurate data as constant tetrahedral elements exhibit slow convergence (ABAQUS, 2010). The total numbers of the tetrahedral elements of natural tooth was 493,742 with 101,091 nodes, the elements of each control model with one-layer core was 534,238 with 112,824 nodes, and the elements of each experimental model was 459,536 with 97,910 nodes (Figure 3.3) (see Appendix A) were used after a pilot study revealed that the error remained below 0.1 % for five mesh sizes (0.5, 1, 2, 4, 6) in all eight models.

3.5.4 Boundary Conditions and Loading

In this study, the boundary conditions were taken from the aforementioned *in-vitro* studies (Kohorst et al., 2007; Dittmer et al., 2009). The outer and bottom surface of the cortical bone was set to have a perfectly fixed boundary with zero displacements in all X-, Y-, and Z-axes as shown in Figure 3.4. Other surfaces were set to have a perfectly free boundary condition. The natural tooth and tooth restored with ceramic crown restoration were considered to be perfectly bonded and the friction coefficient was 0.3 (Couegnat et al., 2006; Santos et al., 2009a).

A static load with a magnitude 200 N (Coelho et al., 2009b; Hasegawa et al., 2010; Rafferty et al., 2010) was applied on the surface of the crown at three different locations and in three different directions with the same concentrated area 2.5 mm². Three different loading conditions were chosen as follows:

An oblique load applied at a 45° oblique angle to buccal cusp of the crown, to simulate the occlusion masticatory force on the tooth; $F_1 = 200 \text{ N}$ (Toparli et al., 2002; Eskitascioglu et al., 2004; Soares et al., 2008b; Hasegawa et al., 2010) with the Vector of the force $F = (-0.707, 0.707, 0)$ as shown in Figure 3.5.

A vertical force applied on the topmost of the buccal and palatal cusps of the crown in order to simulate forcing during bruxism on the tooth; $F_2 = 200$ N (Lee et al., 2002; Eskitascioglu et al., 2004; Al-Omiri et al., 2011) with the Vector of the force $F = (0, 1, 0)$ was applied as seen in Figure 3.5.

A horizontal force applied to the middle third of buccal crown to simulate external traumatic forces on the tooth; $F_3 = 200$ N (Al-Omiri et al., 2011) with the Vector of the force $F = (1, 0, 0)$ as shown in Figure 3.5. All forces were applied on the aforementioned areas as distributed pressure. Any stresses that are likely to be introduced during the crown preparation of the tooth were neglected.

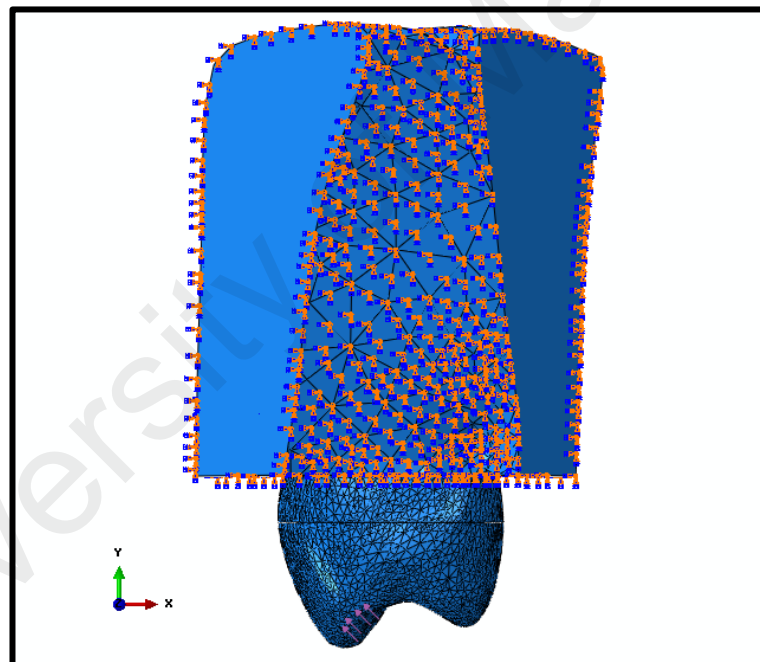


Figure 3.4: Boundary condition of the model.

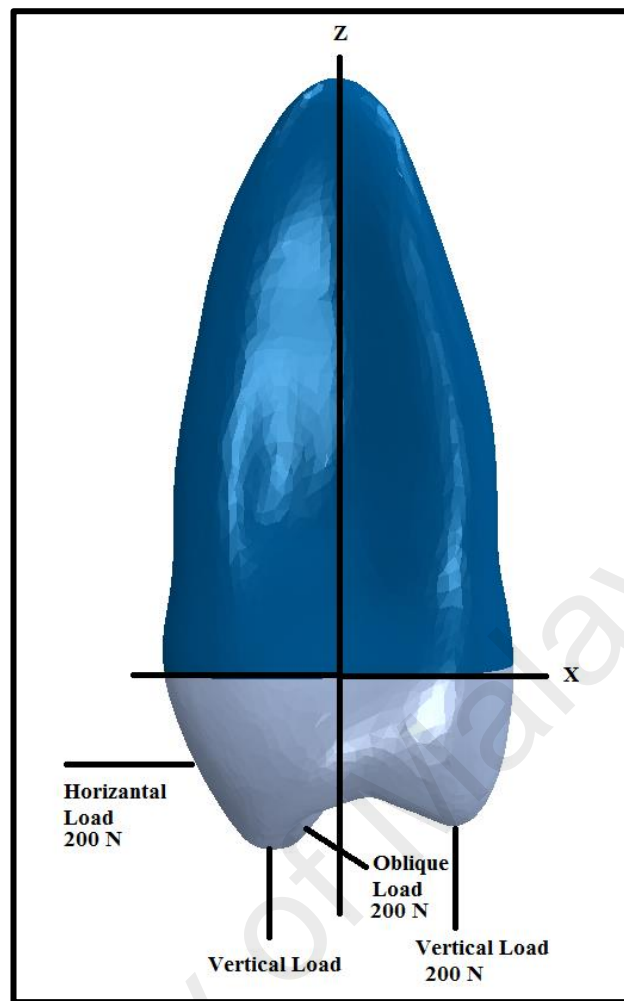


Figure 3.5: A static load in three different directions.

3.5.5 Natural Tooth and Restorative Materials and Material Properties

The elastic Young's Modulus (E) and Poisson's ratio (ν) used for each component in this present study were assumed to be homogeneous, isotropic and linear elastic (Table 3.2.) (Anusavice and Hojjatie, 1992; Thompson et al., 1994; Kelly et al., 1995; Toparli et al., 2002; Denisova et al., 2004; White et al., 2005; Kohorst et al., 2007; Dittmer et al., 2009; Dejaka et al., 2012; Zheng et al., 2012). A pilot study was conducted for many estimated functionally graded dental ceramic (FGDC) designs with varied compositions in order to ensure the best integration for the FGDC. The outcomes revealed that the most significant were shown better in multilayered FGDC than single layer (zirconia with/without alumina) (Models A, B, C, and D).

The elastic Young's Modulus (E) of different synthesised ceramic cores (Models B-G) were calculated by using the "rule of mixture" (ROM) which was inspired by the theory of ceramic composite materials, as shown in the following equation (Vasiliev and Morozov, 2001):

$$E_{composite} = \frac{f_1 E_1 \frac{v_1}{v_2} + f_2 E_2 \frac{v_1}{v_2}}{2} \quad (1)$$

Where,

f_1 and f_2 were representing the fractions of volume for ingredients of the first and second in each synthesised layer. V_1 and V_2 were representing Poisson's ratios (V) for ingredients of the first and second in each synthesised layer. E_1 and E_2 were representing the elastic Young's modulus (E) for ingredients of the first and second in each synthesised layer.

Poisson's ratio (V) for different synthesised ceramic cores (Models B-G) were also calculated utilizing the following equation:

$$V = \frac{V_1 + V_2}{2} \quad (2)$$

Table 3.2: Elastic properties of the tooth and restorative material properties.

No	Tissue/Materials	Young's Modulus (GPa)	Poisson's Ratio
1	Isotropic enamel	80	0.32
2	Dentine	18.6	0.31
3	Periodontal ligament	0.689	0.49
4	Spongy bone	0.345	0.30
5	Coritcal bone	13.8	0.26
6	Veneering	70	0.28
7	Zirconia	210	0.30
8	Alumina	400	0.30
9	Luting cement	15.9	0.33

3.5.6 Finite Element Analysis (FEA)

The simulation of the 3D-FE model pattern, the estimation of the processing and the stress-strain distributions were performed using Professional Version 6.10 of ABAQUS/CAE. Stress patterns were obtained at different locations; along all nodes located centrally from cervical buccally to cervical palatally on the surfaces of the veneer, the ceramic core, the cement, and the dentine as illustrated in Figure 3.6. The points were chosen at cervical from buccal (point 1a) and cervical palatal (point 1b) margins of all parts for all model crown, at the axio-gingival corners (point 2a and 2b), on the midpoint of the buccal and palatal surfaces (points 3a and 3b), and on top of both cusps with the occlusal surface of the veneer, the ceramic core, the cement as shown in Figure 3.6, and the dentine (4a and 4b) as shown in Figure 3.7. The stress distribution (Von Mises, maximum stress principal, minimum stress principal, and shear stress) and strain distribution (maximum strain and minimum strain) were investigated in each component and at the veneer-ceramic core-cement-dentine interfaces (X, Y and Z).

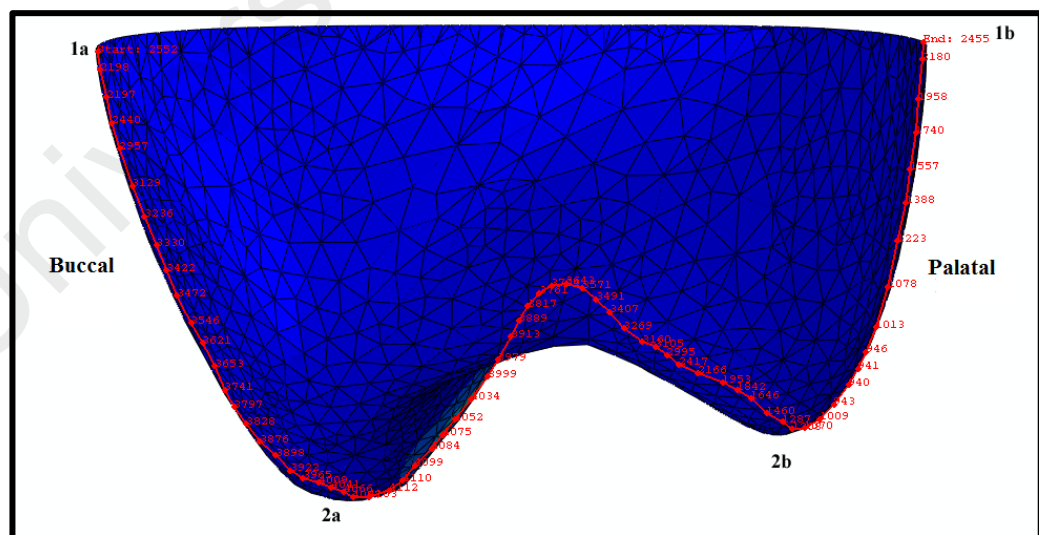


Figure 3.6: Measurements of stress on the model occlusal surface of the veneer, the ceramic core, and the cement.

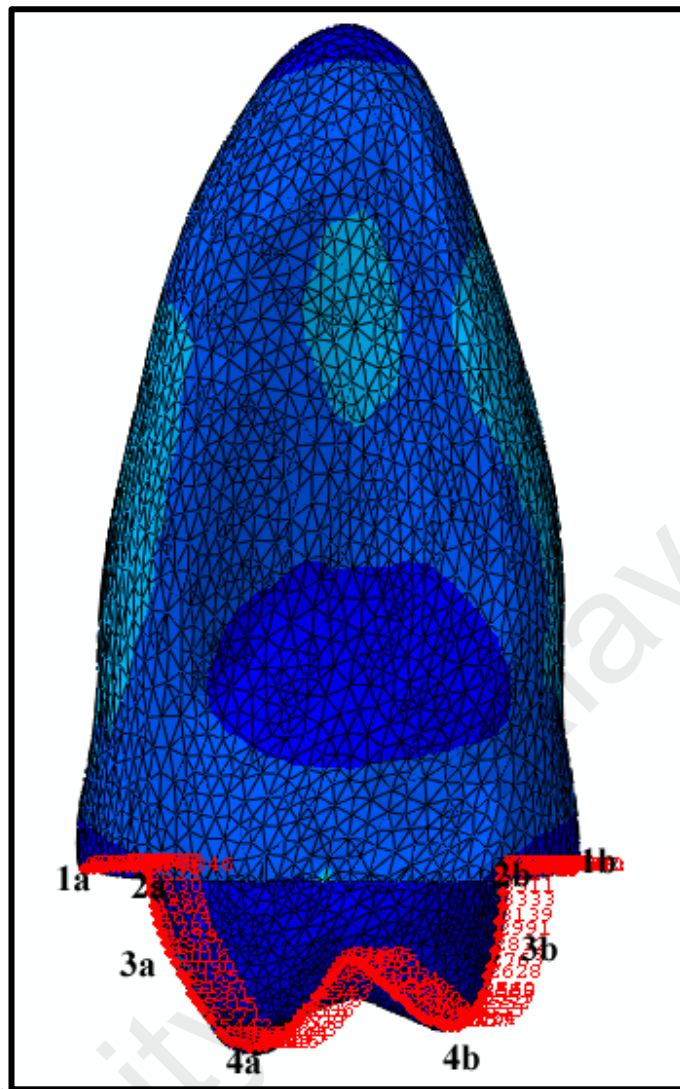


Figure 3.7: Measurements of stress on the model dentine.

3.6 Results

The FEA program almost always registers high stresses at the loading point, especially when a point load was applied in all models under three various loadings. Generally, the results of this study showed that the highest von Mises stress levels were observed within all structures in all models under various loading conditions.

3.6.1 Oblique Load

In the oblique load direction, the results were observed that the von Mises stress started to develop from the load region on the crown and slightly decreased towards the inner parts with maximum stresses of 139.7 MPa (Model A), 139.3 MPa (Model B), 139.5 MPa (Model C), 139.6 MPa (Model D), 109.9 MPa (Model E), 109.8 MPa (Model F), 109.8 MPa (Model G), and 61.5 MPa (Model H) (Figure 3.8). The maximum von Mises stress concentration levels were observed in the ceramic core of Models A to D. However, lower von Mises stress concentration levels were observed in the graded multilayered ceramic core (Models E to G) and natural tooth (Model H). Improvement and reduction were observed in the average von Mises stress values under oblique loading for graded multilayered ceramic cores (Model E to G) compared with the homogenous zirconia ceramic core (Model A) without alumina.

Figures 3.9a and 3.9b showed that the von Mises stress distribution on an obliquely loaded tooth model restored with various types of ceramic cores (Models A to G) and a natural tooth (Model H). The maximum von Mises stress was concentrated at the load region on the crown and spread to the middle of the occlusal surface. The maximum von Mises stress levels were observed directly below the load region for both veneer and ceramic core solids. The highest stress levels were observed at the ceramic core region in contact with the cement layer. Increased levels of stress concentration were also observed at the margin regions of the ceramic core, including the cervical and proximal region. However, stress progressively decreased towards the inner part of cement surface and the tooth (Figure 3.9c and Figure 3.9d).

The maximum tensile stress (maximum principal stress) concentration levels were observed in the veneer and ceramic core of Models A to D. However, lower tensile stress concentration levels were observed in the graded multilayered ceramic core (Models E to

G) and natural tooth (Model H) (Figures 3.10 and 3.11). Additionally, the maximum compressive stress concentration levels were observed in the veneer and ceramic core of models A to D. However, lower compressive stress (minimum principal stress) concentration levels were observed in the graded multilayered ceramic core (Models E to G) (Figures 3.12 and 3.13).

The shear stress between the veneer and core interfaces of the graded multilayered models (Models E to F) was lower than in the single-layer models (Models A to D) (Figure 3.14 in X-Y direction) (in X-Z and Z-Y direction for shear stresses see Appendix A Figures 1 and 2). Meanwhile, the shear stress between the core and cement interfaces of the graded multilayered models (Models E to F) was lower than in the single-layer models (Models A to D).

High stress levels were observed directly below the load region for veneer and ceramic core solids (Figure 3.15a). Higher stress levels were observed at the ceramic core region in contact with the cement layer (Figure 3.15b). Increased levels of stress concentration were also observed at the margin regions of the ceramic core, including the cervical and proximal regions. Stresses on the dentine were considerably lower in Models E to G than in Models A to D (Figure 3.15c).

Figure 3.16 showed that the strain distribution under oblique loading for single layer (Models A-D), multilayered graded (Models E-G), and natural teeth. In all models, strain distribution was observed in the buccal aspect of the whole crown. In contrast, the values of minimum strain were observed on the apical part of the tooth root as shown in Figure 3.17. Progressively, strains increased from the inner to the outer side of the dentine and from the dentine-cement interface nearby the occlusal border of the crown. Also, the lower strain values were noted at the cervical zone, whereas the occlusal and middle thirds of the crown were nearly free of distortions. In all models, strains distributions were quite

similar. Also, all the models restored with a single layer ceramic core showed slightly higher strain values when compared with models restored with multilayered ceramic cores (Models E to G) as seen in Figure 3.18. (a, b, c, and d) in all veneer-core-cement-dentine parts as shown in Figure 3.18.

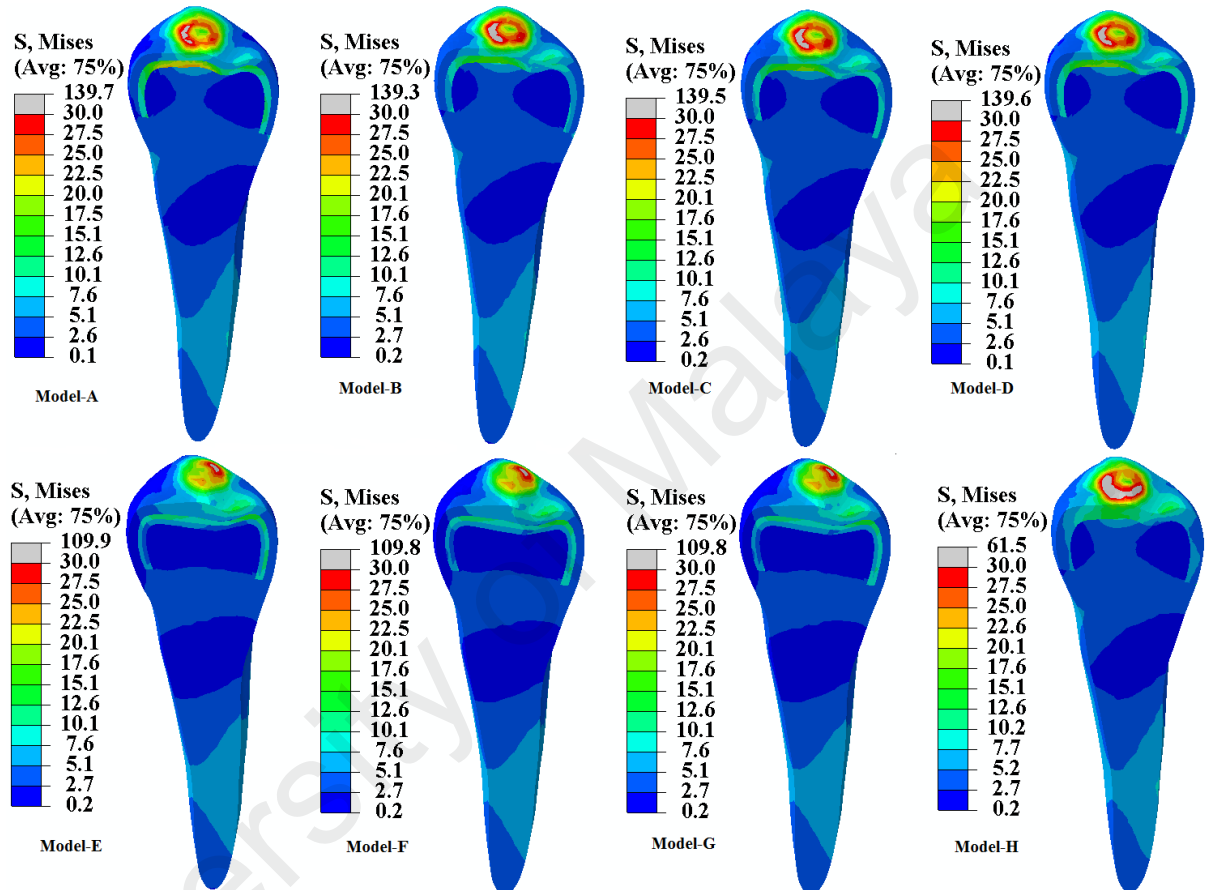


Figure 3.8: Contour plot of the von Mises stress distribution within the tooth and veneer-core-cement of all models when loaded obliquely.

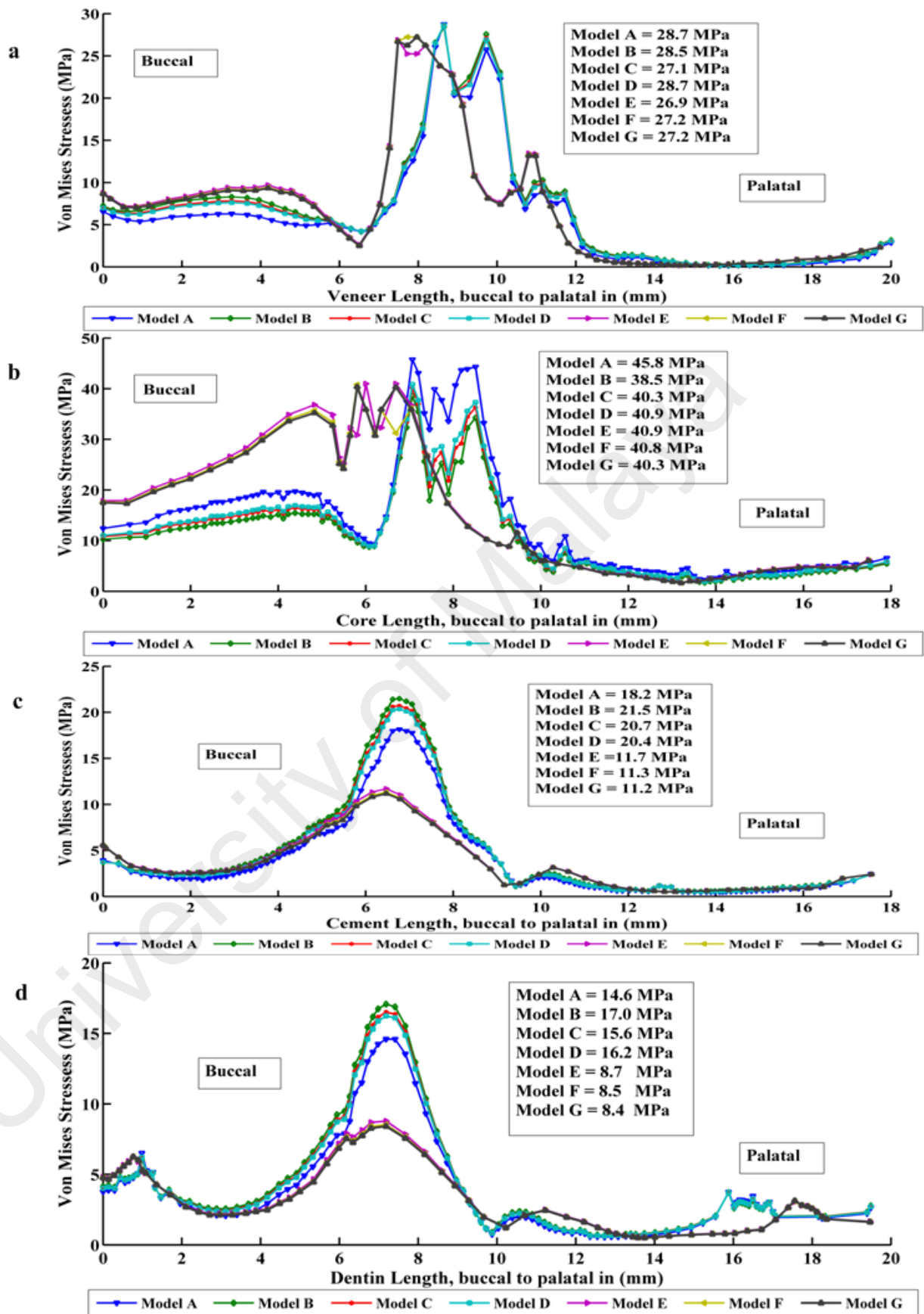


Figure 3.9: The von Mises stress of the veneer-core-cement-dentine in all models when loaded obliquely.

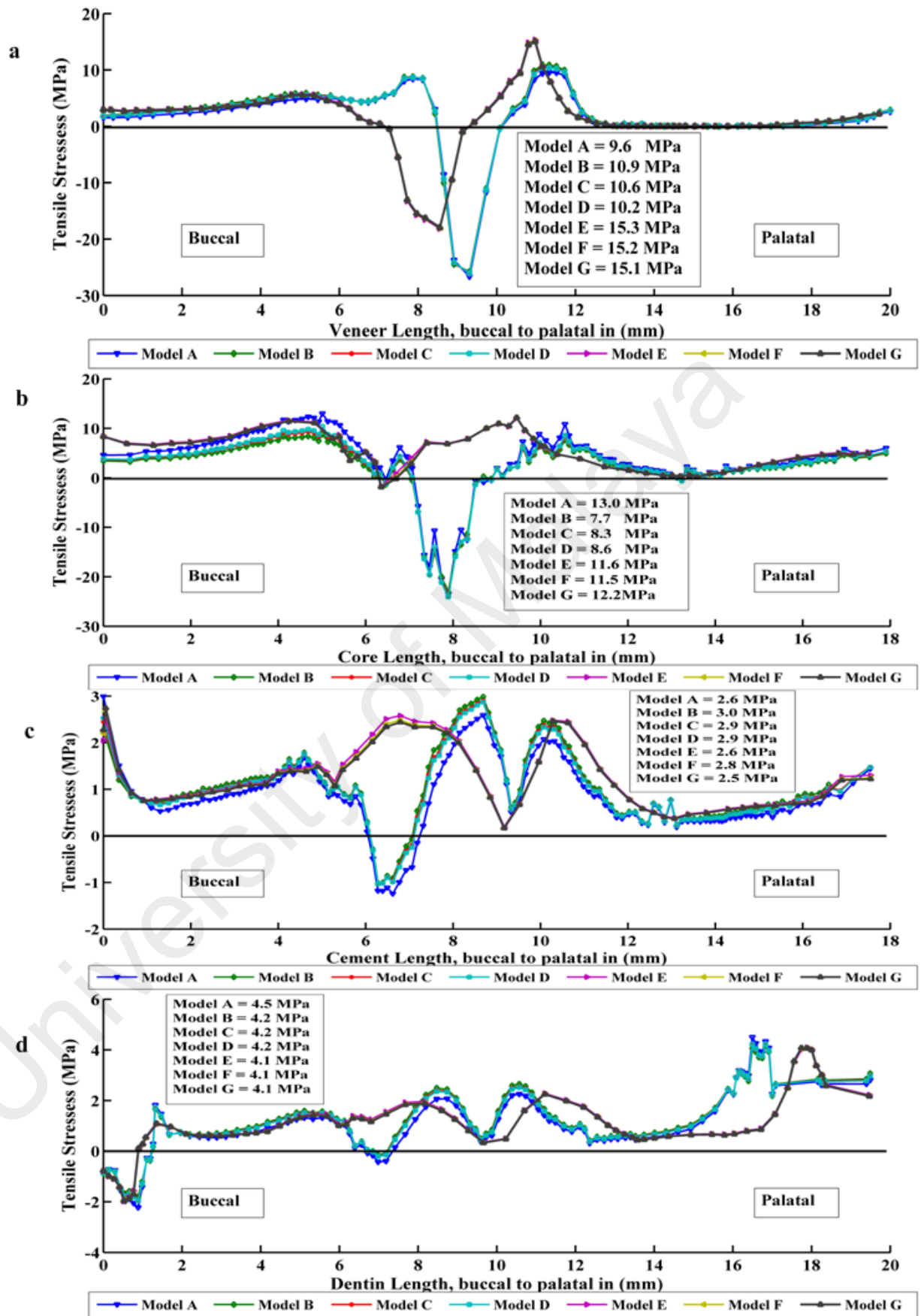


Figure 3.10: The tensile stresses of the veneer-core-cement-dentine in all models when loaded obliquely.

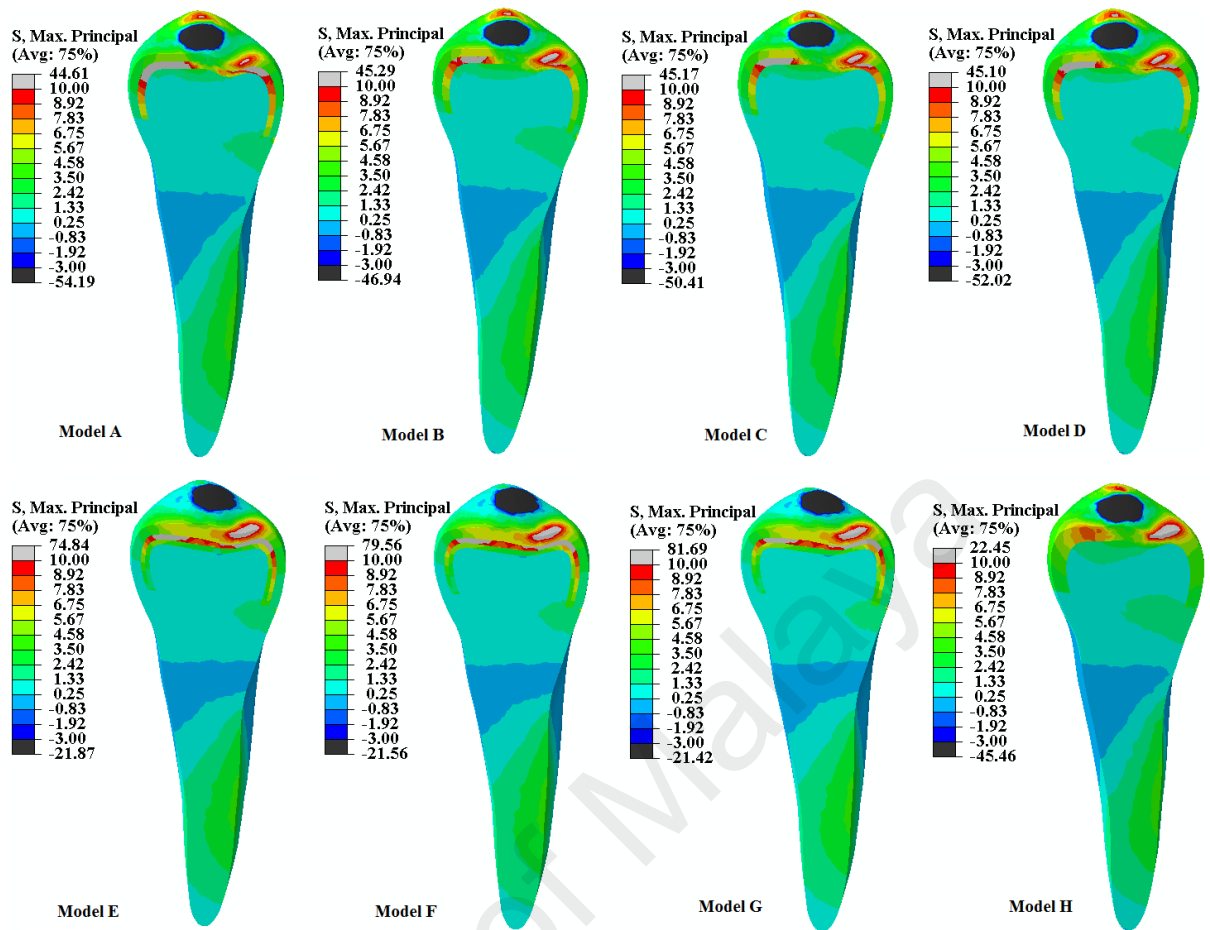


Figure 3.11: Contour plot of the tensile stresses of the veneer-core-cement-dentine in all models when loaded obliquely.

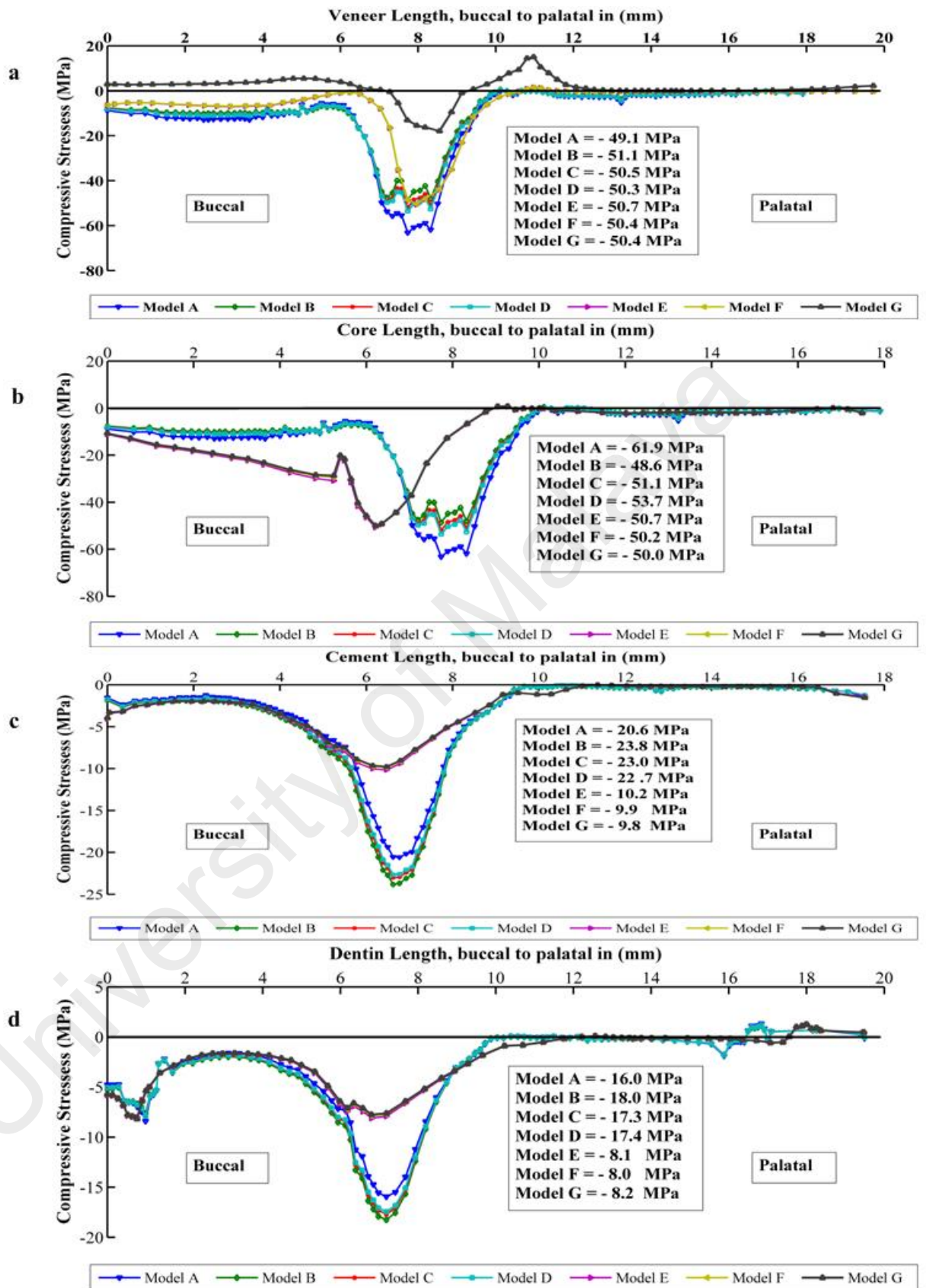


Figure 3.12: The compressive stress of the veneer-core-cement-dentine in all models when loaded obliquely.

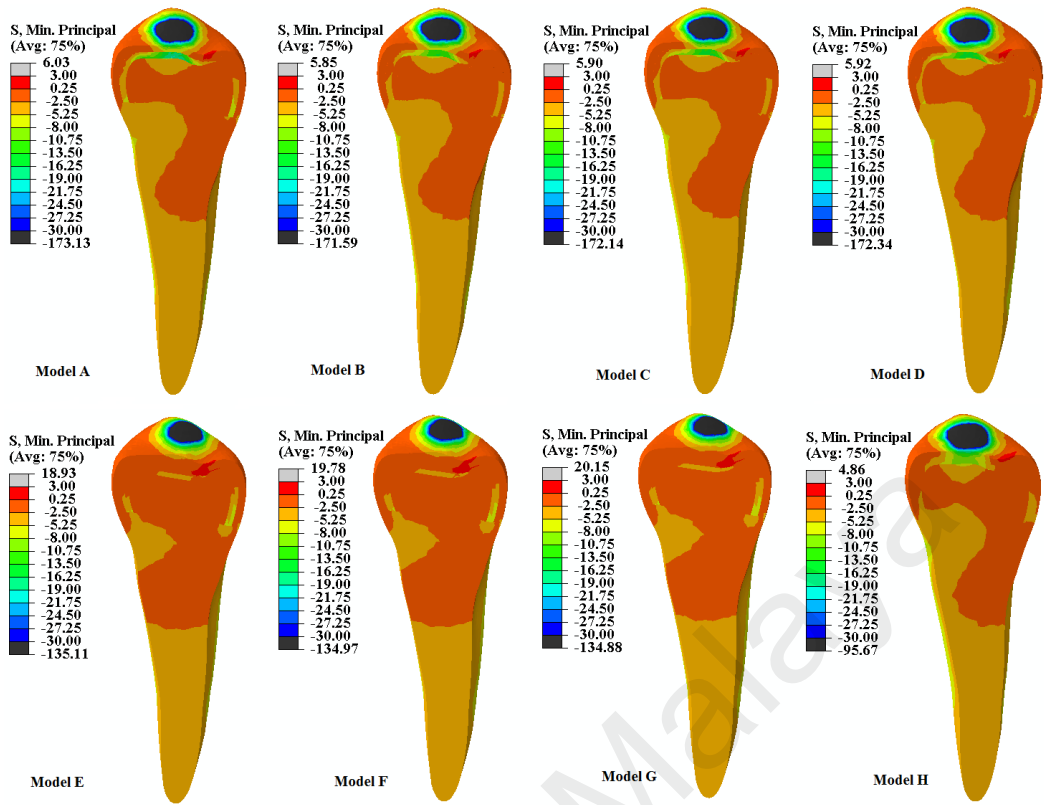


Figure 3.13: Contour plot of the compressive stress of the veneer-core-cement-dentine in all models when loaded obliquely.

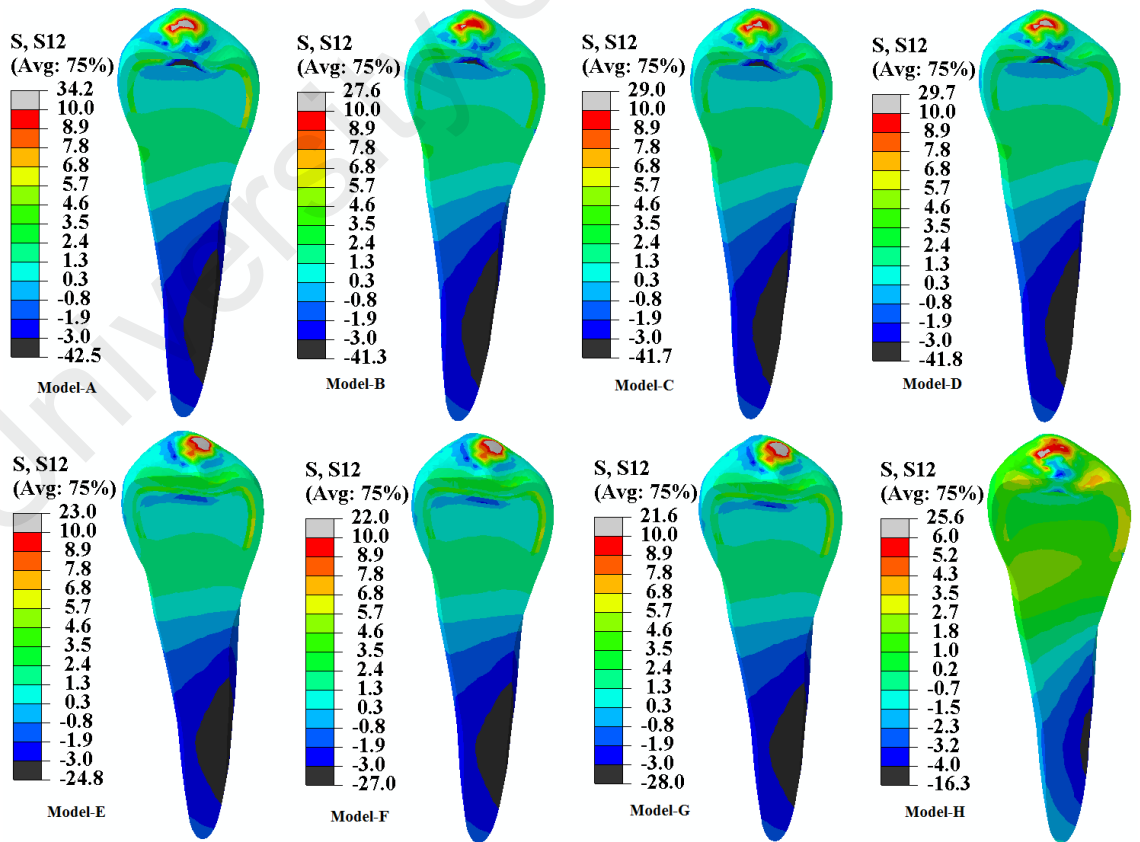


Figure 3.14: Contour plot of the shear stress distribution interface between veneer-core-cement-dentine-S12 (X-Y direction) when loaded obliquely.

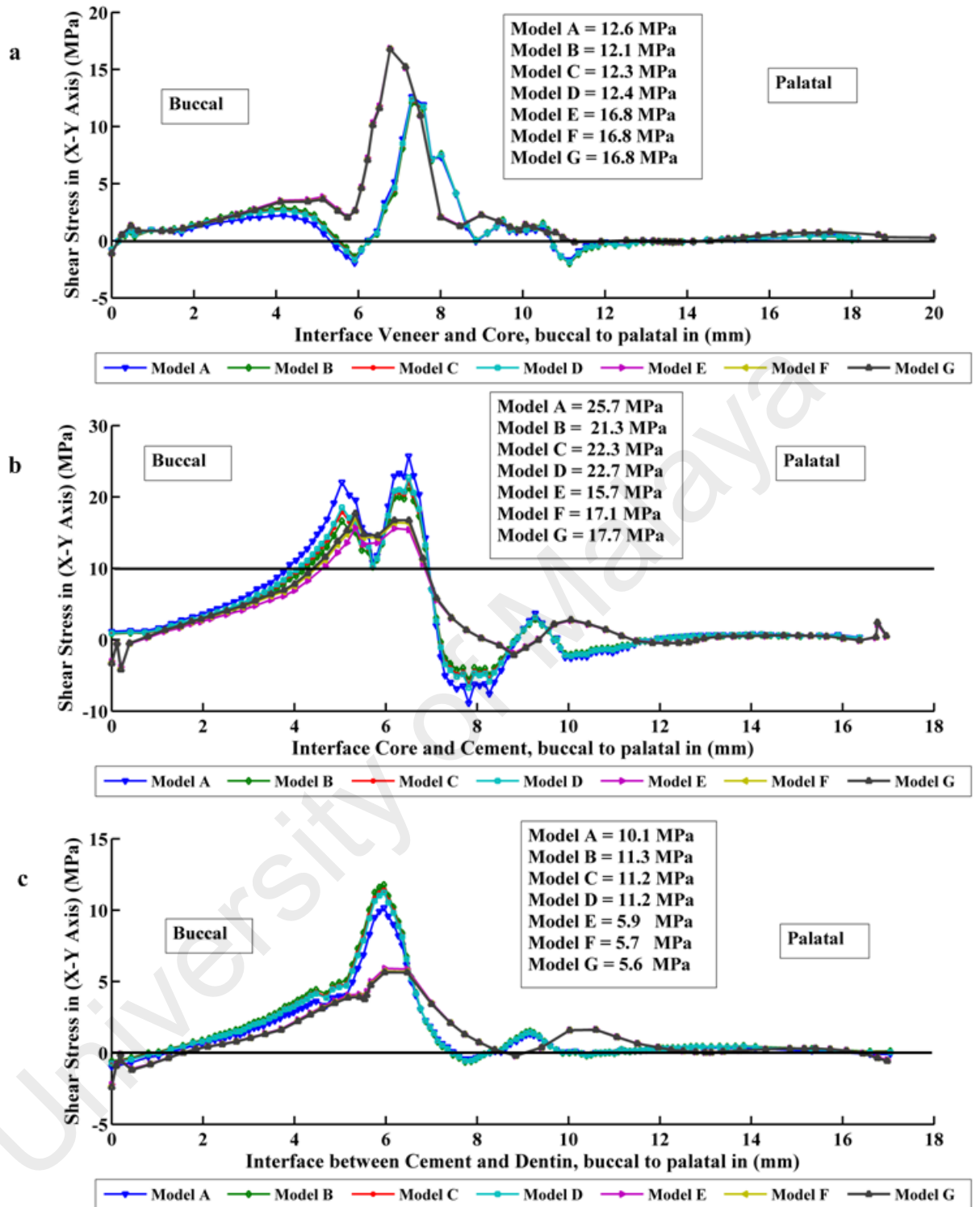


Figure 3.15: The shear stress distribution between the veneer-core-cement-dentine interfaces in all models. S12 (X-Y direction) when loaded obliquely.

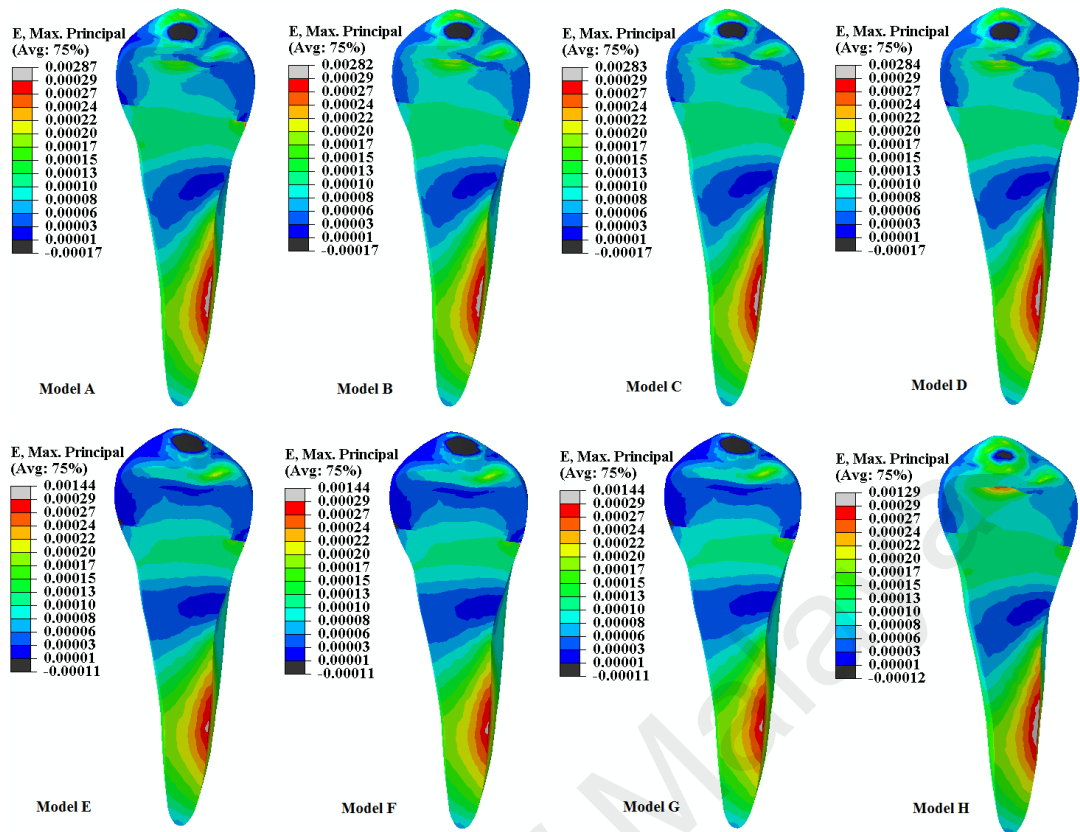


Figure 3.16: Contour plot of the strain maximum distribution within the tooth and veneer-core-cement of all models when loaded obliquely.

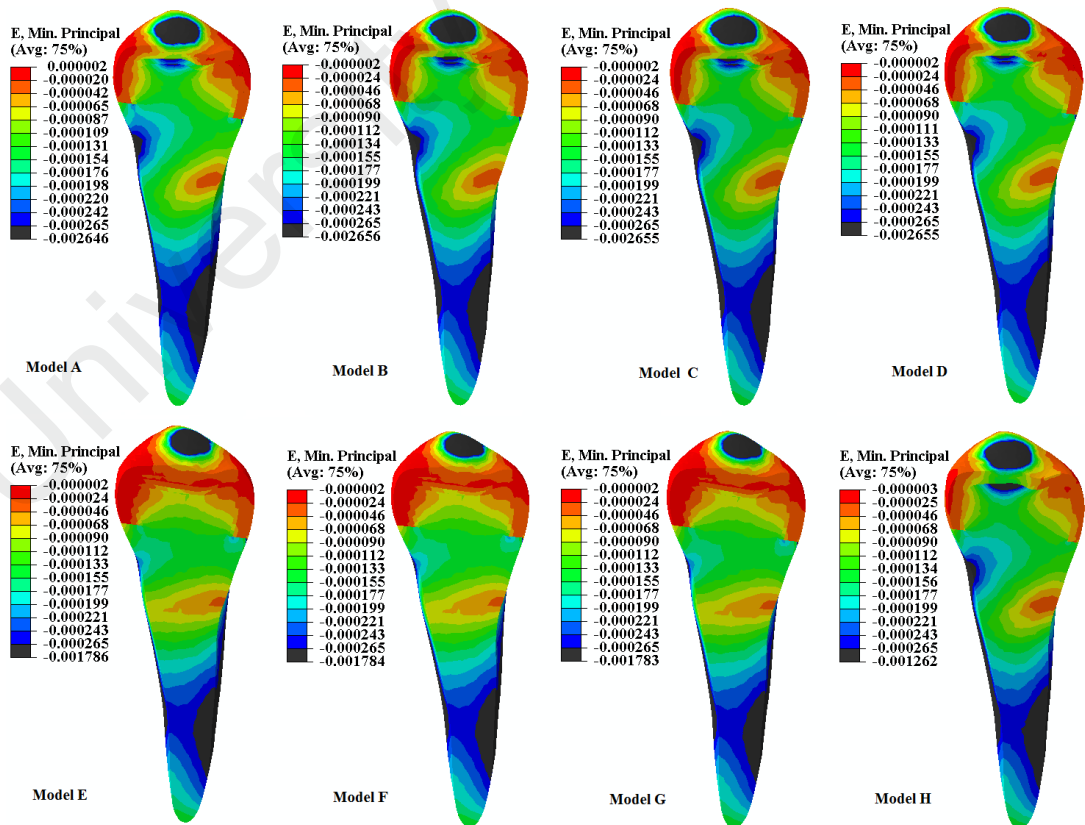


Figure 3.17: Contour plot of the strain minimum distribution within the tooth and veneer-core-cement of all models when loaded obliquely.

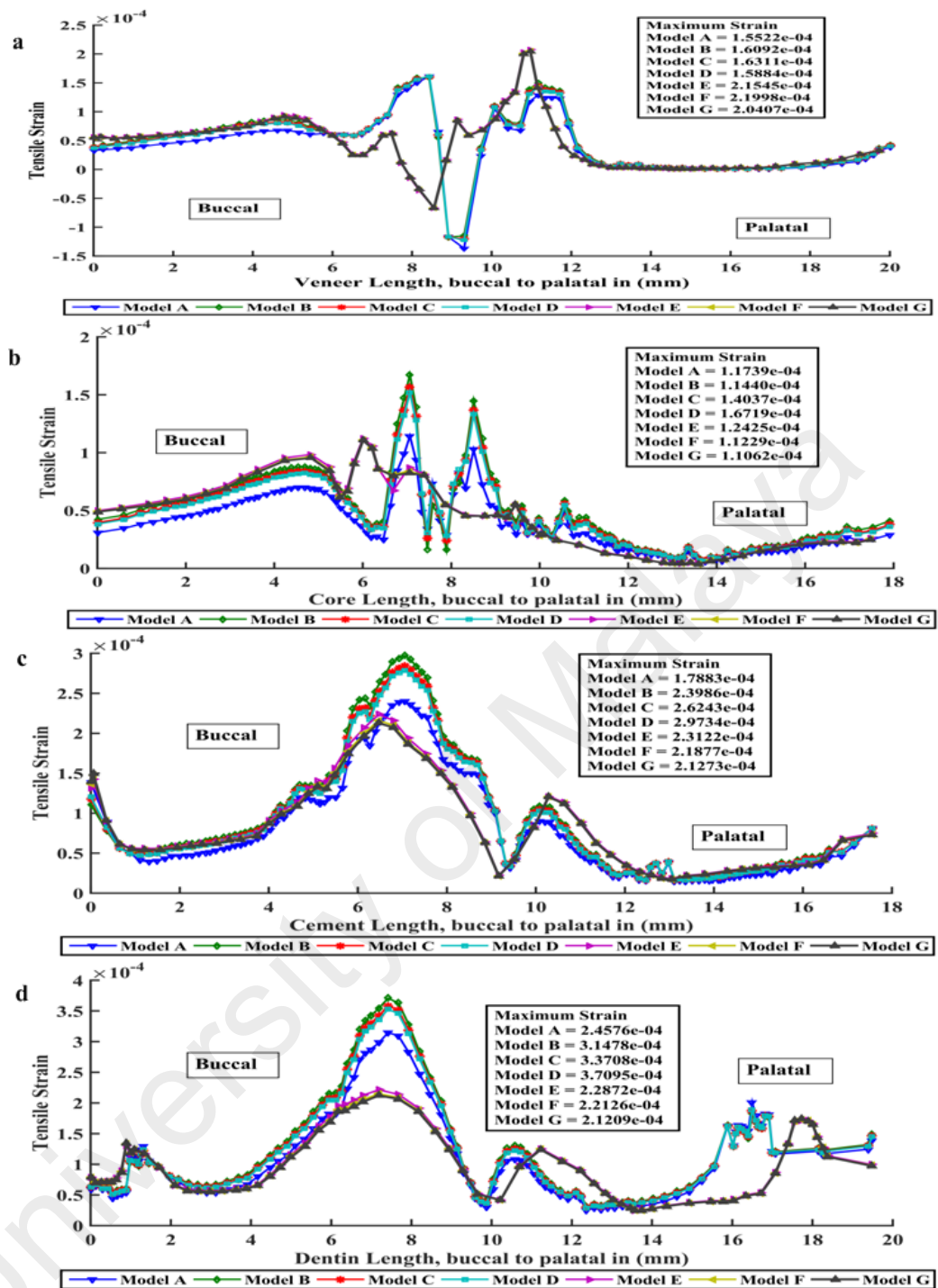


Figure 3.18: The strain maximum distribution within the tooth and veneer-core-cement of all models when loaded obliquely.

3.6.2 Horizontal Load

In the horizontal load direction, the results observed were that the von Mises stress started to develop from the load region at the middle third of buccal crown and slightly decreased towards the inner parts to palatal aspect with von Mises stresses of 217.9 MPa

(Model A), 253.8 MPa (Model B), 245.8 MPa (Model C), 241.9 MPa (Model D), 219.7 MPa (Model E), 234.2 MPa (Model F), 240.7 MPa (Model G), and 126.6 MPa (Model H), respectively as shown in Figure 3.19. The maximum von Mises stress concentration levels were observed in the ceramic core of Models A to D. However, lower von Mises stress concentration levels were observed in the graded multilayered ceramic core (Models E to G) and natural tooth (Model H) as shown in Figure 3.20. In all models, von Mises stress distributions were similar. Slight improvement and reduction were observed in the average von Mises stress values under horizontal loading for graded multilayered ceramic cores (Model E to G) compared with the homogenous zirconia ceramic core (Model A). The magnitude of the von Mises stress distribution under horizontal loading was higher than oblique loading. This indicated that the horizontal load is aggressive and traumatic to the tooth restored ceramic crown and natural tooth in the buccopalatal direction (Figure 3.19 and Figure 3.20) than oblique load.

The maximum tensile stress (maximum principal stress) concentration levels under horizontal loading were observed in the veneer and ceramic core of Models A to D at the loading points buccal. However, lower tensile stress concentration levels were observed in the graded multilayered ceramic core (Models E to G) and natural tooth (Model H) (Figures 3.21 and 3.23). Additionally, the maximum compressive stress concentration levels were observed in the veneer and ceramic core of models A to D. However, lower compressive stress (minimum principal stress) concentration levels were observed in the graded multilayered ceramic core (Models E to G) (Figures 3.22 and 3.24).

The shear stress between the veneer and core interfaces of the graded multilayered models (Models E to F) was lower than in the single-layer models (Models A to D) (Figure 3.25 in X-Y direction) (in X-Z and Z-Y direction for shear stresses see Appendix A figures 3 and 4). Meanwhile, the shear stress between the core and cement interfaces

of the graded multilayered models (Models E to F) was lower than in the single-layer models (Models A to D). High stress levels were observed directly below the load region for veneer-ceramic core interfaces (Figure 3.26a). Higher stress levels were observed at the ceramic core region in contact with the cement layer (Figure 3.26b). Increased levels of stress concentration were also observed at the margin regions of the ceramic core, including the cervical and proximal regions. Stresses on the dentine-cement interface were considerably lower in Models E to G than in Models A to D (Figure 3.26c).

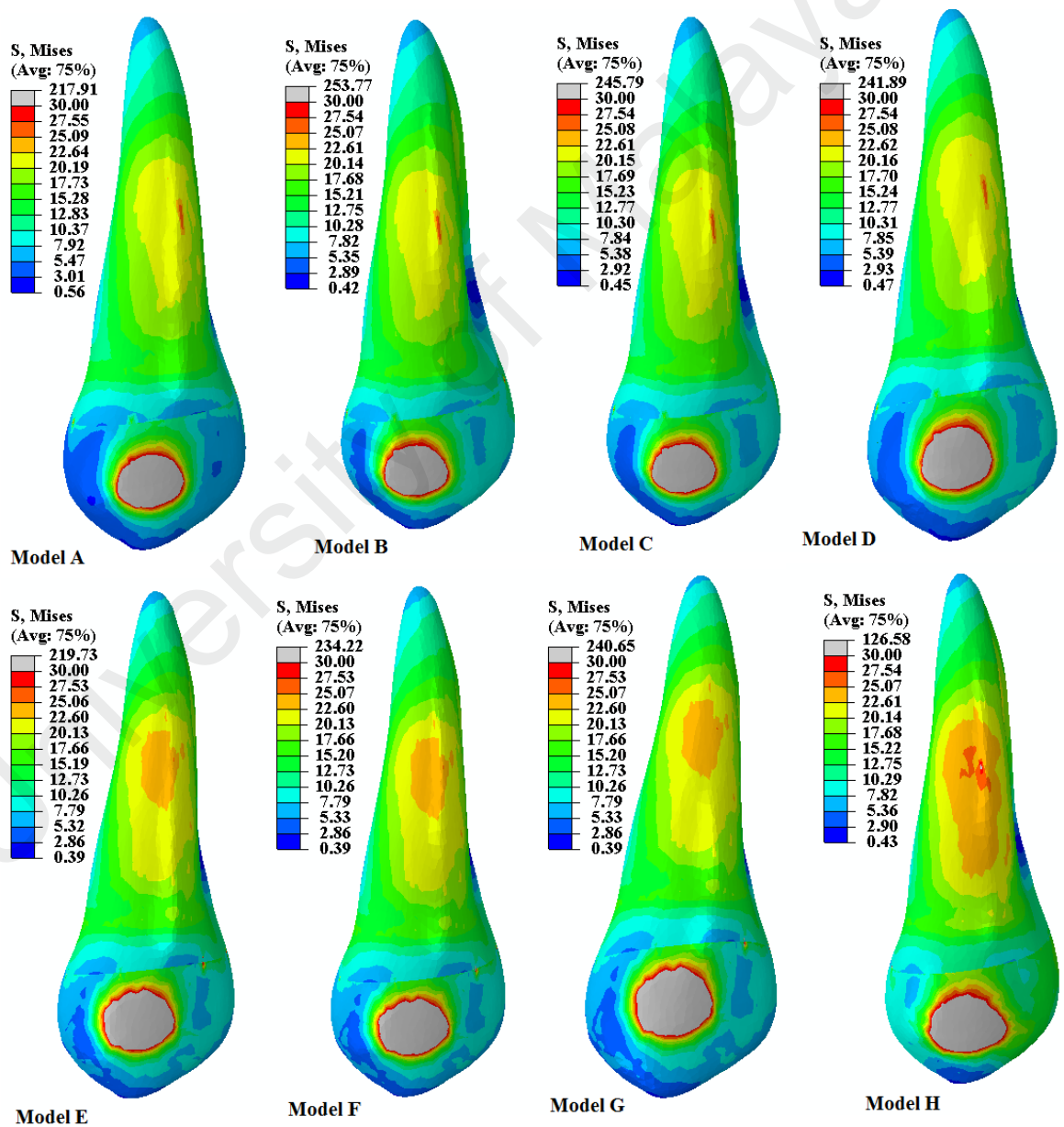


Figure 3.19: Contour plot of the von Mises stress distribution within the tooth and veneer-core-cement of all models when loaded horizontally.

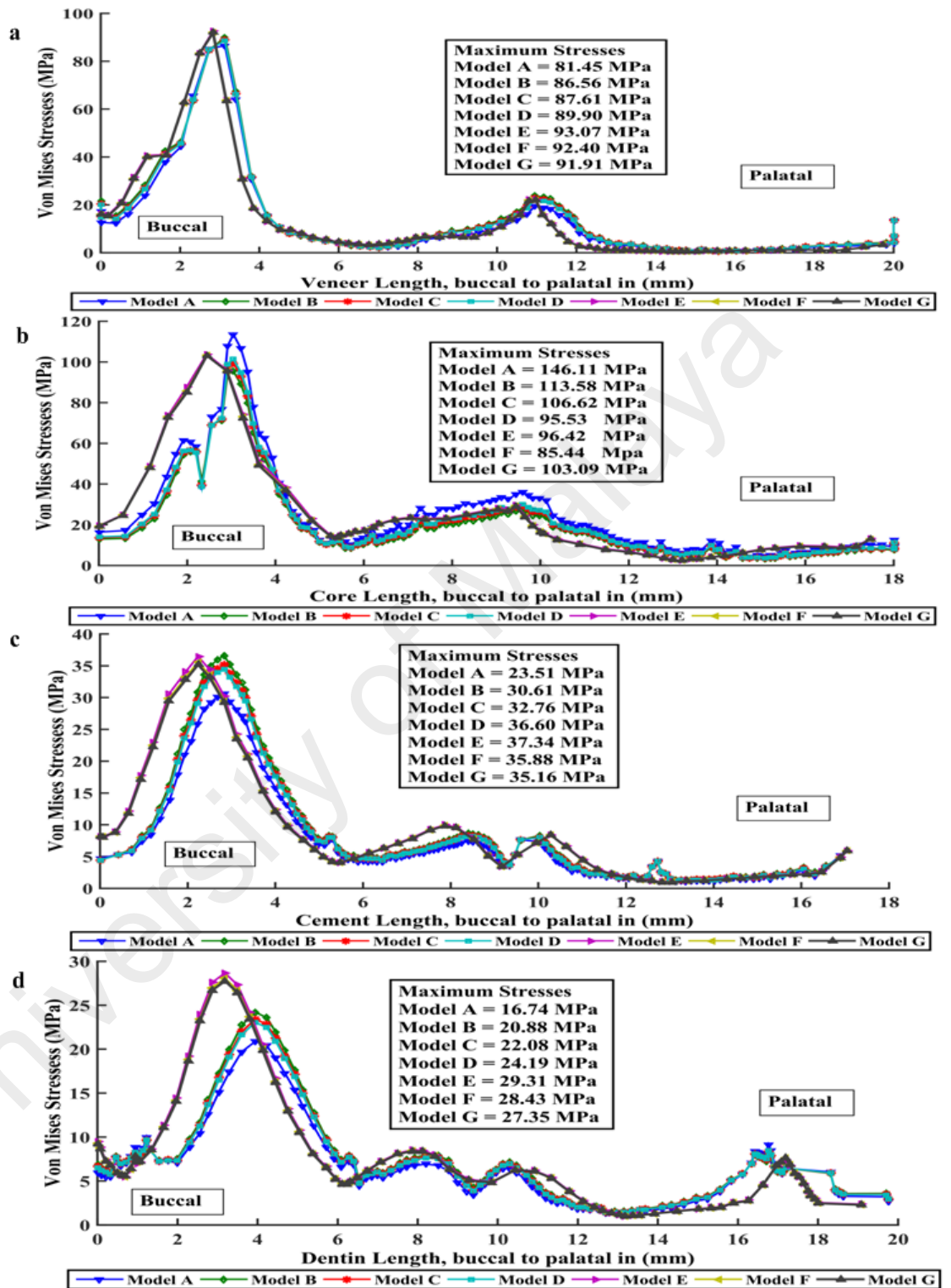


Figure 3.20: The von Mises stress distribution within the tooth and veneer-core-cement of all models when loaded horizontally.

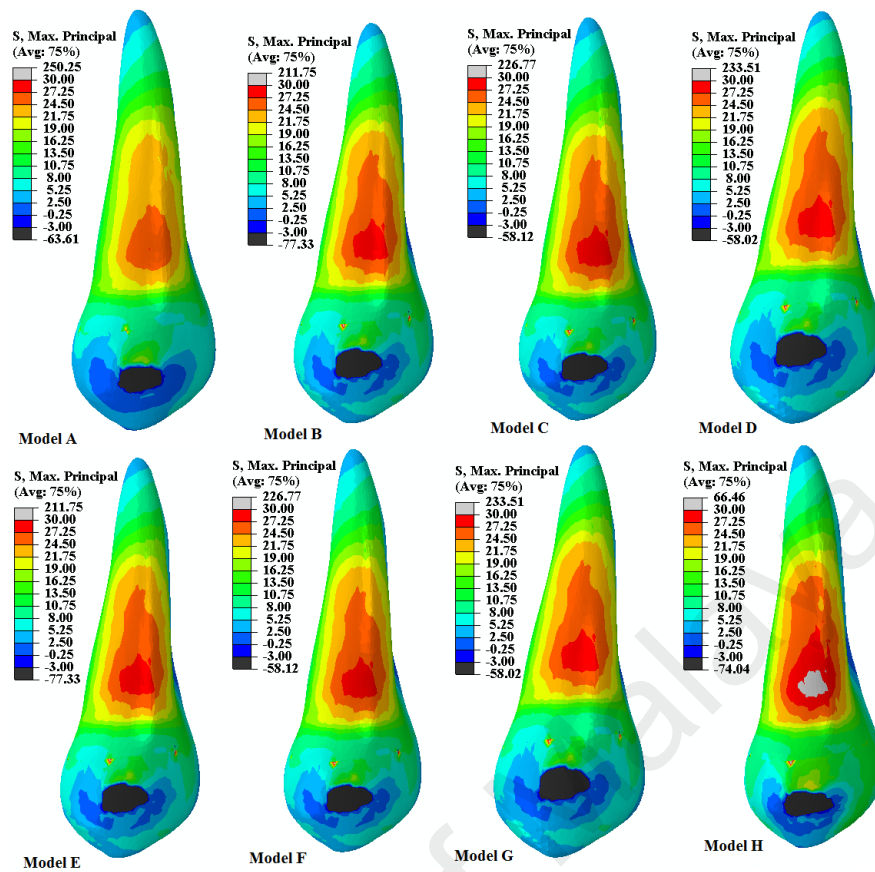


Figure 3.21: Contour plot of the maximum principal stress distribution within the tooth and veneer-core-cement of all models when loaded horizontally.

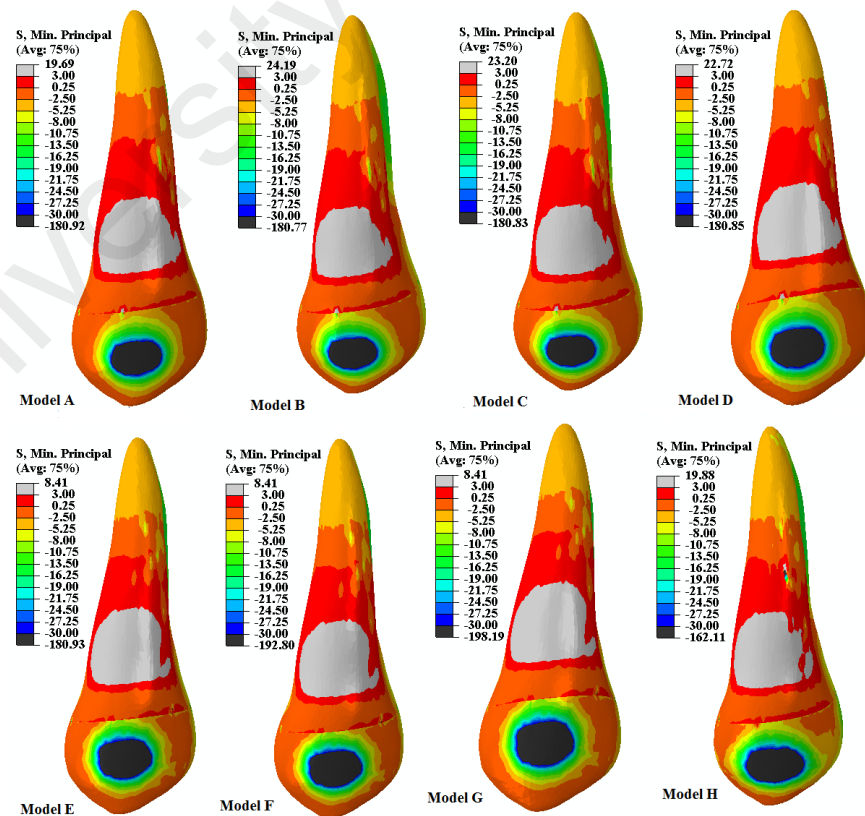


Figure 3.22: Contour plot of the minimum principal stress distribution within the tooth and veneer-core-cement of all models when loaded horizontally.

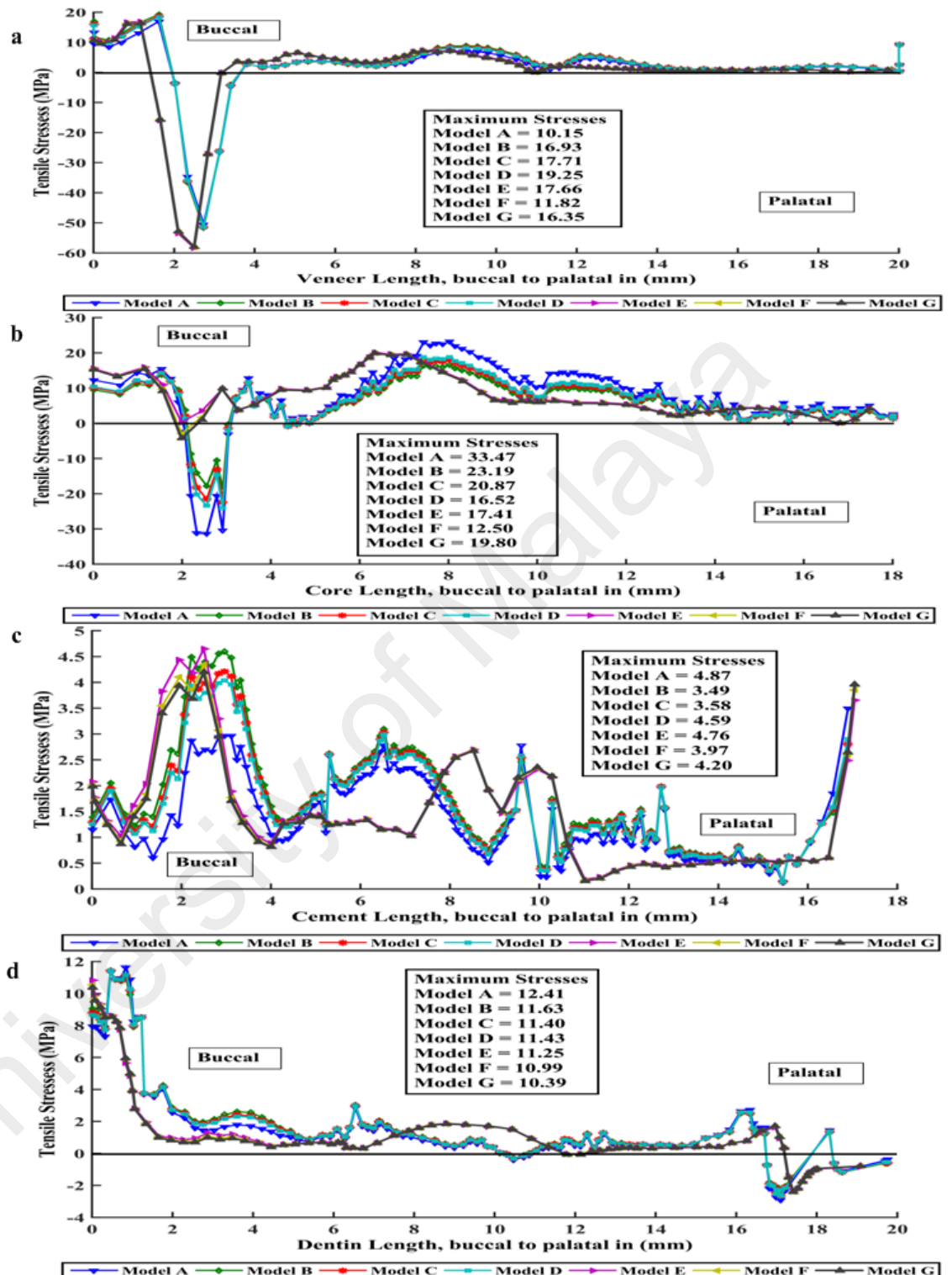


Figure 3.23: The tensile stress distributions within the tooth and veneer-core-cement of all models when loaded horizontally.

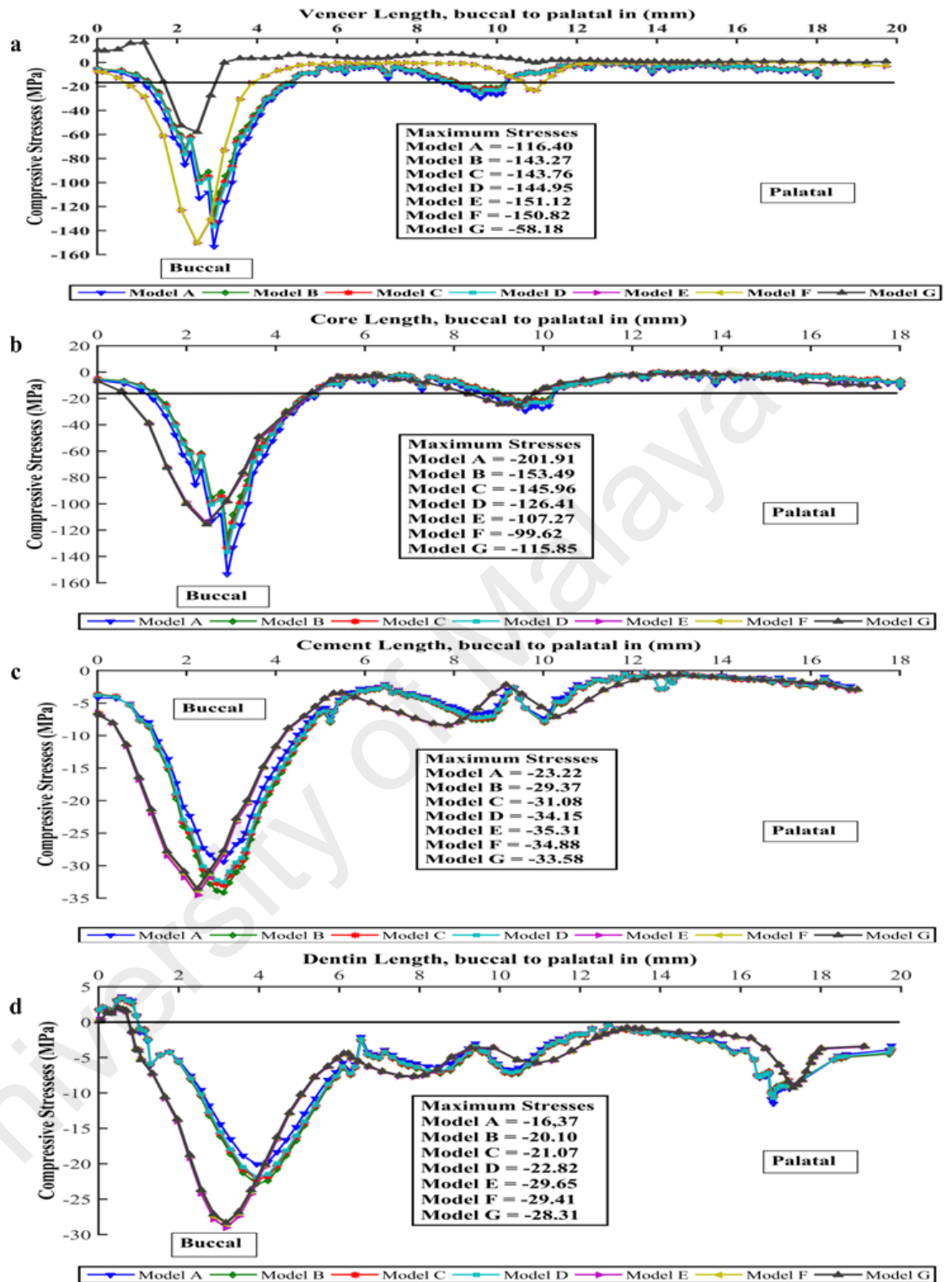


Figure 3.24: The compressive stress distributions within the tooth and veneer-core-cement of all models when loaded horizontally.

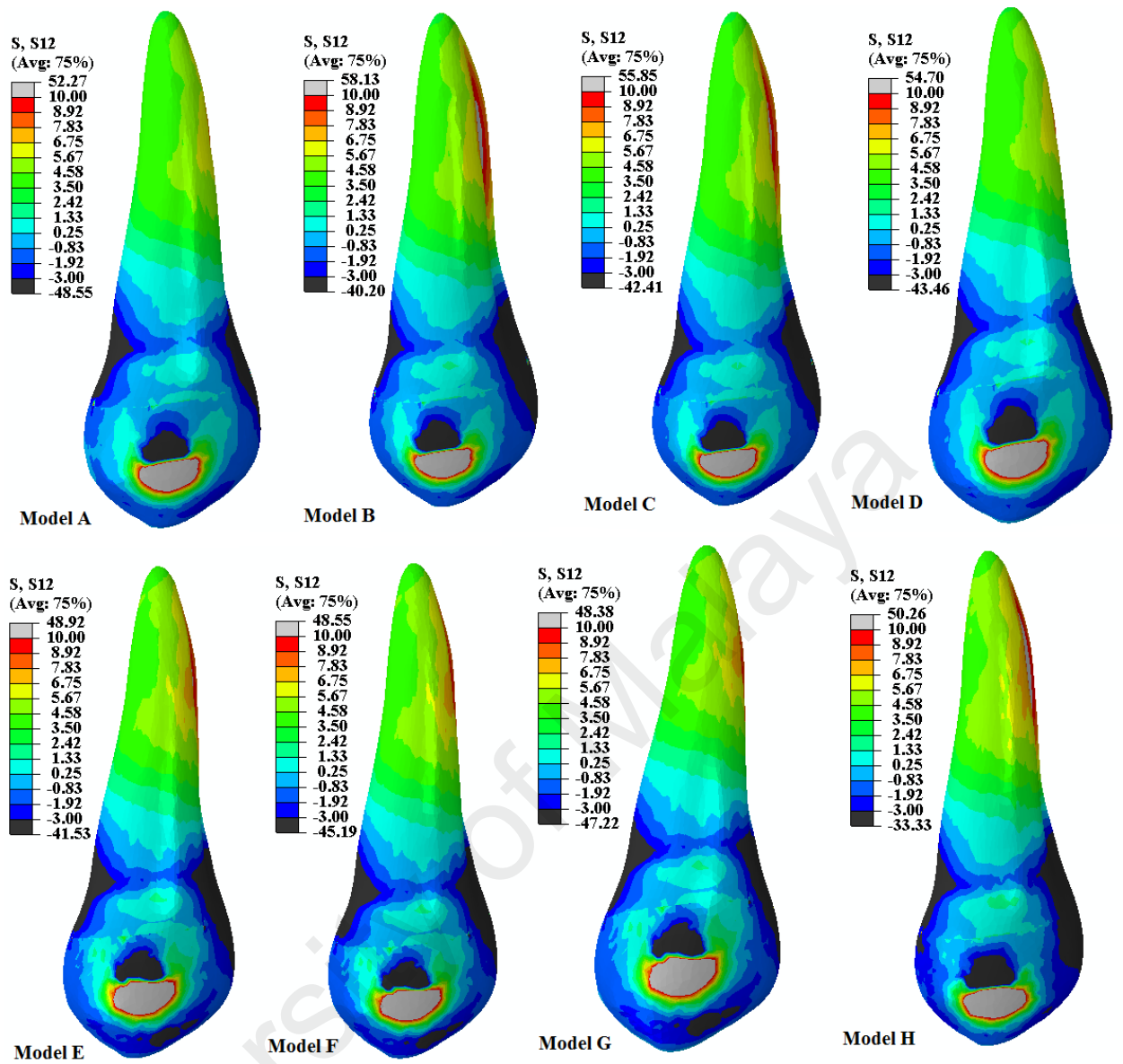


Figure 3.25: Contour plot of the shear stress distributions within the tooth and veneer-core-cement of all models (S12:X-Y direction) when loaded horizontally.

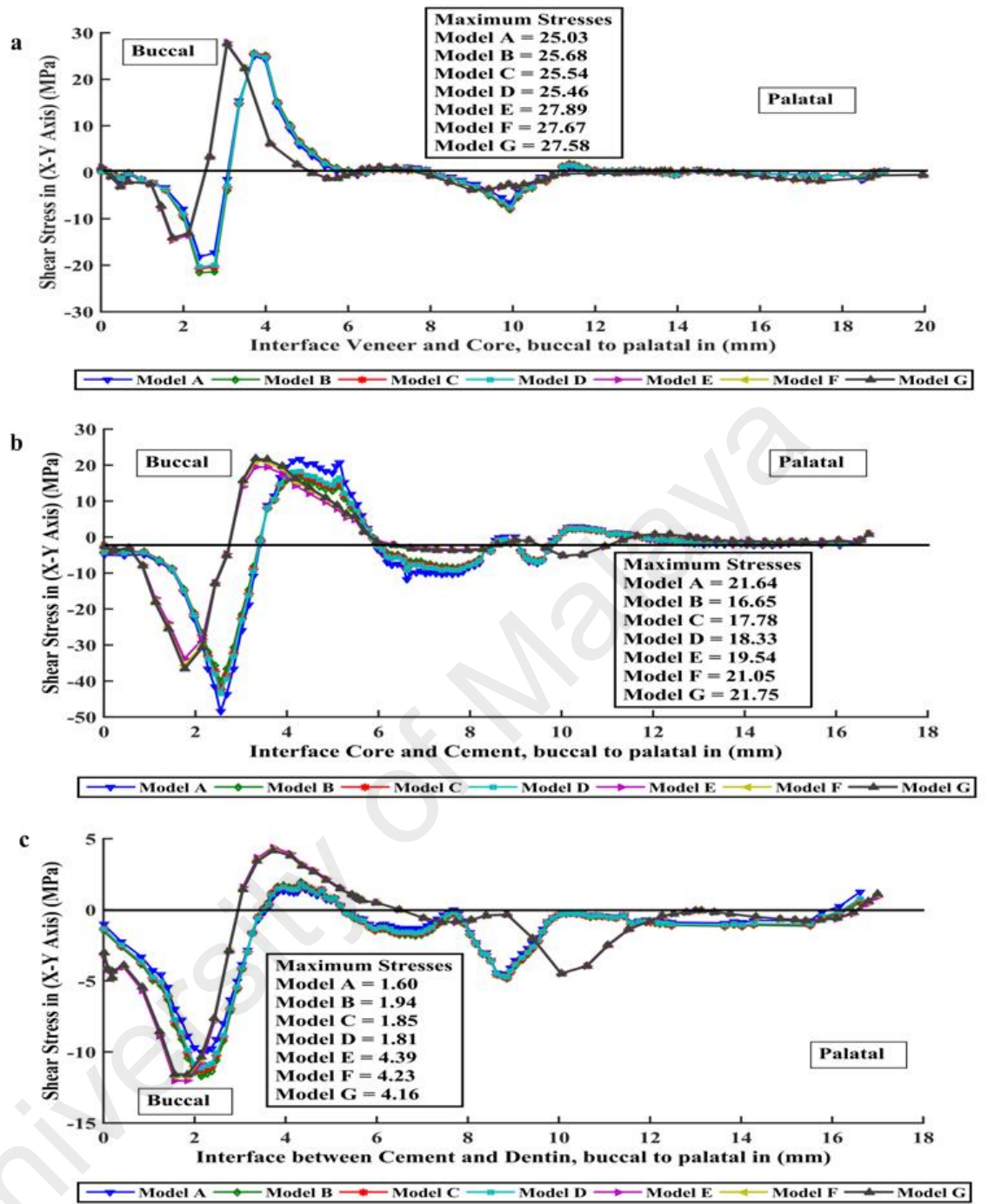


Figure 3.26: The shear stress distributions within the tooth and veneer-core-cement of all models (S12: X-Y direction) when loaded horizontally.

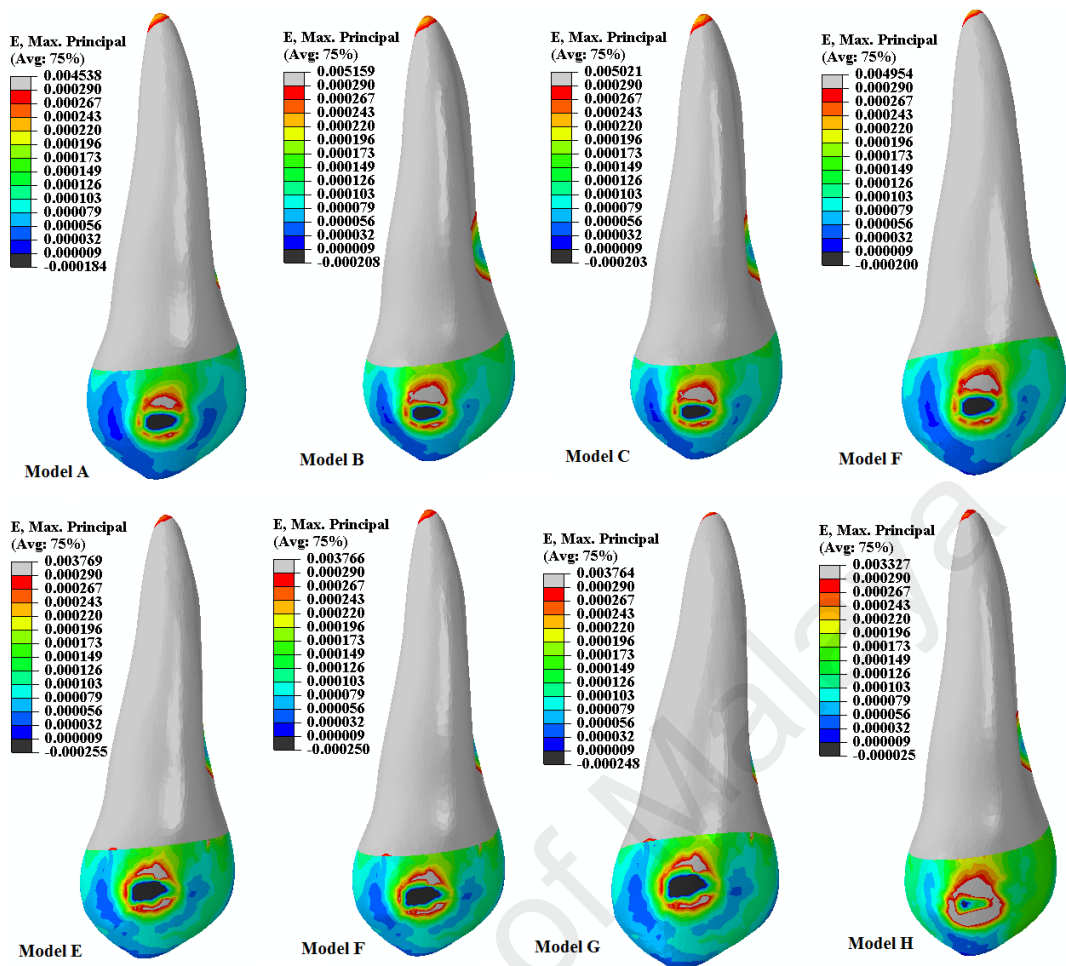


Figure 3.27: Contour plot of the strain maximum distribution within the tooth and veneer-core-cement of all models when loaded horizontally.

Figure 3.27 showed that the strain distribution under horizontal loading for single layer (Models A-D), multilayered graded (Models E-G), and natural teeth. In all models, strain distributions were observed in the buccal aspect of the whole crown. In contrast, the values of minimum strain were observed on the apical part of the root tooth as shown in Figure 3.29. Progressively, strains reduced from the inner to the outer side of the dentine and from the dentine-cement interface towards the occlusal border of the crown. Also, lower values of strain were noted at the cervical zone, whereas the occlusal and middle third of the crown were not nearly free of distortions. In all models, strain distributions were quite similar. Also, all the models restored with single layer ceramic core showed slightly higher strain values when compared with models restored with multilayered

ceramic cores (Models E to G) as seen in Figure 3.28. (a, b, c, and d) in all veneer-core-cement-dentine parts as shown in Figure 3.27.

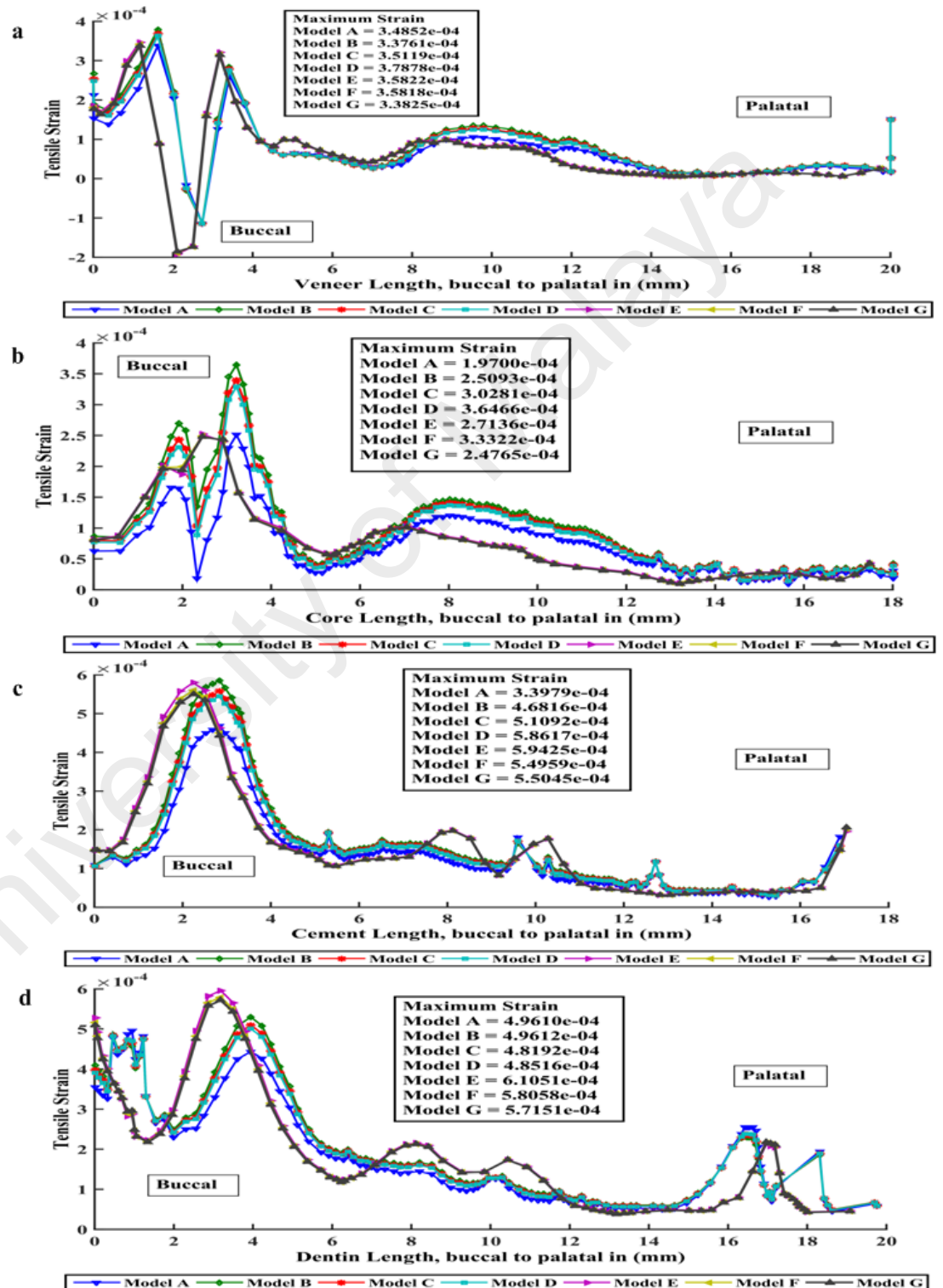


Figure 3.28: The tensile strain distribution within the tooth and veneer-core-cement of all models when loaded horizontally.

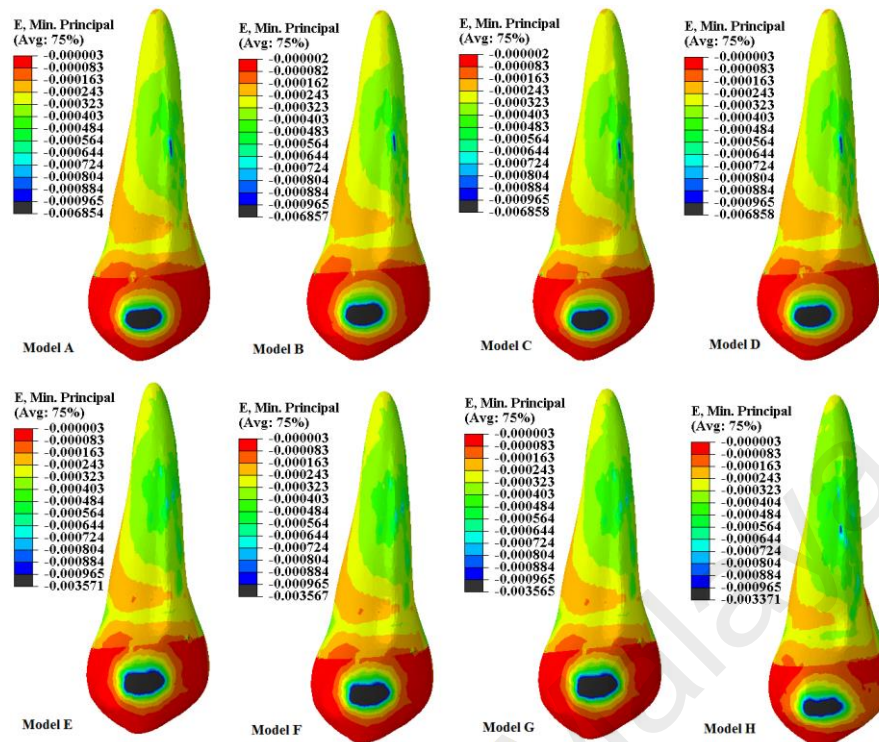


Figure 3.29: Contour plot of the strain minimum distribution within the tooth and veneer-core-cement of all models when loaded horizontally.

The results of the analysis of stresses using a 3D FE model pattern of an upper premolar revealed that the stress concentrated around the region of the buccal cervical of the crown, where the horizontal load was applied at middle third of the buccal aspect. The distribution of stress did not note in the cross-sectional view expand beyond the palatal aspect but stayed within the buccal area. The concentrated stresses around the buccal cervical area due to the horizontally loaded force may powerfully cause distortions.

3.6.3 Vertical Load

Although the von Mises stress distribution was almost similar when the tooth was loaded vertically (Figure 3.30), the magnitude of the von Mises stress distribution was higher than oblique loading, but lower than horizontal loading. This is again reflected in the von Mises stresses distributions in all models where the maximum stresses were 182.9 MPa (Model A), 168.9 MPa (Model B), 172.2 MPa (Model C), 173.7 MPa (Model D),

235.9 MPa (Model E), 222.7 MPa (Model F), 221.9 MPa (Model G), and 147.5 (Model H) as shown in Figure 3.30. The maximum von Mises stress concentration levels were observed in the ceramic core of Models A to D. However, lower von Mises stress concentration levels were observed in the graded multilayered ceramic core (Models E to G) and natural tooth (Model H) as shown in Figure 3.31. In all models von Mises stresses distributions were similar. Slight improvement and reduction were observed in the average von Mises stress values under vertical loading for graded multilayered ceramic cores (Model E to G) compared with the homogenous zirconia ceramic core (Model A). The magnitude of the von Mises stress distribution under vertical loading was higher than oblique loading. This indicated the vertical load is traumatic at buccal and palatal cusps to the tooth restored ceramic crown and natural tooth in the buccopalatal direction (Figure 3.30 and Figure 3.31) than normal masticatory load.

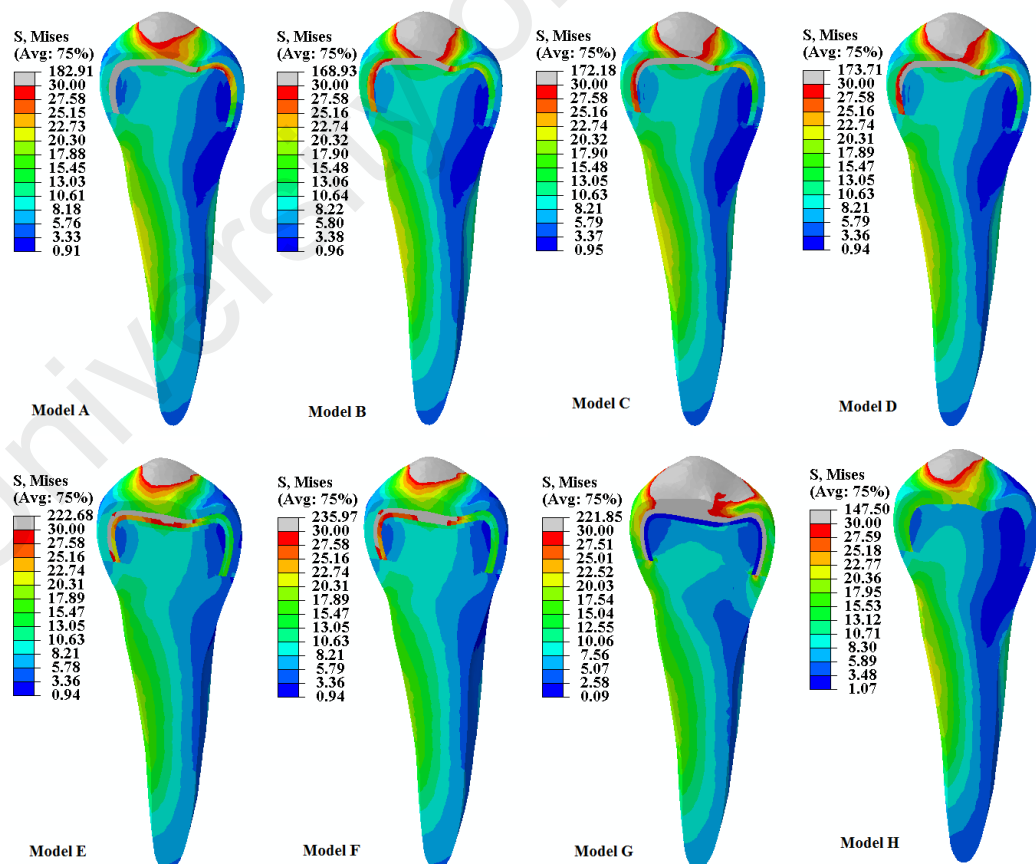


Figure 3.30: Contour plot of the von Mises stress distribution within the tooth and veneer-core-cement of all models when loaded vertically.

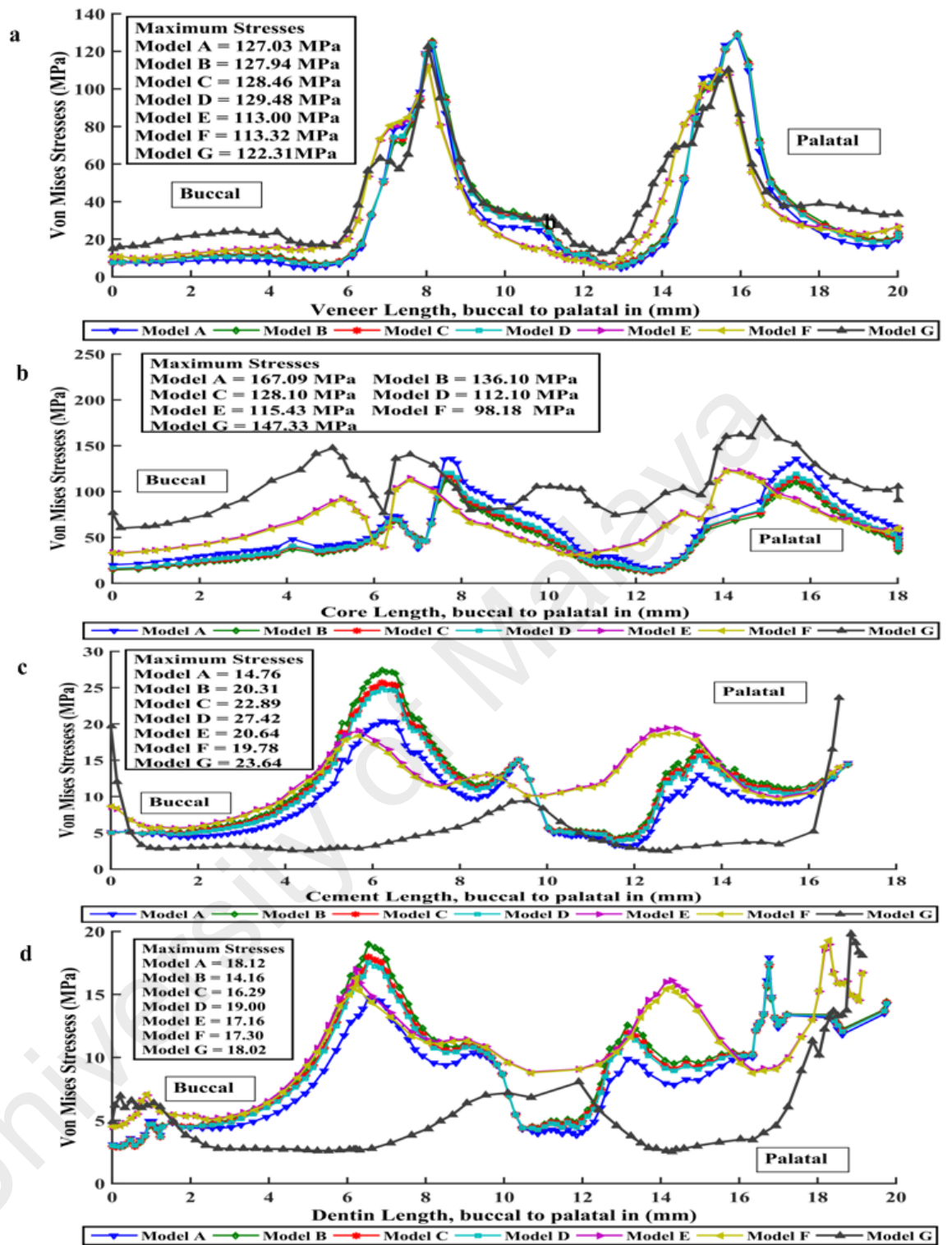


Figure 3.31: The von Mises stress distribution within the tooth and veneer-core-cement of all models when loaded vertically.

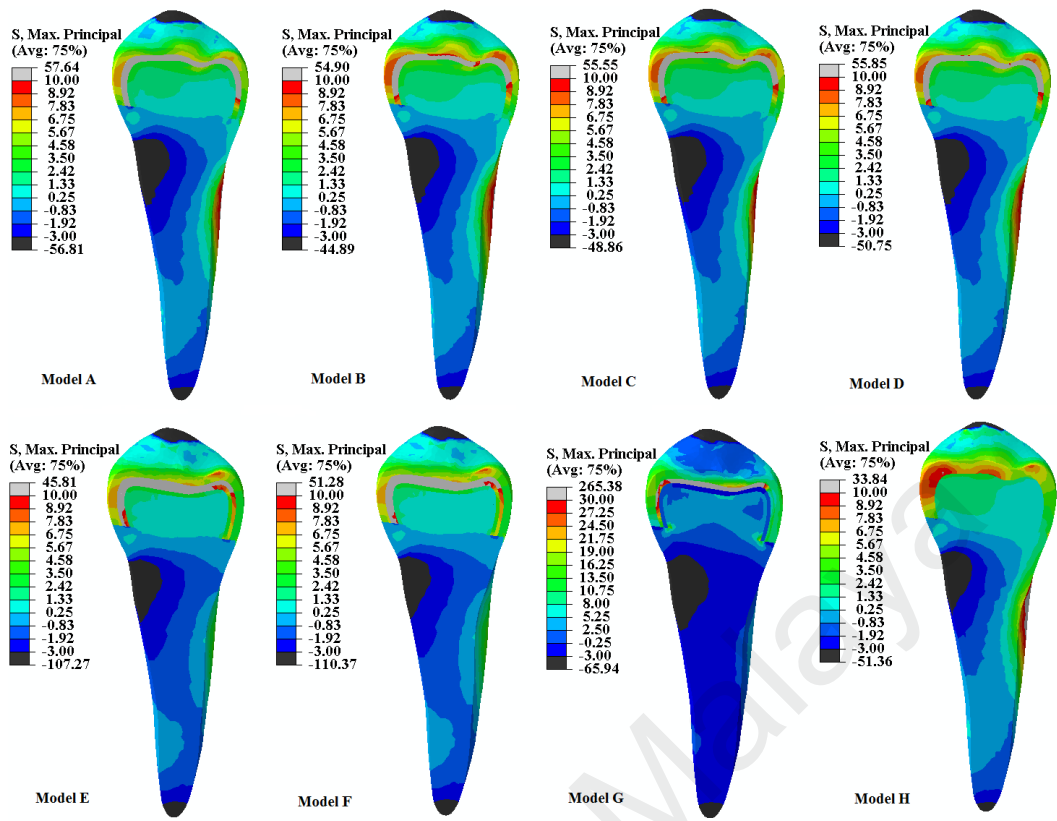


Figure 3.32: Contour plot of the maximum principal stress distribution within the tooth and veneer-core-cement of all models when loaded vertically.

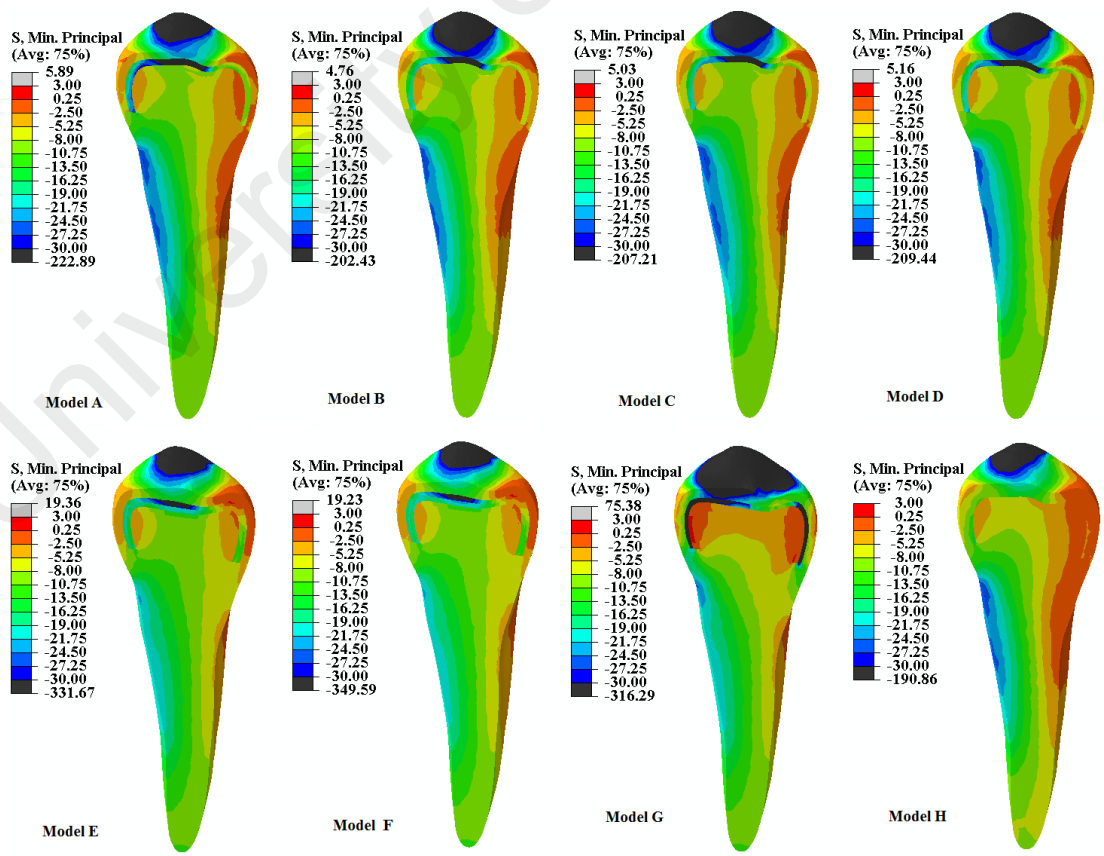


Figure 3.33: Contour plot of the minimum principal stress distribution within the tooth and veneer-core-cement of all models when loaded vertically.

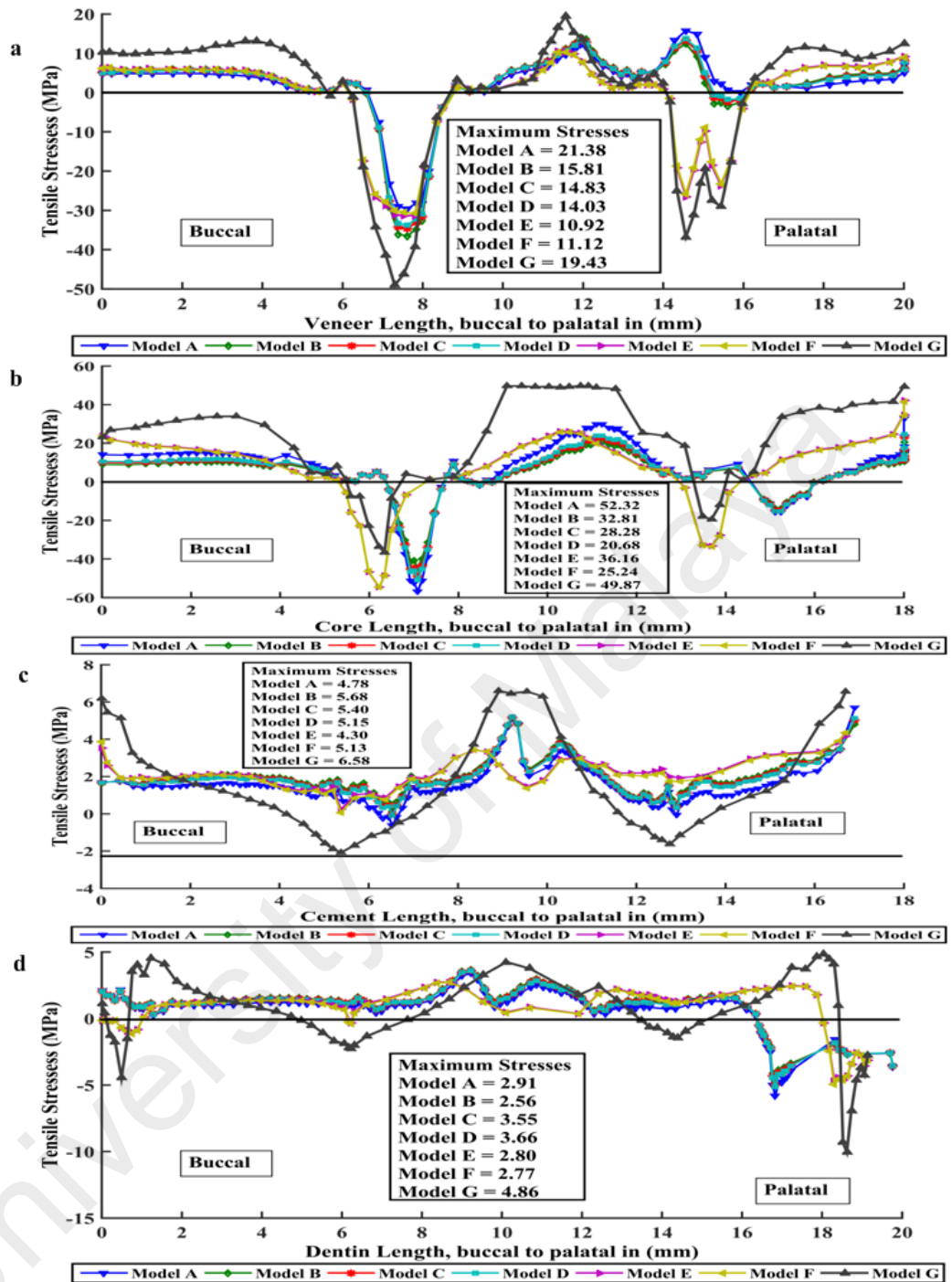


Figure 3.34: The tensile stress distribution within the tooth and veneer-core-cement of all models when loaded vertically.

The maximum tensile stress (maximum principal stress) concentration levels under vertical loading were observed in the veneer and ceramic core of Models A to D at loading point buccally. However, lower tensile stress concentration levels were observed in the graded multilayered ceramic core (Models E to G) and natural tooth (Model H) (Figures 3.32 and 3.34). Additionally, the maximum compressive stress concentration levels were

observed in the veneer and ceramic core of models A to D. However, lower compressive stress (minimum principal stress) concentration levels were observed in the graded multilayered ceramic core (Models E to G) (Figures 3.33 and 3.35).

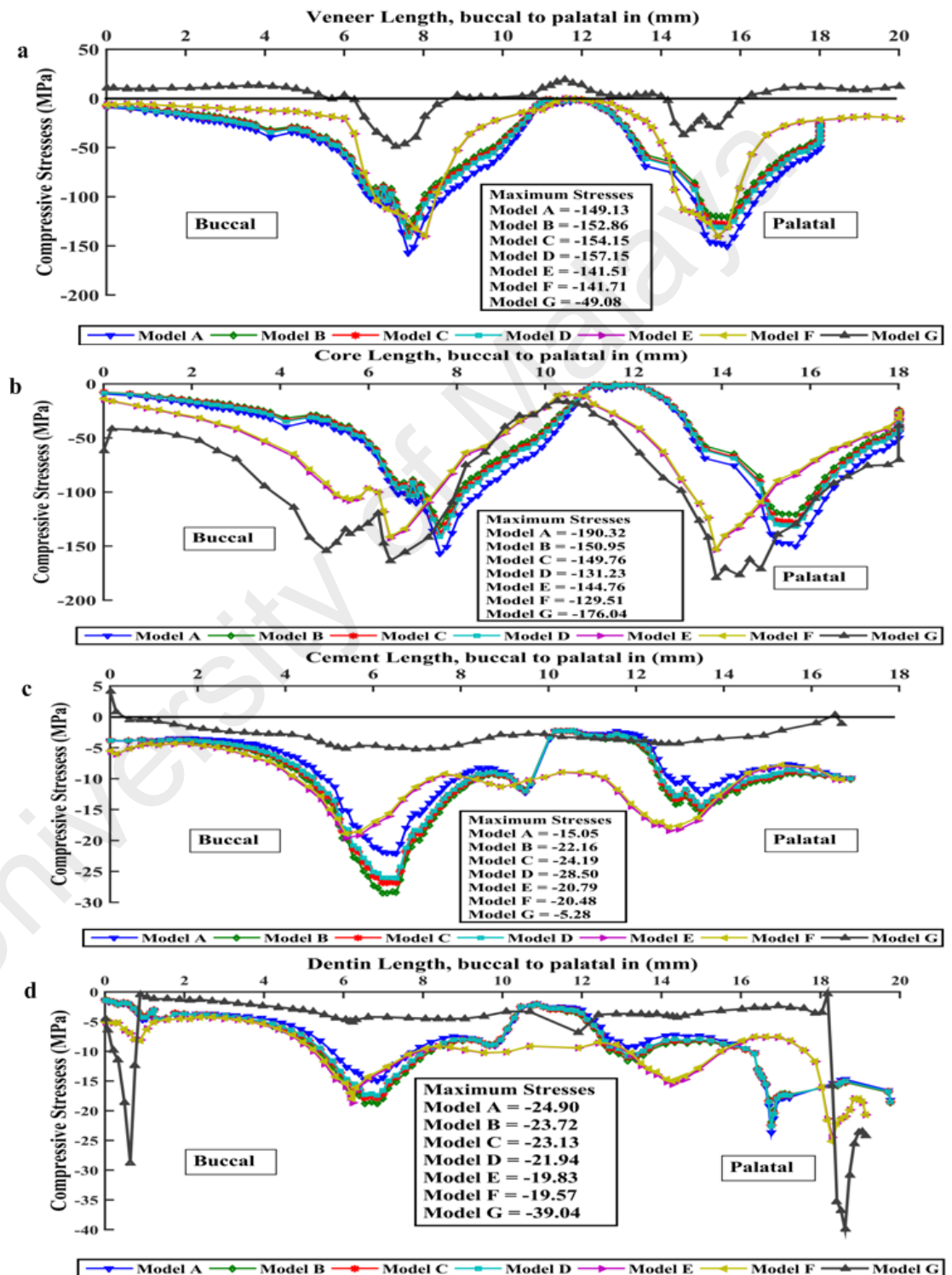


Figure 3.35: The compressive stress distribution within the tooth and veneer-core-cement of all models when loaded vertically.

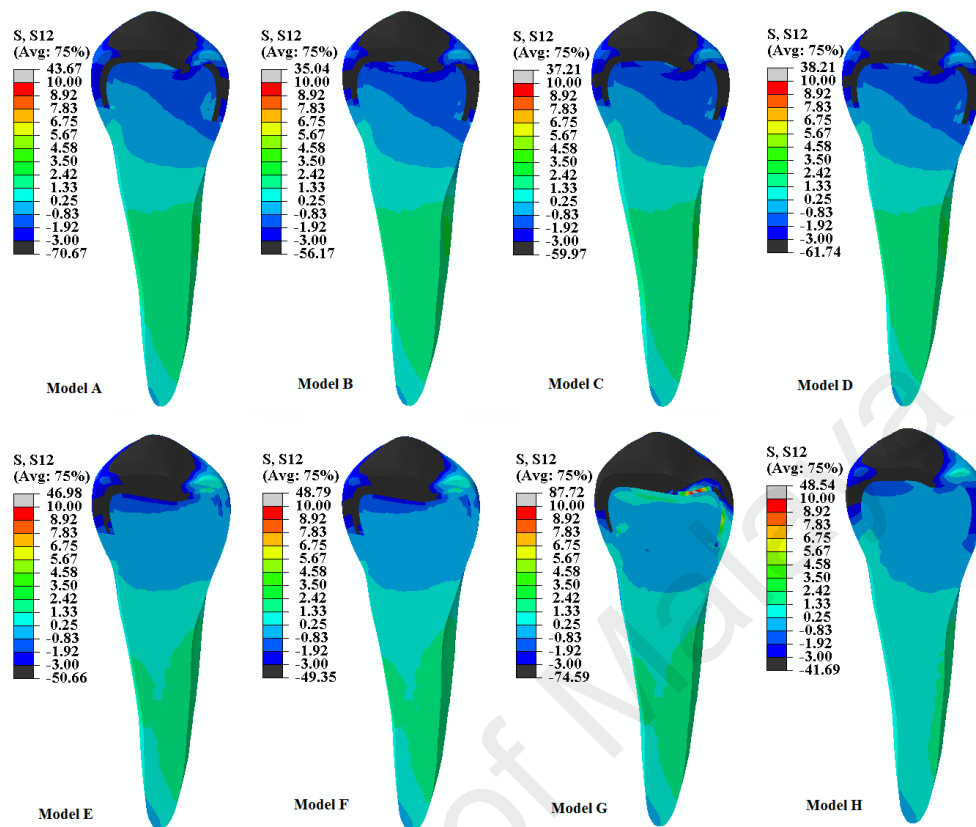


Figure 3.36: Contour plot of the shear stress distribution within the tooth and veneer-core-cement of all models (S12: X-Y direction) when loaded vertically.

The shear stress between the veneer and core interfaces of the graded multilayered models (Models E to F) was lower than in the single-layer models (Models A to D) under vertical loading (Figure 3.36 in X-Y direction) (in X-Z and Z-Y direction for shear stresses see Appendix A figures 5 and 6). Meanwhile, the shear stress between the core and cement interfaces of the graded multilayered models (Models E to F) was lower than in the single-layer models (Models A to D). High stress levels were observed directly below the load region for veneer-ceramic core interfaces (Figure 3.37a). Higher stress levels were observed at the ceramic core region in contact with the cement layer (Figure 3.37b). Increased levels of stress concentration were also observed at the margin regions of the ceramic core, including the cervical and proximal regions. Stresses on the dentine-cement interface were considerably lower in Models E to G than in Models A to D (Figure 3.37c).

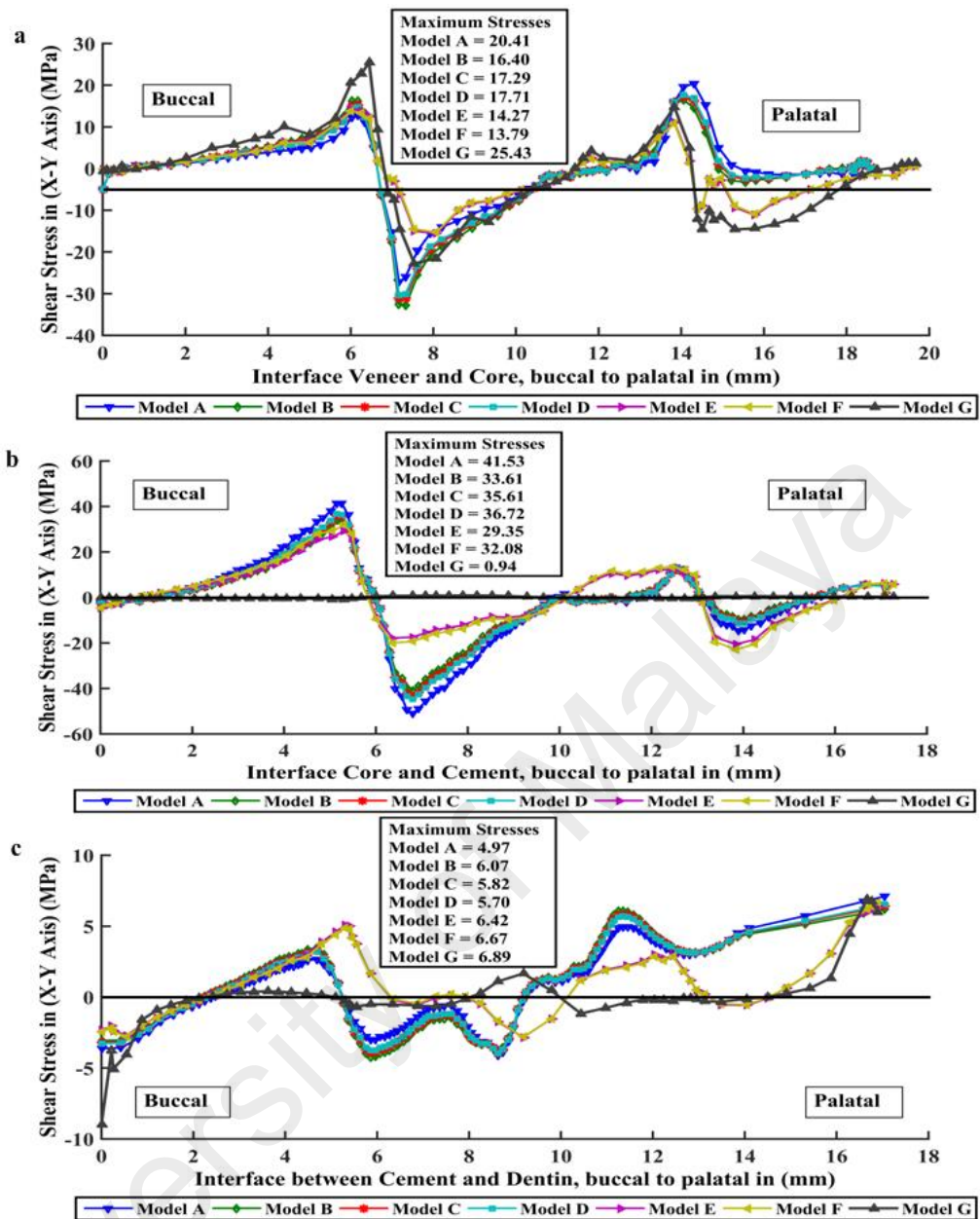


Figure 3.37: The shear stress distribution within the tooth and veneer-core-cement of all models (S12: X-Y direction) when loaded vertically.

Figure 3.38 showed that the strain distribution under vertical loading for single layer (Models A-D), multilayered graded (Models E-G), and natural tooth. In all models, strains distributions were noted in the occlusal aspect of whole crown. In contrast, the values of minimum strains were observed on the apical part of the tooth root as shown in Figure 3.39. Progressively, strains increased from the upper to the lower part of the dentine and from the dentine-cement interface nearby the occlusal border of the crown.

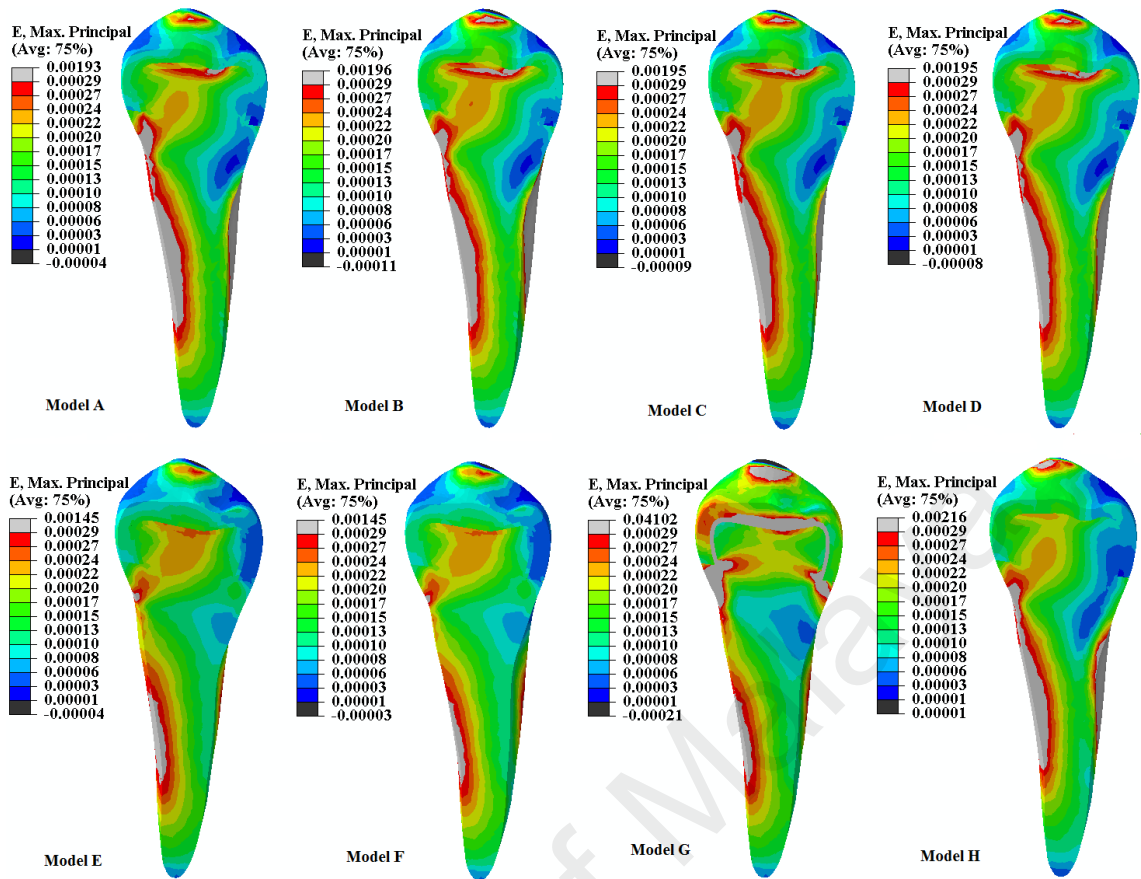


Figure 3.38: Contour plot of the strain maximum distribution within the tooth and veneer-core-cement of all models when loaded vertically.

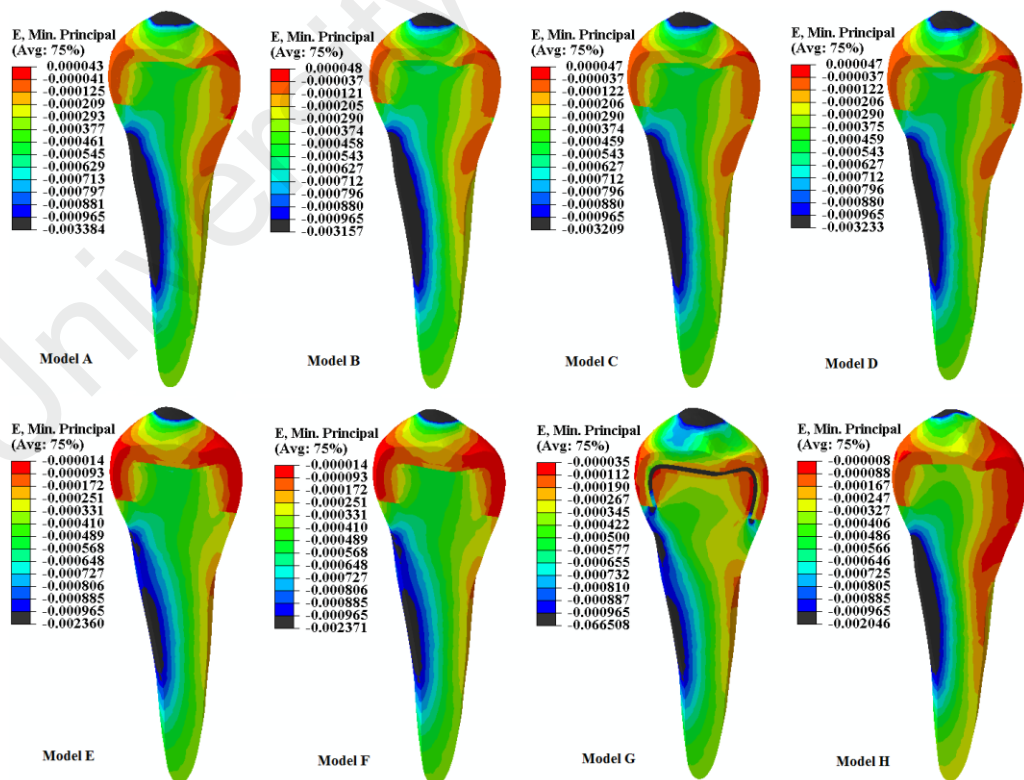


Figure 3.39: Contour plot of the strain minimum distribution within the tooth and veneer-core-cement of all models when loaded vertically.

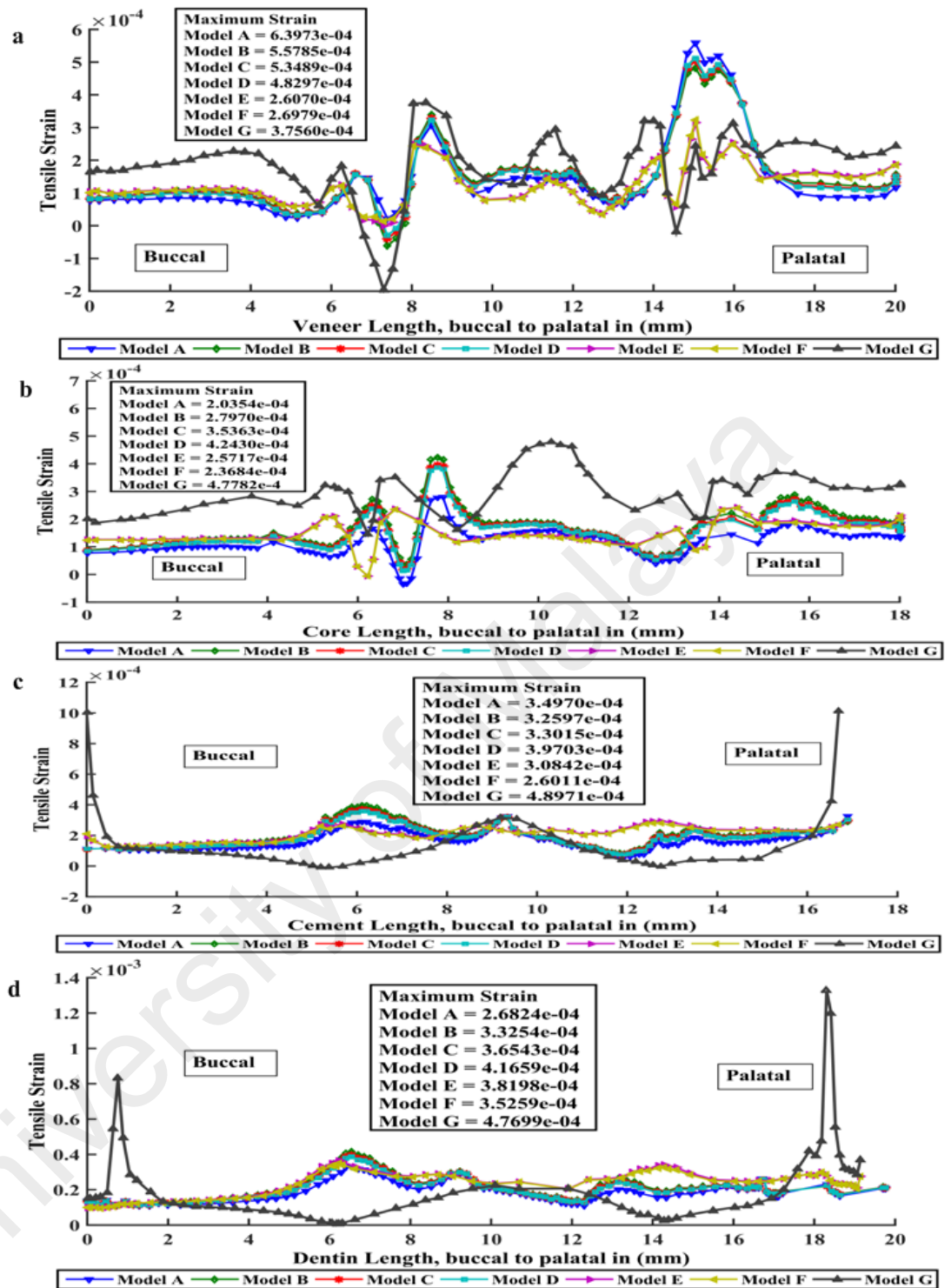


Figure 3.40: The tensile strain distribution within the tooth and veneer-core-cement of all models when loaded vertically.

The minimum strains shown at the cervical area of the crown, whereas the occlusal and middle thirds of the crown were nearly free of distortions. In all models, strain distributions were quite similar. Also, all the models restored with single layer ceramic

core showed slightly higher strain values when compared with models restored with multilayered ceramic cores (Models E to G) as seen in Figure 3.40. (a, b, c, and d) in all veneer-core-cement-dentine parts as shown in Figure 3.39.

The improvement in the average von Mises stress values under oblique, horizontal and vertical loadings for graded ceramic cores (Model B-G) compared to homogenous zirconia (Model A) ceramic cores was calculated in percentage as shown in Table 3.3. The reduction in the average von Mises values by graded one layer ceramic cores compared to zirconia ceramic cores is highlighted in Table 3.3. The percentage difference in average von Mises stress values amongst the two graded ceramic cores was not high.

Table 3.3: The von Mises stress value on tooth restored with various types of ceramic core loaded under different loading directions.

Models	Percentage difference in average Von Mises values (MPa)		
	Oblique loading	Horizontal loading	Vertical loading
A	139.70	217.91	182.91
B	139.30	253.77	168.93
C	139.50	245.79	172.18
D	139.60	241.89	173.71
E	109.90	219.73	222.68
F	109.80	234.22	235.97
G	109.80	240.65	221.85
H	61.50	126.58	147.50

3.7 Discussion

Few methodologies have been utilized for investigation of dental crown restorations and teeth undergone to the action forces, among which computerized tomography (CT) image and the FEM are the technique of preference. This technique is one of the most informative concerning the analysis of 1D, 2D and 3D frameworks subjected to several extrinsic actions. The efficiency of this technique is explained by the approval of results taken by numerical data analysis depend on many experimental and clinical observations and conclusions (appears to be of the most interest to understand sensitive problems related to the restorative dental material choice and optimal application steps definition).

CT permits both the acquisition of bone morphology and measurement of bone density in a living individual. Consequently, it is estimated that the data could be used for 3D FE modelling with material properties put exactly to reflect the detailed morphology and internal bone structures. Accordingly, 3D FE modelling from CT images is of great assistance in understanding the individual simulations of the stress values and distribution of stress. Specially, issue has been directed relating temporomandibular joint defects, enamel lesion, structural design of prosthetic devices, teeth loss, and optimum implant designing (Magne, 2007; Shahmoradi and Swain, 2016).

Recently, a few studies have reported on the optimum design of all-ceramic crowns based on the geometry of a real tooth obtained from computerized tomography (CT) scan and analyzed by FEA. FEA enables simulation of any case, however, the accuracy and validation of the outcomes depend on the build of a suitable model (Magen, 2007; Uddanwadiker, 2012; Shahmoradi and Swain, 2016).

Soares et al., (2008a, and 2008b) suggested that the combination of strain gauge non-destructive test and experimental mechanical destructive tests (fracture resistance test)

with numerical FEM analyses exhibit to be relevant and important for the biomechanical analysis and behaviour of dental restorations.

A simulation computer is clearly unattainable to involve all of the parameters that happened in the oral environment. The applicability of FEA results to oral conditions relate to the similarity among the dimensions, geometry, type of load application of the models, material data, and the natural tooth. In this study, the estimations the 3D tooth patterned model were made after the built-up of the sound natural premolar by CT scan as described in detail in this chapter 3 section 3.2. It was calculated that the materials utilized in the models were isotropic, homogeneous, and linearly elastic, but they had various tensile and compressive strengths. Unfortunately, the properties of tooth structures are anisotropic and are not homogeneous as enamel (because of its prismatic structure) or dentine (because of its capillary morphological structure).

A load position and applied load played significant roles in stress concentration in complex anatomical structures such the full crown which influenced the results of the FEA researches. In the majority of teeth in *in vitro* examinations, a static load was directly applied to the occlusal surfaces of the crown (Imanishi et al., 2003; Ozen et al., 2007; Coelho et al., 2009b). This was a considerable facilitation of true occlusal loads. In this work, three different loads: oblique (to simulate the occlusion mastication), horizontal (to simulate the traumatic force), and vertical (to simulate the bruxism force) were applied on the 3D- FE models created at three different location bases of the natural contact relationship. This innovative method allowed us to reproduce complex and variable loads applied on a tooth during mastication, horizontal, vertical and to determine the 3D stresses in the tooth. In this work, the oblique load was applied on buccal cusp not on palatal cusp, this is a limitation in this study, it is difficulted to applied oblique load on small area (2.5 mm^2) on the palatal cusp by FEA. Further investigations are needed to compare the

models constructed from CT scan and analysed by FEA with applying oblique load on palatal cusp.

In this study, the results revealed that the oblique occlusal load simulates the mastication force better and lower stresses than horizontal and vertical forces. It shown that tensile stresses were concentrated on the buccocclusal side outer on the surfaces of the veneer and core and the compressive stresses were concentrated in the inner surfaces of veneer and core for all models. It had been reported that when a load was applied horizontally, the tensile stress occurred in the buccocervical area of the inner part of the veneer and core, and when the load was applied vertically, the tension occurred on the lower surface of the buccal and palatal functional cusps (Imanishi et al., 2003; Coelho et al., 2009b). This reveals that the oblique and horizontal forces might be attributable to the bending and deformation of the ceramic crown restoration.

FEM models required an experimental validation, that is purposely definitive and prepared. If possible for validation, appropriate laboratory data can also be obtained from the literature in order to reduce cost and time. After validation, the model can be extensively employed for a broad range of studies (Ausiello et al., 2001). The FEA results of this study are in accordance with experimental study carried out by Ausiello et al., (2001), by mean of validation FEA.

In this study, the analysis models composed of the cancellous and cortical bone, periodontal ligament, dentine, enamel, veneer, ceramic core, and cement for real simulation. In this work, there was concentrated on the dental ceramic core (zirconia with/without alumina) with different percentages of its compositions and studying the effects of stress-strain distribution on one layer or two layers of ceramic core with other structures (veneer, cement, and dentine) under static in the three different loads in three different locations.

Generally, the results of this study revealed that the von Mises, tensile, compressive, shear stresses, and strain of all models of synthesised ceramic cores tested during masticatory load simulation (oblique load) in the crown of premolar were lower than the stresses on all models under horizontal and vertical loads. Also, the stress concentrations were noted on the inner surface of the ceramic crown under the functional cusp. Subsequently, the thin-walled crown in premolar teeth made of zirconia with/without alumina and alumina-toughened-zirconia were capable of resisting occlusal loads, while under the same loads (oblique, horizontal, and vertical loads), porcelain veneers crowns can fail. This is in accordance with the fatigue testing outcomes of Magne et al., (2010) and Dejak et al., (2012), indicating that thin-walled leucite-reinforced ceramic crown restorations (1.2 mm occlusal thickness) failed under cyclic loading in 100% of cases.

Additionally, it had been reported that the chipping of the porcelain veneer is the most common complication of zirconia crowns (Lorenzoni et al., 2010). Factorial analysis performed by Rekow et al., (2006) exhibited that the material, cement modulus, load position, thickness of restorative crowns, and crown-tooth supporting are of primary importance in stress magnitude. The higher the tensile strength of the crown material, the thinner can be the crown's walls. The results of this study are in agreement with the studies by Rekow et al., (2006) and Dejak et al., (2012). The study by Coelho et al., (2009b) indicated that an additional variable must be considered in the proximal contours (buccal: palatal ratio).

When there is oblique load, the tensile stresses produced in the proximal and cervical regions were lower than that of horizontal and vertical loads. The magnitude of the tensile stress at the cervical region depends not only on the direction and magnitude of the load but also the leverage effect and resistance. The outcomes of this work are in agreement with studies by Xhohga (1977) and Lee et al., (2002). The malocclusion and bruxism with

intensive lateral occlusal load should generate much greater tensile stress of the teeth and teeth restored ceramic crowns, which may cause a higher prevalence of fracture (Xhohga, 1977; Lee et al., 2002).

In this study, during mastication load simulation, the von Mises stress in the tooth structures decreased with an increase in the Young's modulus of elastic of the used crown material. The previous work carried out by Rosentritt et al., (2009) on fracture performance of 96 restored teeth with zirconia-based, alumina-based, and metal–ceramic crowns demonstrated only one case of fracture. Also, the higher the elastic Young's modulus of the crown material, the lower the equivalent stresses that happened in luting cement and contact tensile and shear stresses at cement–dentine interface. It can therefore be supposed that in clinical conditions, gold and all-ceramic crowns will be more able to withstand marginal microleakage than composite crowns. The study by Vanoorbeek et al., (2010) confirmed the presumption that demonstrate a worse marginal fit and more frequent debonding of composite crowns than all-ceramic crowns after 3 years of function.

In the present study, the FE stress analysis proposes that the inner surface towards the cement-core interface of the all-ceramic crown within the occlusal area has undergone the highest tensile stress (Anusavice and Hojjatie, 1992; Scherrer and de Rijk, 1993). The fracture initiation sites of the dental ceramic crown are primarily controlled by the location and size of the critical flaw (Thompson et al., 1994; Kelly et al., 1995). Campbell (1989) reported that the support of veneer porcelain is related to Young's modulus and not to the strength of the substructure materials. According to Scherrer and de Rijk (1992), increasing the length of an all-ceramic crown on a die with an elastic modulus of 3 GPa increased the resistance to fracture, while Derand (1974) reported that crown length played only a small role in the fracture resistance.

With single-layer ceramic cores, maximum tensile stress occurred either at the outer surface adjacent to the loading site or in the inner surface of the ceramic core. Location of maximum tensile stress strongly depended on Young's modulus of the supporting substrate. In the current study, when the substrate which simulated dentine had Young's modulus of 18 GPa, maximum principal stress occurred at the outer surface adjacent to the loading site. This high stress level was the dominant cause of failure. With multilayered ceramic cores, the maximum principal stress was located in the subsurface region below the loading site, near ceramic core-cement interface. The presence of such a high bending stress level in a non-rigid supporting substrate (material with low Young's modulus) became the dominant reason which caused a fracture.

In the most multilayered dental crown, Young's elastic modulus of the top ceramic layer is between 70–400 GPa, while that of the substrate polymeric layer is around 18 GPa. The Young's elastic moduli of dental luting cements are commonly between 3–5 GPa (Kelly, 1997). The mismatch in Young's moduli outcomes in high stresses that can give rise to sub-surface radial cracks (Huang et al., 2007b) in the top ceramic layer.

In a ceramic crown restoration, the supporting substrate of the remaining dental structure is dentine with Young's modulus of 18 GPa. A more probable fracture site would be located on the inner surface of the dental crown instead of the outer surface near the biting area. This finding agreed with the numerous investigations on dental crown fractures conducted by Thompson et al., (1994), Anusavice and Hojjatie, 1992, Kelly et al., (1990), Dejak et al., (2012), Ha et al., (2016), Hondo et al., (2016), and Jalali et al., (2016).

In each model, the stress level in the dentine core was of extremely low magnitude (Models A to H). In Models E to H, the stress level was almost neutral and which was lower than that in Models A to D. This phenomenon suggested that the ceramic core

“protected” the dentine core from bearing loads or stresses of significant magnitude. In addition, the ceramic core with significantly higher elastic modulus than the abutment material bore the full brunt of the applied compressive load. The stiff ceramic core material effectively transferred the compressive load to the base of the tooth through the chamfer margin. This compression diversion around the dentine core caused the latter to experience relatively low compressive stress at approximately 0 MPa to 20 MPa. A higher elastic modulus would imply a greater role in absorbing the applied load and diverting it around the tooth abutment. The marginal area should be cautiously designed because of increased tensile stress, although not critical, occurred in this region.

The results of this present study revealed that the stress distribution and strain values were directly effected by the quantity of teeth structures removed and the kind of restorative placed. Also, a force applied to the dental ceramic crown and natural tooth causes structural strain and stress concentration. When this happens within the elastic limit, the ultrastructural integrity of the body is not influenced. Concentrated stress may result in crack formation and propagation causing fracture and structural failure. The linear and direct relation between strain and stress is primarily confirmed by the Young’s elastic modulus, an important mechanical property, essential to understanding the biomechanical behaviour of materials and their relationships (Rees et al., 1994).

In this study, the models restored with single layer ceramic core showed high stress concentration levels and higher strains values when compared with models restored with multilayered ceramic cores under three different loads at three different locations.

Clinically, restored upper premolars teeth may be subjected to buccal and palatal strains, as a result of occlusal force application, that may be related with high levels of stress concentration inside the restoration-tooth complex. However, if the values of strains exceed the maximum resistance ability of tooth structures, the restoration may be

compromised; there may be gap formation at the adhesive interface, microleakage, crack formation, and even fracture (Lohbauer et al., 2003; Soares et al., 2008b).

When the FEA models were restored with graded multilayered ceramic cores (models E to G), the stress distribution patterns were identical to that of an intact non-restored tooth (control model H) in the three various load directions. It may directly depend on the constructed models in this study, which presented a bond between the veneer and core and cement and the dentine of the tooth to simulate the interaction between tooth structure and all components of the dental crown system.

When comparing the behaviour of the constructed models by varying the kind of ceramic cores in single and multilayers in this study, it was observed that the veneer and core and adhesive cement materials promoted minimum values of strain when subjected to occlusal force, as found in the study of Soares et al., (2008b) as well as reduction of the stress levels inside the tooth structure, primarily in the coronal and cervical root dentine.

The differences in stress behaviour among models were observed perhaps due to the variance between the laboratory processed resin and mechanical properties of the ceramic material, which may have had a direct effect on the distribution of stresses resulting from load application (Magne and Belser, 2003). The ceramic restoration model concentrated stresses within the restorations, due to the greater rigidity and high elastic modulus of the ceramic material (Magne and Belser, 2003; Couegnat et al., 2006), as illustrated by FEA models (Figure 3.8). This behaviour was an important factor in the strain values estimated by FE for the graded multilayered models (E to G). Moreover, cores in the models E to G showed higher values of strain when compared with cores of the models A to D, possibly due to the lower rigidity related to the lower elastic modulus of this graded core

material (Magne and Belser, 2003), that also noted by the distribution of stress shown in the models A to D (Figure 3.8) under oblique load than horizontal and vertical loads.

This study described the biomechanical behaviour when calculating the stress-strain distributions in veneer-core-cement-dentine and determining interfaces stress of the tested models at three different load direction. It was noted that intact premolar maxillary and those restored models with single and multilayered ceramic core with adhesive cement material showed a lower stress-strain distribution in oblique load (mastication simulation) than horizontal (traumatic simulation) and vertical (bruxism simulation) loads as shown in Table 3.3. An important factor in this behaviour was the high concentrated stress within the ceramic core material (Holand et al., 2000), when compared with different ceramic cores. This behaviour was observed in this study.

This study has an advantage because of the real sound premolar tooth with the more complexity of anatomical structures and restored with different ceramic cores by using the CT scanning with mimics and 3D-FEA for more complex structures and show complex anatomical details than 2D analysis and 3D analysis. This study, has a limitation as it did not use a strain gauge test and thermomechanical analysis. Further investigation is needed to compare the models constructed in this study by combination FEA and strain gauge test. However, other studies that used strain gauge tests, the same specimen was used for different strain measurements (Toparli et al., 1999; Soares et al., 2008b). Also, a previous study by Toparli et al., (2003) had conducted 3D-FEA on upper premolar to study temperature and thermal stress. Thermal mechanical stresses under masticatory loads may increase the failure rate of the ceramic crown restorations in oral conditions.

It is important to consider the clinical significance of this study. Conservation of tooth structures and the selection of dental ceramic core restoration biomaterials with a

biomechanical behaviour similar to an intact tooth would exhibit to be a fast, and relatively low cost alternative when compared with indirect dental restorations.

3.8 Conclusions

In this chapter, it can be concluded that:

- 1- Compared with single-layer ceramic cores (Models A, B, C, D), FGDCs (Models E, F, G) reduced the levels of von Mises stress, tensile stress, compressive stress, and strain within the tooth which was restored with a multilayered ceramic core when subjected to oblique, horizontal, and vertical loadings.
- 2- Compared with single-layer ceramic cores (Models A, B, C, D), FGDCs (Models E, F, G) reduced shear stress at veneer-ceramic core-cement-dentin interfaces, when subjected to oblique, horizontal, and vertical loadings.
- 3- The CT images with FEM can be used to construct 3D models and to develop a technique to analyze stresses on the tooth, to support the jawbone, and to restore a tooth using the dental crown system (veneer-core-cement) during masticatory load based on FEM. The described method can produce detailed and valid 3D FE models of the maxillary premolar tooth with FGMs of single layer and multilayered dental crown restoration and can also be used for others biomechanical applications. In addition to that, a novel biomechanical clinical diagnostic standard may be clinically utilized based on this study to understand the stress-strain analysis of the dental ceramic crown system.

Significance finding: The finite element method with graded multilayered material approach can be used to design new ceramic cores in order to reduce stress concentrations and interfacial stresses successfully in the dental crown restoration.

CHAPTER 4: SYNTHESIS AND CHARACTERIZATION OF BIOCERAMIC POWDERS FOR DENTAL CROWN RESTORATIONS

4.1 Introduction

All-ceramic dental crowns and bridges exhibit outstanding aesthetics, mimic enamel properties, and have excellent biocompatibility. However, cracks cannot be totally prevented since most are custom fabricated into dental restorations and contain porosity and/or stress risers. Dental crown restorations are still custom made without much fundamental control or engineering of the microstructures whether PFM or all-ceramic frameworks are used. Therefore, crack-tolerant designs or more crack-resistant are still very much needed in dental ceramic engineering (Bayne, 2005). Nevertheless, a challenging attribute of such ceramic materials is their insufficient loading capability that is related to the comparatively low fracture strength and time-dependent strength decrease instigated by progressive crack growth. This happens to be one of the main obstacles restricting the exploitation of ceramic materials to fully replace metals in major dental restorations such as bridges, where tensile stress levels are considerable. The ability to predict and assess the crack initiation and growth in the bridge prior to its construction would offer a significant advantage in providing criteria for an improved design (Li et al., 2006; Zhang et al., 2016a; Zhang et al., 2016b).

The concept of FGM is a new technique for enhancing the performance of dental ceramic core material. Compared with conventional uniform and homogeneous materials, FGM permits the fabrication of materials with various characteristics within the similar material at different interfaces (Shevchenko et al., 2003; Hedia and Mahmoud, 2004; Yanga and Xiang, 2007).

According to Cattani-Lorente et al., (2011), the rough cracks and/or micro-cracks, as have been reported in many researches were usually found in the dental all-ceramic zirconia crown restorations as the varying moisture and temperature of the oral condition may cause low temperature degradation (LTD) for 3–5% volume expansions and 8% shear strain. Under occlusal loads such cracks extend and weaken the mechanical properties or even lead to failure. Moreover, there are other ancillary contributing factors that are unpreventable for all-ceramic dental bridges and crowns in clinical practice, which include impurities, micro-cracks, pores and other defects (Cesaria et al., 2006; Zmudzki et al., 2006; Zhang et al., 2014). Degradation increases when the grains are large in size (Li and Watanabe, 1998; Gremillard et al., 2004) and the Y_2O_3 content is low (Sato and Shimada, 1985). Furthermore, the rate of phase transformations intensifies with increasing aging time and temperature (Chevalier et al., 1999). Residual stresses stimulated by surface preparation may produce additional effects (Deville et al., 2006) and the cubic phase acting as nucleation places for the t–m transformation (Chevalier et al., 2004; Harada et al., 2016).

It has been reported that the addition of CeO_2 or Al_2O_3 to Y-TZP might prevent the t–m transformation (Sato and Shimada, 1985; Tsubakino et al., 1991; Li and Watanabe, 1997; Ross et al., 2001). Moreover, supplementing the zirconia with up to 40 wt.% Al_2O_3 decreased the t–m transformation rate, but did not completely prevent the transformation (Sato and Shimada, 1985). A previous study by Tsubakino et al., (1991) indicated that the inclusion of 1.2–12 wt.% Al_2O_3 to Y-TZP matrix limited the t–m phase transformation to the surface layers. At difference with Tsubakino et al., (1991) and Li and Watanabe (1997) were able to inhibit the t–m phase transformation during hydrothermal degradation of 2Y-TZP and 3Y-TZP by adding 3–5 vol.% Al_2O_3 (Cattani-Lorente et al., 2011; Cattani-Lorente et al., 2016).

Recently, there are many approaches to reduce defects and/or inhibit cracks of zirconia including surface stabilization, particle reduction, and second phase solid oxide dissolution. It has been focused on second phase solid oxide dissolution due to successful developments of dental all-ceramic materials. Many mechanisms exist for second phase oxide to enhance the fracture toughness. It can cause martensitic transformation of zirconia from the tetragonal to monoclinic phase under externally applied stresses. Compressive stresses caused by the stress stimulated transformation at the vicinity of a propagating crack shield the crack tip from the applied stress and thus, enhances the fracture toughness. Crack deflection, micro-crack formation and crack “bridging” can also be involved (Annamaria et al., 2003; Cesaria et al., 2006; Zhang et al., 2014).

Recently, several graded alumina- zirconia ceramic composites have been evolved to limit distribution and crack propagation and to provide improved mechanical properties (Moraes et al., 2004; Santos et al., 2009b; Zhang et al., 2012; Zhang et al., 2014; Zhang et al., 2015; Kaizer et al., 2016; Kohal et al., 2016; Ender et al., 2016).

This chapter describes the experimental methods performed; this chapter also presents the strategies developed to serve as guidelines throughout the study and aid in achieving the desired objectives. An outline of the methodology is presented using a flow chart in Figure 4.1. The outline provides an overview of the whole process and followed by a detailed discussion regarding the procedures and techniques used for experimental. The main activities in this study include synthesis of ceramic powders, characterization, and experiment tests which are described in detail in this chapter.

4.2 Aim of this Chapter

The aim of this chapter was to synthesise bioceramic multilayered graded core and characterization of microstructures, chemical composition, physical, thermal, and mechanical properties.

4.3 Objectives of this Chapter

4.3.1 Synthesis of bioceramic powders for dental crown restorations

4.3.1.1 To synthesise a ceramic core of 3Y-TZP with/without alumina.

4.3.1.2 To synthesise graded glass $\text{SiO}_2\text{-Al}_2\text{O}_3\text{-K}_2\text{O-Na}_2\text{O-CaO-Tb}_4\text{O}_7$ system.

4.3.2 Characterization of microstructure and chemical compositions of synthesised ceramics

Field emission scanning electron microscopy (FESEM) and Energy dispersive X-ray (EDX) were used to evaluate topographically and surface elemental compositions. X-ray diffraction (XRD) was used to determine the crystalline and amorphous material in natural or synthetic samples.

4.3.3 Physical, mechanical and thermal properties evaluation

In order to validate the synthesised ceramics for dental crown restoration as a ceramic core, the physical, mechanical, and thermal properties were evaluated.

4.3.3.1 Physical and mechanical properties: namely,

The density (ρ), the volume of shrinkage, porosity, Vickers hardness (H_v), compressive strength, Young's modulus (E), and strain were measured, which were based on pure zirconia and alumina.

4.3.3.2 Thermal properties

Thermomechanical analysis (TMA) analyzer was used to evaluate the coefficient of thermal expansions of the synthesised ceramic specimens.

4.4 Null Hypothesis of this Chapter

The null hypothesis of this study there was no improvement of a new synthesised bioceramic and technique by using the layering technique with FGM to obtain the multilayers of ceramic cores produced from different ceramic powders with different percentages to less or avoid a crack in all-ceramic dental crown restorations.

4.5 Materials and Methods

4.5.1 Materials

Eleven different ceramic powders with different particles size (micro-nano particles size) were used in this study as shown in Figures 4.2, 4.3, 4.4, 4.5, 4.6, 4.7, 4.8, 4.9, 4.10, 4.11, and 4.12. The ceramic phases were 99.99% pure. The specifications of ceramic powder materials used to prepare multilayered ceramic cores were listed in Table 4.1 and Table 4.2.

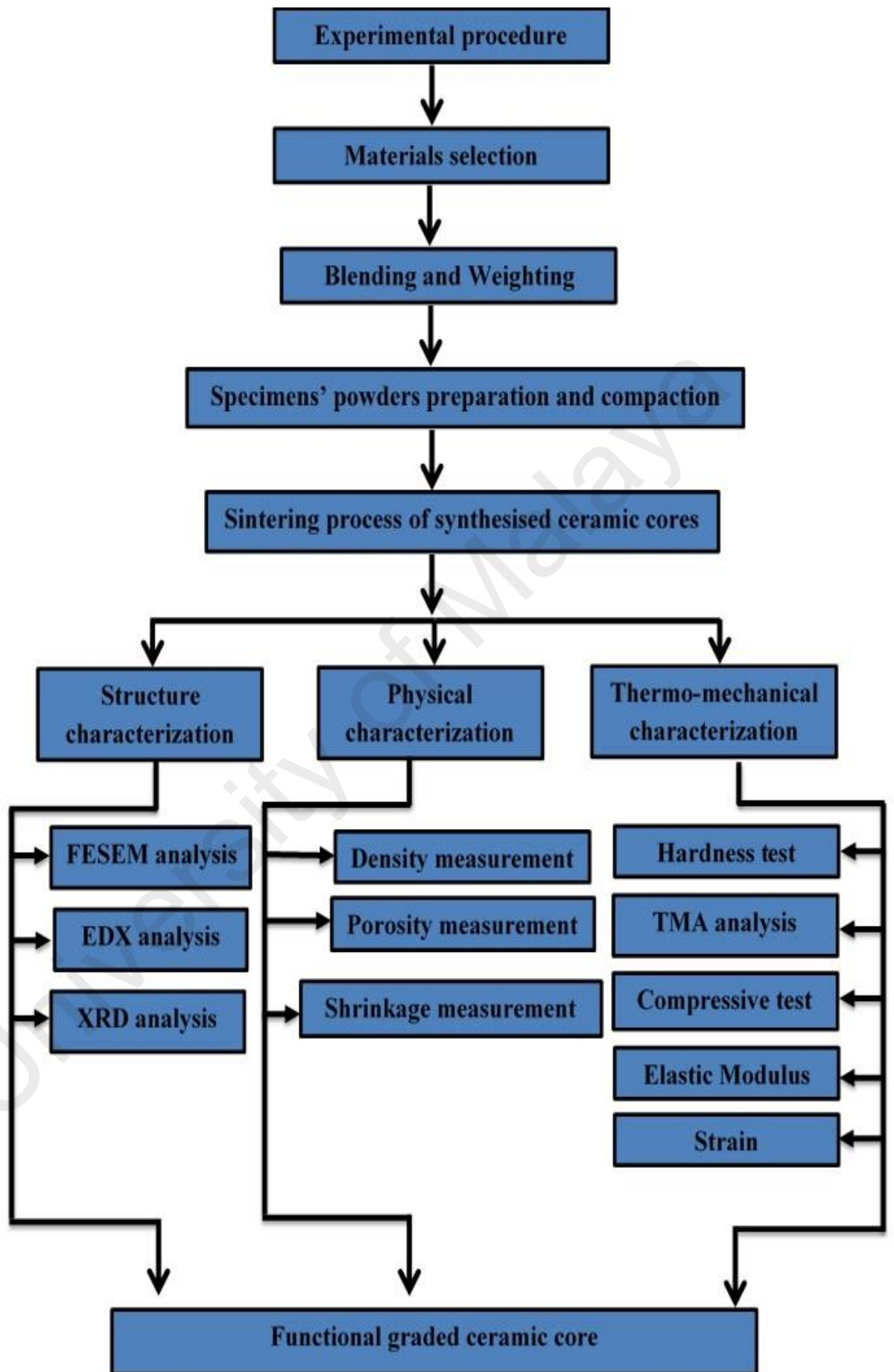


Figure 4.1: A flow chart of the experimental methodology.



Figure 4.2: Zirconium oxide (micro-size). **Figure 4.3:** Zirconium oxide (nano-size).

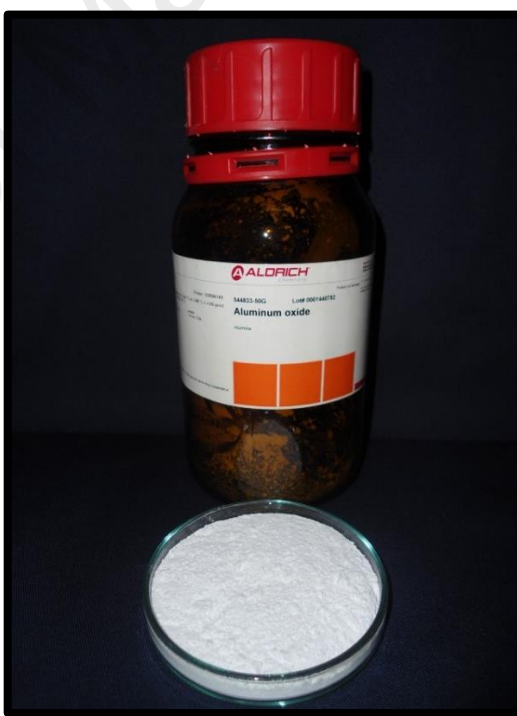


Figure 4.4: Aluminum oxide (micro-size). **Figure 4.5:** Aluminum oxide (nano-size).



Figure 4.6: Yttrium (III) oxide (nano-size). **Figure 4.7:** Magnesium oxide (nano-size).

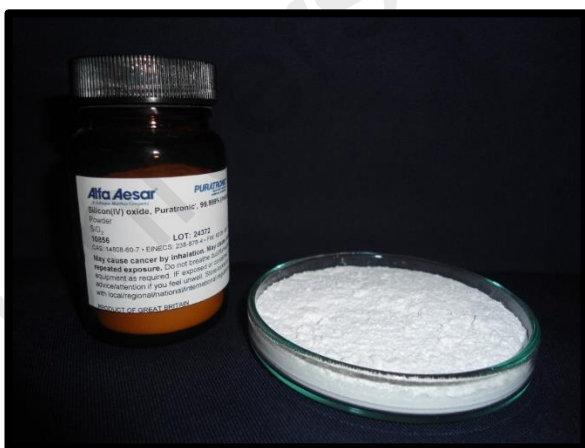


Figure 4.8: Silicon (IV) oxide (nano-size). **Figure 4.9:** Potassium oxide (micro- size).



Figure 4.10: Calcium oxide (micro-size).



Figure 4.11: Barium Sodium oxide (micro-size).

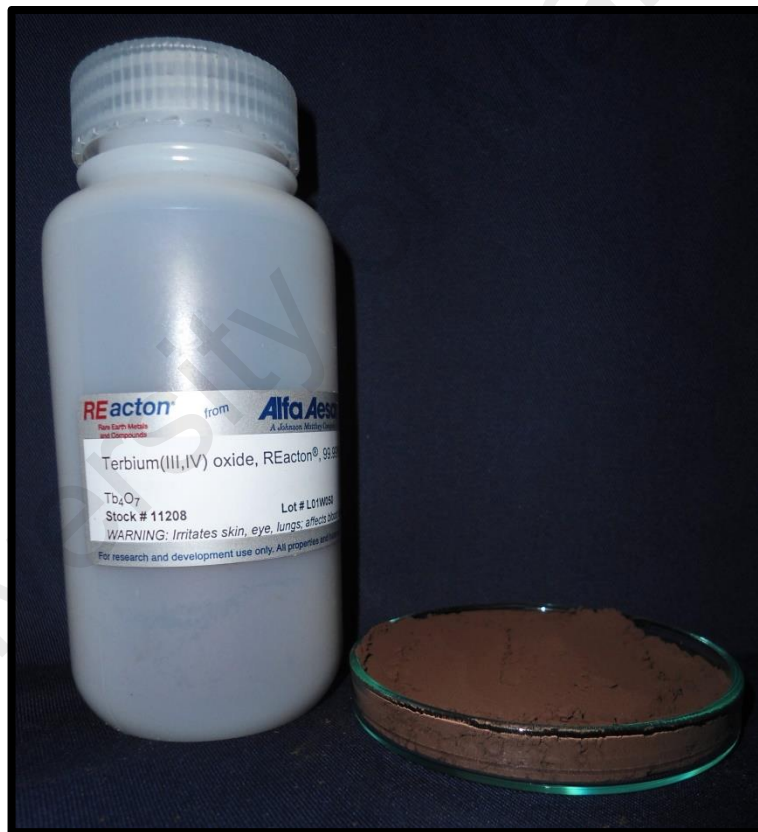


Figure 4.12: Terbium (III, IV) oxide (micro powder).

Table 4.1: Specification of materials used in the study.

Properties	Aluminum oxide	Aluminum oxide	Magnesium oxide	Yttrium(III) oxide	Zirconium (IV) oxide	Zirconium (IV) oxide
Formula	Al ₂ O ₃	Al ₂ O ₃	MgO	Y ₂ O ₃	ZrO ₂	ZrO ₂
Physical state	Powder, white	Nanopowder, white	Nanopowder, white	Nanopowder, white	Nanopowder, white	Powder, white
Particle size	~10µm	<50 nm	<50 nm	<50 nm	<50 nm	~5 µm
Purity	~99.8%	~99.99 %	99.999%	~99.99 %	~99.99 %	~99.8 %
Density	4.000 g/cm ³	4.000 g/cm ³	3.580 g/cm ³	5.01 g/cm ³	5.89 g/cm ³	5.89 g/cm ³
Molecular weight	101.96 g/mol	101.96 g/mol	40.3 g/mol	225.81 g/mol	123.22 g/mol	123.22 g/mol
Boiling point	2980°C	2980°C	3600°C	4300°C	5000°C	5000°C
Melting point	2038°C	2038°C	2852°C	2410°C	2700°C	2700°C
Solubility in water	Insoluble	Insoluble	Insoluble	Insoluble	Insoluble	Insoluble
Brand	Sigma-Aldrich USA	Sigma-Aldrich USA	Sigma-Aldrich USA	Sigma-Aldrich USA	Sigma-Aldrich USA	Sigma-Aldrich USA
Batch No	MKBB8879	0001440782	MKBF8384V	MKBF5726V	MKBC3615	BCBG0412V

Table 4.2: Specification of materials used in the study.

Properties	Silicon Oxide (IV)	Terbium Oxide (IV)	Potassium Oxide	Sodium Oxide	Calcium Oxide
Formula	SiO ₂	Tb ₄ O ₇	KO ₂	Ba ₂ NaNb ₅ O ₁₅	CaO
Physical state	Powder, white	Powder, dark brown	Powder, yellow	Powder, white	Powder, white
Particle size	0.5-10 μm (approx. 80% between 1-5 μm)	-	-	-	<10μm
Purity	99.999%	99.99%	96.5%	99.999%	99.95%
Density	2.2-2.6 g/cm ³	7.3 g/cm ³ at 25 °C	2.14 g/cm ³		3.25-3.38 g/cm ³
Molecular weight	60.90 g/mol	747.70 g/mol	71.1 g/mol	1002.19 g/mol	56.08 g/mol
Boiling point	2230 °C	-	Decomposes	-	2850 °C
Melting point	1710 °C	2340 °C	400 °C	-	2572 °C
Solubility in water	Insoluble	Insoluble	Reacts violently	-	Reaction
Brand	Puratronic [®] . All American Element Inc., USA.	AlfaAesar [®] , A Johnson Matthey Company, USA	AlfaAesar [®] . All American Element Inc., USA	Puratronic [®] . All American Element Inc., USA	AlfaAesar [®] . A Johnson Matthey Company, USA
Batch No	24372	L01W050	A08W021	10649	J25W013

4.5.2 Methodology

Figure 4.1 shows the experimental steps performed in the present study. The various steps used to produce the required materials are outlined in the following sections:

4.5.2.1 Metallurgy of Powders for Fabrication of the Graded Multilayered Ceramic Cores

Multilayered ceramic cores were prepared using a powder metallurgy method schematically as show in Figure 4.1. The process of metallurgy powder for fabrication of the graded homogenous single layer and multilayered ceramic cores was divided into 2 steps as follows:

(a) Drying of Powder

ZrO₂, Al₂O₃, Y₂O₃, MgO, SiO₂, KO₂, CaO, NaO, and Tb₄O₇ powders were dried in an oven at 120°C overnight to prevent the particles from sticking during mixing, thus minimizing the formation of agglomeration of the particles during mixing as shown in Figure 4.13.

(b) Blending of Pure Powder

Once the selected powders had been weighted (30 g), the starting ceramic powders were blended completely together to affirm maximum particles dispersion for typical mechanical properties. The benefits of the blending are to reduce the particle size and to obtain a more homogenous shaped particle. The blending process of starting powders was achieved by using a planetary ball mill machine (Retsch 200 GmbH, Haan, Germany) (Figure 4.14 and Figure 4.15) filled with 50 zirconia ceramic balls of half an inch diameter

(weight 150 g). The blending process was carried out at 400 rpm with reverse action for 15 min for 7 hours based on a pilot study of this work.



Figure 4.13: Drying of the substrate powders.



Figure 4.14: Zirconium jar and balls.



Figure 4.15: A planetary ball mill machine used.

4.5.2.2 Powders Mixing and Milling

Mixing and milling are the crucial steps in specimens' preparation. Effective milling and mixing process were results in the lower amount of agglomeration and a uniform composition in the mixture. The powders were poured into the bowl of the zirconia ball mill with ethanol (99.99%) and the top is then closed tightly. The ZrO_2 , Al_2O_3 , Y_2O_3 , MgO , SiO_2 , KO_2 , CaO , NaO , and Tb_4O_7 of various combination powders were then mixed for seven hours. In order to minimize or prevent particle agglomeration and sticking onto the wall of the bowl, ethanol absolute was poured with powders, wet milling and mixing.

4.5.2.3 Compaction of the Specimens Using Uni-Axial Hydraulic Press

Customize-made stainless steel compaction die (Figure 4.16) was used to produce the individually graded specimens. The die consisted of five parts as illustrated in Figure 4.17. Prior to specimen fabrication, the mould was cleaned using ethanol and cotton tissue to remove any debris to prevent contamination of specimens. The mould was lubricated using zinc stearate and this was to facilitate the removal of specimens easily from the mould after compaction of specimens.

In order to locate the amount of the powder to be placed into the mould, the desired sintered layer thickness, t , was multiplied by the cross-sectional area, A . this will determine the final sintered volume of the layer. This volume was then multiplied by the theoretical density of the powder composition, ρ_{layer} based on a rule of mixture (ROM) formulation, to ultimately determine the mass of the powder to be added as following:

$$m_{layer} = \rho_{layer} At \quad (3-1)$$

The specimen was then placed layer by layer into the mould. It was found that layering with a combination of 80 % YZrO_2 and $\text{Al}_2\text{O}_3\text{MgO}$ powders first, made removal of the specimen after compaction easier and efficient without causing any damage to the specimen. After each layer, has been placed, the plunger was inserted to flatten each layer using gentle figure pressure. This pressing stage does not constitute adequate load to integrate the powders, but it is just adequate to flatten the layer to permit for the formation of smooth interfaces. Once all of the powders had been added into the mould, the plunger was put on top for final compaction. The powder was then compacted using the uni-axial hydraulic pressing machine (Figure 4.18) at 200 MPa for 10 minutes forming a circular shaped specimen and then ejected slowly from the mould. The graded ceramic green specimens' height was approximately 8 mm (Figure 4.19) and 10 mm in diameter. The finished green specimens were then ready for sintering in the furnace. Ninety specimens were fabricated for all nine groups (10 specimens for each group) as listed in Table 4.3.

Table 4.3: Grouping of compactions of specimens.

groups	Designs	Materials and percentage (%)
A	First layer ceramic core	Zirconia (100%)
B	First layer ceramic core	Zirconia (80%) + Alumina (20%)
C	First layer ceramic core	Zirconia (60%) + Alumina (40%)
D	First layer ceramic core	Zirconia (50%) + Alumina (50%)
E	First layer ceramic core	AlMgO 100%
F	Graded silica	SiO_2 , AlMgO , KO_2 , CaO , NaO , Tb_4O_7
G	Two layers ceramic core	First layer: Zirconia (100%) Second layer: Zirconia (80%) + Alumina (20%)
H	Two layers ceramic core	First layer: Zirconia (100%) Second layer: Zirconia (60%) + Alumina (40%)
I	Two layers ceramic core	First layer: Zirconia (100%) Second layer: Zirconia (50%) + Alumina (50%)

4.5.2.4 Sintering of Specimens by Using Pressureless Furnace

Sintering is a method whereby compacted powder are heated so that particles fused together, thus, resulting in a solid particle with improved mechanical strength. After die compaction, all specimens were sintered by using pressureless sintering.

The prepared specimens were placed into the furnace (XY-1700, Nanyang XINYOO Furnace, Nan Yang city, China) as shown in Figure 4.20. The specimens were sintered under flowing inert argon gas to avoid more oxidation of specimens at high temperatures.

A sintering cycle was selected as shown in Figure 4.21. The temperature of the furnace was set and monitored using the digital program controller. The initial temperature of 30°C was maintained for 5 minutes, and then increased gradually to 500°C within 94 minutes (increment of 5°C/min). This stage is to precondition the high temperature sintering. Once the temperature reached 500°C, it was then maintained for 120 minutes. After that, the temperature was increased gradually to 1500°C within 190 minutes for sintering process. The temperature of 1500°C was again maintained for 120 minutes. This stage allows densification of the specimens. Finally, the temperature was decreased gradually from 1500°C to 30°C within 145 minutes and cooling rate 3°C/min, following which the specimens were kept in the furnace overnight. The furnace was set to cool down to 30°C (Figure 4.22 and Figures 4.23).



Figure 4.16: A custom made stainless steel compaction die used.

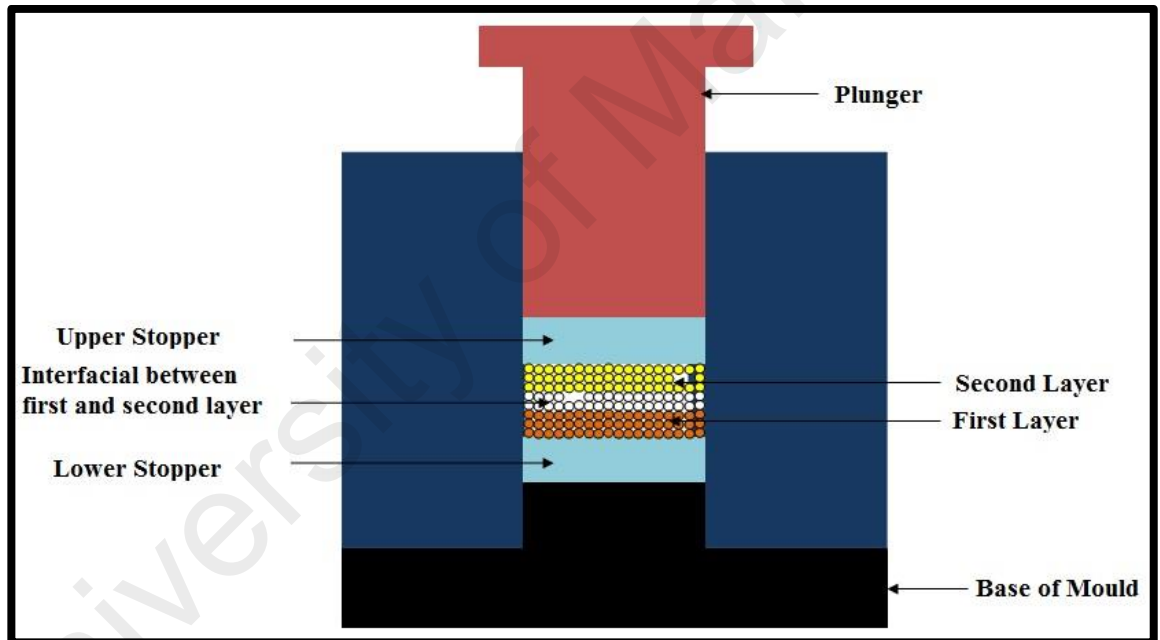


Figure 4.17: Schematic of die compaction mould.



Figure 4.18: Uni-axial hydraulic pressing machine used.



Figure 4.19: The graded ceramic green specimen.



Figure 4.20: The furnace used.

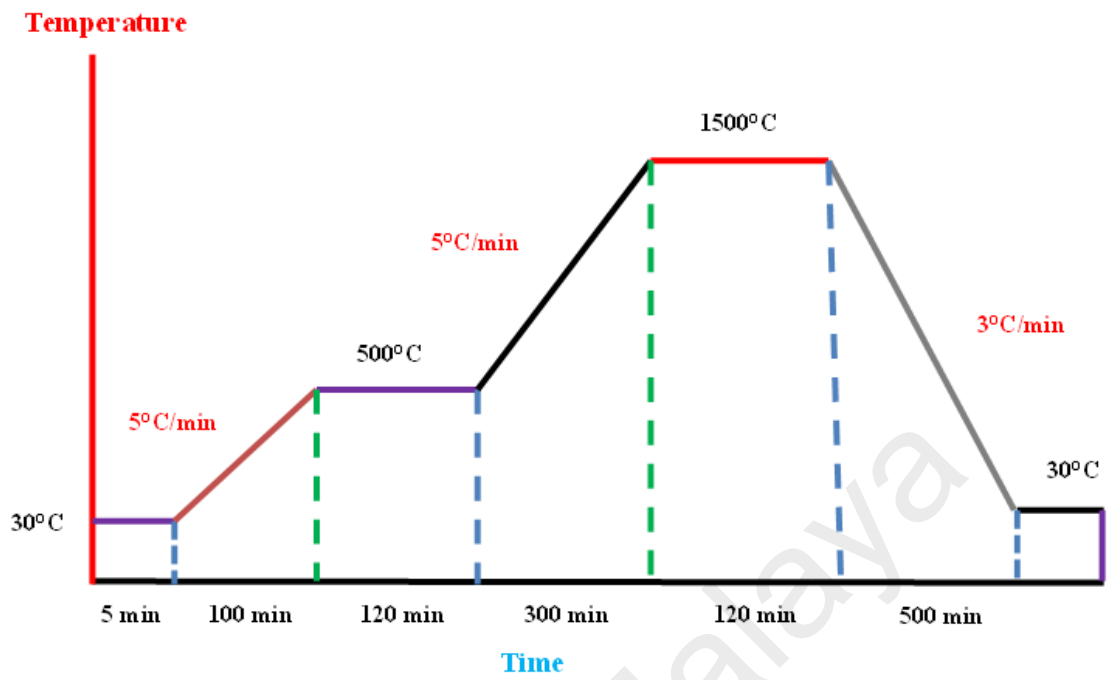


Figure 4.21: Sintering schedule and densification of the graded multilayered ceramic composite.



Figure 4.22: The graded ceramic green specimens before sintering.



Figure 4.23: The graded ceramic green specimens after sintering.

4.5.2.5 Characterization and Optimization of the Multilayered Graded Ceramics

In order to define the characteristic of the graded specimens with/without coating by graded glass silica, the starting point of the graded multilayered ceramic was the determination of the microstructure and chemical composition. Field emission scanning electron microscope (FESEM), energy dispersive X-ray analysis (EDX)-element analysis and X-ray diffraction system (XRD) phase analysis are the most convenient techniques for this purpose. The second part of the experiment was to assess the physical, mechanical, and thermal properties. The assessment of physical properties included the determination of the experimental density, theoretical density, relative densities, experimental porosity, and volume of shrinkage. The evaluation of the mechanical properties such as microhardness, compressive strength, modulus of elasticity, strain and thermomechanical analysis (TMA) was carried out.

4.5.2.6 Microstructure Characterization Analysis

(a) FESEM Analysis

Microstructure characterization is an important feature of this study in view of the pronounced influence of microstructure on various properties of synthesized multilayered graded ceramic. These characterizations are important to determine if the microstructure depicted shows particle reinforcement or interpenetrating phase between different particle composition; which will not only determine the sintering behaviour but also have an impact on the mechanical properties.

The microstructure, morphology, and distribution of the particles were investigated by using FESEM (Low Vacuum Operating Mode, Quanta 200 F, FEI, Dawson Creek Drive

Hillsboro, Oregon, USA) as shown in Figure 4.24. Prior to mounting on the aluminum stub, the surface of the specimens was polished and then cleaned with ethanol. Each specimen was then mounted on the aluminum stub using adhesive carbon tape and was subsequently mounted on the 7-holder specimen stage. Imaging was done under 10 and 20 Kv accelerating voltage at a magnification between 200x to 4000x using both the secondary electron and back scattered electron signals. 27 specimens were fabricated for all nine groups (3 specimens for each group) as listed in Table 4.3.

Micrographs were taken by focusing on the different areas of each layer. It is considered advantageous to observe various locations through each layer, since the materials are likely to be non-homogenous on the microscale, and there may be features that are not present throughout the material.

(b) Element Analysis (EDX)

Element analysis was carried out by using the EDX equipped in the same FESEM to determine the composition of synthesised ceramic composites.

(c) X-Ray Diffraction (XRD) Phase Analysis

X-ray diffraction (XRD) (Bruker X-RD D8 Advance, Frankfurt, Germany) was utilized to determine the phase stability of synthesised graded multilayered ceramic composite for both powders and sintered specimens as shown in Figure 4.25. Specimens were mounted onto the holder using various adhesive and adjusted to the correct height with a glass slide. Scanning angle (2θ) ranged from 20° to 70° using $\text{CuK}\alpha$ radiation ($\lambda = 1.54056 \text{ \AA}$). In order to obtain the graded composition profile, the specimens were cut using a diamond blade Highspeed-2000, Isomet-Buehler, (USA) into consecutive slices of 2 mm thick at each layer representing the different composition. The obtained peaks were then compared to the standard reference JCPDS-ICCD files to assess the phases in specimens (X'Pert HighScore, Version: 1.0d, PANalytical B. V., Almelo, Netherlands).



Figure 4.24: FESEM used.



Figure 4.25: XRD machine used.

4.5.2.7 Physical Characterization

Densities (ρ , g/cc) of specimens were calculated using Archimedes' method and is presented by Equation (3.2), whilst the volume shrinkage (ϵ %) of the sintered specimens was estimated with Equation (3.3). a minimum of ten similar samples of each group was

taken. The average of mean and standard deviation (SD) for each sintered specimen were determined using the water density of 0.99704 g/mL at 25 °C (Sartorius Mechatronics AX224, Göttingen, Germany) (Figure 4.26). Ninety specimens were fabricated for all nine groups (10 specimens for each group) as shown in Table 4.3.

The relative density of each specimen was calculated by using the measured experimental density divided by the theoretical density.

$$\text{Density } (\rho) = \frac{\text{Weight in air}}{\text{Weight in air} - \text{Weight in water}} \times \text{Water density} \quad (3.2)$$

$$\text{Volume shrinkage percentage } (\epsilon \%) = \frac{\text{Initial volume} - \text{Final volume}}{\text{Initial volume}} \times 100 \quad (3.3)$$

Porosity is the measurement of the void spaces in the material. This measurement uses its specific characteristics as a volume fraction which is from 0 to 1 or as a percentage from 0-100%. There are two types of pores in the specimen: open pores and close pores. The saturated surface dry technique was used to measure the void spaces by the open pores by Equation (3.4). The samples were treated in desiccators vacuum for 30 minutes at 1 atm as shown in Figure 4.27. This is to ensure that trapped air bubbles in the samples were eliminated.

$$\text{Porosity } (\%) = \frac{W_s - W_d}{W_s - W_w} \times 100 \quad (3.4)$$

where;

W_d : Weight of the specimens in air, g.

W_s : Weight of the specimens in water, g.

W_w : Weight of the surface dry specimen, g.



Figure 4.26: Electronic densitometer used.



Figure 4.27: Vacuum desiccators used.

4.5.2.8 Mechanical Characterization

4.2.2.8.1. Vickers Hardness Test (VH)

Total of ninety synthesized ceramic cores bars (13 mm height and 6 mm in diameter) were consecutively polished with 400-, 600-, 800-, 1000-, and 1200- grit silicone polisher papers and the diamond polishing solutions (1 μm) on polishing machine (Buehler, Binghamton, NY, USA) under water-cooling in order to obtain a mirror-like surface. Ninety specimens were tested for all nine groups (10 specimens for each group) as shown in Table 4.3.

Vickers hardness test (VH) was performed on the polished surfaces of the sintered specimens using a micro Vicker's hardness tester (HMV-2 T, Shimadzu Coroperation, Tokyo, Japan), (Figure 4.28). The diamond indenter pyramid-shaped was utilized at a fixed load of 9.807 N for 5s to get a minimum of seven indentations from each specimen (ASTM C 1327, 2001). The VH with units of GPa was estimated as follows:

$$VH = 0.0018544 (P/d^2)$$

Where:

P = load, N, and

d = average length of the two diagonals of the indentation, mm.

4.2.2.8.2. Compressive Strength Test

Total of 90 synthesised ceramic cores bars (13 mm height and 6 mm in diameter) were consecutively polished with 400-, 600-, 800-, 1000-, and 1200- grit silicone polisher papers and the diamond polishing solutions (1 μ m) on polishing machine (Buehler, Binghamton, NY, USA) under water-cooling in order to obtain a mirror-like surface.

The samples were subjected to compressive strength test at room temperature to determine the compressive strength (σ_{UCS}), compressive elastic modulus (E_C), and compressive strain of the synthesised ceramic cores. The test was carried out using a universal testing machine (Instron, Shimadzu Cooperation, Tokyo, Japan) as presented in Figure 4.29. The test was performed under load control condition at a displacement rate of fixed cross-head speed of 1 mm/min. The compressive test was carried out and standardised by ASTM C773-88 (1999). Ninety specimens were tested for all nine groups (10 specimens for each group) as shown in Table 4.3. The compressive strength of each specimen was calculated as follows:

$$C = L / A$$

Where

C = compressive strength of the sample, MPa;

L = total load on the sample at failure, N; and

A = area of the bearing surface of the sample, mm^2 .



Figure 4.28: MicroVickers hardness testing machine used.



Figure 4.29: A universal testing machine used.

4.2.2.8.3. Thermomechanical Analysis (TMA) Test

The measurements of the coefficient of thermal expansion (CTE) of the synthesised ceramic cores were carried out and standardised by the ISO-6872- (E) (2008). Ninety specimens were measured for all nine groups (10 specimens for each group) as shown in Table 4.3. All ceramic core specimens had a cylindrical shape with a length of 20 mm and a diameter of 5 mm (with cross-sectional area 19.634 mm^2) as shown in Figure 4.30. Each sample was heated from 25°C to 500°C at $5^\circ\text{C}/\text{min}$ in an air atmosphere with a constant load -0.1mN . Alumina ceramic probe and sample cylinder were used. Dried sample stayed vertically. The CTE for the ceramic cores and graded glass silica were measured with an apparatus for thermo-mechanical analyzer (TMA) (TMA-60H, Model 04000 SCI 00034, Shimadzu Cooperation, Tokyo, Japan) (Figure 4.31). The CTE for all specimens were calculated automatically between 25°C to 500°C by TMA. The average mean values and standard deviation of the coefficients of thermal expansion were used for the calculations in this study.



Figure 4.30: Specimens of ceramic cores fabricated for TMA.



Figure 4.31: TMA machine used to measure the CTE.

4.6 Results

4.6.1 Characterization of Synthesised Graded Ceramic Cores

4.6.1.1 Morphology and Microstructures Analysed by FESEM

For the microstructural observation of synthesised ceramic powders and sintered pure zirconia, alumina, and YTZP-Al composite, the microstructure of YTZP-alumina composite (Figure 4.33 to Figure 4.39) indicates that a uniform distribution of Al and Zr elements is clearly observed in the composite and resembles their relative amounts. This homogeneous distribution is due to homogeneous particle size distribution of the starting powders as shown in Figures 4.32 and 4.34. The microstructural characterization was also performed for the zirconia to quantify the grain size and shape using image analysis for FESEM. The alumina was seen to have grains of equal size and distribution, with the grains tending to be uniform (Figure 4.33).

Figure 4.33 to Figure 4.38 present microstructural of 3YTZP-Al₂O₃ ceramic composites with varying Al₂O₃ contents (0, 20, 40, 60, and 100 wt%) sintered at 1500 °C in 2 h in air. The micrograph exhibited the Al₂O₃ and ZrO₂ grains as dark and whitish colour respectively, where zirconia grains were embedded around the alumina grain and/or within the grain. However, small fractions of intragranular zirconia were also being noticed. Figure 4.35 and Figure 4.36 showed that the zirconia grains eventually coalesce with each other were located at grain junctions and responsible for a grain boundary pinning effect. The higher volume fraction of zirconia causes the zirconia to be less isolated and more continuous and interconnected. Figure 4.37 showed relatively more isolated pores and these pores were interconnected in some

occasions. Micropores were presented at the triple junction of the ZrO_2 grains. The presence of pores tends to increase the diffusion distance between particles thereby reducing the driving force for pores shrinkage. In this context, the final relative density of the compositions was lower than the other compositions. Figure 4.38 showed the zirconia particles were isolated at grain boundaries between bigger alumina grains and some isolated pores were observed. Most of the ZrO_2 grains were located at the junctions of the Al_2O_3 grains and the grain boundaries should be due to the strong self-diffusion of zirconia, which revealed the intergranular nature of the ZrO_2 grains. Although some small ZrO_2 grains were located within the Al_2O_3 grains and had a spherical geometry, processing the intergranular type. Figure 4.39 showed the microstructure of graded silica revealed that the silicon particles with another element such as KO, CaO, Al_2O_3 are slightly homogenous also some pores were observed.

For the microstructural observation of interfaces between two layers, sintered pure zirconia, alumina, and ATZ, the sintered body was cut and polished and then buffed with alumina paste of 1 μm in particle size. FESSEM analysis of the all-ceramic cores tested groups revealed porosities in the zirconia and alumina interfaces (Figure 4.40 to Figure 4.45).

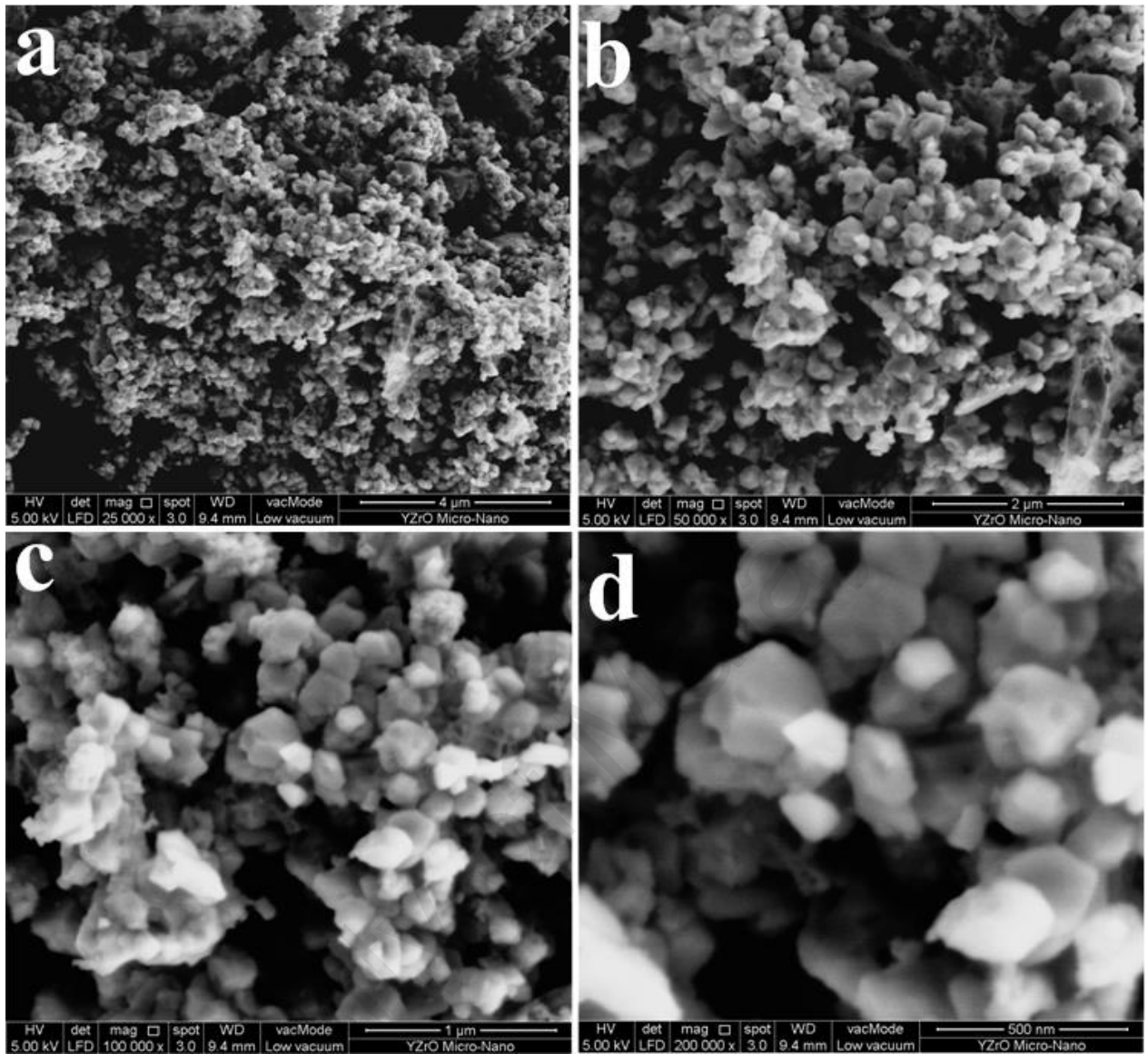


Figure 4.32: FESEM for zirconia powder 100%. (a) mag x25000, (b) mag x50000, (c) mag x100000, and (d) mag x200000.

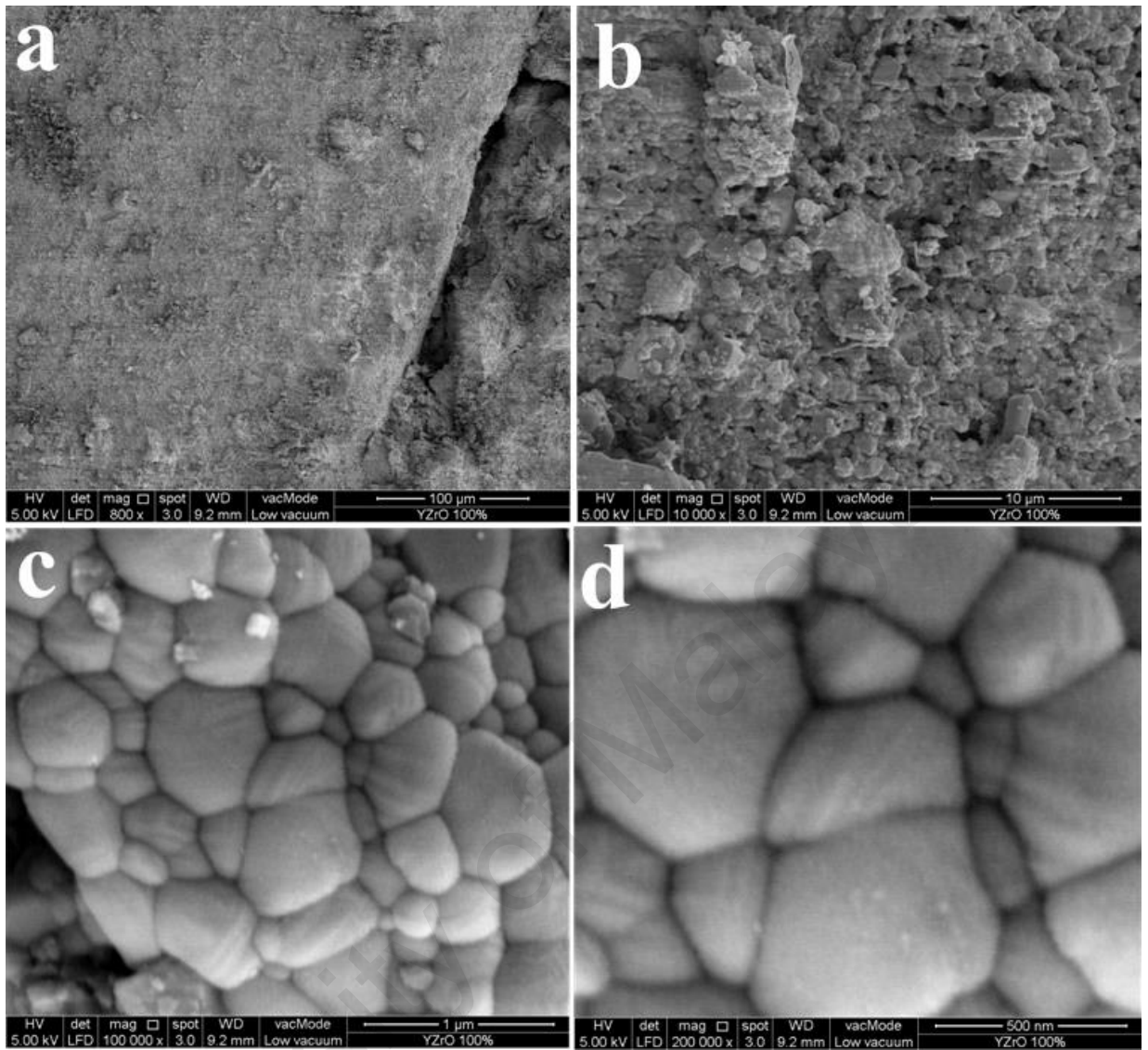


Figure 4.33: FESEM for sintered zirconia 100%. (a) mag x800, (b) mag x50000, (c) mag x100000, and (d) mag x200000.

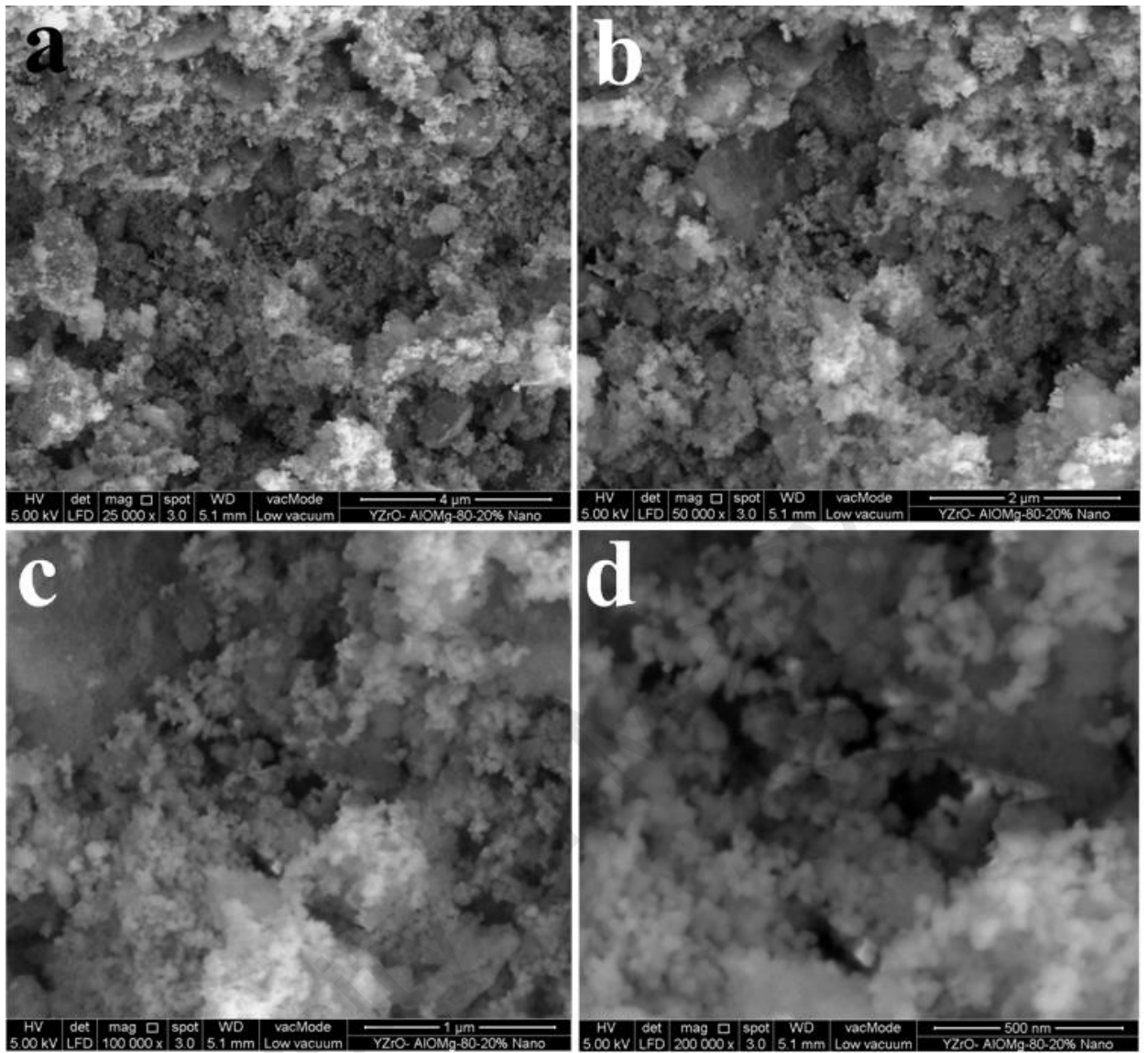


Figure 4.34: FESEM for zirconia 80% (white grain)-alumina 20% (dark grain) powder. (a) mag x25000, (b) mag x50000, (c) mag x100000, and (d) mag x200000.

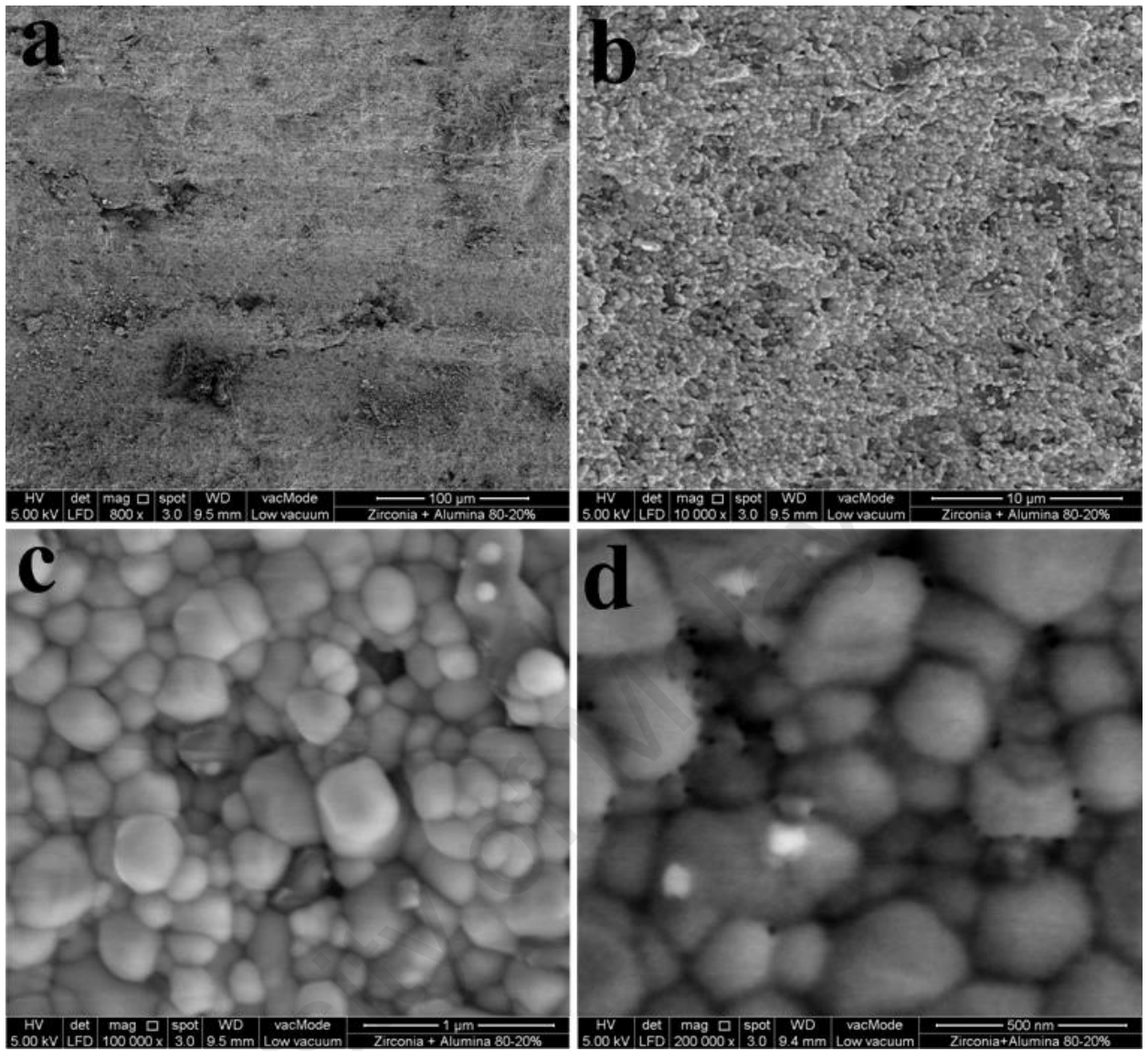


Figure 4.35: FESEM for sintered zirconia 80% (white grain)-alumina 20% (dark grain). (a) mag x800, (b) mag 10000, (c) mag x100000, and (d) mag x200000.

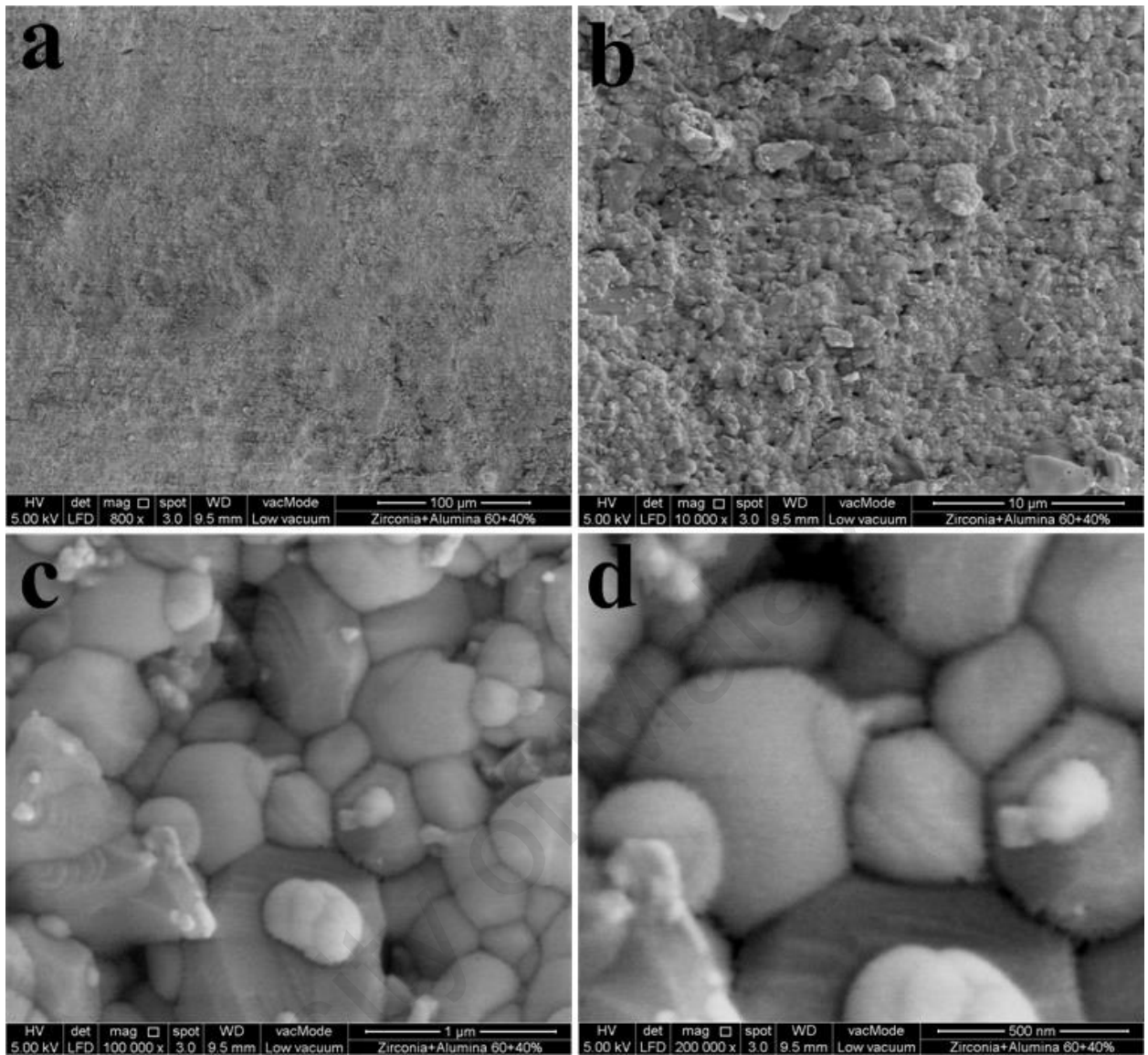


Figure 4.36: FESEM for sintered zirconia 60% (white grain)-alumina 40% (dark grain). (a) mag x800, (b) mag 10000, (c) mag x100000, and (d) mag x200000.

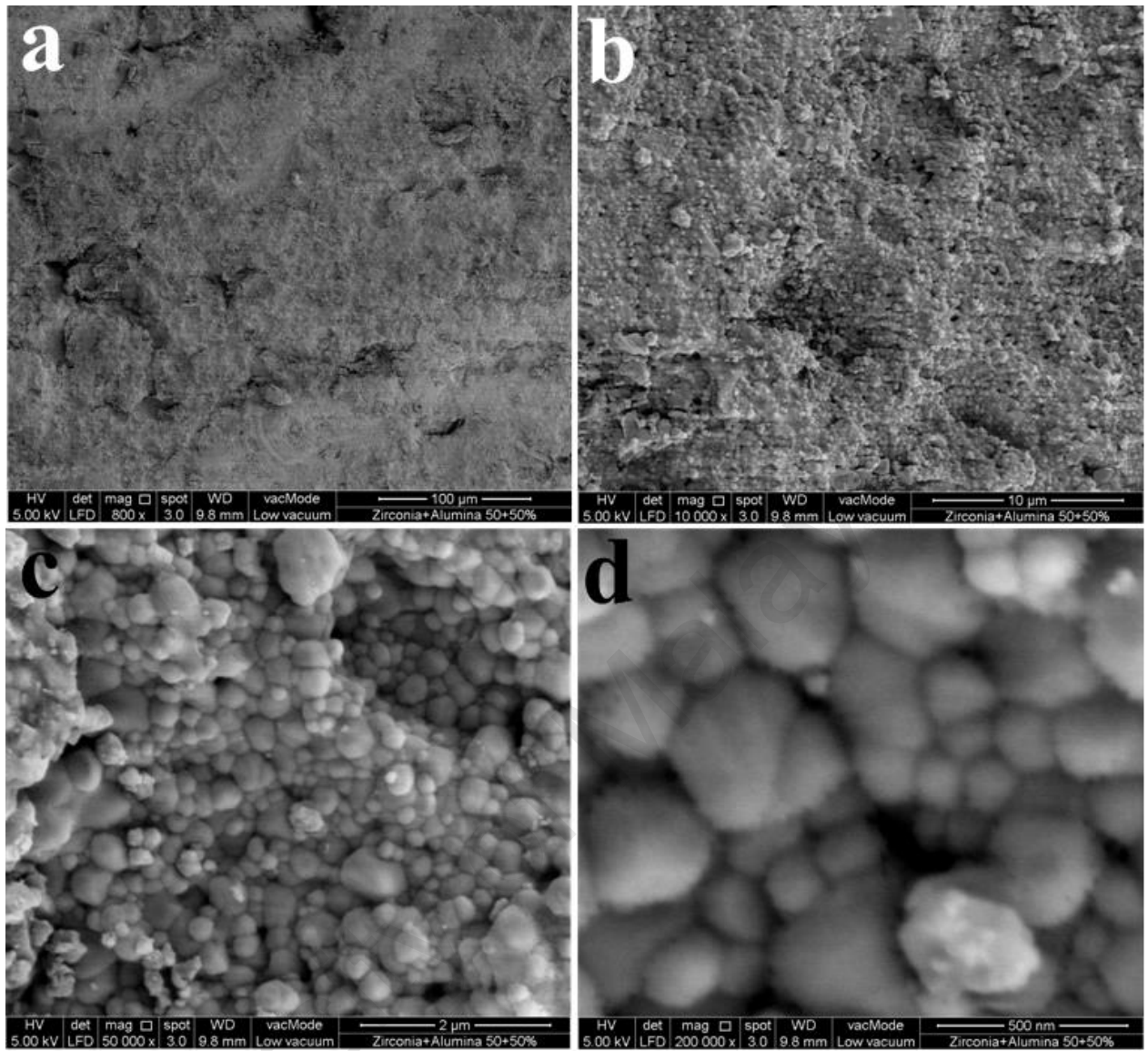


Figure 4.37: FESEM for sintered zirconia 50% (white grain)-alumina 50% (dark grain). (a) mag x800, (b) mag 10000, (c) mag x100000, and (d) mag x200000.

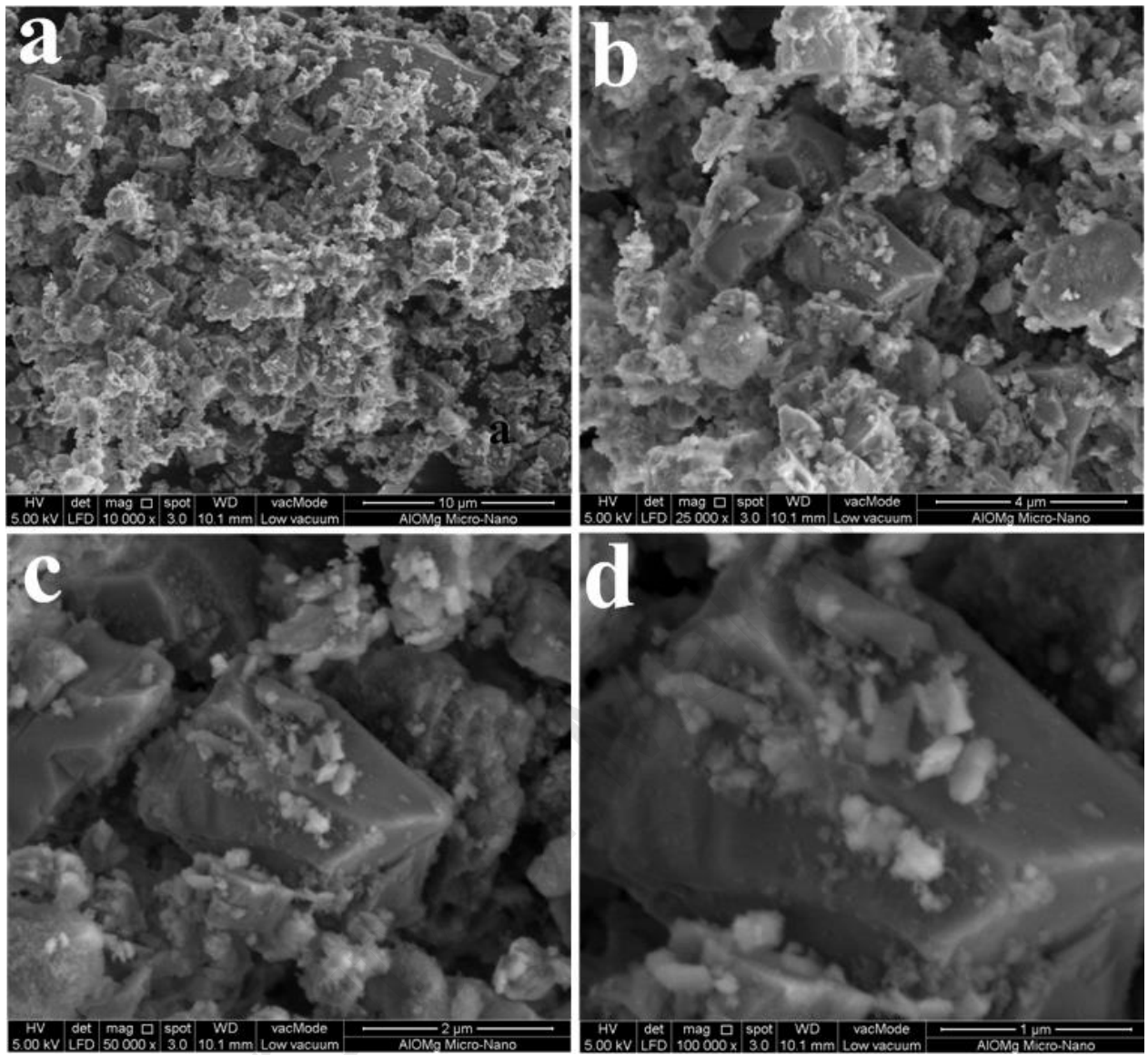


Figure 4.38: FESEM for alumina 100% after sintering. (a) mag x10000, (b) mag x25000, (c) mag x500000, and (d) mag x100000.

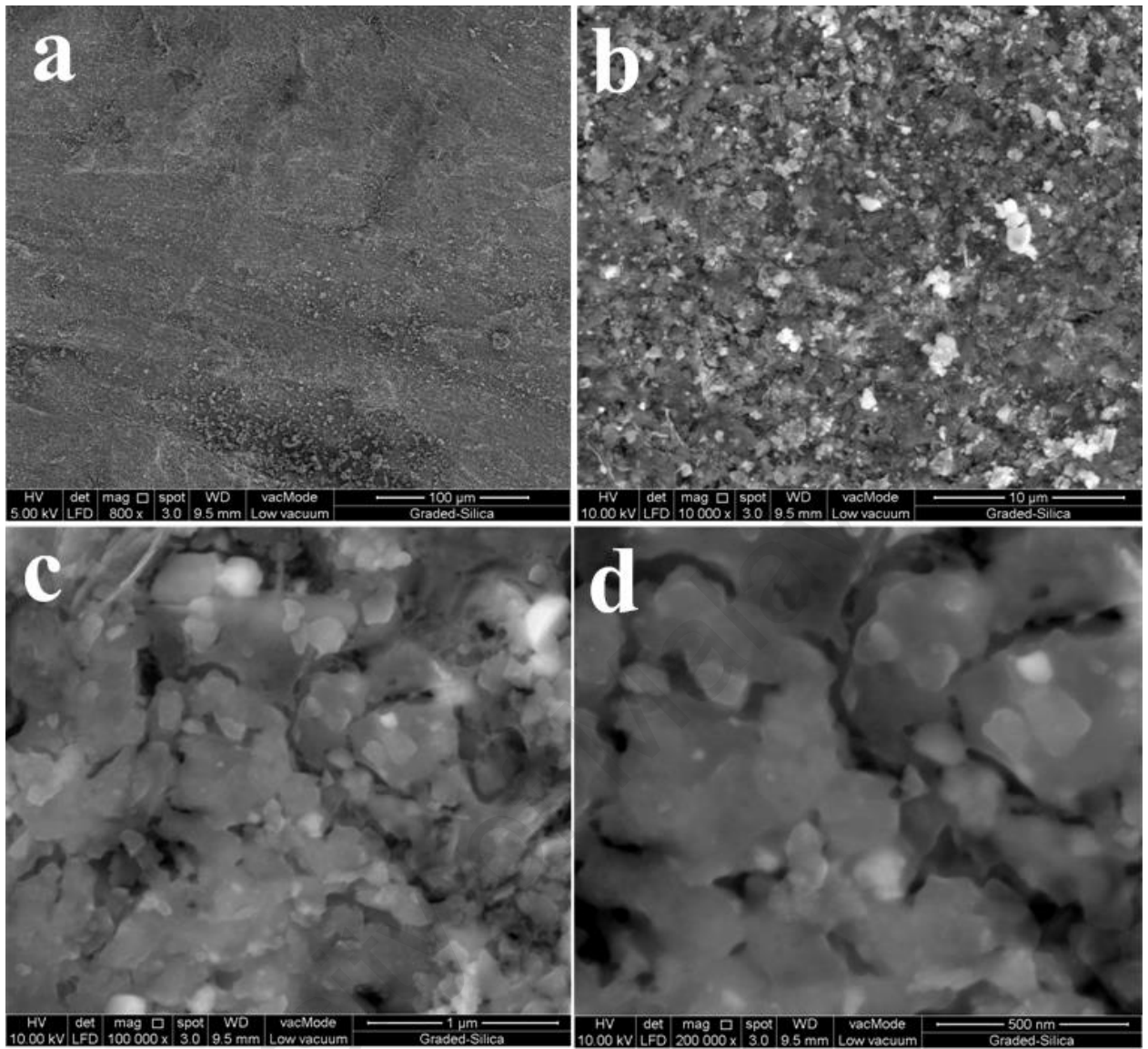


Figure 4.39: FESEM for sintered graded silica. (a) mag x800, (b) mag 10000, (c) mag x100000, and (d) mag x200000.

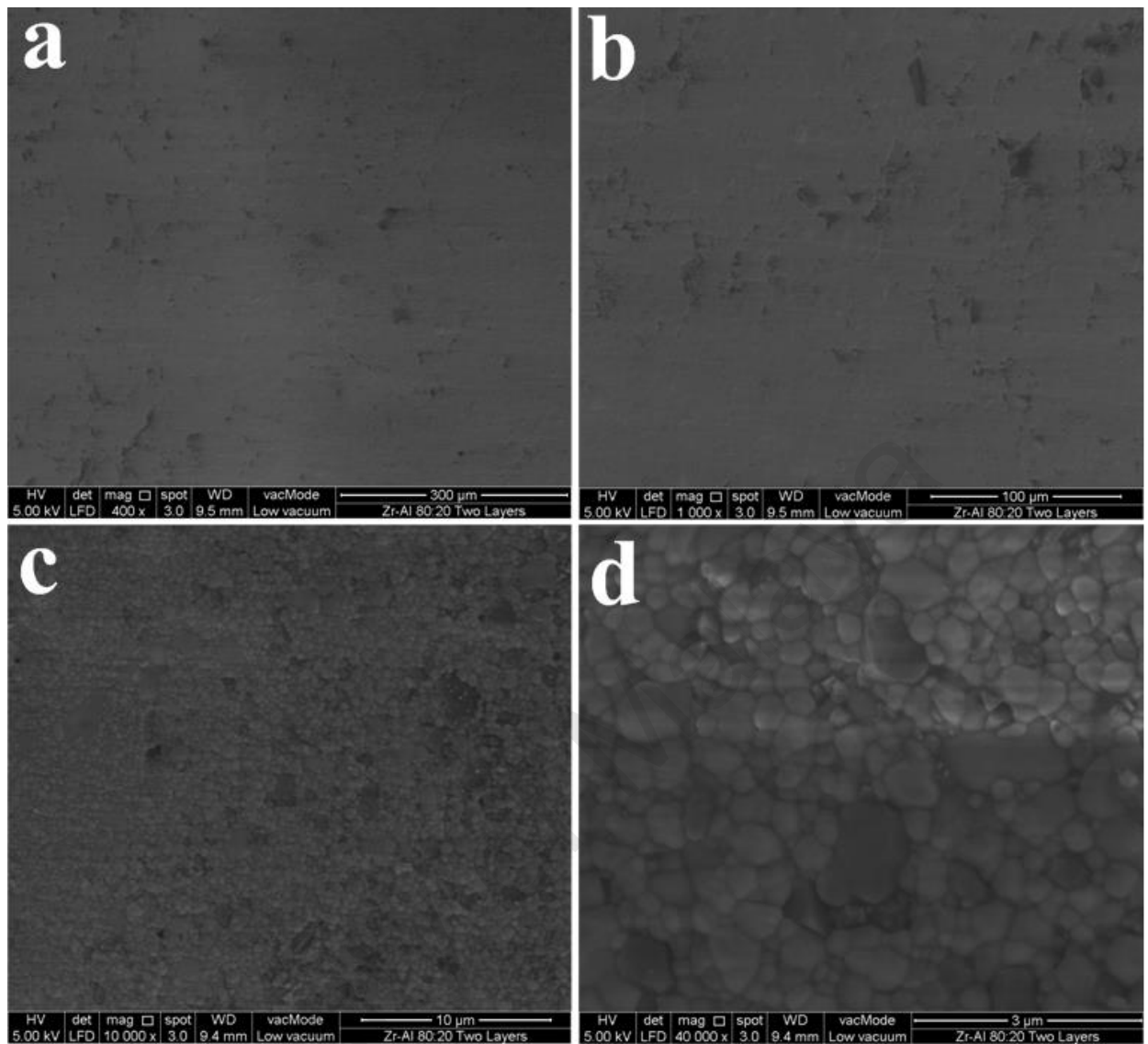


Figure 4.40: FESEM for sintered two-layers zirconia 100% (white layer)-zirconia 80%-alumina 20% (dark layer). (a) mag x400, (b) mag 1000, (c) mag x10000, and (d) mag x40000.

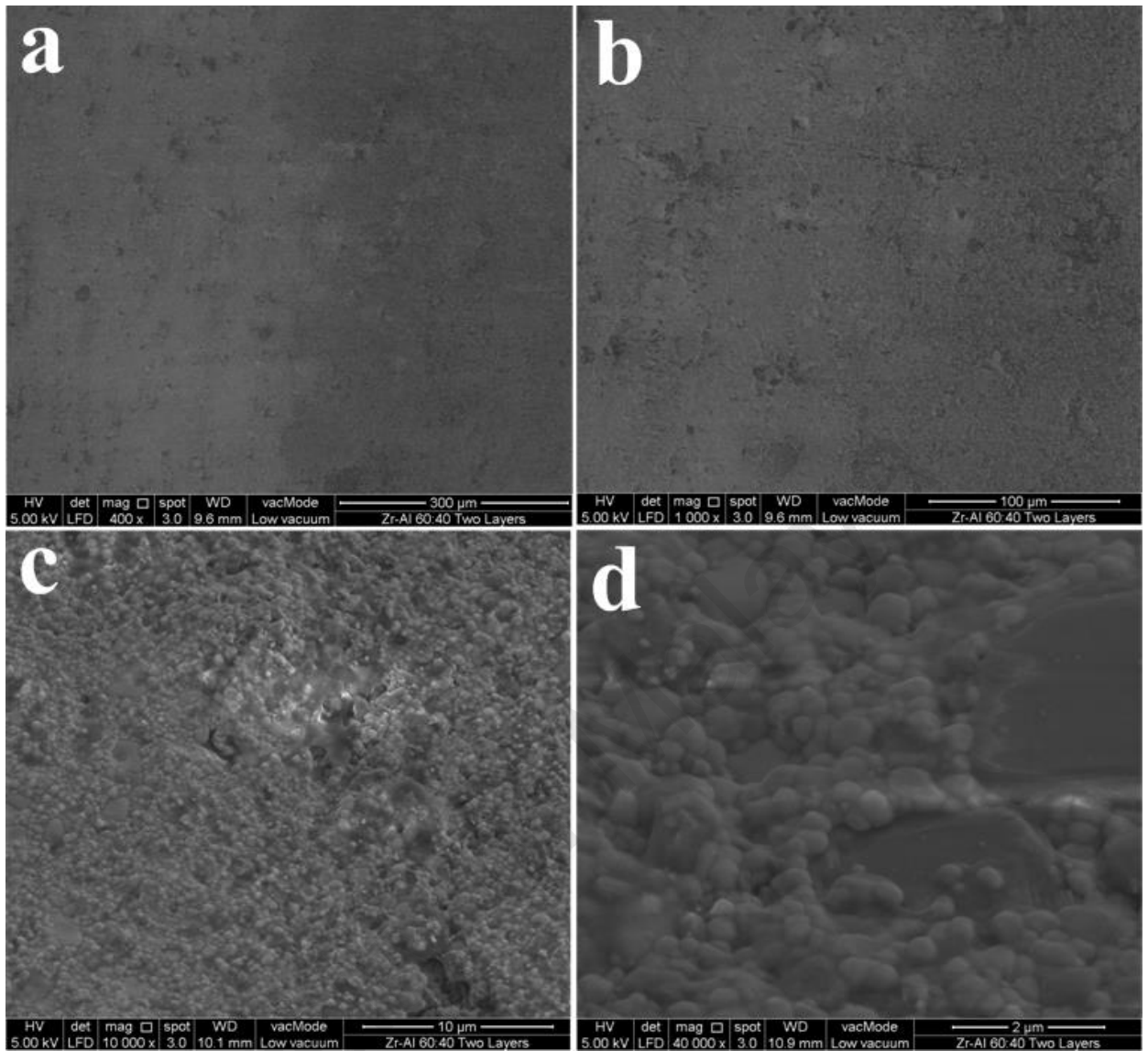


Figure 4.41: FESEM for sintered two-layers zirconia 100% (white layer)-zirconia 60%-alumina 40% (dark layer). (a) mag x400, (b) mag x1000, (c) mag x10000, and (d) mag x40000.

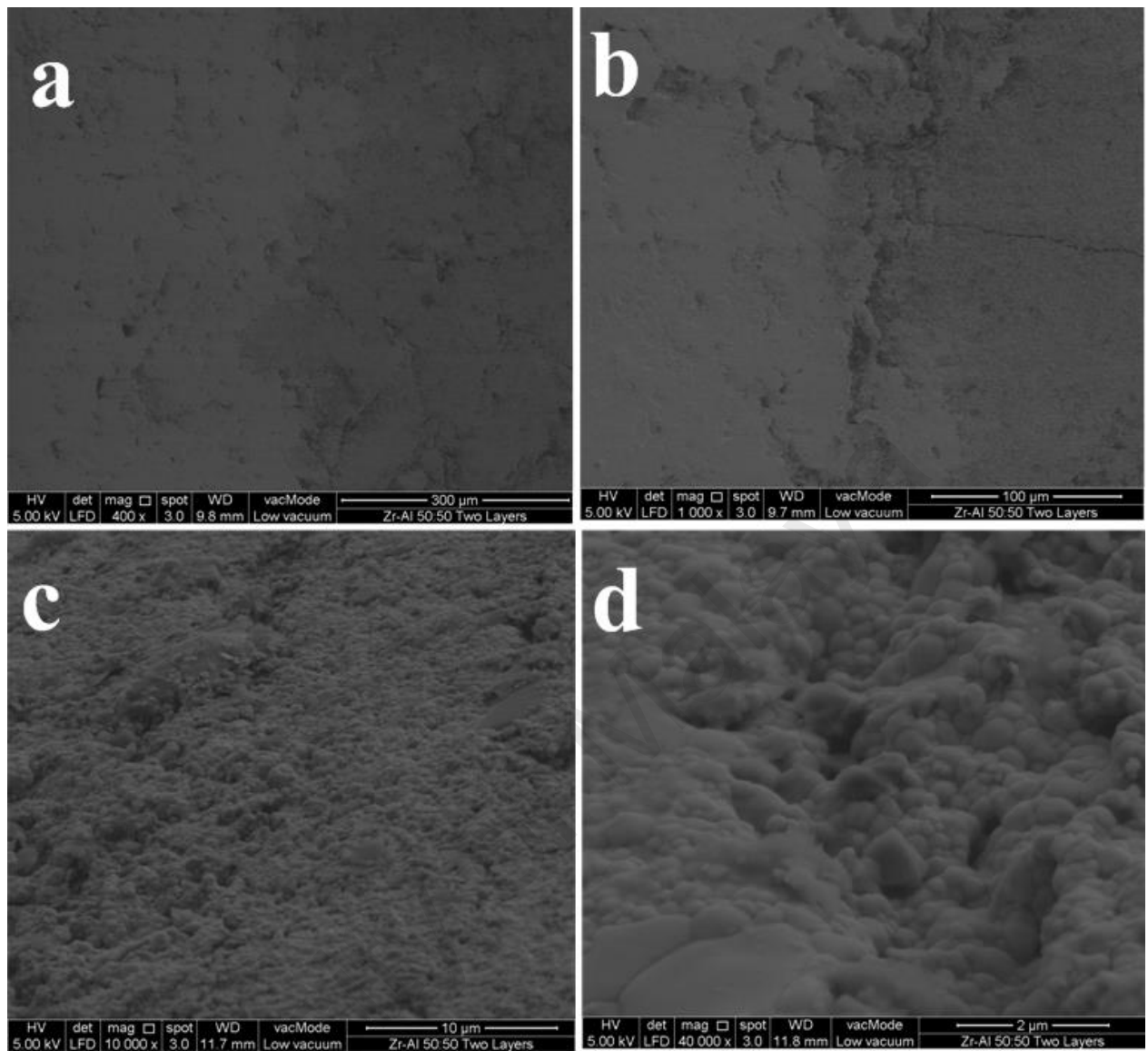


Figure 4.42: FESEM for sintered two-layers zirconia 100% (white layer)-zirconia 50% alumina 50% (dark layer). (a) mag x400, (b) mag x1000, (c) mag x10000, and (d) mag x40000.

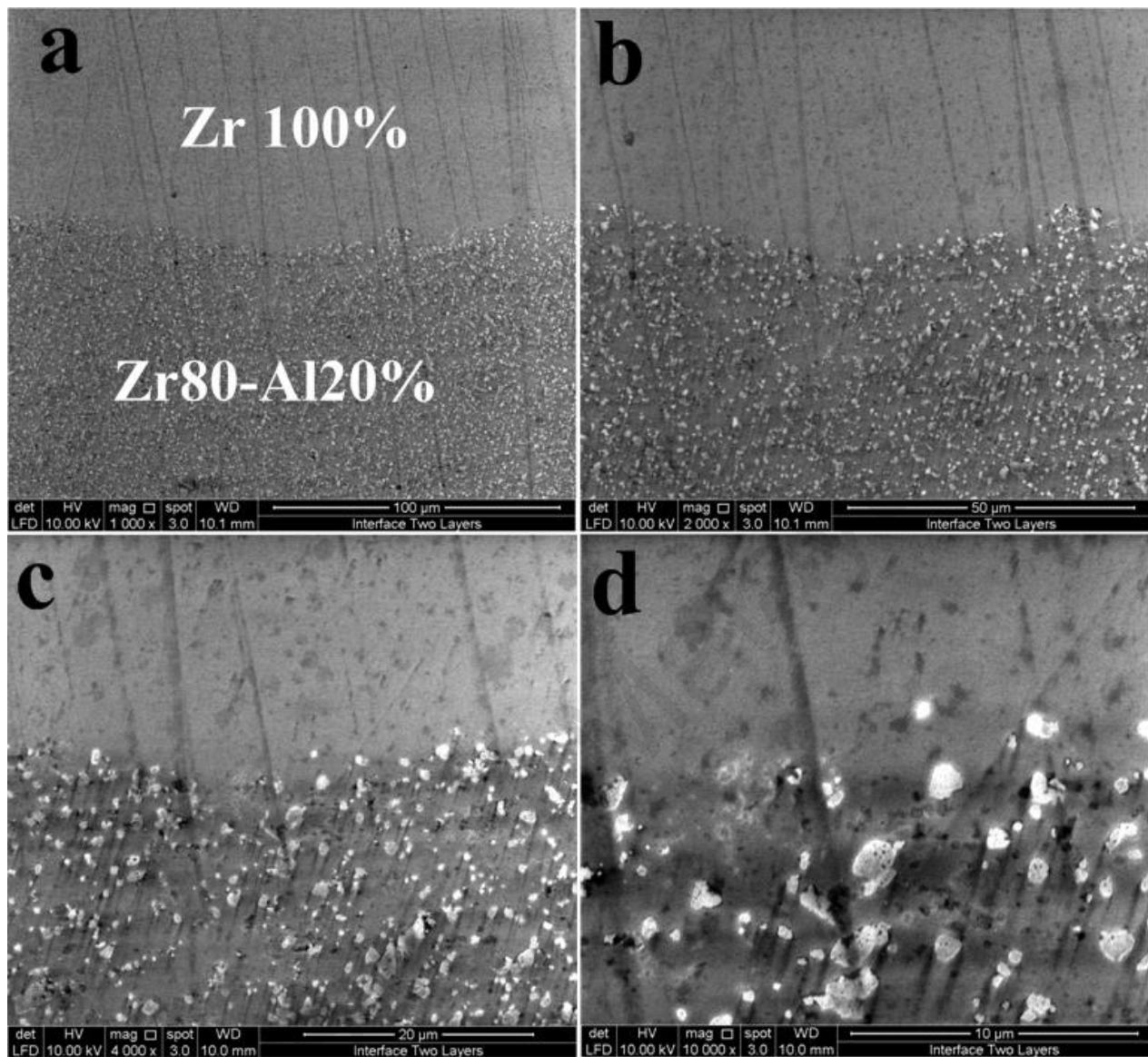


Figure 4.43: FESEM of interface between two-layers zirconia 100% (white layer) zirconia 80%-alumina 20% (dark layer). (a) mag x1000, (b) mag 2000, (c) mag x4000, and (d) mag x10000.

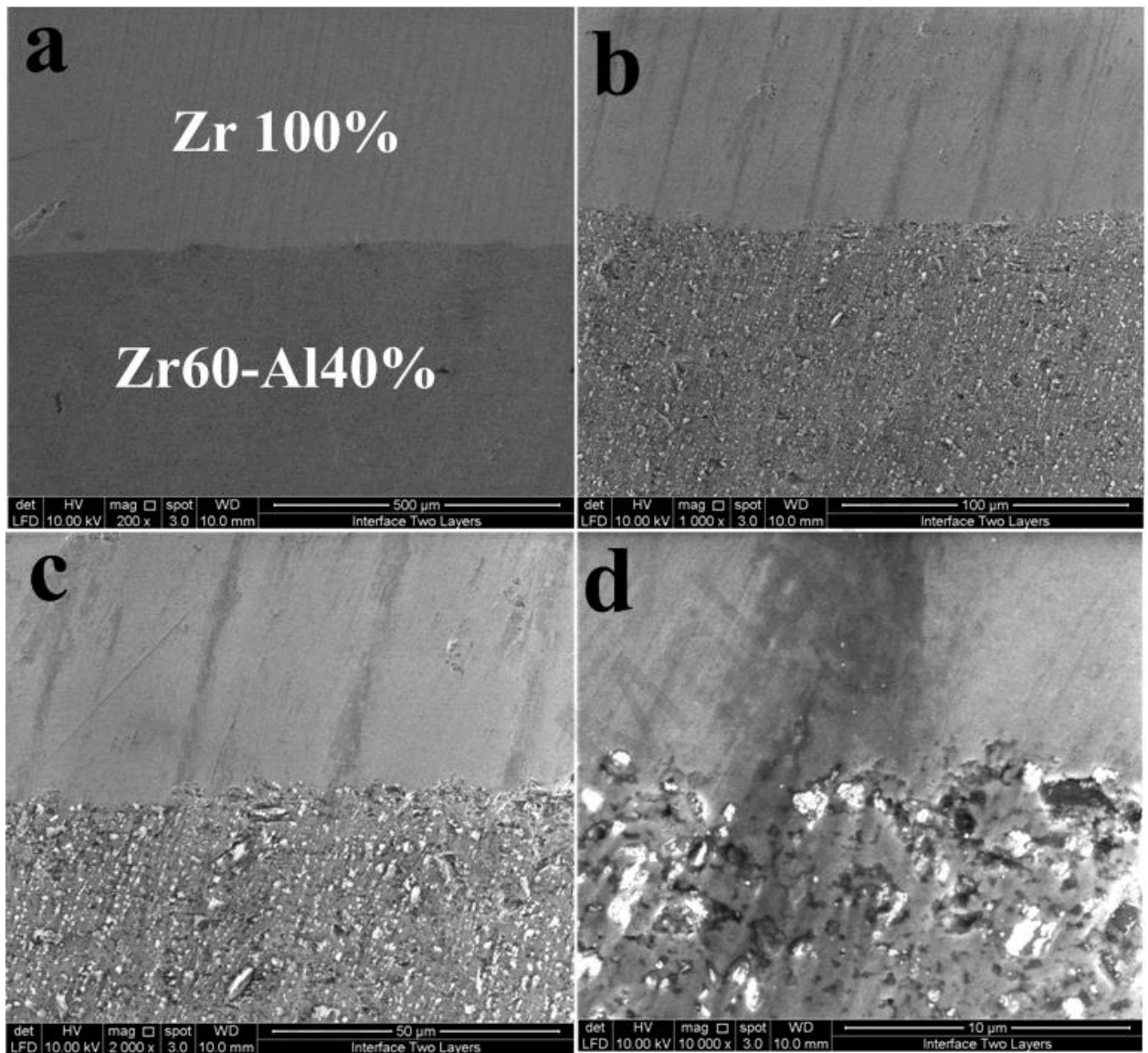


Figure 4.44: FESEM of interface between two-layers zirconia 100% (white layer) Zirconia 60%-alumina 40% (dark layer). (a) mag x200, (b) mag x1000, (c) mag x2000, and (d) mag x10000.

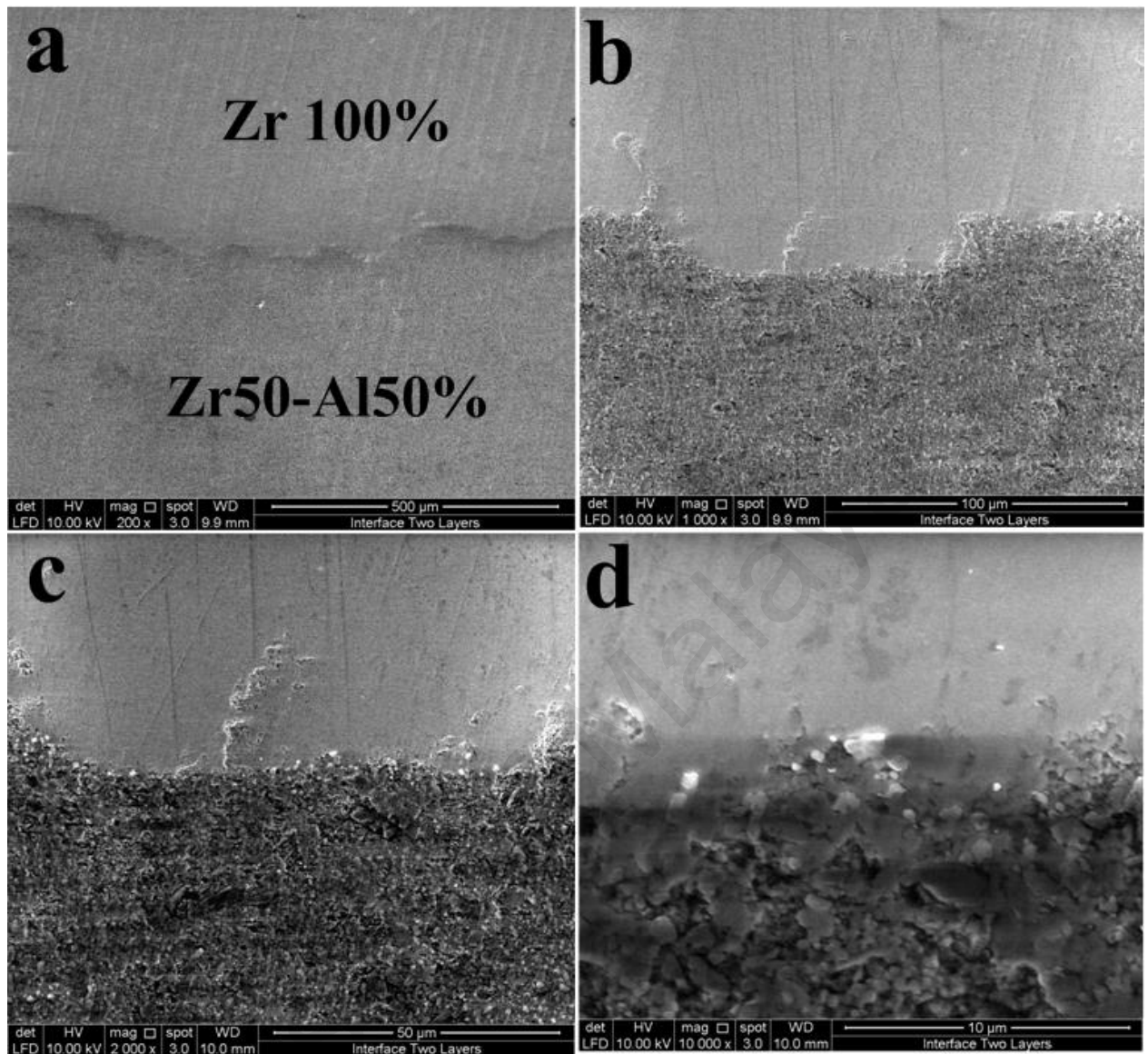


Figure 4.45: FESEM of interface between two-layers zirconia 100% (white layer)-zirconia 50%-alumina 50% (dark layer). (a) mag x200, (b) mag x1000, (c) mag x2000, and (d) mag x10000.

4.6.1.2 Composition Mapping Analyses by EDX

The single layer of synthesised ceramic cores zirconia, alumina, graded silica, and interface between layers of multilayered structure ceramics specimens were investigated by EDX before and after sintering process (from Figures 4.46 to Figure 4.57) and revealed that the composition elements were equivalent.

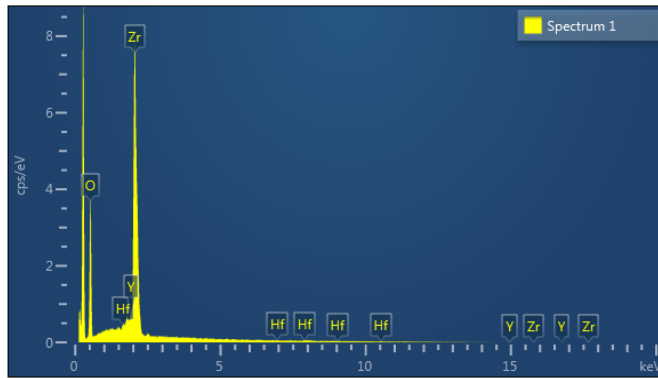


Figure 4.46: EDX of YZrO 100% powder.

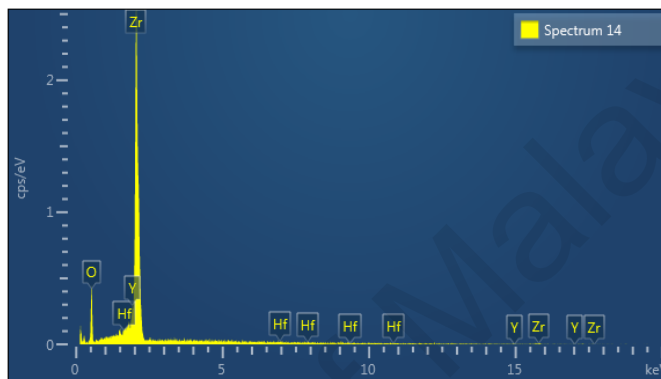


Figure 4.47: EDX of YZrO 100% layer after sintering.

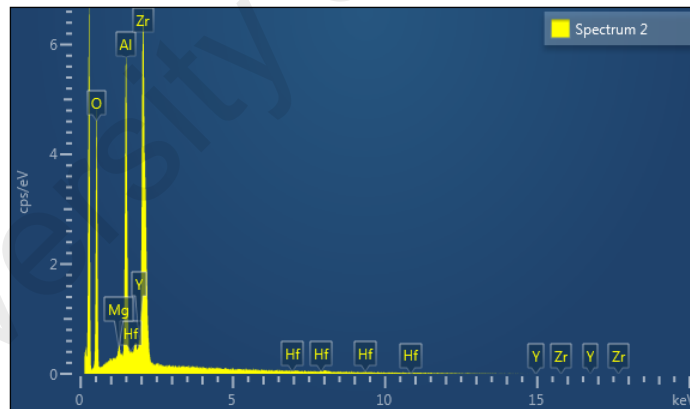


Figure 4.48: EDX of Zr80%-Al20% powder.

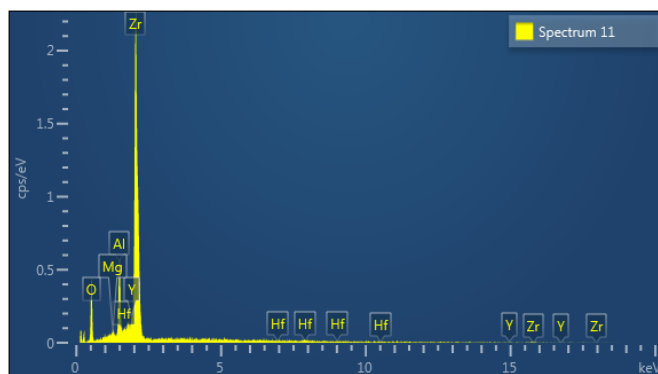


Figure 4.49: EDX of Zr80%-Al20% layer after sintering.

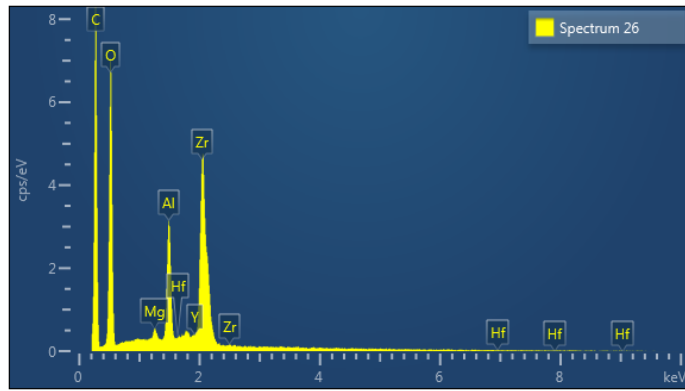


Figure 4.50: EDX of Zr60%-Al40% powder.

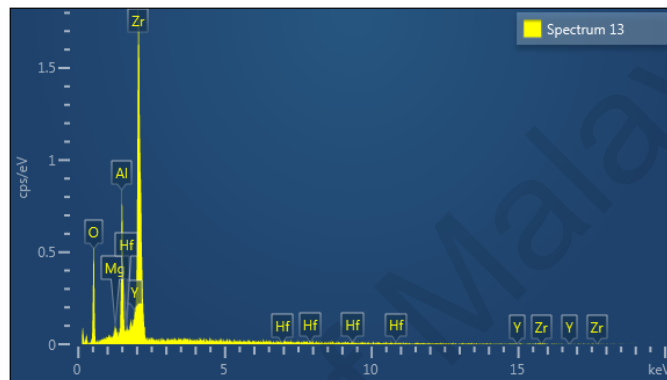


Figure 4.51: EDX of Zr60%-Al40% layer after sintering.

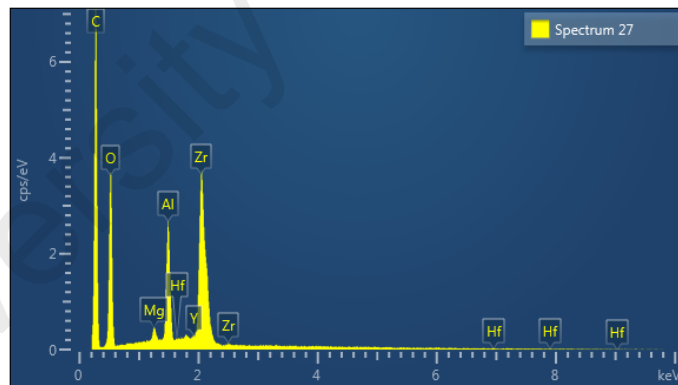


Figure 4.52: EDX of Zr50%-Al50% powder.

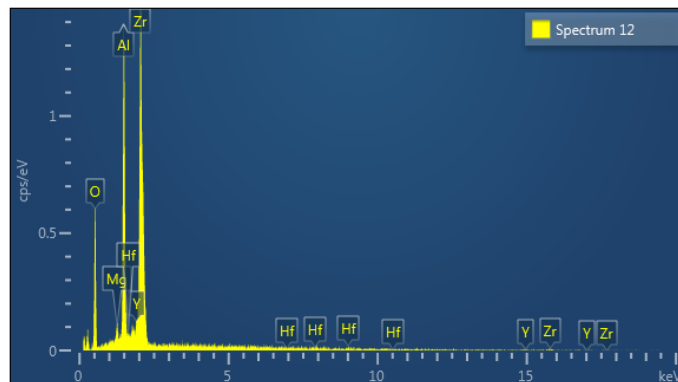


Figure 4.53: EDX of Zr50%-Al50% layer after sintering.

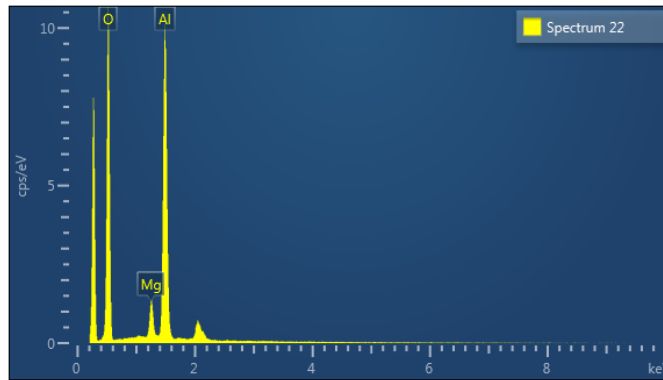


Figure 4.54: EDX of MgAlO100% powder.

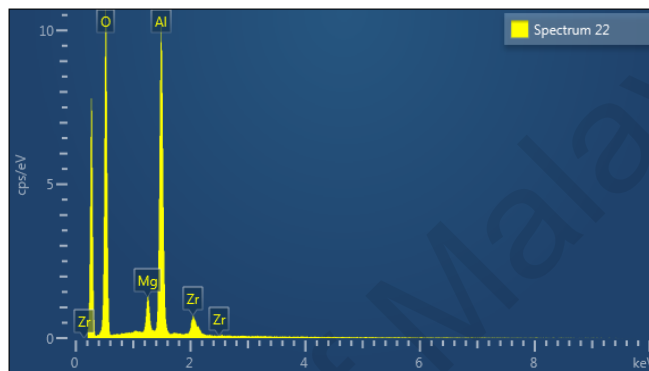


Figure 4.55: EDX of MgAlO 100% layer after sintering.

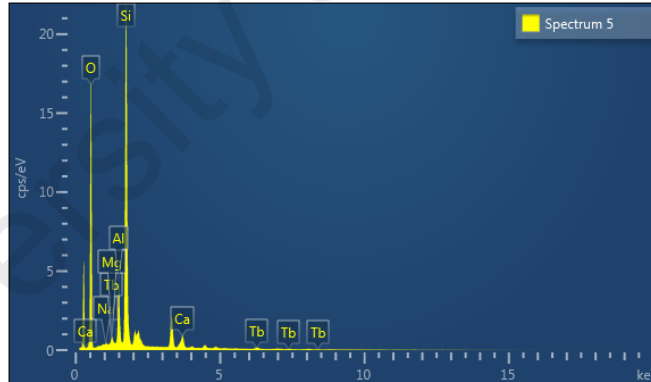


Figure 4.56: EDX of graded silica powder.

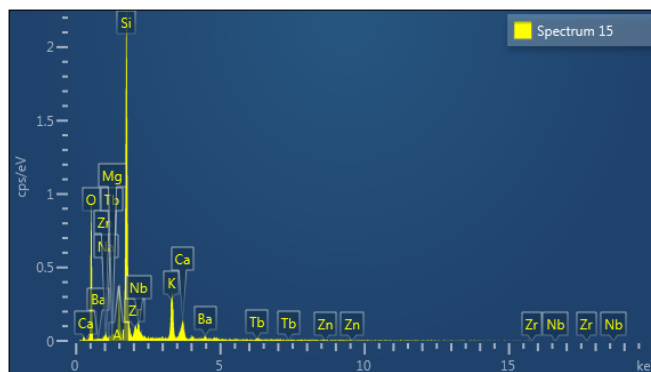


Figure 4.57: EDX of graded silica layer after sintering.

4.6.1.3 Phase Analysis by XRD

Single layer of synthesised ceramic cores were analysed in both phases (powder and solid) by XRD. It has been shown that, for YZrO 100%, 16 peaks were found as seen in Figure 4.58a attributed to the presence of monoclinic zirconia (M-Zr) (code No:00-013-0307) between 20 to 70, 2-Theta scale. But in solid form (after sintering), 14 peaks were found as seen in Figure 4.58b attributed to the presence of monoclinic zirconia (M-Zr) (code no:00-013-0307, 8 peaks), which is present as foreign phase in the samples of tetragonal zirconia (code no: 00-050-1089; 6 peaks) with monoclinic Hafnium oxide (code no: 00-034-0104) in both phase of zirconia. Also for single synthesised ceramic alumina core was analysed in both phase (powder and solid forms), in powder form before sintering, 10 peaks were found as seen in Figure 4.59a attributed to the presence of alumina (hexagonal phase (rhombohedral), corundum, aluminum oxide, code no:01-071-1126, density =4.03), but in solid form after sintering 12 peaks were found as seen in Figure 4.59b attributed to the presence of cubic zirconium oxide (code no: 00-049-1642), which is present as foreign phase in the sample of alumina having 10 peaks (density=4.02 code no:01-071-1126). Figure 4.60a showed the diffraction pattern for graded silica in powder and solid form (before and after sintering). In both powder and solid form, 11 peaks were found as seen in Figure 4.60b attributed to the presence 3 peaks of cubic zirconium oxide (code no: 00-027-0997, density= 6.20), which is present as foreign phase in the sample of graded silica (hexagonal phase, code no:01-083-2469, silicon oxide, density =2.74) and presence alumina (code no: 00-046-1212) (see Table 1, Appendix B).

The alumina toughened zirconia (ATZ) synthesised ceramic cores were analysed in both phases (powder and solid) by XRD. In Zr80%-Al20% ceramic powder, it was observed 13 peaks as seen in Figure 4.61a attributed to the presence 2 peaks of magnesium aluminum oxide (code no:00-033-0853, $MgAl_2O_4$, orthorhombic phase) in monoclinic

zirconia (code no:00-013-0307) mixed with lower amount phase tetragonal of zirconia in the mixture (code no: 01-083-0113) which was detected by XRD. In Zr80%-Al20% ceramic solid after sintering to 1500 °C, 14 peaks were found as seen in Figure 4.61b, 6 peak of tetragonal phase of zirconia (code no:00-050-1089) and 3 peaks of cubic phase of zirconia (code no: 01-083-0431) with 1 peak corundum (code no 00-46-1212) and 4 peaks of monoclinic phase of zirconia (code no: 00-013-0307). For Zr60%-Al40% ceramic powder, 14 peaks were found as seen in Figure 4.62a, 12 peaks of monoclinic phase of zirconia (code no: 00-013-0307) with 2 peak alumina (code no: 00-046-1212). After sintering as seen in Figure 4.62b, it was found 17 peaks, 8 peaks of tetragonal phase of zirconia (code no: 01-088-1007) with 4 peaks monoclinic phase of zirconia (code no: 00-013-0307) and 5 peaks of alumina (code no: 00-046-1212). For Zr50%-Al50% ceramic powder as shown in Figure 4.63a, it was found 18 peaks 13 peaks of monoclinic phase of zirconia (code no: 00-013-0307) and 4 peaks of alumina (code no: 00-042-1468) and 1 peak of tetragonal phase of zirconia (code no: 01-083-0113). After sintering, it was found 12 peaks as seen in Figure 4.63b, 7 peaks of tetragonal phase of zirconia (code no:01-083-0113), and 3 peaks of alumina (code no:00-042-1468), and 2 peaks lower amount of monoclinic phase of zirconia (code no:00-013-0307) (Table 1, Appendix B).

Figure 4.64a showed the diffraction pattern for the interface between the two layer Zr100-YZrO80%-Al20%, which had 6 peaks with 4 peaks of tetragonal phase of zirconia (code no: 00-050-1089) and 2 peaks of alumina (code no: 00-046-1212). Figure 4.64b showed the diffraction pattern for the interface between two layers of Zr100-Yzr60-Al40%, 4 peaks were found, 2 peaks of tetragonal phase of yttrium zirconium oxide (code no:01-083-0113) with 2 peaks of cubic phase magnesium zirconium oxide (code no: 01-083-0432). Figure 4.64c showed the diffraction pattern for the interface between the two layers Zr100%-YZr50%-Al50%, 7 peaks were found with 4 peaks of tetragonal phase of

zirconium yttrium oxide (code no:01-083-0113) and 3 peaks of alumina (code no:00-046-1212) (Table 1, Appendix B).

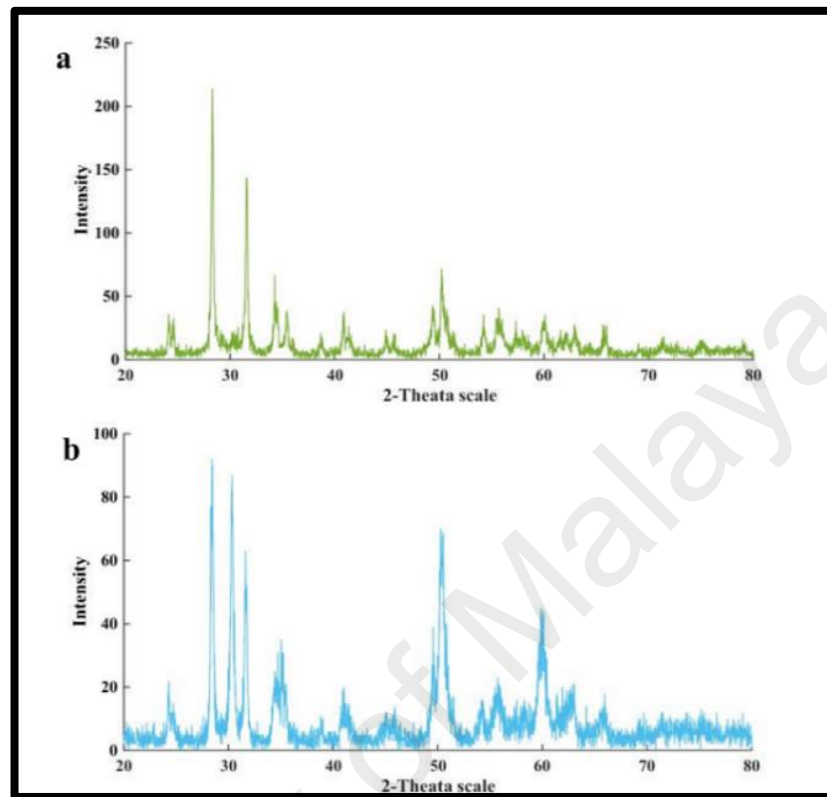


Figure 4.58: XRD pattern of ZrO₁₀₀ powder (a) and solid (b).

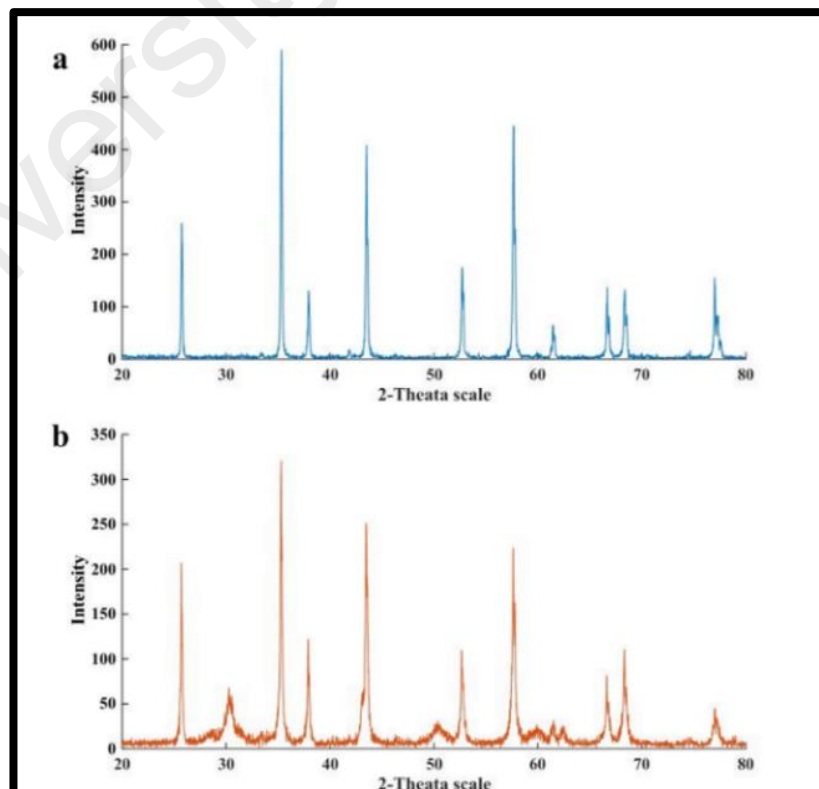


Figure 4.59: XRD pattern of Al₁₀₀ powder (a) and solid (b).

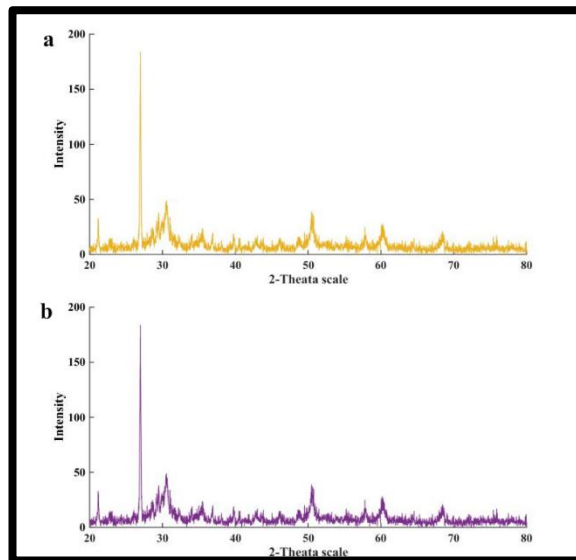


Figure 4.60: XRD pattern of silica powder (a) and solid (b).

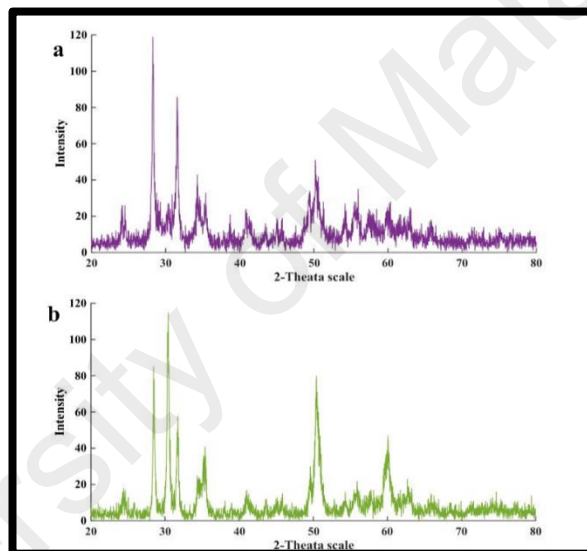


Figure 4.61: XRD pattern of ZrO₈₀Al₂₀% powder (a) and solid (b).

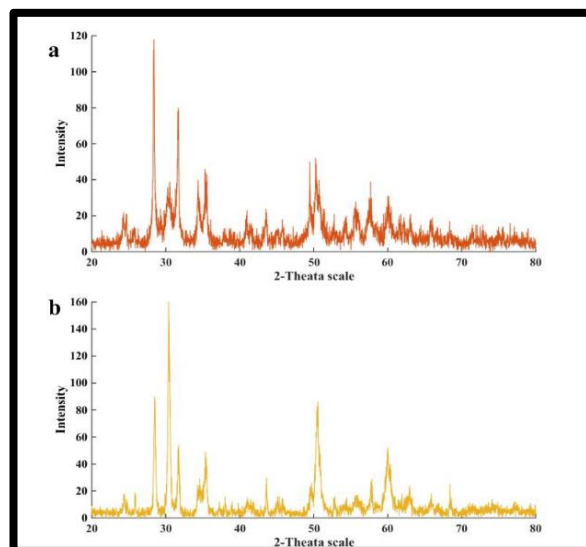


Figure 4.62: XRD pattern of ZrO₆₀Al₄₀% powder (a) and solid (b).

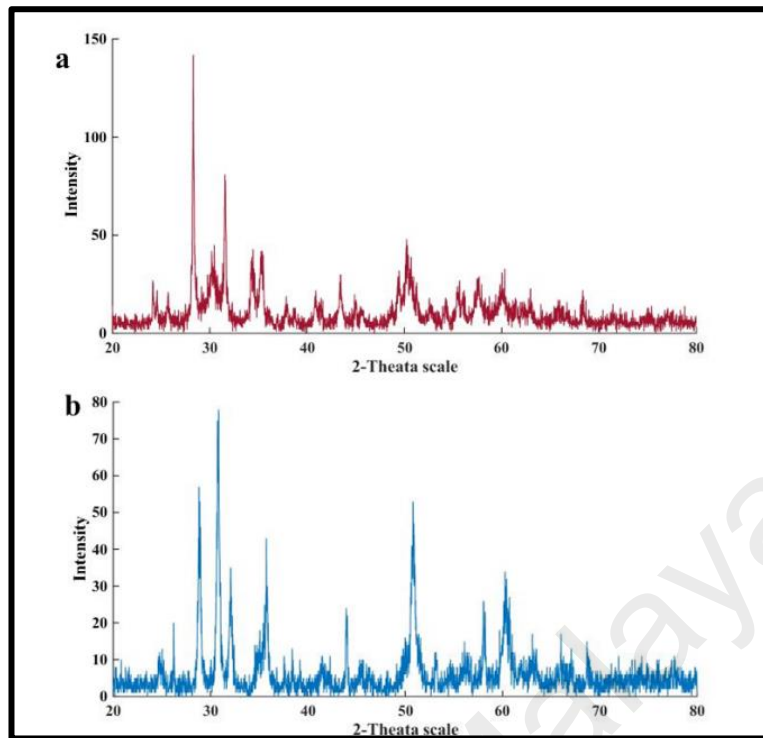


Figure 4.63: XRD of Zr50%-Al50% powder (a) and solid (b).

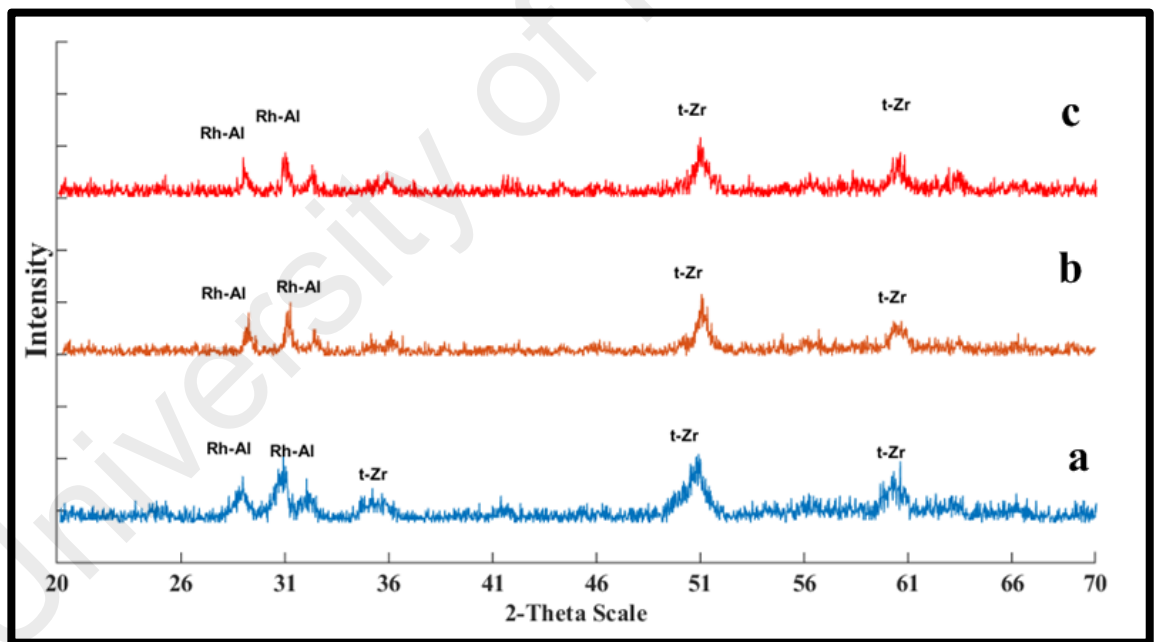


Figure 4.64: XRD of interface layers between two layers (a) Zr100%-Zr80%-Al20%, (b) Zr100%-Zr60%-Al40%, and (c) Zr100%-Zr50%-Al50%.

4.6.2 Results of Experimental, Relative density, and Porosity

The results of density (g/cm^3) were presented in Table 4.4. and Figure 4.65. Experiment density decreased with increasing alumina content for both single and

multilayered synthesised ceramic core composites, resulting in the differences in density between the synthesised ceramic core composites systems in this study as shown in Table 4.4.

The results of relative density (g/cm^3) were presented in Table 4.4. and Figure 4.66. Relative density decreased with increasing alumina content for both single and multilayered synthesised ceramic core composites, resulting in the differences in relative density between the synthesised ceramic core composites systems in this study as shown in Table 4.4.

The results of porosity (%) were presented in Table 4.4. and Figure 4.67. Porosity decreased with increasing alumina content for both single and multilayered ceramic composites, resulting in the differences in porosity between the synthesis ceramic cores composites systems in this study as shown in Table 4.4.

Table 4.4: Mean of experimental, relative density, and porosity of synthesised bioceramic cores.

Groups	Bioceramic Cores	N	Experimental density (g/cm^3)		Relative density		Porosity (%)	
			Mean	SD \pm	Mean	SD \pm	Mean	SD \pm
A	YZrO100%	10	5.318	0.17	0.90	.029	7.82	0.48
B	YZrO80%-MgAlO20%	10	5.240	0.01	0.95	.002	5.05	0.24
C	YZrO60%-MgAlO40%	10	4.720	0.05	0.93	.014	4.53	0.31
D	YZrO50%-MgAlO50%	10	4.503	0.02	0.91	.005	4.50	0.28
E	MgAlO100%	10	3.898	0.09	0.98	.022	2.37	0.30
F	Graded Silica	10	2.177	0.10	0.84	.037	8.30	0.29
G	YZrO100%-YZrO80% +MgAlO20%	10	4.888	0.18	0.86	.029	9.67	0.31
H	YZrO100%-YZrO60% +MgAlO40%	10	4.972	0.05	0.90	.009	8.45	0.28
I	YZrO100%-YZrO50% +MgAlO50%	10	4.954	0.05	0.91	.010	7.63	0.31

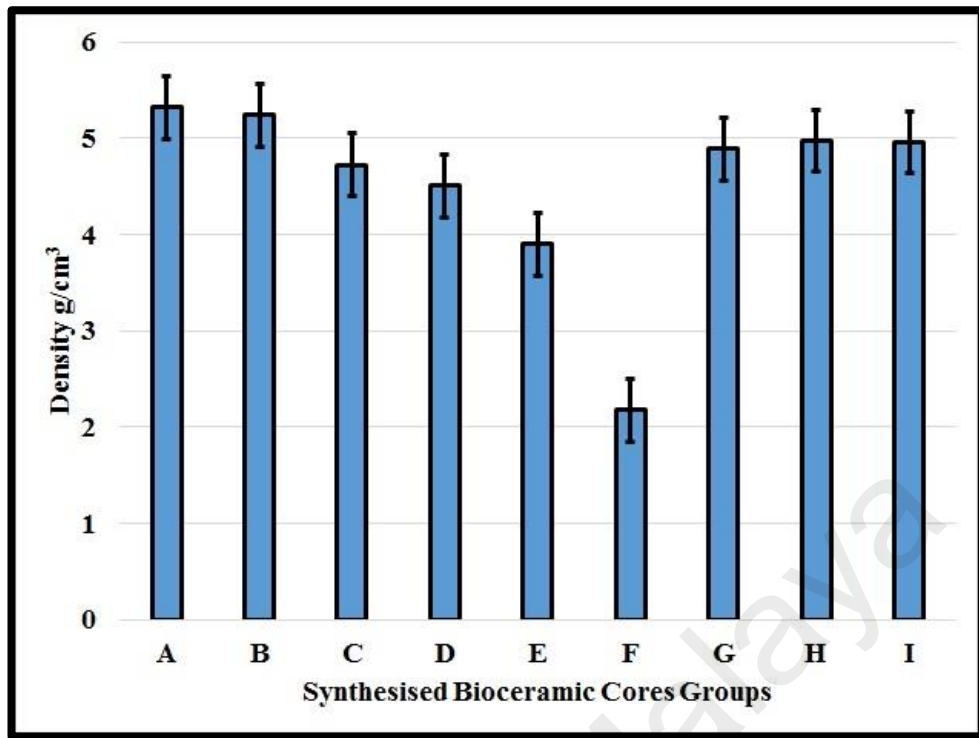


Figure 4.65: Experimental density of all synthesised ceramic cores.

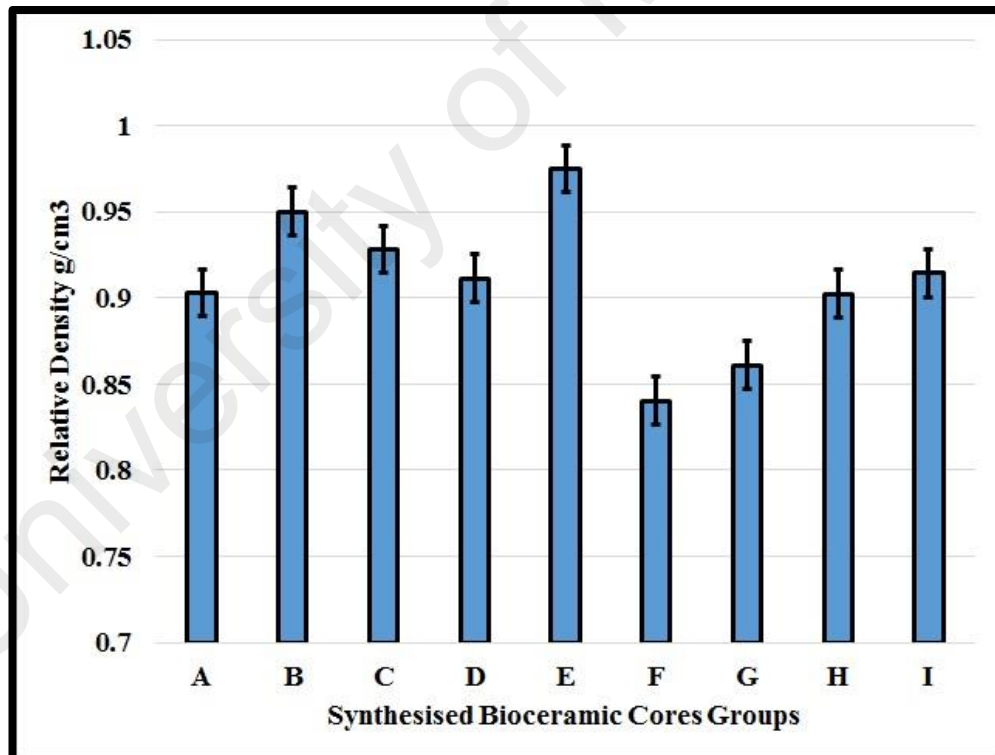


Figure 4.66: Relative density of all synthesised ceramic cores.

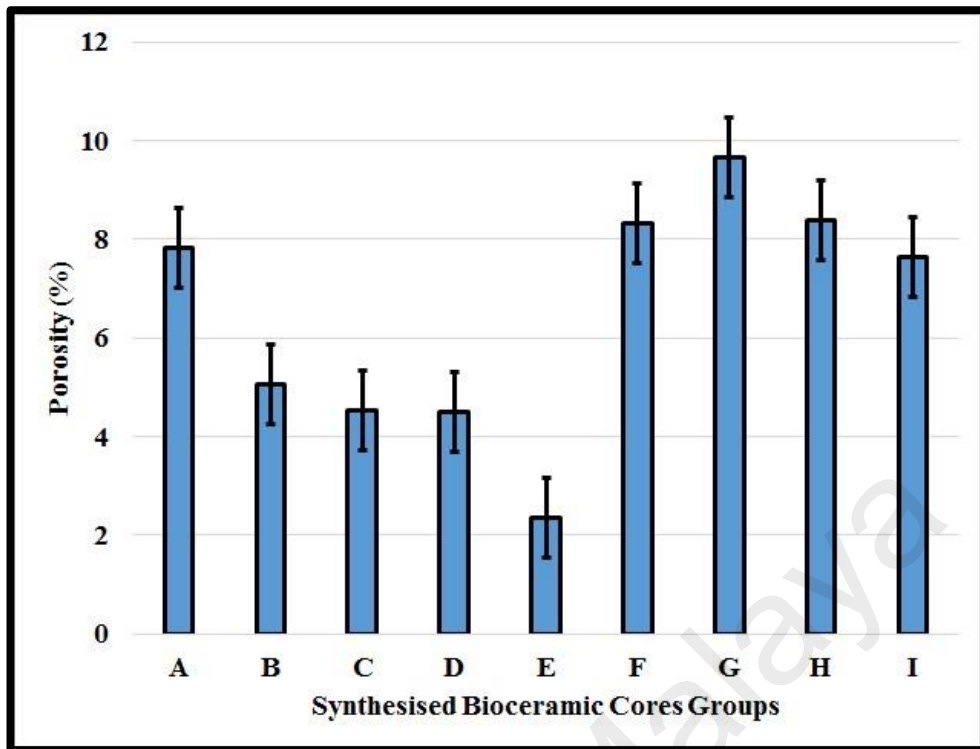


Figure 4.67: Porosities of all synthesised ceramic cores.

4.6.3 Results of the Volume Shrinkage, Vickers Hardness, and CTE

The results of volume shrinkage (%) were presented in Table 4.5. and Figure 4.68. The volume shrinkage decreased with increasing alumina content for both single and multilayered ceramic composites, resulting in the differences in shrinkage between the synthesised ceramic cores composites systems in this study as shown in Table 4.5.

The results of Vicker hardness were presented in Table 4.5. and Figure 4.69. Vickers hardness increased with increasing alumina content for both single and multilayered ceramic composites, resulting in the differences in Vickers hardness between the composites systems in this study as shown in Table 4.5.

Figure 4.70 to Figure 4.77 showed the indentation load areas with different sizes into each layer of different synthesised ceramic cores.

Table 4.5: Mean of volume shrinkage, Vickers Hardness, and CTE of synthesised bioceramic cores.

Groups	Bioceramic Cores	N	Volume shrinkage (%)		Vickers Hardness (MPa)		CTE ($10^{-6}/K$)	
			Mean	SD \pm	Mean	SD \pm	Mean	SD \pm
A	YZrO100%	10	37.70	0.61	1292.8	26.82	10.5	0.03
B	YZrO80%-MgAlO20%	10	36.66	0.57	1432.6	16.94	10.2	0.03
C	YZrO60%-MgAlO40%	10	34.20	0.86	1545.7	26.55	10.1	0.03
D	YZrO50%-MgAlO50%	10	33.78	0.53	1583.9	27.37	10.0	0.03
E	MgAlO100%	10	21.24	1.60	1711.9	26.61	8.4	0.05
F	Graded Silica	10	35.77	2.71	942.1	13.23	8.2	0.04
G	YZrO100%-YZrO80% +MgAlO20%	10	35.69	1.16	1260.9	21.40	10.4	0.03
H	YZrO100%-YZrO60% +MgAlO40%	10	37.82	1.40	1349.9	27.25	10.4	0.03
I	YZrO100%-YZrO50% +MgAlO50%	10	38.16	1.97	1457.0	27.23	10.4	0.03

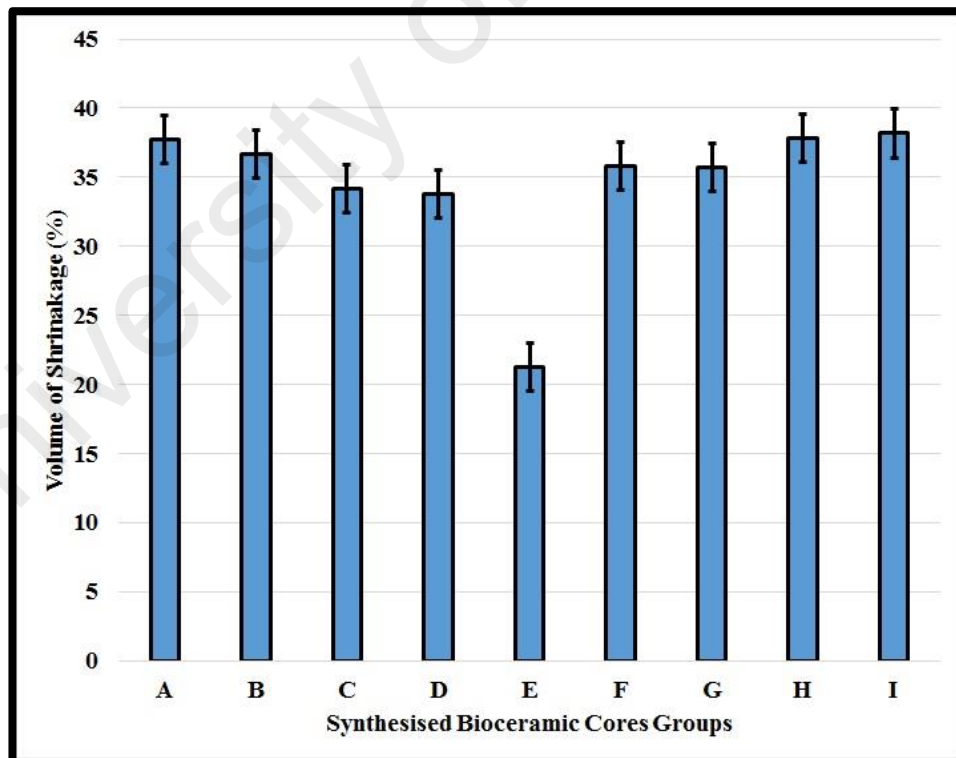


Figure 4.68: Volume shrinkage of all synthesised ceramic cores.

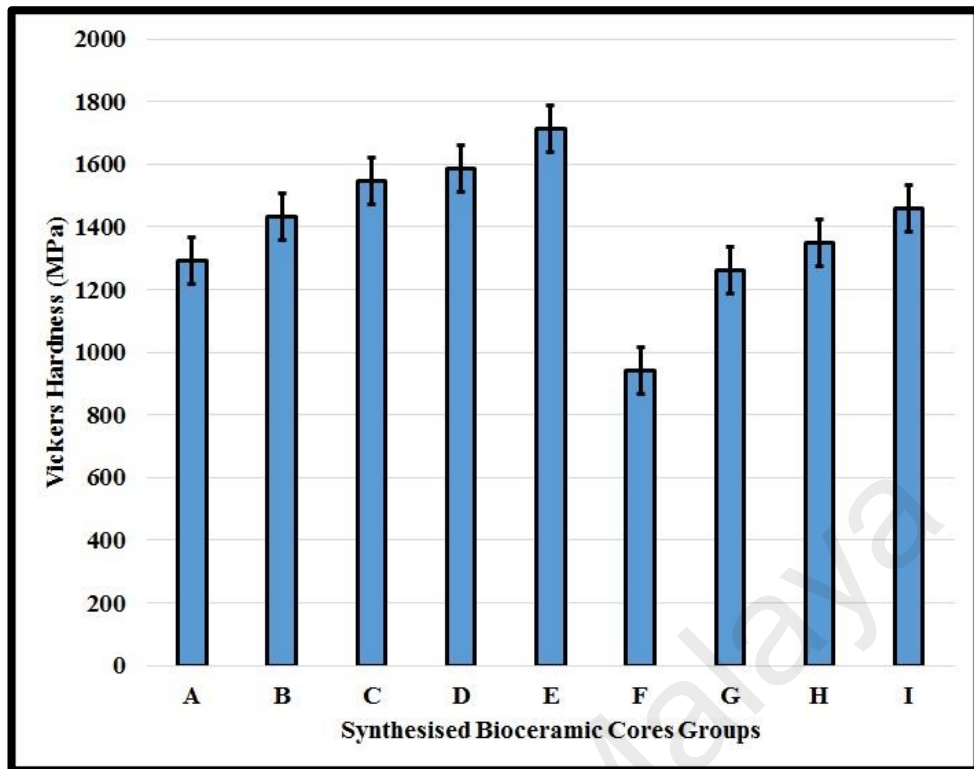


Figure 4.69: Vickers Hardness of all synthesised ceramic cores.

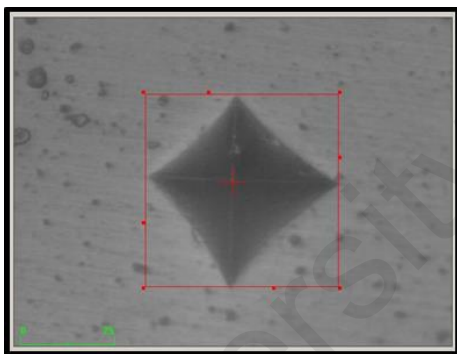


Figure 4.70: Vickers indentation of YZr100% layer.

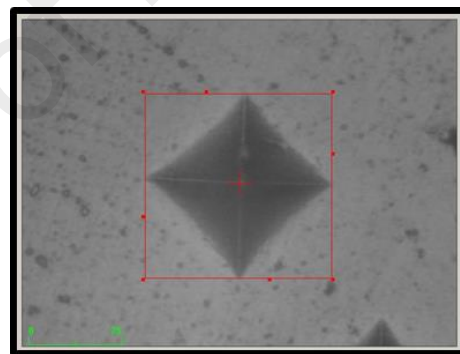


Figure 4.71: Vickers indentation of Zr80%-Al20% layer.

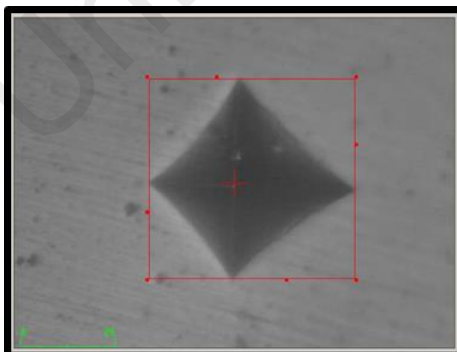


Figure 4.72: Vickers indentation of Zr60%-Al40% layer.

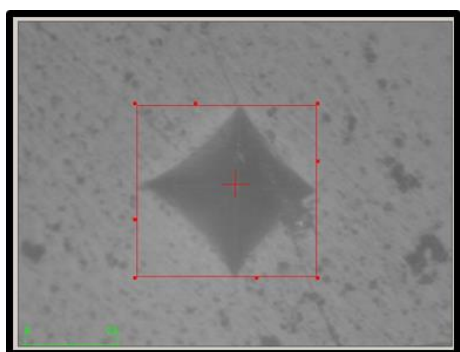


Figure 4.73: Vickers indentation of Zr50%-Al50% layer.

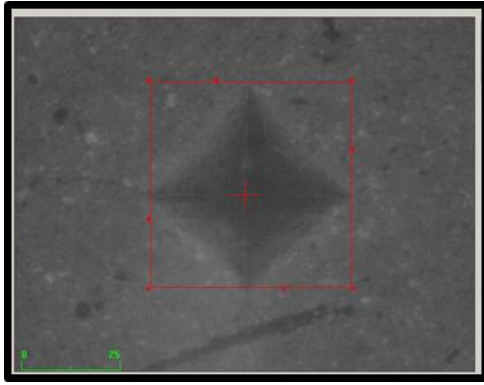


Figure 4.74: Vickers indentation of graded silica layer.

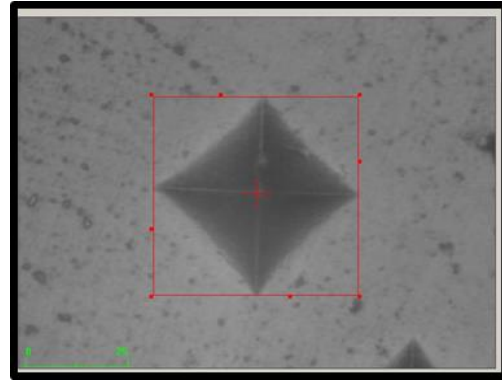


Figure 4.75: Vickers indentation of Zr100%-Zr80%-Al20% layer.

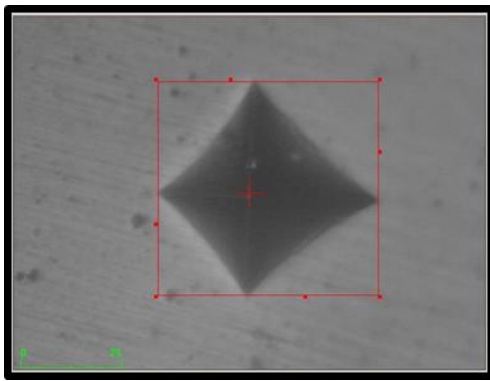


Figure 4.76: Vickers indentation of Zr100%-Zr60%-Al40% layer.

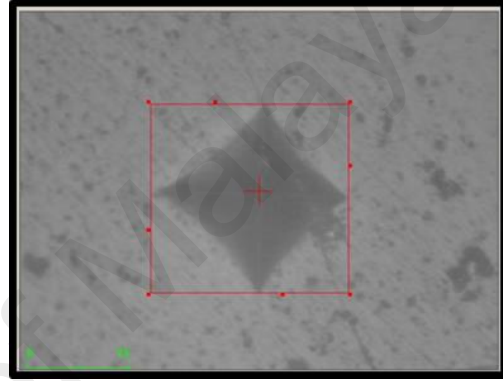


Figure 4.77: Vickers indentation of Zr100%-Zr50%-Al50% layer.

The results of TMA for determination of the coefficient of thermal expansions of synthesised ceramic cores were presented in Table 4.5. and Figure 4.78. The volume shrinkage decreased with increasing alumina content for both single and multilayered ceramic composites, resulting in the differences in shrinkage between the synthesised ceramic core composites systems in this study as shown in Table 4.5.

From the Figure 4.79 to Figure 4.87 showed the thermal expansion of zirconia, MgAl_2O_3 alumina, ceramic composites containing 100, 80, 60, 50 wt% Y-TZP, and graded silica have been determined as a function of temperature utilizing the TMA when the temperature increase from 25 °C to 500 °C.

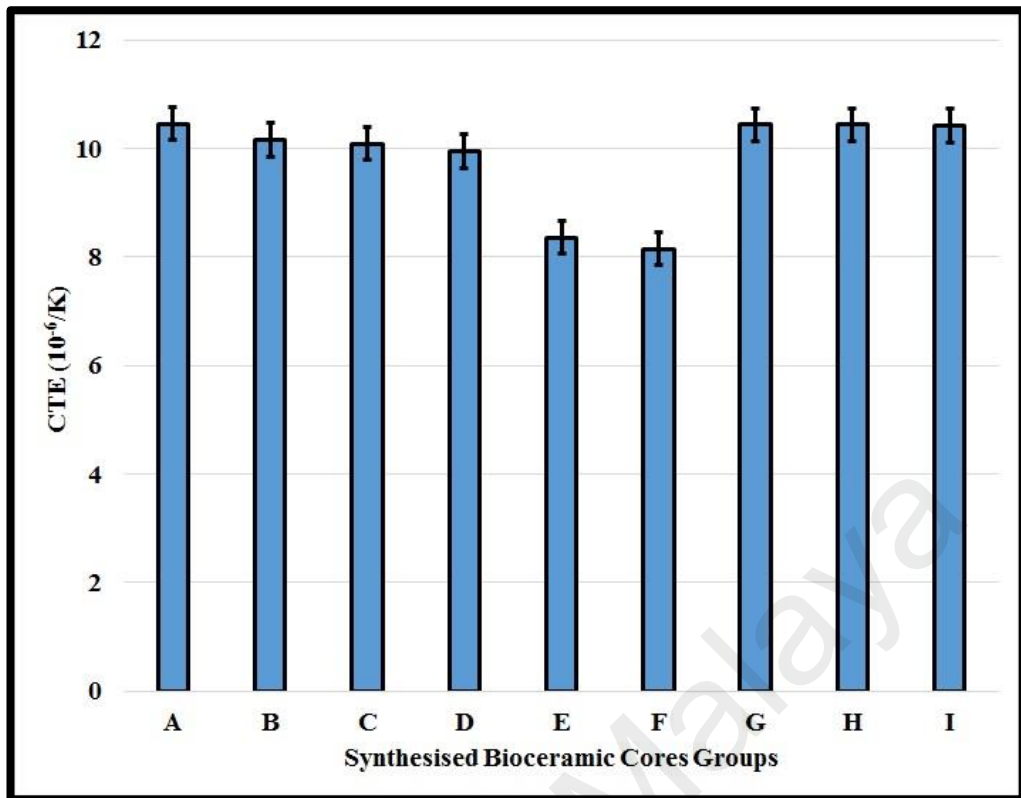


Figure 4.78: CTE of all synthesised ceramic cores.

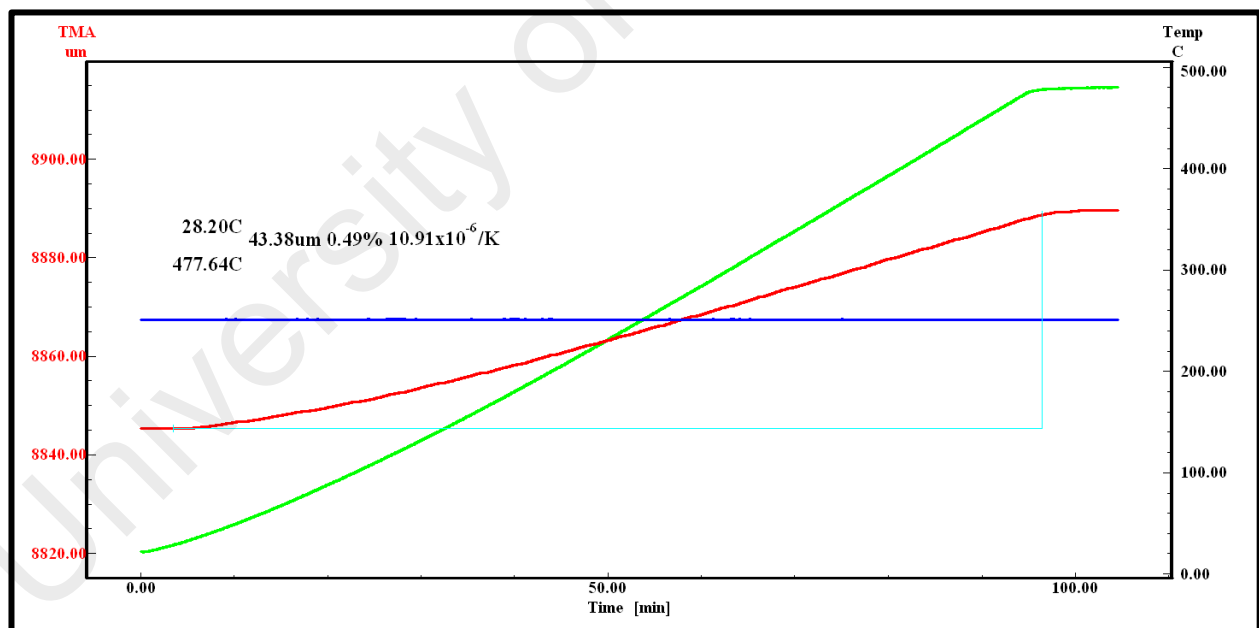


Figure 4.79: CTE of zirconia 100% ceramic core layer.

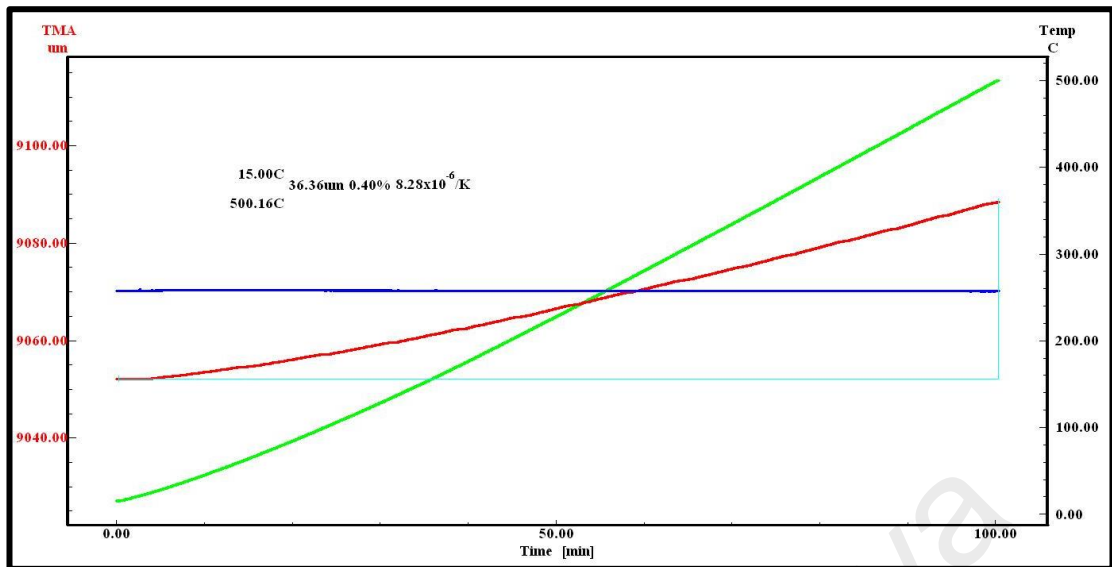


Figure 4.80: CTE of alumina 100% ceramic core layer.

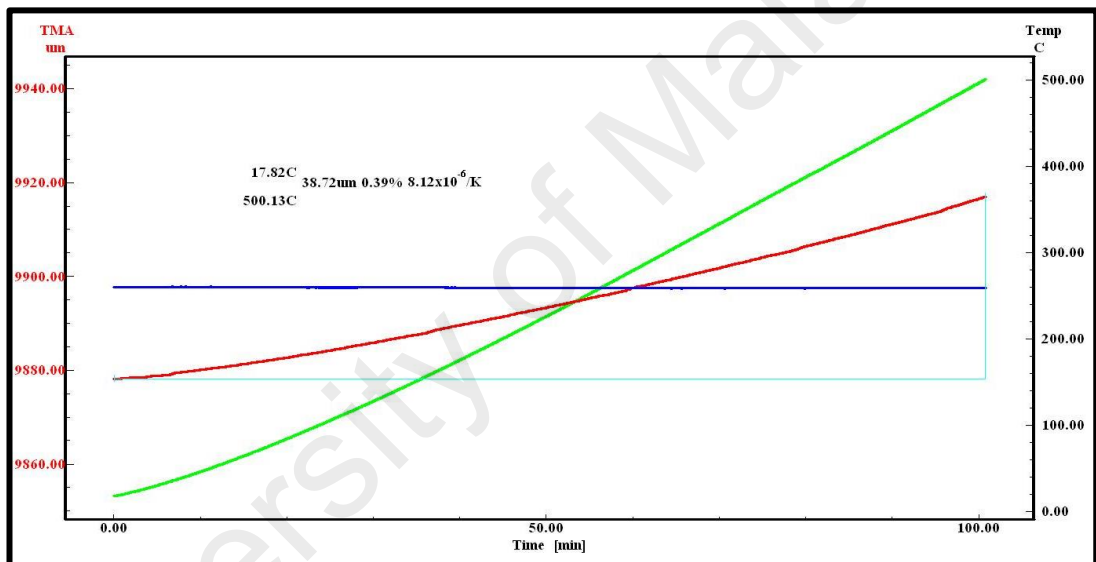


Figure 4.81: CTE of graded silica layer.

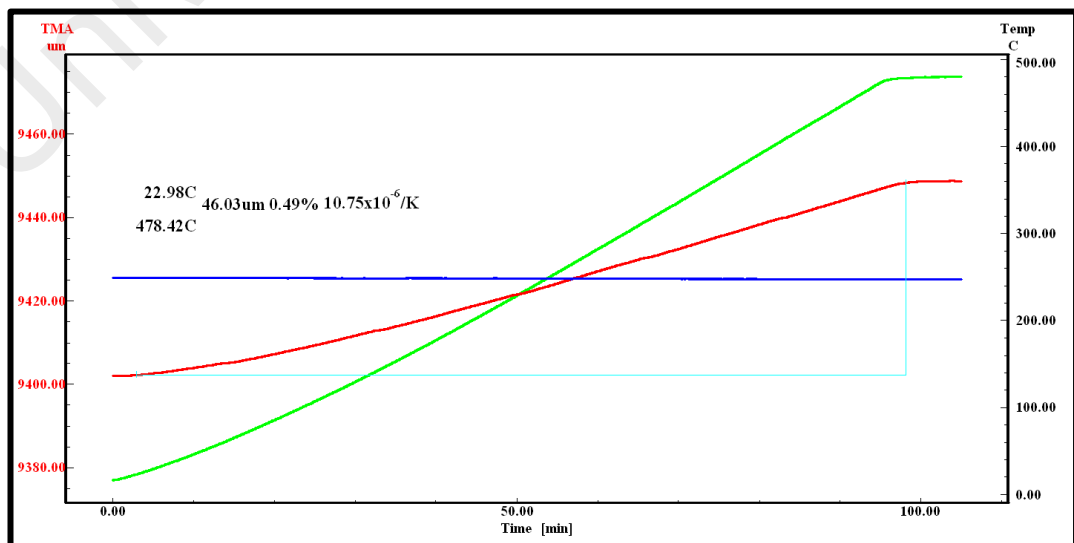


Figure 4.82: CTE of Zr80%-Al20% ceramic core layer.

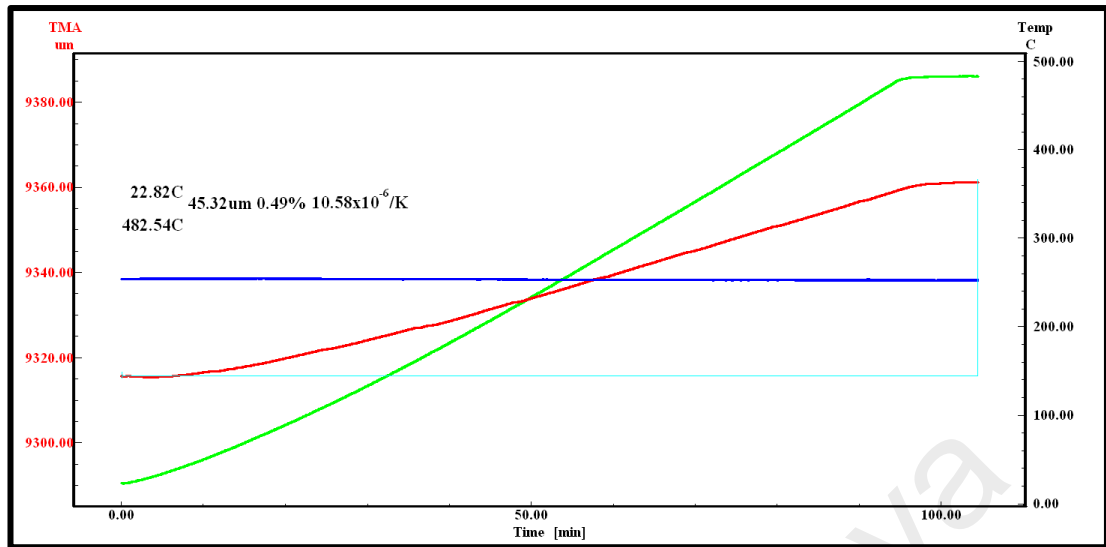


Figure 4.83: CTE of Zr60%-Al40% ceramic core layer.

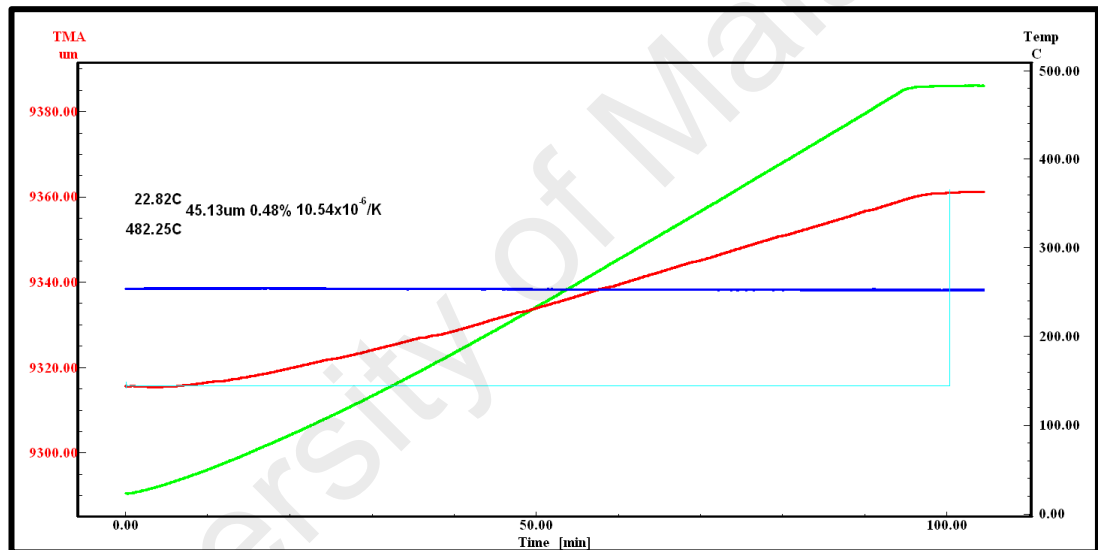


Figure 4.84: CTE of Zr50%-Al50% ceramic core layer.

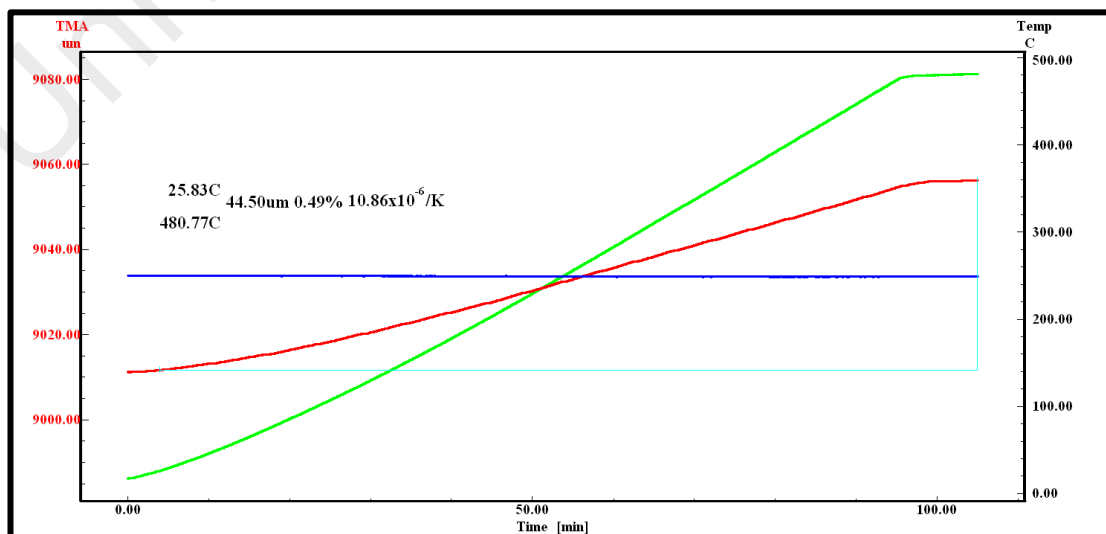


Figure 4.85: CTE of Zr100%-Zr80%-Al20% ceramic two layers.

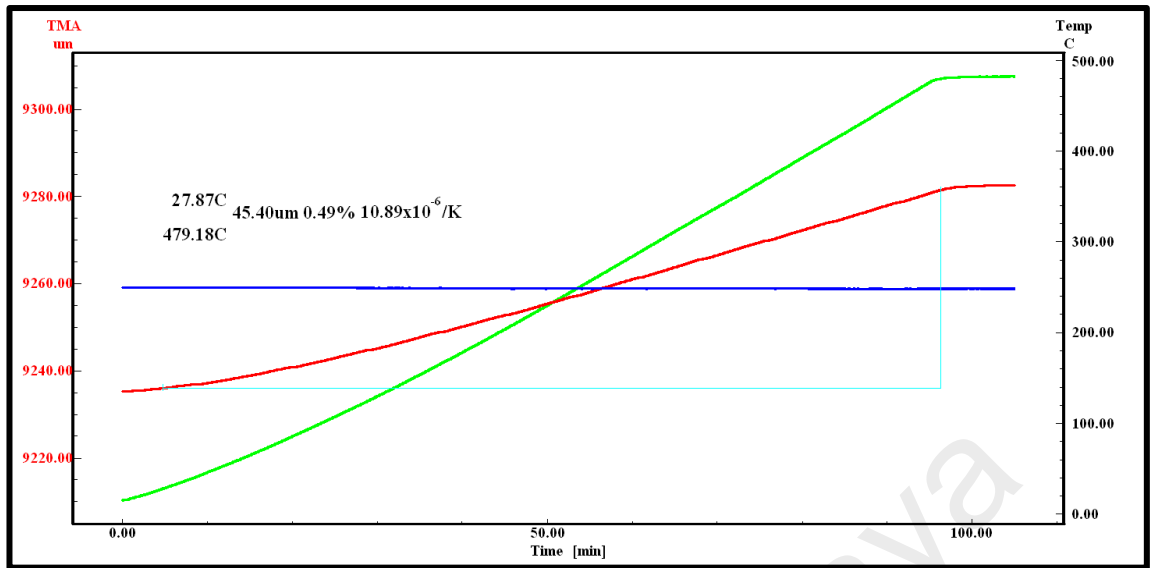


Figure 4.86: CTE of Zr100%-Zr60%-Al40% ceramic two layers.

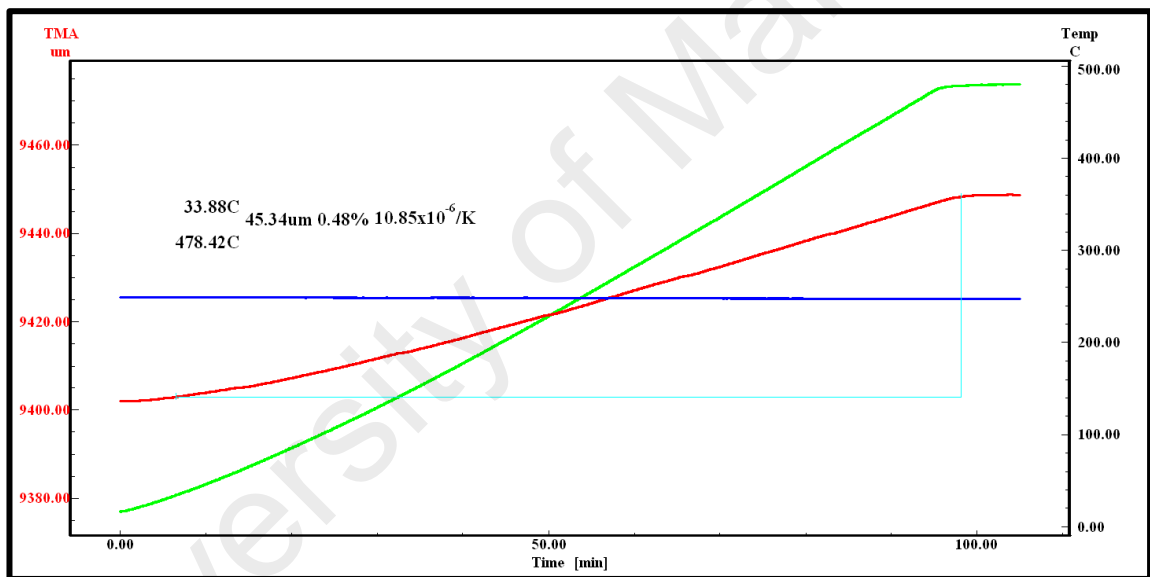


Figure 4.87: CTE of Zr100%-Zr50%-Al50% ceramic two layers.

4.6.4 Results of the Compressive Strength, Elastic Young's Modulus, and Strain

The mean values and standard deviations of the compressive strength (MPa), strain (%), and elastic Young's modulus (E) (GPa) for synthesised bioceramic cores were tested. Here, the compressive strength, strain, and elastic modulus were obtained at the yield point. SPSS statistical software (version 21, USA) was used to conduct one-way ANOVA test to examine the significance of the compressive strength, strain, and elastic modulus values.

The results of compressive strength (MPa) were presented in Table 4.6. and Figure 4.88. The compressive strength for multilayered synthesised ceramic cores slightly increased with increasing alumina content than single ceramic composites, resulting in the little differences in compressive strength between the synthesised ceramic composites systems compared to homogenous zirconia and alumina groups in this study as shown in Table 4.7 by one-way ANOVA.

The results of elastic modulus were presented in Table 4.6. and Figure 4.89. Elastic modulus increased linearly with increasing alumina content for both single and multilayered ceramic composites, resulting in the significant differences in elastic modulus between the synthesised ceramic composites systems in this study as shown in Table 4.8 by one-way ANOVA.

Table 4.6: Mean of compressive strength, elastic modulus, and strain of synthesised bioceramic cores.

Groups	Bioceramic Cores	N	Compressive strength (MPa)		Elastic modulus (GPa)		Strain (%)	
			Mean	SD	Mean	SD	Mean	SD
A	YZrO100%	10	743.9 ^a	26.1	210.1 ^{a,c}	4.2	3.3 ^b	.9
B	YZrO80%-MgAlO20%	10	642.9 ^{a,b}	32.4	306.7 ^{a,b,c}	10.6	2.7 ^{a,b}	.5
C	YZrO60%-MgAlO40%	10	654.3 ^{a,b}	20.2	329.5 ^{a,b,c}	12.5	3.8 ^b	.8
D	YZrO50%-MgAlO50%	10	669.9 ^{a,b}	25.0	341.2 ^{a,c}	23.2	4.3 ^{a,b}	1.5
E	MgAlO100%	10	844.0 ^a	29.7	377.2 ^{a,c}	16.8	3.3 ^b	.8
F	Graded Silica	10	445.1	18.4	187.0	8.5	2.1	.4
G	YZrO100%-YZrO80% +MgAlO20%	10	645.1 ^{a,b}	26.2	287.5 ^{a,b,c}	10.5	3.1 ^{a,b}	.6
H	YZrO100%-YZrO60% +MgAlO40%	10	657.1 ^{a,b}	32.2	313.0 ^{a,b}	30.2	3.6 ^b	.5
I	YZrO100%-YZrO50% +MgAlO50%	10	659.7 ^{a,b}	32.1	320.1 ^{a,b,c}	14.0	3.3 ^b	.6

^a Significant difference ($P < 0.05$) at same column based on the Tukey test.

^b No significant difference ($P > 0.05$) at same column based on the Tukey test.

^c significant difference ($P < 0.05$) at same column based on the Tukey test.

The results of strains were presented in Table 4.6. and Figure 4.90. the strains increased linearly with increasing alumina content for both single and multilayered ceramic composites, resulting in the significant differences in the strains between the synthesised ceramic composites systems in this study as shown in Table 4.9 by one-way ANOVA.

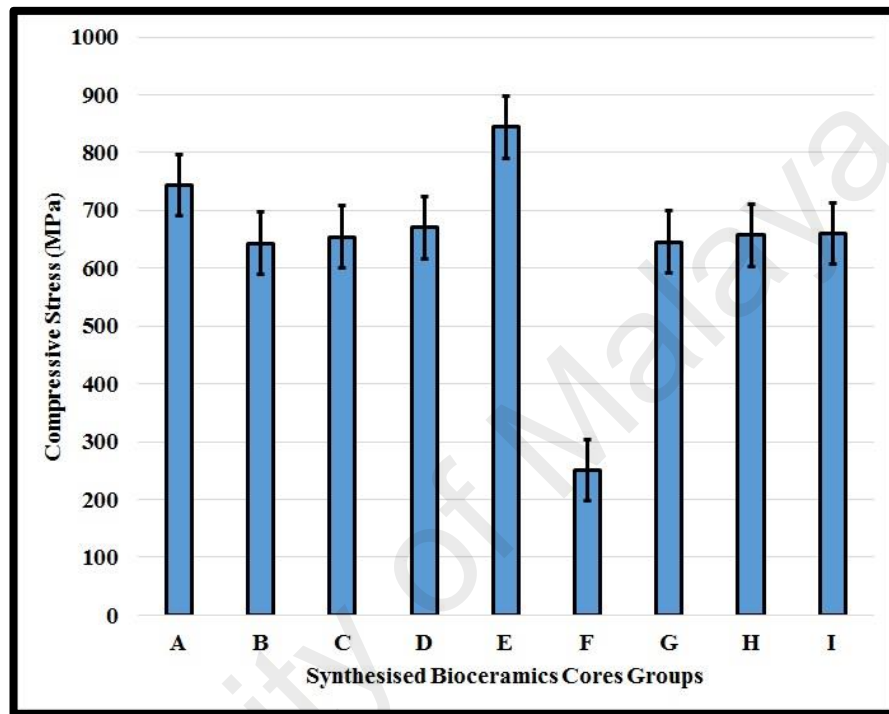


Figure 4.88: Compressive strength of all synthesised ceramic cores.

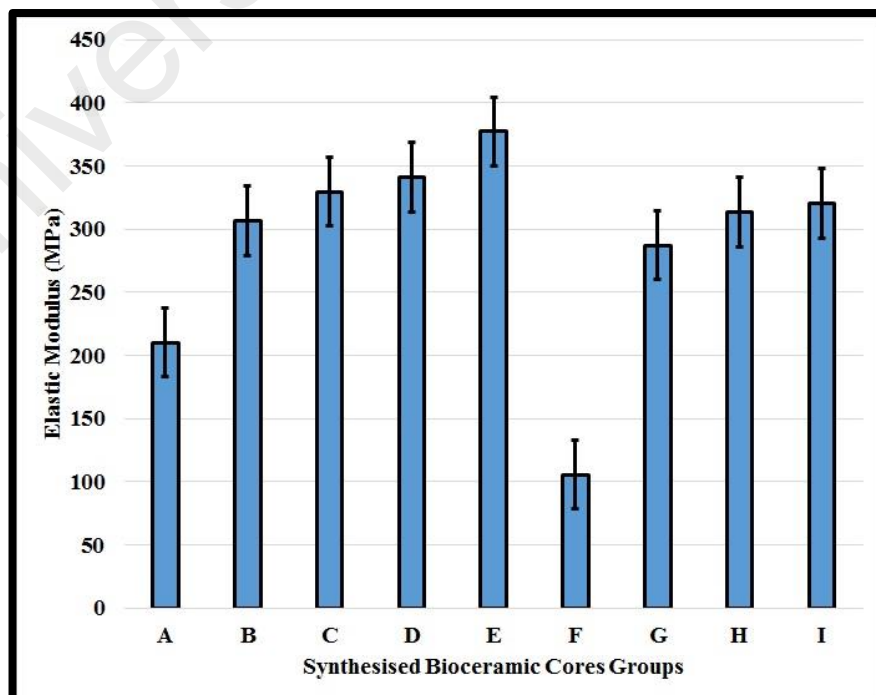


Figure 4.89: Elastic modulus of all synthesised ceramic cores.

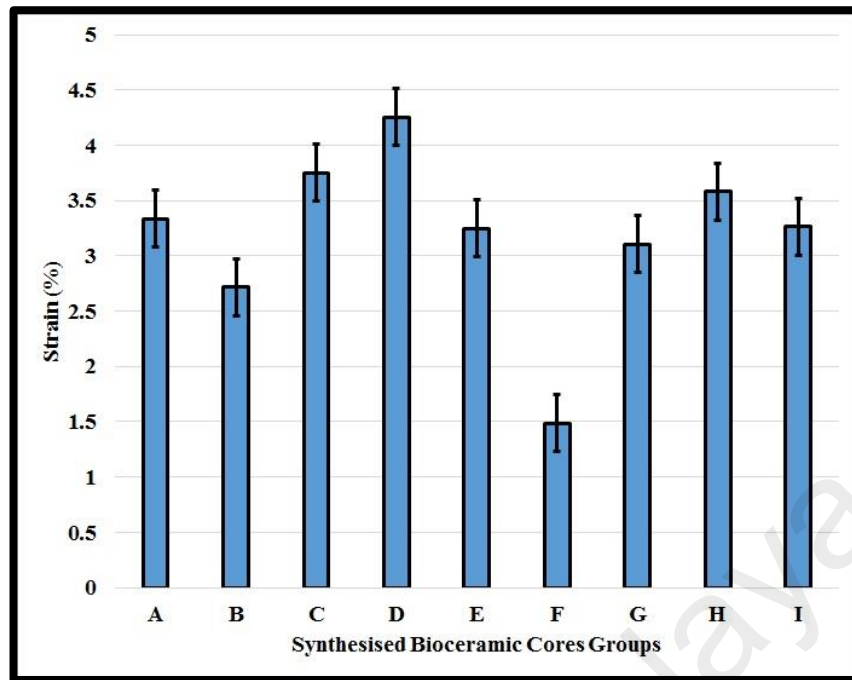


Figure 4.90: Strains of all synthesised ceramic cores.

The results of the comparisons by Tukey test for the compressive strength of all synthesised ceramic cores were shown in Table 4.5. Compressive strength in homogenous zirconia and alumina was more than in synthesised single and multilayered ceramic cores, there was significant differences ($P < .05$) between homogenous zirconia and alumina and synthesised single layers and multilayers ceramic cores in the mean of compressive strength. Also, there was a significant difference between homogenous alumina and zirconia ($P < .05$). The slightly similar results were obtained the compressive strength of synthesised single and multilayered ceramic core except zirconia (743.9 MPa) and alumina (844.0 MPa) ceramic cores were different. There was also no significant difference between synthesised single layers and multilayers ceramic cores in mean of compressive strength ($P > .05$) as shown in Table 4.5 and Table 4.6.

Table 4.7: Compressive stresses of synthesised ceramic cores.

	Sum of Squares	Df	Mean Square	F	Sig.*
Between Groups	345506.537	7	49358.077	61.006	.000
Within Groups	58253.397	72	809.075		
Total	403759.934	79			

*. One-way ANOVA (Levene test of homogeneity of variances = 0.485).

The results of the comparisons by Tukey test for the elastic modulus of all synthesised ceramic cores were shown in Table 4.5. Elastic modulus in homogenous zirconia was lesser than in homogenous alumina, synthesised single, and multilayered ceramic cores, there was significant difference ($P < .05$) between homogenous zirconia and alumina and synthesised single layers and multilayers ceramic cores in the mean of elastic modulus. Also, there was a significant difference between homogenous alumina and zirconia ($P < .05$). However, there was no significant difference between ZrO80%-Al20% synthesised single layers and multilayers ceramic cores in mean of elastic modulus ($P > .05$), and there was only significant difference between ZrO60%-Al40% synthesised single layers and ZrO100%-ZrO80%-Al20% multilayers ceramic cores in mean of elastic modulus ($P < .05$). There no significant difference between ZrO50%-Al50% single layer and ZrO60%-Al40% and ZrO100%-ZrO50%-Al50% multilayers ($P > 0.05$) as shown in Table 4.5 and Table 4.7.

Table 4.8: Effect of the elastic modulus of all synthesised ceramic cores.

	Sum of Squares	Df	Mean Square	F	Sig.*
Between Groups	164999.414	7	23571.345	81.202	.000
Within Groups	20900.187	72	290.280		
Total	185899.601	79			

*. One-way ANOVA (Levene test of homogeneity of variances = 0.231).

The results of the comparisons by Tukey test for the strain of all synthesised ceramic cores were shown in Table 4.5. There were no significant differences ($P < .05$) between homogenous zirconia and alumina and synthesised single layers and multilayers ceramic cores in the mean of strain. There was a significant difference between ZrO80%-Al20% single layer and ZrO50%-Al50% single layer ($P = .002$). There was also a significant difference between ZrO50%-Al50% synthesised single layer and ZrO100%-ZrO80%-Al20% multilayers ceramic cores in mean of strain ($P = .049$) as shown in Table 4.5 and Table 4.8.

Table 4.9: Effect of the strains on all synthesised ceramic cores.

	Sum of Squares	Df	Mean Square	F	Sig.*
Between Groups	14.914	7	2.131	3.157	.006
Within Groups	48.594	72	0.675		
Total	63.508	79			

*. One-way ANOVA (Levene test of homogeneity of variances = 0.104).

University of Malaya

4.7 Discussion

Kim and Paulino (2003), Paulino et al., (2003), and Walters et al., (2004) have developed precise graded finite elements for the modelling of FGM. Such models could obviously form the fundamental for future study to calculate crack driving loads and assist with developing a better understanding of fracture processes in FGM. They could also be applied to the design of future bio-inspired structures with nonlinear material laws that have a more advanced scope (Huang et al., 2007b). There is, therefore, a need for further research on FGMs for the future applications in dentistry.

The previous study by Huang et al., (2007b) added FGM layer with its Young's modulus varying gradually from dental cement layer to enamel-like dental layer ceramic (Huang et al., 2007b). FE simulations of the structure showed that adding an FGM adhesive layer can significantly reduce the concentrated stresses in the sub-surface of the top ceramic layer. This increases the resistance of the structure to radial cracking. Moreover, the calculated lengths of critical cracks were much higher than those calculated in both existing dental crowns and the natural tooth enamel-dentine complex (Huang et al., 2007a). This suggests the possibility of building synthetic, bio-inspired, functionally graded dental multilayers that have better durability or comparable than those of natural teeth. However, the study of Huang et al., (2007b) did not provide experimental validation of the concept.

Depending on the results of the simulated FEA of the synthesised graded bioceramic, results, and discussion in chapter 3, the experimental study was conducted and discussed in detailed in this current chapter 4.

In this current study, observations of the sintered synthesised ceramic composite biomaterials by FESEM observed highly homogeneous microstructures without

agglomerates, abnormally grown grains of alumina or some pores. XRD analyses of the specimens indicated that only monoclinic, tetragonal zirconia and α -alumina, are the crystalline phases present in both the pure (zirconia and alumina) and in the ATZ composites. A bimodal and a fine distribution of particles size permitted the most effective fulfilling of the matrix socket for uniaxially pressing, reinforcing better densification of the powders. The utilization of 0.6 wt.% of ethanol (99.99%) as a dispersant was efficient to avoid agglomerates that were sources of imperfections during sintering (Kunes et al., 2000; Mukherjee et al., 2001).

The results of this study revealed that the pinning effect of $3Y\text{ZrO}_2$ on the grain growth of Al_2O_3 is distinct in the synthesised ceramic composite. That is, with the increase in ZrO_2 , two phenomena were evident. One is the morphology change of Al_2O_3 grain. It changed gradually from plate-like to equiaxed. The suppressing effect of ZrO_2 on the formation of plate-like Al_2O_3 grains is obvious. The other is the decrease of Al_2O_3 grain size. At low volume, fractions of 3Y-TZP the ZrO_2 particles (white grains) are inefficient in pinning the Al_2O_3 grain boundaries, so that exaggerated or abnormal grain growth happens easily, as shown in Figure 4.36 and Figure 4.37 (60 and 50 vol% 3Y-TZP). Some ZrO_2 particles are trapped into Al_2O_3 grains. The results of this current study, therefore is in agreement with previous studies by Lange and Hirlinger (1984), Kibbel and Heuer (1986), Huang et al., (2003), and Weimin et al., (2008).

Lange and Hirlinger (1984) reported that the abnormal growth of Al_2O_3 was prevented by the ZrO_2 inclusions at volume fractions 55%. The discrepancy suggests that other parameters besides ZrO_2 volume fraction influence microstructural development. Kibbel and Heuer (1986) observed that the break up of grain growth in a ATZ with a higher volume fraction of ZrO_2 than that possibly required to prevent exaggerated grain growth. They showed that the reason was linked to impurities altering the properties of the

ubiquitous and continuous glassy grain-boundary phase (Huang et al., 2003). The ZrO_2 has an action of transformation toughening on the Al_2O_3 matrix, and it also can suppress Al_2O_3 grain growth. There is a little solid solubility between Al_2O_3 and $ZrO_2(Y_2O_3)$. Al^{3+} (0.57\AA), Zr^{4+} (0.87\AA) and Y^{3+} (1.015\AA) form interpenetration boundaries which can hinder Al_2O_3 growth. In addition, a little ZrO_2 has an action of pinning Al_2O_3 boundary (Lange, 1982; Weimin et al., 2008).

The results of this study revealed that the microstructure of the sintered 95vol% Al_2O_3 , at $1500\text{ }^\circ\text{C}$, had irregular grains growth or was not fully dense with grains and pores although 5% of MgO was added to the alumina powder to prevent abnormal grain growth. Wang et al., (2001) indicated that plate-like grains of Al_2O_3 can be found when the body contained a small amount of impurities, especially when SiO_2 is present with other oxides. However, the formation of plate-like grains usually needs higher temperature ($\geq 1500\text{ }^\circ\text{C}$) and longer holding time (Koyama et al., 1993). In the present work, observation by EDX found small amounts of SiO_2 and other oxides in alumina powder.

In this study, by adding Al_2O_3 into the ZrO_2 matrix, the presence of the two featured grains, ZrO_2 (white grain) and Al_2O_3 (dark grain) can be obviously seen, as well as an increasing amount of Al_2O_3 grains due to the increasing Al_2O_3 wt% content in the ceramic composites. With the increasing amounts of Al_2O_3 (wt%), larger grain sizes of both phases, Al_2O_3 and ZrO_2 , were observed. Also, it can be noted that the grain growth rate of the ZrO_2 phase is lower than that of the Al_2O_3 phase. Additionally, the grain growth of both phases Al_2O_3 and ZrO_2 can be obviously observed after sintering. A similar behaviour had been noted by Alexander et al., (1994) and Santos et al., (2009b) for ZrO_2 - Al_2O_3 ceramic composites. However, this study did not measure the kinetic grain growth in different sintering time and sintering process using the hot isostatic press. It is a limitation and further investigations are needed.

Zhang et al., (2006a) investigated the pressureless sintering behaviour of the nanocrystalline $\text{Al}_2\text{O}_3\text{-Y}_2\text{O}_3\text{-ZrO}_2$ system with YSZ (3 mol%) as a function of alumina content from 5 up to 30 mol% (Zhang et al., 2006a). It had reported that the fully dense pellets after sintering for 4 h at 1200 °C with the alumina-free yttria-stabilized specimen. The particle sizes of their starting material were around 10 nm. An addition of 5 mol% alumina resulted in a density of 99% whereas an addition of 30 mol% Al_2O_3 lowered the density to 80%. They concluded that alumina suppressed densification and inhibited grain growth. Similar results were reported by Srdić et al., (2000). The higher sintering temperature was required due to the larger particle sizes of the initial powders and the higher alumina content in the specimens. Fully dense specimens were obtained by hot isotatic pressing for 30 min at 1400 °C or 2 h at 1350 °C (Oelgardt et al., 2010).

In this study, the phase compositions were seen to be almost identical and thus independent of the starting powders. The specimens consisted of 20, 40, and 50 wt% Al_2O_3 for the ATZ composite system and 100 wt% Al_2O_3 and 100 wt% Y-TZP for the synthesised single layer and multilayers ceramic systems. After sintering the zirconia phase was tetragonal and lower amount of monoclinic phase. An interesting phenomenon is that the amount of monoclinic zirconia phase decreased when the volume fraction of zirconia increased in the ceramic composites (Huang et al., 2003). According to Lange (1982), when increasing the volume fraction of zirconia, the constraint from Al_2O_3 matrix decreased and the grain size of ZrO_2 increased. As a result, the amount of the monoclinic phase increased. In this experiment results were observed a reversible way. This phenomenon may be related to the sintered densities of the synthesised ceramic composites. It was found that the relative density of the synthesised ceramic composite containing more ZrO_2 is slightly higher than that of synthesised ceramic composite containing less ZrO_2 . A higher degree of densification is beneficial to the retain tetragonal ZrO_2 at room temperature.

In general, sintered specimens with higher relative density exhibit greater mechanical properties. However, there is also an influence of microstructure uniformity on mechanical properties. In this study, the highest experimental densities were obtained for synthesised pure YZR100%, Zr80-Al20%, Zr60-Al40%, Zr50-Al50%, Zr100-Zr80-Al20%, Zr100-Zr60-Al40%, Zr100-Zr50-Al50%, Al100%, and silica (Table 4.3). From pure alumina (Al) until 80 wt.% zirconia (80 Zr), the density of the synthesised ceramic composites increases with the decrease of alumina content, indicating that the addition of alumina particles allowed the densification of zirconia matrix. In the same way, starting from pure zirconia to 50 wt% Zr, the addition of alumina enhanced the synthesised ceramic composite densification.

In this study, the sintered pure zirconia, alumina oxides and $ZrO_2-Al_2O_3$ ceramic composites showed relative density in the range of 99.13% to 99.86% (Table 4.4). The results showed the differences of relative densities for homogenous mixtures 3YTZP with various percentages of Al_2O_3 (20, 40, and 50 wt%) after sintering 2 h at 1500 °C in air. It can be noted that the maximum sintered relative density (95%) was attained for compositions 3YTZP 80 wt % with Al_2O_3 20 wt% content. It is important to focus that the relative density decrease with increasing the Al_2O_3 wt% content, indicating that the addition of Al_2O_3 suppressed the densification of 3Y-TZP matrix. These results were in good agreement with findings of Moares et al., (2004), Zhang et al., (2006a), Santos et al., (2009b), Abden et al., (2014), Zhang et al., (2015) who reported that the relative density decreases as the Al_2O_3 wt% content increases in zirconia matrix.

According to ASTM F 1873-9836 (1998), the total porosities less than 1% vol is required to high pure ceramics of zirconia, alumina, and Zr-Al ceramic composite for biomedical applications (ASTM F 1873-9836, 1998; ASTM F 603-0035, 2000). Therefore, in this study, the total of porosities for synthesised ceramic cores was less than 1%vol. The

mechanical strength of the ceramic is mainly related to the porosity distribution. It has been shown that decreasing the porosity distribution of synthesised ceramic results in increasing Vickers hardness and compressive strength (Moraes et al., 2004).

In this study, the volume shrinkages ranged from 21.7% to 37.7% of synthesised graded ceramic cores. The results indicated that when alumina wt% decreased, the volume shrinkage increased and also when porosities increased in the synthesised graded ceramic cores, the volume of shrinkage is increased. The results of this study is in agreement with the previous studies by Zhang et al., (2010) and Zhang et al., (2015).

The defects in the sintered specimens, such as frustum formation, delamination, and cracking, which originated from the sintering behaviour and various shrinkage of ceramic cores, could be controlled by the modifications in terms of the phase type and particle size of zirconia. The residual stresses induced in the ceramic regions of FGM were characterized by the XRD method, which was relaxed as the number and thickness of compositional gradient layers were increased. The residual stresses in Y-TZP/Alumina-FGM showed non-uniform patterns resulting from CTE mismatch and sintering defects (Choa et al., 1998; Bamba et al., 2003).

In this study, the compressive strength of specimens Al_2O_3 sintered at 1500 °C is lower than the value reported in the literature (Lange et al., 1988; Sudre and Lange, 1992). This is because over firing of Al_2O_3 has occurred at 1600 °C. It can be noted that the compressive strength of the synthesised composites did not increase with increasing volume fraction of 3YTZP. The results of this work are in disagreement with a study by Haung et al., (2003). Also, previous studies showed that ZrO_2 - Al_2O_3 powder compacts need a higher sintering temperature (>1550 °C) to obtain a comparable relative density to their ingredients because the densification is significantly retarded by the presence of ZrO_2 inclusions (Lange et al., 1988; Sudre and Lange, 1992). Besides, stresses arising

from the presence of the agglomerates and heterogeneities give rise to differential sintering rates within the compact during sintering (Kellett and Lange, 1984; Tuan and Brook, 1989). Thus, the composite can only be densified by hot-pressing or post-hot isostatic pressing in most cases (Huang et al., 2003).

In multilayered ceramic cores, compressive stress is induced on the ceramic regions by the volume expansion of m-ZrO₂ that resulted from the t→m ZrO₂ phase transformation on cooling could be caused by the difference in the CTE. As a consequence, it has been verified that the residual stresses generated on FGM are dominantly effected by the number and thickness of compositional gradient layers, and the sintering defects and residual stresses can be controlled by the decrease of the sintering behaviour and difference of the shrinkage of each component (Choa et al., 1998; Zhang et al., 2015).

The CTE tested by TMA for the single layer and multilayered synthesised ceramic cores composite is shown in Figure 4.78. There were differences in CTE between synthesised ceramic cores in this study, indicating that the thermal expansion showed significant effect on strength degradation and volume of shrinkage for the composite under the test condition utilized. Internal residual stresses and/or microcracks due to CTE mismatches between alumina grains and zirconia matrix perhaps occurring in thermal fatigue were negligible to affect flexure strength of the composite material of interest (Bamba et al., 2003). Hence, it is concluded that CTE mismatch would not have been sufficient enough to degrade the strength of the synthesised ceramic composite systems (Zhang et al., 2015).

On the other hand, alumina particles have high elastic modulus (the elastic modulus is double that of zirconia). This makes the stress of zirconia phase transformation very clearly improve, and contributes more in crack tip position. Moreover, the CTE of

alumina is about $8 \times 10^{-6} \text{ K}^{-1}$, less than zirconia. When alumina is uniformly distributed in the zirconia matrix, alumina grain is in a compressive stress state. So, zirconia and alumina grains combine well in the boundary. Correspondingly, they have the highest boundary strength, and a crack does not easily to happen in the grain boundary (Hbaieb et al., 2007; Rong et al., 2008; García and Hotza, 2012). In addition, alumina can change the internal structure of the zirconia so that more t-phase zirconia is retained. The retention of the t-phase at ambient temperature permits it to generate martensitic transformation under externally applied stresses (Zhang et al., 2014).

Thermal expansion of the alumina decreased with the increasing in yttria stabilized zirconia content for a given temperature, whereas the variations of thermal expansions for pure alumina Al_2O_3 -100 wt.% is much higher than those for Al_2O_3 -20 wt%, Al_2O_3 -40 wt%, and Al_2O_3 -50 wt.% Y-TZP. It is also worth noting that, as the temperature increases, the difference among their thermal expansions of multilayered Zr100%-Zr80%-Al20 wt%, Zr100%-Zr60%-Al40 wt%, Zr100%-Zr50%-Al50 wt%, and graded silica were reduced especially at the 500°C. Additionally, the thermal expansion increased with the increasing temperature in the alumina and Al_2O_3 -25 wt% Y-TZP. The increase in temperature from 25°C to 500°C leads to a slight increase in the thermal expansion of alumina and Al_2O_3 -25 wt.% Y-TZP, while the thermal expansion decreases slowly after 100°C with an increase of temperature when increasing the Y-TZP content to the 50wt%. The low thermal conductivity of Y-TZP is generally associated with phonon scattering derived from oxygen vacancies (Ghosh et al., 2009; Sasaki et al., 2010; Song et al., 2011). The oxygen vacancies are introduced into the zirconia fluorite structure to charge compensate for Y^{3+} substituting onto Zr^{4+} site. At room temperature, ZrO_2 has a monoclinic crystal structure. Above 2370°C, ZrO_2 possesses a cubic fluorite structure. When ZrO_2 is doped with Y_2O_3 , the resultant solid solution may have a mixture of phases or a defective single phase (Walker and Anderson, 1984). For Y_2O_3 concentrations of 5

to 40 mol% Y_2O_3 , the $ZrO_2 \cdot Y_2O_3$ solid solution is stabilized into a cubic fluorite structure. In addition to the above, the thermal conductivity of YTZP is sensitive to its extrinsic features, such as the porosity and its distribution.

Generally, the Vickers hardness of ceramic materials is influenced by the intrinsic deformability of the ceramic and microstructural features such as grains size, multiphase, and orientation, porosity as well as boundary constitution (Tekeli, 2005; Zhang et al., 2015).

The results of this study showed that the Vickers hardness obtained for ATZ composites as a function of Al_2O_3 content. It is well known that the hardness of Al_2O_3 - ZrO_2 composites is mainly effected by relative density (He et al., 2009; Zhang et al., 2015). It is noteworthy that the lower hardness value obtained for 3YTZP80%-20 wt% Al_2O_3 composite may be due to its lower relative density. Kim and Khalil (2006) reported that the hardness of Al_2O_3 -27.8 wt% 3YSZ composite increased from 12 GPa to 17 GPa when the density increased from 96% to fully densified ceramics. Chen et al., (2008) reported that the Al_2O_3 -40wt% 3YSZ coating had a hardness of 11.8 GPa with 4.4% porosity and 15.8 GPa when porosity decreased to 1%. Also, it was observed that the maximum Vickers hardness was 15.9 GPa for the composition containing 50 wt% Al_2O_3 . It was observed that the microstructure with ZrO_2 grains distributed as intergranular and intragranular particles in the Al_2O_3 grains increases the hardness (Ye et al., 2008). In previous studies, similar hardness results were obtained in 3YSZ- Al_2O_3 composites, with hardness varying between 12 and 15 GPa (Choi & Bansal, 2005; Tekeli, 2005; Daguano et al., 2007; Ye et al., 2008; Santos et al., 2009b; Oelgardt et al., 2010; Abden et al., 2014).

The Vickers hardness of the ceramic composites obeys the rule of mixture (Lange, 1982). It can be noted that with the increase of zirconia content, the hardness of the ceramic composites diminishes. Higher values of hardness imply in scratch resistance and

good wear. Also, it had been reported that many ceramics show a reduce of hardness with the load increase (Krell, 1995; Celli et al., 2003).

In this study, a slight reduction in the hardness of the sintered ZrO_2 - Al_2O_3 ceramic composites was observed. This observation is attributed to the increasing grain size, reducing the number of grains per area and causing a smaller degree of crack deflection by the grain boundaries (Santos et al., 2009b). The decrease in the hardness of $Al_2O_3/3Y$ -TZP composites with increasing micro-alumina content is consistent with the relative density decrease. This is believed to be due to the reason that micro-alumina, as a rigid particle, can inhibit the densification behaviour of the composites, as reported in the previous studies by Shi et al., (1993) and Zhang et al., (2015).

It is important to note that the residual stress from the CTE-mismatch cannot explain that the fraction of m- ZrO_2 with 10 vol% micro-alumina is more than that of 3Y-TZP ceramic (0 vol% micro-alumina). According to previous studies by Choa et al., (1998) and Bamba et al., (2003), the dislocations caused by compressive stress from the CTE mismatch can enhance the transformability of t- ZrO_2 . Although, the compressive stress decreased with increasing micro-alumina content, it may be sufficient to form the dislocations. The volume expansion due to the transformation of t- ZrO_2 can also increase its compressive stress. Therefore, the transformation of t- ZrO_2 is more prominent by adding micro-alumina (Zhang et al., 2015).

An addition of 10 wt% of Al_2O_3 to ZrO_2 matrix can reinforce the grain boundary, improve the phase transformation, enhance the strength of the ceramic and make fracture path twists and turns (Zhang et al., 2014). In a practical application, more external force can lead to sample fracture. Probably the alumina addition can affect the fracture curve extension (Burak et al., 2008).

However, a previous study by Santos et al., (2009b) discovered that there is no prominent influence of the Al_2O_3 addition on fracture toughness, demonstrating values near $8 \text{ MPa m}^{1/2}$ for all sintering conditions and constituents studied. Several studies showed that the K_{IC} of these materials is greatly impacted by the zirconia transformation. Toughening mechanisms, instances of crack bridging, crack spreading and crack deflection, may also be activated when alumina is added to Y-TZP as a dispersed second phase. Another study by Choi and Bansal (2005) showed flexural strength and fracture toughness of both particulate and platelet composites increased with alumina content increased in the zirconia matrix.

The outcome of this work showed that the compressive strength in the ATZ composites is lower than the zirconia and alumina ones when the Al_2O_3 content is increased as shown in Table 4.5. Standard deviation values for each composition in both the single layer and multilayers ATZ composites, suggest that a variability in compressive strength can be indicative of the presence of multiple defect distributions such as compositional inhomogeneities, inclusions as well as pores producing an irregular strength as reported in previous work by Shi et al., (1993) and Nevarez-Rascon et al., (2011).

The results of this study showed that the addition of alumina has a large effect in increasing the Young's elastic modulus, but the influence on compressive strength was much smaller. The reason for this behaviour can be the absence of two of the main toughening mechanisms of ATZ: crack bridging and the transformation toughening. The crack bridging is negligible because of the large grain size of alumina (only small bridges were detected in pure alumina). It has been found greater values of elastic modulus when the grain size of zirconia matrix and alumina particles had been increased with thermal treatments of grain growth. The size of the tetragonal particle and the stabilizer content, have a great influence in the tension required for the transformation of the tetragonal

particle (Gupta et al., 1978; Moraes et al., 2004; Zhang et al., 2015). The critical grain sizes increase with Young's modulus of the composite, which is related with the restrictions imposed to the matrix. The Young's modulus found in this study is in agreement with studies by Moraes et al., (2004); Hbaieb et al., (2007); Rong et al., (2008); Frank and Rainer (2012); and García and Hotza (2012).

The results of this present study revealed that the strain values in the ATZ composite are almost similar. However, the results of the present study are in disagreement to previous studies by Radovic et al., (2004) and Studart et al., (2007). The variation of the strain data is related to the inherently scattered nature of elastic properties determined with mechanical tests (Radovic et al., 2004). It is commonly known that in producing the same strain by the same external force, composite components with a higher elastic modulus undergo a larger load. Therefore, Al₂O₃ particles, with a higher elastic modulus than zirconia, have a dispersion strengthening effect on the composites, as reported in a previous work by Zhang et al., (2012).

4.8 Conclusions

Using synthesised ceramic composite cores reinforced with Al_2O_3 , and graded silica; it can conclude the following:

- 1- The synthesise of ceramic core 3Y-TZP using a pressureless sintering is being developed.
- 2- The synthesis of graded silica $\text{SiO}_2\text{-Al}_2\text{O}_3\text{-K}_2\text{O-Na}_2\text{O-CaO-Tb}_4\text{O}_7$ system is being developed.
- 3- Various dense $\text{ZrO}_2\text{-Al}_2\text{O}_3$ synthesised ceramic graded composites were developed and comparable when sintered at $1500\text{ }^\circ\text{C}$ by using pressureless sintering. In all sintered ceramic cores materials, only the tetragonal ZrO_2 phase with α -alumina phase were observed. Also, the m- ZrO_2 phase content in the starting powder was observed, indicating the complete stabilization of the tetragonal phase during cooling. Also, the microstructures of the graded silica were characterized by FESEM, EDX, and XRD.
- 4- Relative densities ranging from 91 to 98% were attained in the different synthesised ceramic composites at the processing temperature of $1500\text{ }^\circ\text{C}$ for 24 h with pressureless sintering. An increase in hardness of the synthesised ceramic composite materials with increasing amounts of Al_2O_3 (wt%) has been observed.
- 5- A wide range of volume of shrinkage, CTE, compressive strength, elastic modulus, and strain were obtained for all tested synthesised ceramic composites.

CHAPTER 5: SHEAR BOND STRENGTH BETWEEN SYNTHESISED BIOCERAMIC CORES INFILTRATED WITH GRADED SILICA AND VENEER

5.1 Introduction

This chapter describes the shear bonding strength of a new synthesised bioceramic cores with/without infiltrated graded silica and ceramic veneer.

The use of toughened ceramics such as Y-TZP has broadened the application of ceramics in dentistry and facilitated the exploitation of all-ceramic restorations even in posterior areas where high-strength structures are needed (Guazzato et al., 2005).

However, a limitation of dental all-ceramic materials is their vulnerability to fatigue mechanisms that can significantly reduce their strength over time, hence, the lifetime of structural force-bearing components. The propagation of natural cracks initially present in the components' microstructure stands behind the fatigue that leads to the reduction of mechanical strength. On the other hand, the stress assisted reaction of water molecules with the metal-oxide bonds at the crack tip caused the crack propagation under subcritical conditions (Snyder and Hogg, 2005; Harada et al., 2016; Zhang et al., 2016a, and 2016b).

There remains a lot to be revealed about the zirconium oxide–ceramic relationship. One of the weakest aspects of such restorations happens to be the veneer-core interface, which makes ceramic chipping or cracking possible. Several factors may affect veneer cracking and these include: differences in CTEs among the core and veneering ceramic, flaws on veneering, firing shrinkage of ceramic and poor wetting by veneering of the core. Currently, special ceramics are being developed for zirconia in order to limit such an adverse aspect. However, further evaluation of the zirconia veneer-core bond should be

conducted. The luting of restorations can be performed following the completion of veneering control and finishing (Manicone et al., 2007; Al-Harbi et al., 2016).

Kelly and Denry (2008) have shown that an *in vitro* and clinically failed veneering ceramic and all-ceramic FPDs made with a glass-infiltrated alumina core fractured at the connector region where there is a peak of tensile stress.

Kelly et al., (1995) concluded that the properties of the veneering ceramic of the stronger core material influence the failure of the connector. An *in vitro* replica of the clinical failure at the connector has been obtained by loading bi-layered veneer-core disc- or bar-shaped samples with the veneer on the bottom and the core material on top.

Aboushelib et al., (2007) confirmed that the failure of a layered structure is expected to occur in the weakest interface or in the weakest material of the framework; the inferior zirconia veneer bond strength was an observation of interest. On the other hand, the efforts of manufacturers and researchers centred on increasing the strength of the veneer and the core ceramic materials, while the bond among them was not sufficiently addressed (Aboushelib et al., 2007; Hamza et al., 2016).

Silva et al., (2011) revealed that the modified design of the zirconia core exhibited the benefit of additional veneer ceramic support compared with a standard design by improving the reliability of this all-ceramic crown framework.

All-ceramic restorations provide superior esthetic properties, which are well documented in the literature (Raigrodski, 2004). However, the main focus of the researcher was to improve the strength properties of the ceramic materials. Different techniques and methods have been recommended to strengthen dental ceramic, including: controlled crystallization, microstructure tailoring, ion exchange, the use of resin luting agents, and the use of supporting sub-structure (Albakry et al., 2004; Özcan and

Bernasconi, 2016). The superior physical properties of zirconia material make it a good foundation material for prosthetic dental restorations (Pilathadka et al., 2007; Al-Harbi et al., 2016; Luthra and Kaur, 2016; Xie et al., 2016). In the present study, different synthesised graded zirconia-alumina cores with/without infiltrated graded silica were used to strengthen the veneering ceramic.

Further, the dimensions of veneer and core materials, inherent and processing flaws within the materials and the preparation design are among several variables that may influence the fracture and fatigue behaviour of the materials used in all-ceramic crowns. Other factors that may have an affect include the luting agent, location, direction, and the testing condition and type of the applied load (Tsalouchou et al., 2008; Tzanakakis et al., 2016).

According to Zhang et al., (2012), large amounts of residual stresses exist in the dental ceramic crown and are of different magnitude at different locations due to the shape complexity of the crown. All-porcelain restorations must therefore have sufficient strength in order to avoid the damage caused by stress concentration. Consequently, it is of paramount importance to ensure the sufficient thickness of the veneer layer especially in the incisal of anterior teeth and the function of the molar tooth tip and inclined plane.

5.2 Objective of this Chapter

The aim of this chapter was to evaluate the shear bond strength of synthesised zirconia and alumina ceramic core with/without infiltrated graded silica with their corresponding veneering porcelains. Scanning electron microscopy (SEM) was used to classify the failure pattern, and the interface chemistry was evaluated using energy dispersive X-ray (EDX).

5.3 Null Hypothesis of this Chapter

There are no significant differences in shear bond strength between synthesised zirconia and alumina ceramic core with/without infiltrated graded silica with their corresponding veneering porcelains.

5.4 Materials and Methods

5.4.1 Materials

The materials and their specifications were described and mentioned in Table 5.1 and Table 5.2.

Table 5.1: Properties of veneering material as provided by the manufacturer.

Veneer Material	Composition	CTE ($\mu\text{m}/\text{m}$ $10^{-6}/\text{K}$ between 25 and 500°C)	Manufacturer	Batch No.
Cercon [®] Ceram Kiss Liner	Selenium, Feldspathic porcelain	10.3	DeguDent GmbH, Hanau- Wolfgang, Germany	PL B4 73712
Cercon [®] Ceram Kiss	Feldspathic veneering ceramic (SiO ₂ 60.0- 70.0; Al ₂ O ₃ 7.5-12.5; K ₂ O 7.5-12.5; Na ₂ O 7.5-12.5)	9.2	DeguDent GmbH, Hanau- Wolfgang, Germany	D A4 73247

Table 5.2: Groups of synthesized ceramic cores.

Groups	Material Groups	No.
A	Zr100% + Veneer	10
B	Zr100%+ Silica + Veneer	10
C	Zr80%+20%Al + Silica + Veneer	10
D	Zr60%+40%Al + Silica + Veneer	10
E	Zr50%+50%Al + Silica + Veneer	10
F	Al 100%+ Veneer	10
G	Al 100% + Silica + Veneer	10

5.4.2 Methods

5.4.2.1 Preparation of Synthesized Zirconia and Alumina Ceramic Cores

Seventy synthesised ceramic cores zirconia and alumina with/without infiltrated silica system, 10 disc-shaped samples of 4 mm height and 8 mm diameter were produced. The synthesised bioceramic cores were described previously as in Chapter 4 Section 4.2.1. and in Table 4.5.

A new graded glass silica in the $\text{SiO}_2\text{-Al}_2\text{O}_3\text{-Na}_2\text{O-K}_2\text{O-Tb}_4\text{O}_7\text{-CaO}$ system has been developed to infiltrate Y-TZP and MgAlO. The major composition (>1 wt.%) of the infiltrating glass contained: SiO_2 (65.5 wt.%), Al_2O_3 (11.7 wt.%), Na_2O (7.3 wt.%), K_2O (10.0 wt.%), Tb_4O_7 (2.5 wt.%), and CaO (3.0 wt.%). This composition was selected so that the final product was highly translucent with a light-yellow shade, and had a high melting point coupled with superior resistance to crystallization during the cooling from the raised temperatures. The CTE of the selected glass composition was around $8.2 \times 10^{-6} \text{ K}^{-1}$ (between 25 and 500 °C).

To produce graded structures (producing an infiltrated silica/zirconia and silica/alumina.), another group was presintered between 1100 °C and 1400 °C for 1h in air, producing a somewhat porous template for glass infiltration. The bottom and top

surfaces of presintered Y-TZP were coated with a slurry of the above-mentioned powdered glass composition (Figures 5.1. and Figure 5.2.). Densification and glass infiltration were performed simultaneously at 1500 °C for 2h in air. This way the glass infiltration depth can be tailored by manipulating the porosity of the infiltrating structures, and the grain growth (Zhang and Kim, 2009) and/or destabilizing of the tetragonal zirconia form (Piascik et al., 2006) associated with the post-sintering heat treatment can be avoided. Both grain growth and/or destabilizing of the tetragonal phase are known to be deleterious for the hydrothermal stability of Y-TZP in the body (Chevalier et al., 1999; Piconi and Maccauro, 1999; Zhang and Kim, 2009). A heating and cooling rate of 900 °C/h were used in all cases (Figure 5.3). After the plates cooled, the surface excess glass was removed by polishing.



Figure 5.1: Silica infiltrated to synthesised ceramic cores.



Figure 5.2: Infiltrated core with silica before sintering.

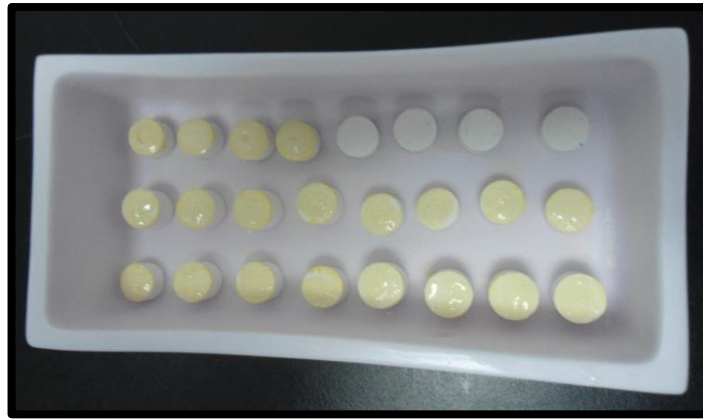


Figure 5.3: Infiltrated core with silica after sintering.

Airborne particle abrasion was then utilized on the bonding surfaces with 50 μm aluminum oxide (Al_2O_3) particles for then 15 s at 3.5 bar pressure and at 10 mm distance from the surface (Figure 5.4). Then, all bonding ceramic cores surfaces discs were acid-etched with 1 % hydrofluoric acid liquid (e-max[®] Etching Liquid, Ivoclar Vivident, Schaan, Liechtenstein) on the bonding surface for 10 min, washed with distilled water for 30 s. Finally, the discs' samples were both ultrasonically cleaned (Model WUC-A02H, Daihan Scientific Co., Ltd., Seoul, Korea) in 99% isopropyl alcohol for 2 min and steam-cleaned for 10 s, then dried with oil-free compressed air.

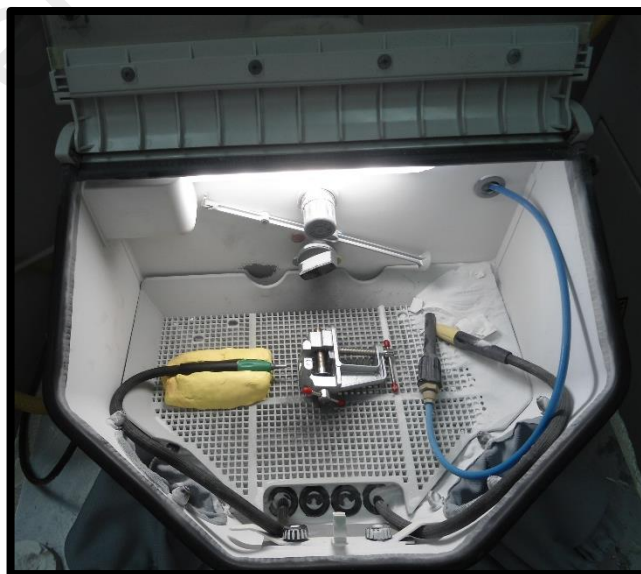


Figure 5.4: Ceramic cores samples abrasived.

5.4.2.2 Preparation Veneer-Core Ceramic Specimens

One type of veneer ceramic was selected for this work, Cercon[®] Ceram Kiss (DeguDent, Hanau-Wolfgang, Germany) as shown in Figure 5.5. Ten samples of each synthesised bioceramic core system were veneered according to manufacturer's recommendations for veneering ceramic.



Figure 5.5: Materials used to build up veneer.



Figure 5.6: Silicone mould used to build up the veneer.

Using a specially-designed, separable silicone mould, a prepared ceramic core disc sample was put in the mould where clearance of 3 mm height and 5 mm diameter was available above the core material for condensing the veneer ceramic as shown in Figure 5.6. The mould was isolated (Picosep Isolating Agent, Renfert[®], Hilzigen, Germany) to

prevent the adhesion of ceramic powder to the mould during layering. The veneering step was carried out utilizing the manual layering technique. First, the liner material, which was a single, thin, continuous layer provided by the manufacturers, was applied and fired independently according to the manufacturer's recommendations (Table 1 in Appendix C). After firing the liner, the veneering ceramic powder was mixed with the manufacturer-supplied condensing liquid and condensed utilizing the vibration blotting technique for 2 s at 50 Hz (Porex Elektro Vibrator, Renfert®, Hilzigen, Germany). The obtained slurry was blotted with a tissue to remove additional water and then condensed into the mould.

After a thin liner layer (Cercon® Ceram Kiss Liner, Degudent Hanau, Germany) was fired, then, the veneering ceramic (Cercon® Ceram Kiss, Degudent, Hanau, Germany) (Figure 5.7) was constructed to the final dimension (5 mm diameter with 3 mm thickness). The prepared veneer-core discs were fired in a programmable vacuum veneer furnace according to the firing program of the manufacturer (Programat® EP 5000, Ivoclar Vivadent, Schaan, Liechtenstein) (Table 1 in Appendix C) as shown in Figure 5.8 and Figure 5.9. Due to the shrinkage of veneer, three separate firings were needed to establish the precise dimension. Owing to firing shrinkage, the accurate diameter of the veneer layer of the samples was measured with a micro-measuring device (Mitutoyo® Digimatic Caliper, Mitutoyo Corp., Kawasaki, Japan) before shear bond strength (SBS) testing. The minimum reading value of the caliper was set at ± 0.01 mm.

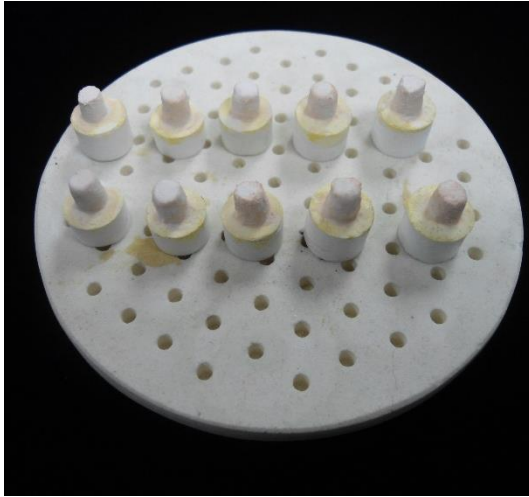


Figure 5.7: Samples before sintering.

Figure 5.8: Samples after sintering.



Figure 5.9: Vacuum furnace used.

5.4.2.3 Surface Analysis

Surface roughness (R_a in μm) measurements were carried out on each disc utilizing an atomic force microscope (AFM) (AMBIOS Technology, Santa Cruz, CA, USA) (Figure 5.10) operated in contact mode set to a $10\ \mu\text{m}$ tip height, $125\ \mu\text{m}$ cantilever length and no rotation of cone angle, was utilized to get qualitative and quantitative data. This created a 3D image of the microstructural surface, located in the center of the specimens as shown in Figure 5.11.



Figure 5.10: Atomic force microscope used.

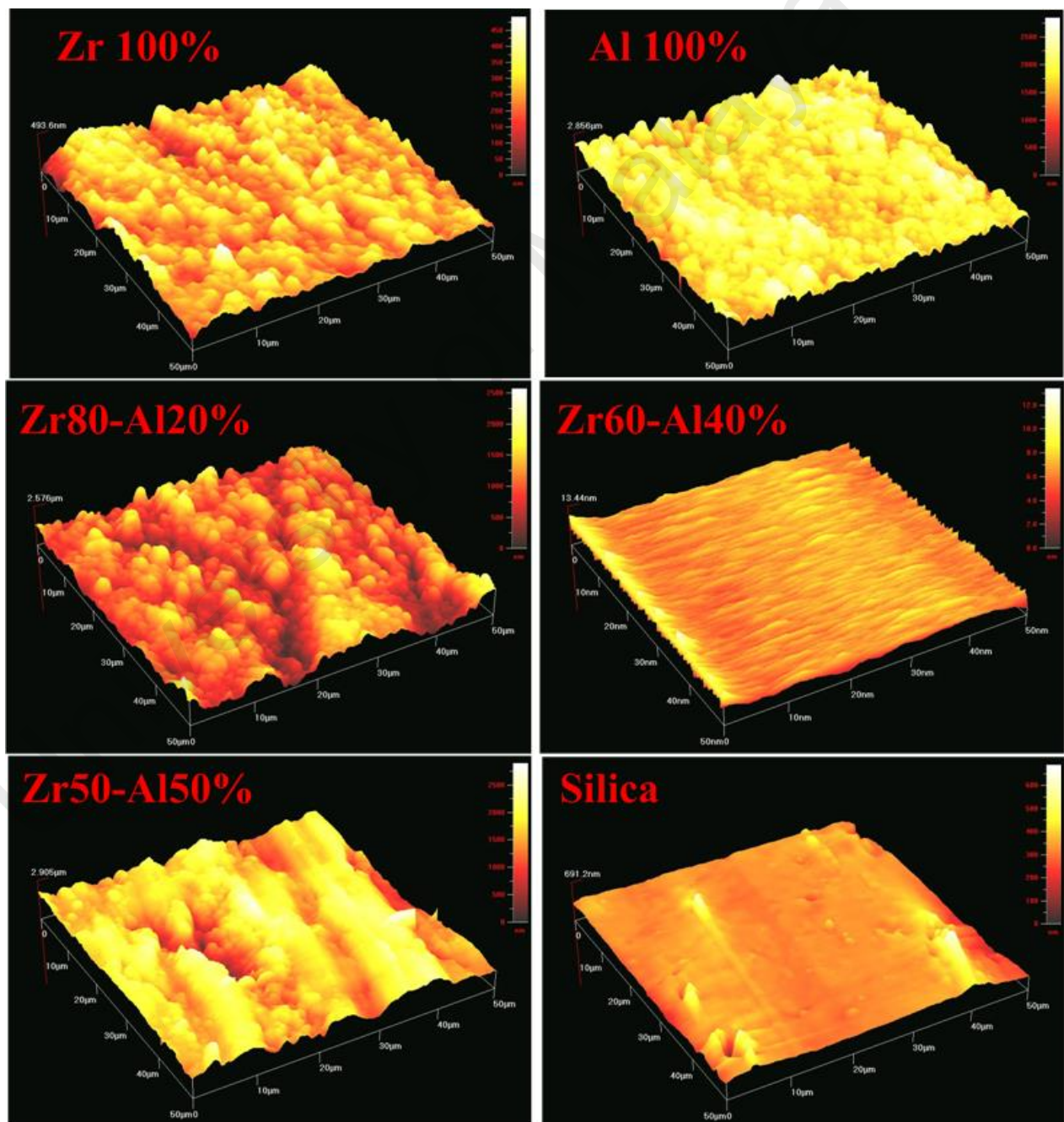


Figure 5.11: Surface roughness of synthesised ceramic cores measured by AFM.

5.4.2.4 Shear Bond Strength (SBS) Test

Each disc was embedded at the center of the customized polytetrafluoroethylene (PTFE) mould using epoxy resin (Mirapox[®] A and B, Miracon[®], Malaysia) as shown in Figure 5.12 and Figure 5.13. Every attempt was made to put the veneer-core interface on the same level as the upper plane of the mould. The veneer-core interface of the sample was put on the same level as the upper plane of the mould utilizing discs for horizontal plane adjustment. All samples were stored in distilled water at 37°C for 24 hours before testing.



Figure 5.12: Mould of specimens.



Figure 5.13: Specimens embedded into epoxy.

After 24 h water storage, the specimens were mounted in a universal testing machine (Model 3345, Shimadzu Cooperation, Tokyo, Japan) (Figure 5.14). Specimens were tightened and stabilized into a custom-made shear test jig (Figure 5.15) and the jig was secured in a bench vice to ensure that the 1 mm thick edge of the shearing device was in contact with the core surface and was located as close as possible to the core-veneer interface (Fig. 5.16). The shear load was applied vertically to the bonding interface at a crosshead speed of 0.5 mm/min until fracture happened. The ultimate load to failure was recorded in Newton (N). As for the average shear bond strength (MPa), it was calculated by dividing the load (N) at which failure occurred by the bonding area (mm²) as follows:

Shear stress (MPa) = Load (N) / Area (mm²);

where Area = $(\pi \times d^2) / 4$ (mm²);

where d = exact diameter of the bonding surface. As for the mean failure load and standard deviation for each group, they were calculated from these data. The test was carried out at room temperature.

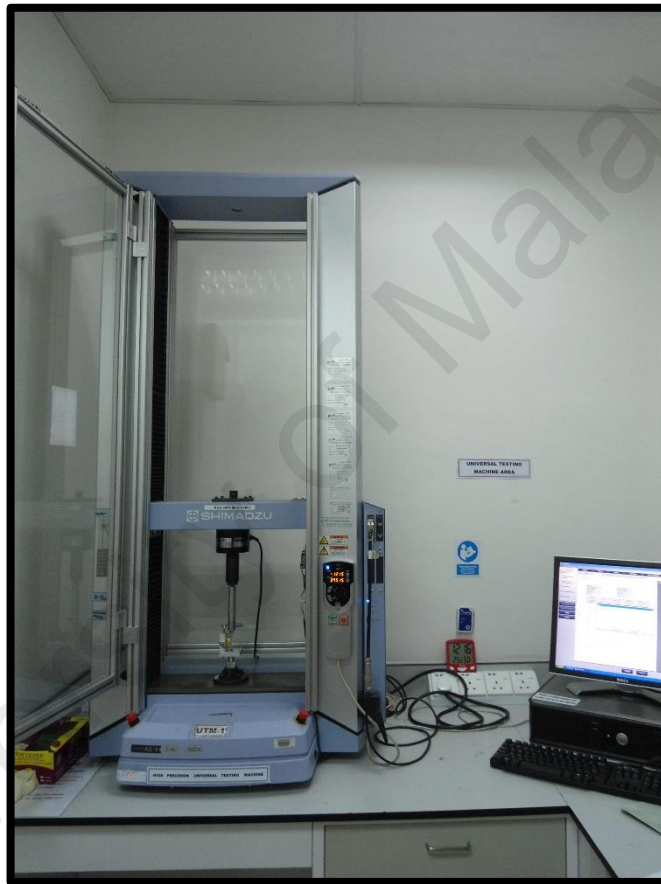


Figure 5.14: Instron universal machine used.

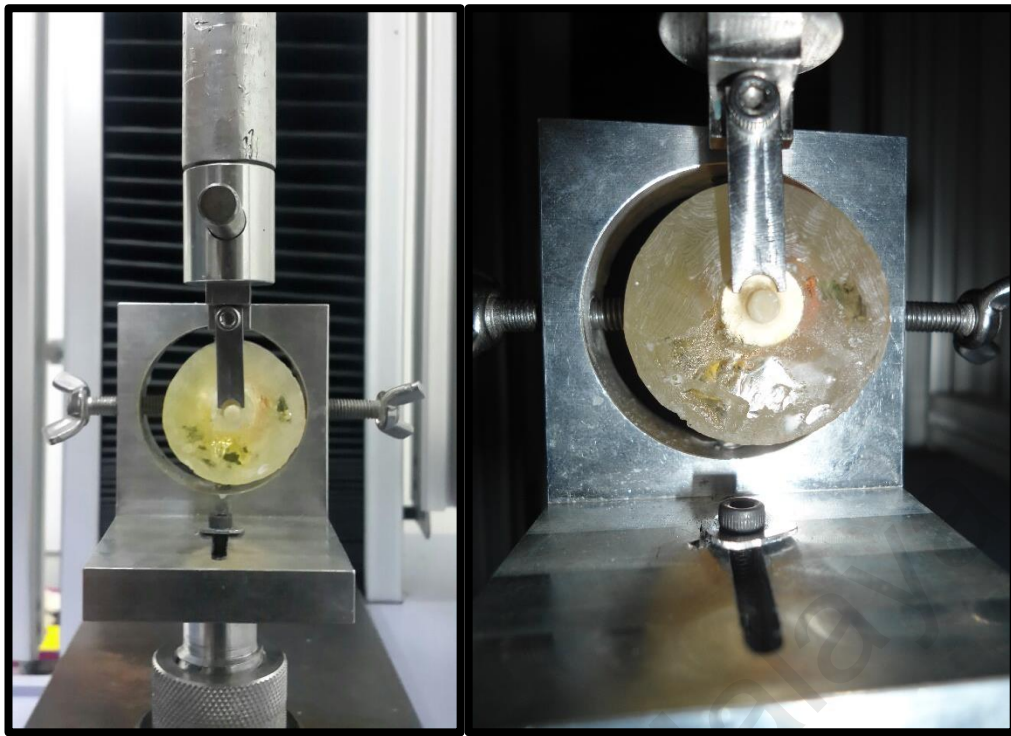


Figure 5.15: Specimens mounted into jig mould for SBS testing.

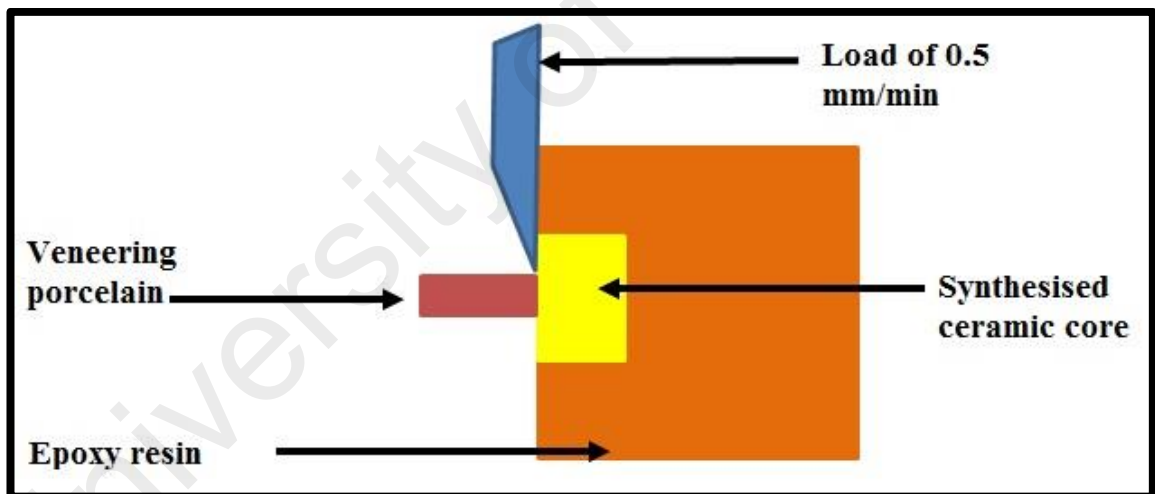


Figure 5.16: Schematic of specimens mounted into jig mould for SBS testing.

5.4.2.5 Fracture Surface Analysis

The fractured surfaces were visually analysed with a stereomicroscope (OLYMPUS SZX7, Model SZ2-ILST, Tokoyo, Japan; $\times 1.5$ magnification) (Figure 5.17) to determine the failure modes of the samples. SEM was utilized to determine the failure modes of the samples.

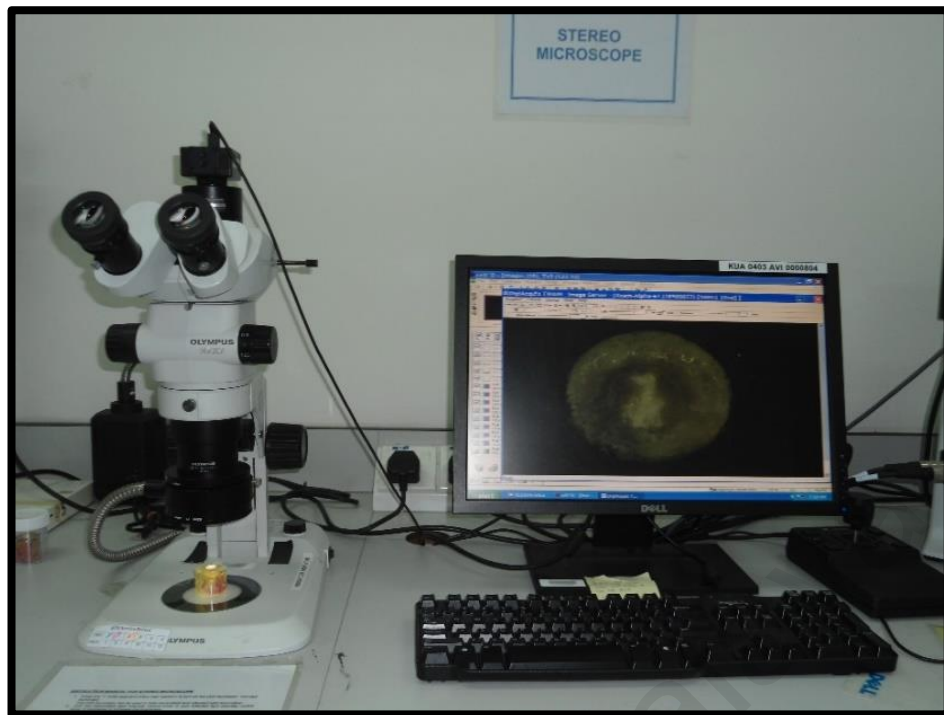


Figure 5.17: Stereomicroscope used.

To determine the mode of failure, the broken samples were examined under SEM (QUANTA FEG 250, Hitachi, Tokyo, Japan) under $\times 30$ to $\times 1000$ magnifications. The definition for failure modes is presented in Table 5.3. And the chemical composition at the fractured core was analysed utilizing EDX (X-Max, Oxford Instrument, Oxford, UK).

Table 5.3: Fracture surface criteria.

Failure type	Definition
Adhesive failure	Complete delamination of veneering porcelain from the core material.
Cohesive failure	Fracture occurs completely and only within veneering porcelain or within core material.
Mixed adhesive/cohesive failure	Fractured surfaces are within veneering porcelain with areas of core materials exposed indicating localized adhesive failure.

Statistical analysis was performed utilizing statistical software (SPSS 21.0, SPSS, Inc., Chicago, IL, USA). The data was analysed utilizing one-way ANOVA to compare the mean shear bond strength between the groups and the Tukey's multiple comparisons test. The level significant level was set to be 0.05.

5.5 Results

5.5.1 Results of the Shear Bond Strength

The Table 5.4. showed the mean and standard deviation of SBS of each group and as shown in Figure 5.18. According to the results, the highest bond strength was found to be the zirconia core (Zr80% +Al20%) coated with graded silica (25.42 MPa). The lowest value of the SBS was noted in the group with alumina core without coated silica (19.06 MPa).

Table 5.4: Mean of shear bond strength of synthesised bioceramic cores and veneer*.

Bioceramic Cores	N	Mean	SD ±	95% Confidence Interval for Mean	
				Lower Bound	Lower Bound
YZrO100% + V	10	21.02	4.27	17.9704	24.0773
YZrO100% + S + V	10	24.51	4.31	21.4261	27.5926
YZrO80%-MgAlO20% + S + V	10	25.42	4.78	21.9992	28.8308
YZrO60%-MgAlO40% + S + V	10	23.14	4.34	20.0329	26.2407
YZrO50%-MgAlO50% + S + V	10	21.92	4.20	18.9131	24.9236
MgAlO100% + V	10	19.06	3.85	16.3028	21.8170
MgAlO 100% + S+ V	10	21.98	3.40	19.5484	24.4076

*. Mean of shear bond strength expressed by (MPa).

The one-way ANOVA (the data distribution was normal distributed and the Levenes' test of homogeneity of quality of variance assumed $P=.993$ as seen in Table 2 and Table 3 in Appendix C) observed a significant difference for the SBS between the synthesised ceramic core with/without coated graded silica to veneer tested at $P < 0.025$ as shown in Table 5.5. The Tukey multiple comparisons test was calculated to make all pairwise comparisons between the five groups in this work plus the two control groups. These comparisons were recorded in Table 3 (Appendix C). The P -values of the various comparisons showed that, YZrO100%, YZrO80%-MgAlO20%, YZrO60%-MgAlO40%,

YZrO50%-MgAlO50%, and MgAlO100% ceramic cores coated with graded silica were comparable and not significantly different to the control groups YZrO100% and MgAlO100% without coated graded silica; but there was a significant difference between YZrO80%-MgAlO20% coated with graded silica and MgAlO100% without coated graded silica ($P=0.019$). All ceramic cores coated with graded silica groups had higher values than the control groups without coated graded silica.

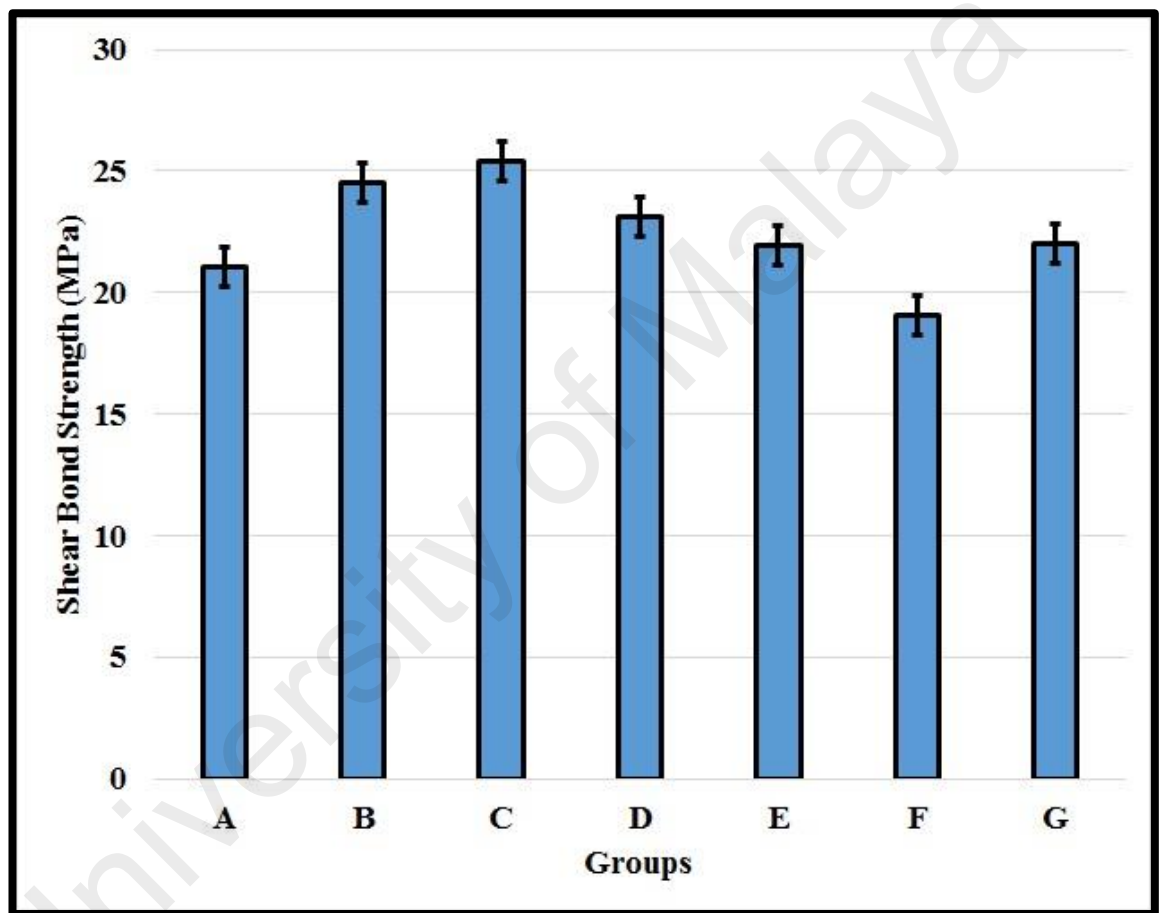


Figure 5.18: The mean shear bond strength of synthesised ceramic cores coated with silica bonded to veneering ceramic.

Table 5.5: Shear bond strength of synthesised bioceramic cores and veneer (MPa).

	Sum of Squares	Df	Mean Square	F	Sig.*
Between Groups	275.342	6	45.890	2.623	.025
Within Groups	1102.159	63	17.495		
Total	1377.501	69			

5.5.2 Results of the Fracture Failure

The values percentage for the fracture surface analysis were computed and presented in Table 5.6. All tested groups demonstrated an adhesive failure between the veneer and the core as well as cohesive failure within the veneer. Only alumina demonstrated cohesive failure within the core. Alumina core without coated graded silica observed more surface failure at the veneer-core interface.

Table 5.6: Failed bonded surfaces by percentage (%).

Bioceramic Cores	A	C	A/C
YZrO100% + V	55	8	37
YZrO100% + S + V	41	18	41
YZrO80%-MgAlO20% + S + V	33	8	51
YZrO60%-MgAlO40% + S + V	47	12	41
YZrO50%-MgAlO50% + S + V	71	2	27
MgAlO100% + V	35	2	63
MgAlO 100% + S+ V	45	11	44

(A = Adhesive, C = Cohesive, A/C = mixed adhesive/cohesive)

In all the samples, the fracture initiated at the veneer-core interface and progressed into the veneering ceramic, observable in the SEM image after debonding (from Figure 5.18 to Figure 5.24). Veneering ceramic remaining on alumina and the zirconia surfaces coated with graded silica was clearly visible. Also, debonding surfaces were observed by EDX (from Figure 5.25. to Figure 5.31.).

According to evaluation under the SEM ($\times 30$), the alumina and zirconia without infiltrated silica groups showed mixed adhesive/cohesive failures with only small remnants of veneer attached to the ceramic core material. A SEM images of the alumina and zirconia groups under high magnification exhibited several small pores in the veneering ceramic, where fracture originated and propagated in the veneering porcelains. Careful evaluation showed a thin layer of veneering porcelain covering the fracture

surface (from Figure 5.19. to Figures 5.25 -a, b, c, d). Additionally, EDX results revealed that fractured alumina and zirconia with/without infiltrated silica surfaces were mainly covered by veneer or liner material and some alumina and zirconia crystals were exposed (Figure from 5.26. to Figure 5.32). The results observed the presence of a thin layer of veneer layer over the alumina and zirconia ceramic cores.

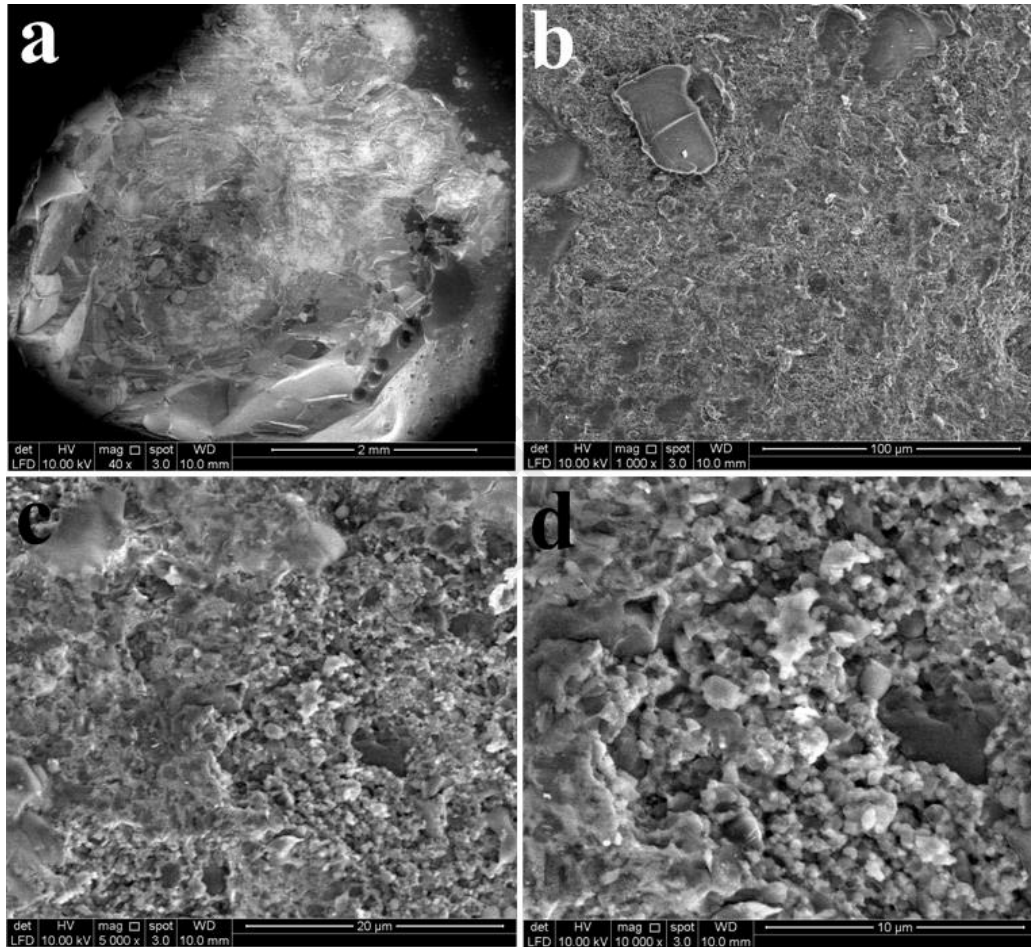


Figure 5.19: SEM of YZrO₂ 100%-veneer. (a) mag x10, (b) mag x1000, (c) mag x5000, and (d) mag x10000.

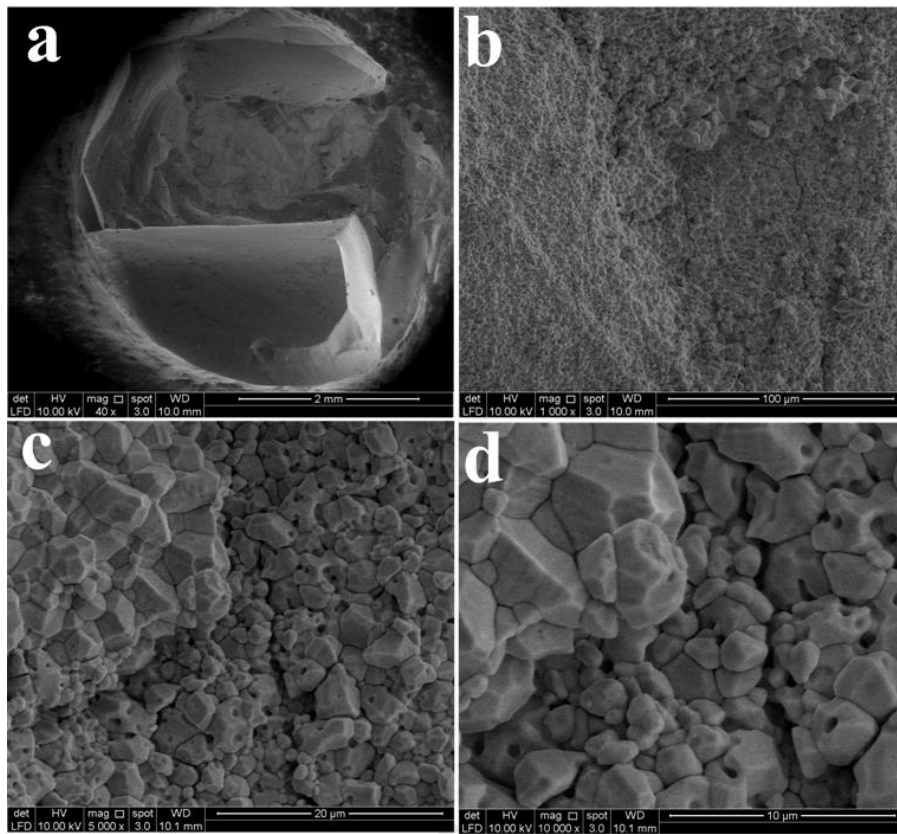


Figure 5.20: SEM of YZrO₂ 100%-silica-veneer. (a) mag x10, (b) mag x1000, (c) mag x5000, and (d) mag x10000.

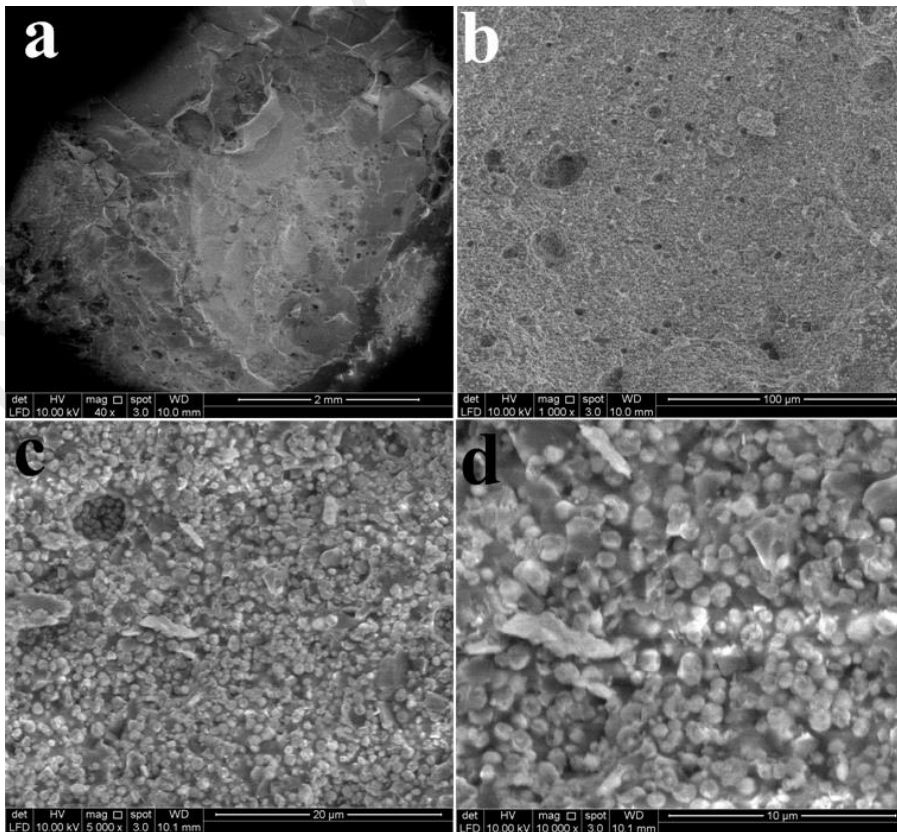


Figure 5.21: SEM of Zr80%-Al20%-silica-veneer. (a) mag x10, (b) mag x1000, (c) mag x5000, and (d) mag x10000.

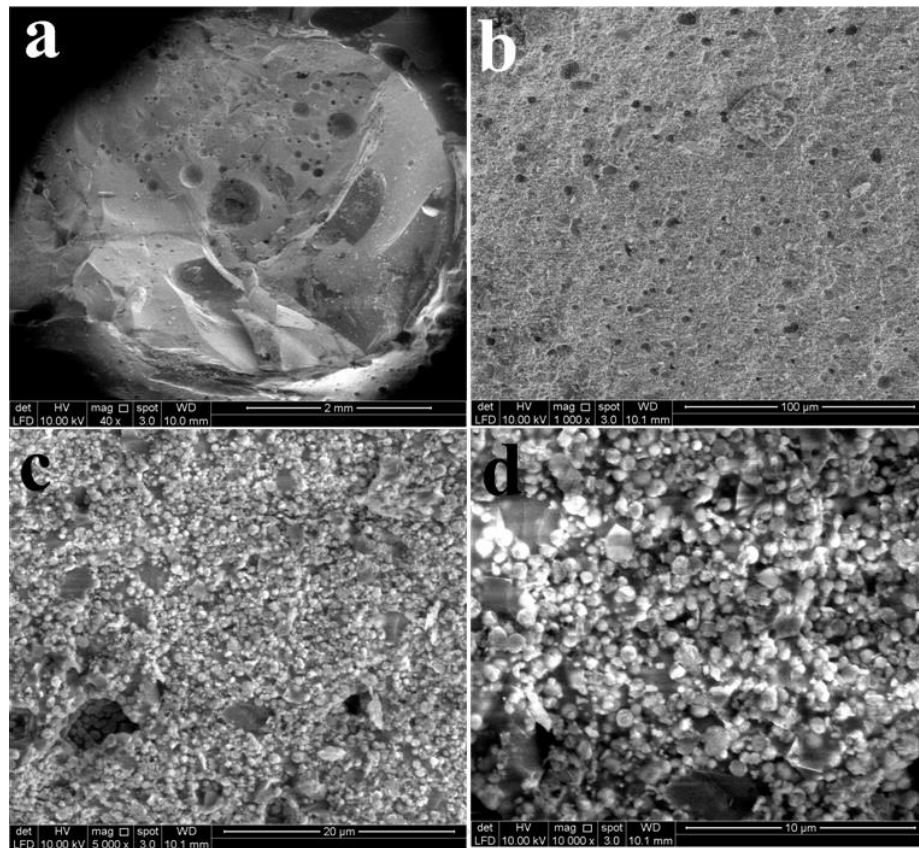


Figure 5.22: SEM of Zr60%-Al40%-silica-veneer. (a) mag x10, (b) mag x1000, (c) mag x5000, and (d) mag x10000.

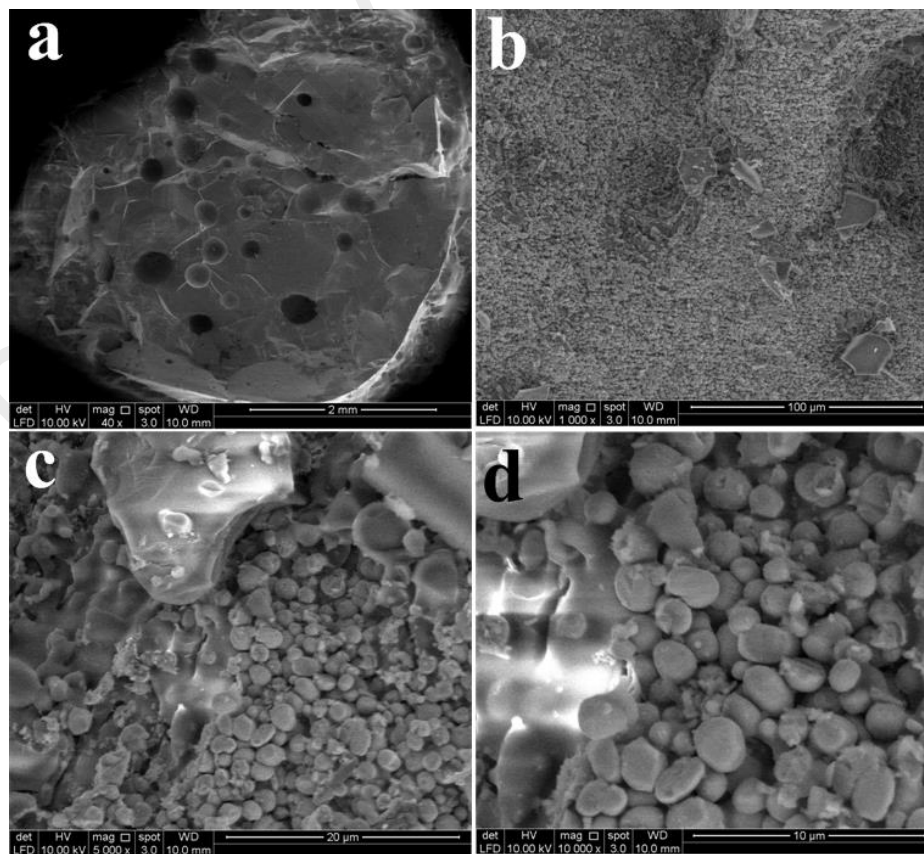


Figure 5.23: SEM of Zr50%-Al50%-silica-veneer. (a) mag x10, (b) mag x1000, (c) mag x5000, and (d) mag x10000.

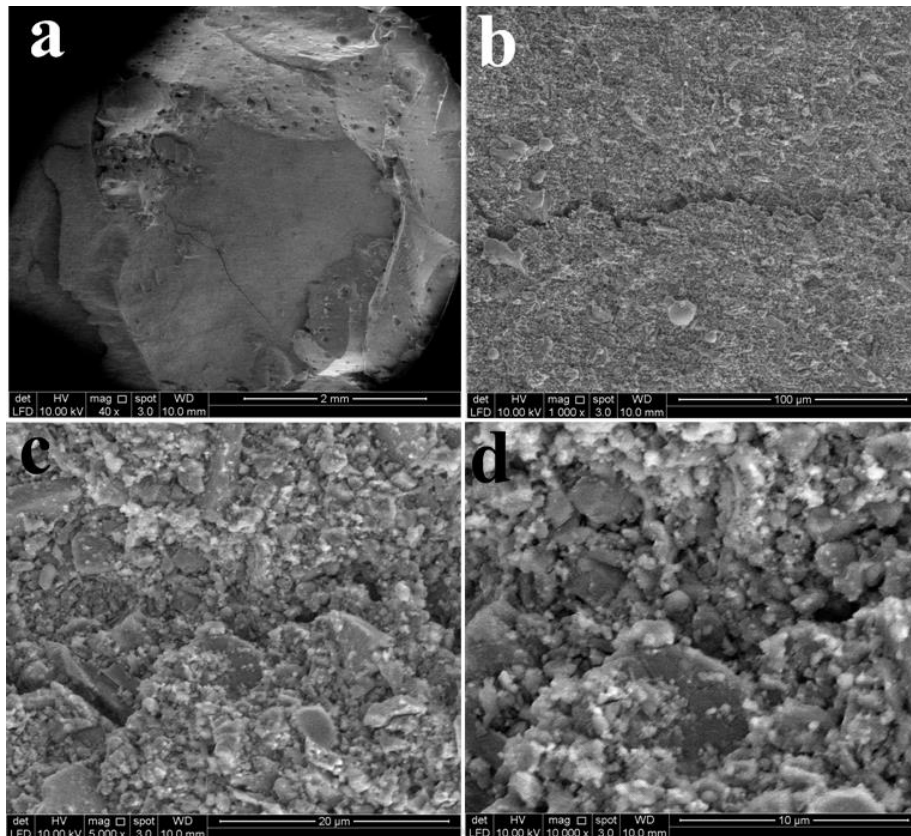


Figure 5.24: SEM of Al₂O₃ 100%-veneer. (a) mag x10, (b) mag x1000, (c) mag x5000, and (d) mag x10000.

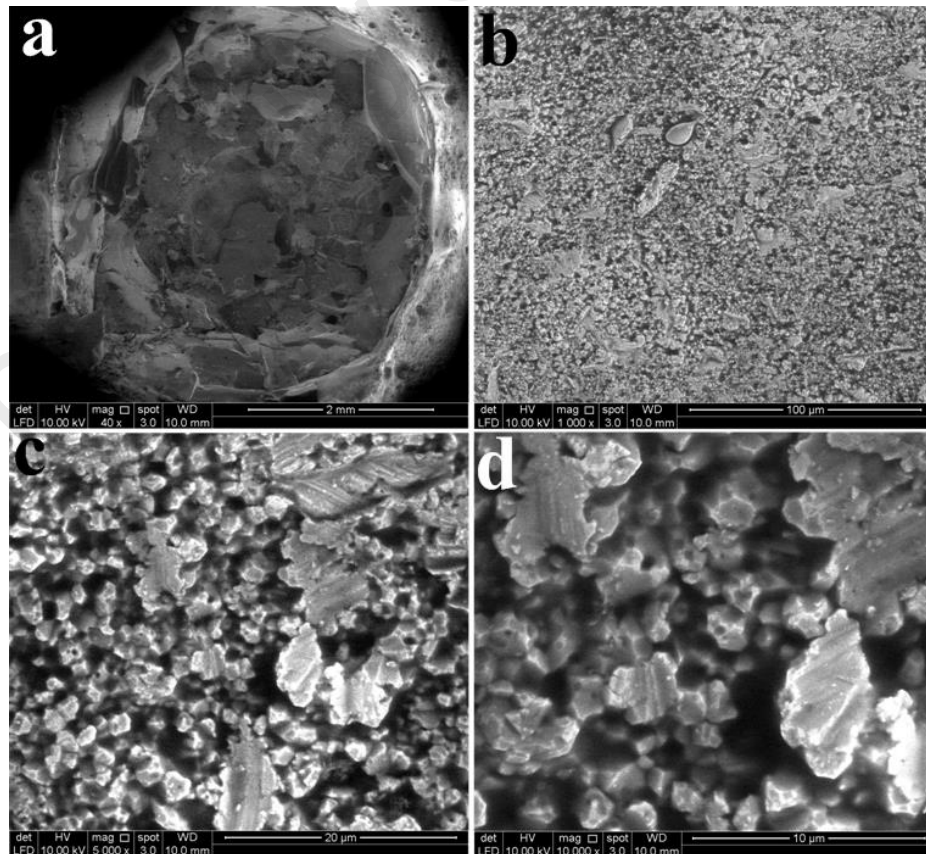


Figure 5.25: SEM of Al₂O₃ 100-silica-veneer. (a) mag x10, (b) mag x1000, (c) mag x5000, and (d) mag x10000.

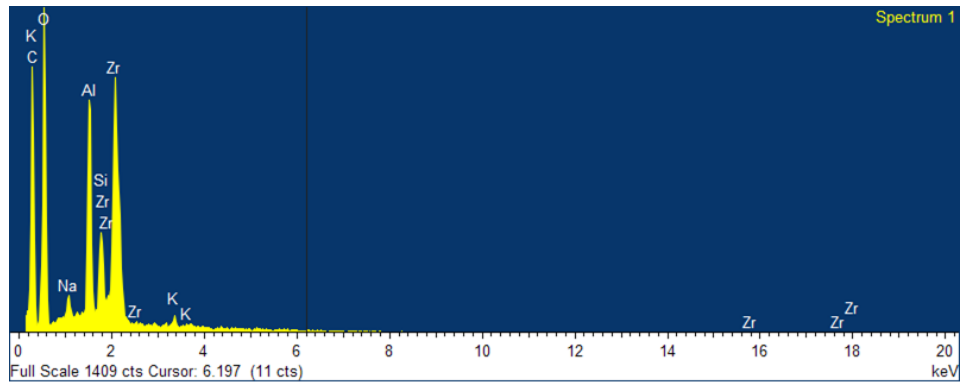


Figure 5.26: EDX of interface surface between Zr100 and veneering.

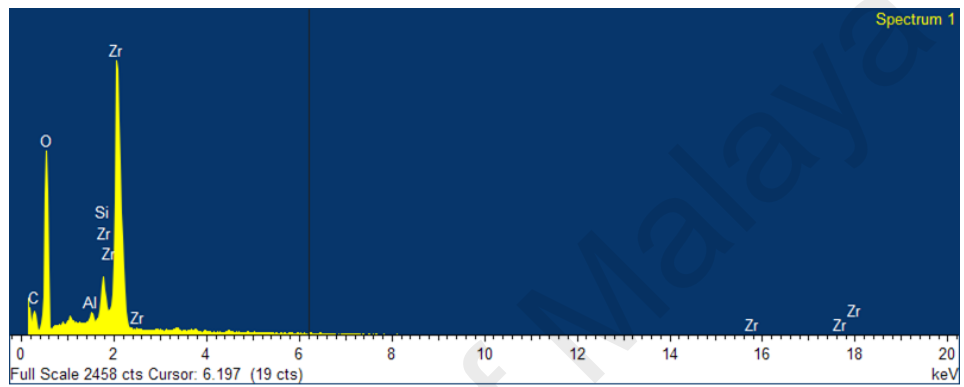


Figure 5.27: EDX of interface surface between Zr100, graded silica, and veneering.

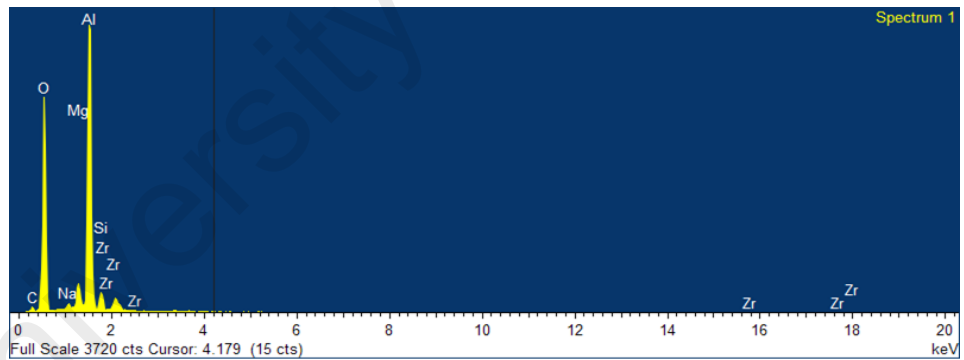


Figure 5.28: EDX of interface surface between Al100 and veneering.

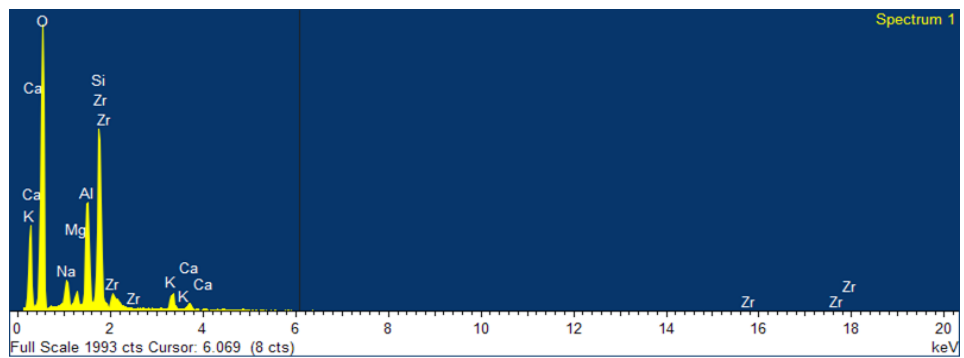


Figure 5.29: EDX of interface surface between Al100, graded silica, and veneering.

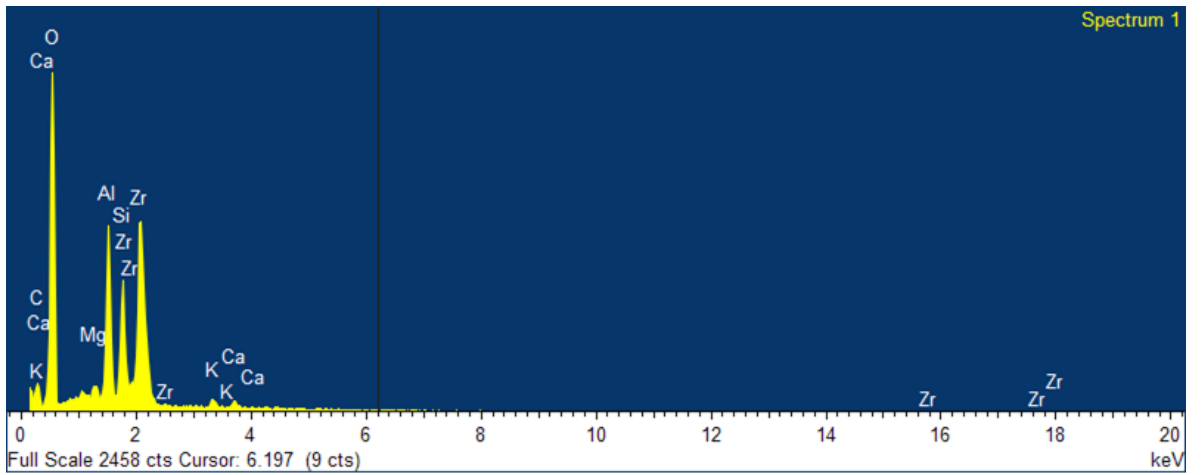


Figure 5.30: EDX of interface surface between Zr80-Al20%, graded silica, and veneering.

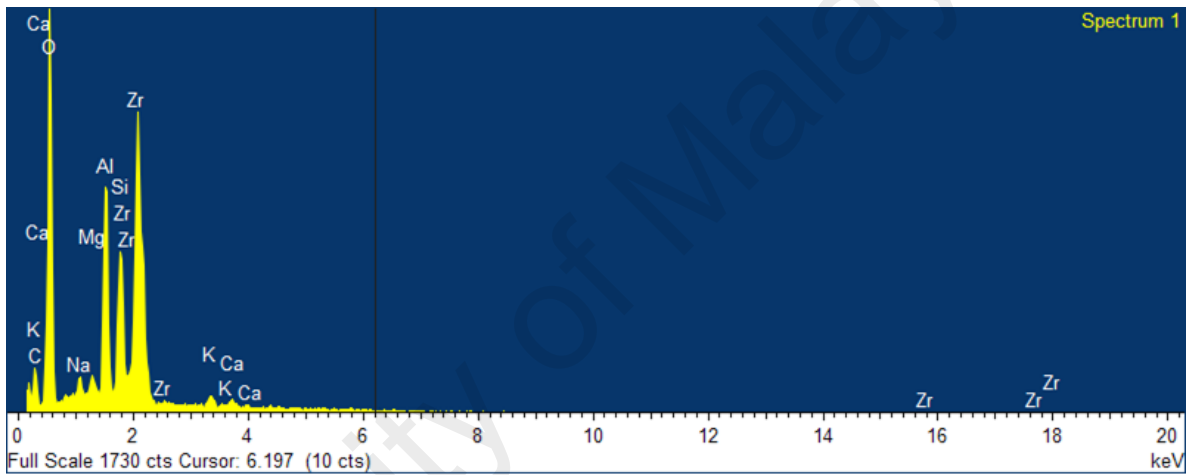


Figure 5.31: EDX of interface surface between Zr60-Al40%, graded silica, and veneering.

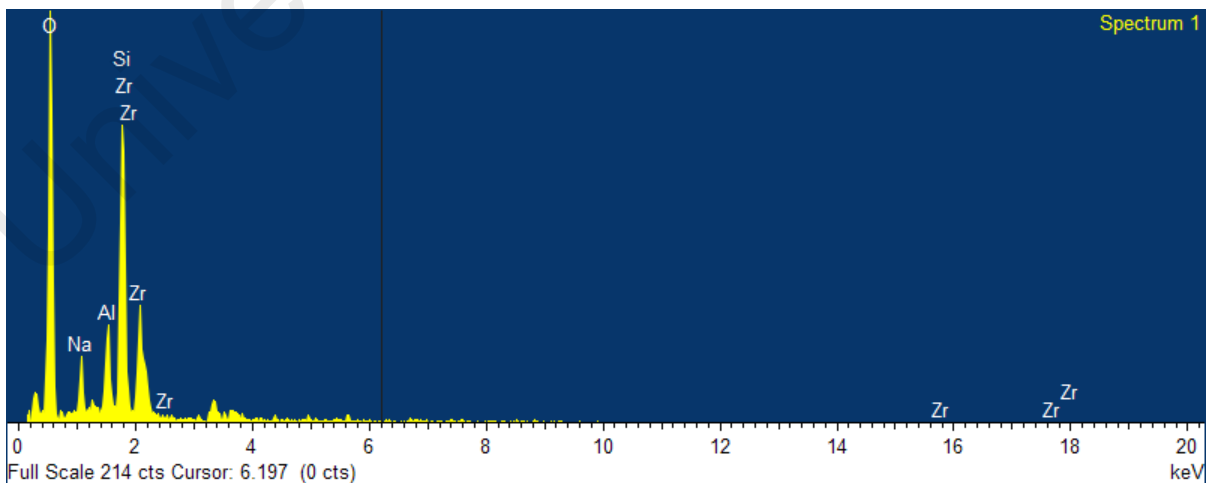


Figure 5.32: EDX of interface surface between Zr50-Al50%, graded silica, and veneering.

5.6 Discussion

To meet the ISO requirements of ISO 9693 (1999), the measurement of the bond strength of the ceramic metal framework should be tested by the Schwickerath crack initiation standardised test (three-point bending test) where the mean de-bonding strength/crack initiation strength should be higher than 25 MPa. However, it is important to note that this test approach cannot be subjected to multilayered all-ceramic frameworks as an outcome of the essential brittleness of all-ceramic core biomaterials (Albakry et al., 2003). An appropriate standardised test setup with a lower bond strength that is needed for multilayered all-ceramic core materials is still to be determined (Al-Dohan et al., 2004; Guess et al., 2008; Chio et al., 2009).

From a clinical point of view, some compositional and microstructural differences are exhibited in the veneering ceramics for the different cores, but in terms of mechanical properties, these are manufactured according to identical international standards (ISO 6872, 2008). Therefore, the similar veneering ceramic was applied to seven types of synthesised ceramic cores materials in this work.

A few studies used different test techniques of the bond strength for veneering ceramics and all-ceramics cores, such as the SBS test (Albakry et al., 2003; Al-Dohan et al., 2004; Dündar et al., 2005; Dündar et al., 2007; Guess et al., 2008; Fischer et al., 2008; Chio et al., 2009; Komine et al., 2010; Özkurt et al., 2010; Moon et al., 2016; Al-Harbi et al., 2016), microtensile test (Aboushelib et al., 2005; Aboushelib et al., 2006), three and four point bending (White et al., 2005), and biaxial flexure strength tests (Isgrò et al., 2003). Nevertheless, a common limitation was traced in all tests, which is hardly in determining the bond strength of veneer-core from subjected load at failure on the specimens in the particular test setting (Mecholsky, 1995).

In this work, the SBS test approach was chosen due to the simplicity and reliability of the test. That includes easier preparation of the specimen, the application of a simple protocol test and the capability to classify various products appropriate to values of the bond strength. However, some disadvantages are associated with the SBS test such as incidences of non-uniform interfacial stresses, high standard deviations, and the impact related to the geometry of the specimen. Therefore, in order to improve the clinical practicality of the SBS test, it becomes important that the specimen preparation, rate of forcing application, and cross-sectional surface area are standardised.

Moreover, to simplify the standardisation of the cross-sectional area, the samples tested in this current study were produced in bar shapes. Nevertheless, some limitations do exist in terms of the methodology applied in this research. The first issue is related to the fixing of the tested samples by embedding in the customized polytetrafluoroethylene mould using epoxy resin. Failures continued to occur within the epoxy resin when the bond strength of the veneer-core framework was stronger than the strength of the epoxy resin. Thus, an improved method for the fixation of samples is needed. Additionally, other limitation may have generated some cutting defects and/or flaws due to the fact that the samples have to be custom created and subjected to grinding.

On the other hand, delamination may happen easily between the two layers causing the crack to expand within the interface and then restart at confirmed stress concentration regions of the weaker layer upon additional forcing because of the largest fracture toughness difference and the weakest interfacial bonding among the glass veneer and the ceramic core. In an earlier study, Quinn et al., (2010) explored the chipping resistance of PFM samples compared with the chipping resistance of veneered zirconia specimens and revealed the relationship between substrate hardness and chipping. In this work, it has been found that under the simulative loading condition, the interfacial fracture of alumina-

based, zirconia-based, and alumina-toughened-zirconia (ATZ) multilayered frameworks resulted in an enhancement stress generating from the variances in elastic of Young's modulus among the veneer and the synthesised graded ceramic core. Similar issues have been reported in earlier studies of the alumina structures. Kelly et al., (1995) stated that up to 78% of fractured veneer ceramics and all-ceramic core with a glass-infiltrated alumina originated between the veneering ceramics and core ceramics interfaces.

Guess et al., (2008) found that the high values of bond strength of the combination of ceramic metal could not be attained by the veneering ceramics and zirconia core. Therefore, the development of new laboratory guidelines for the use of zirconia as a framework biomaterial is strongly recommended. Zheng et al., (2012) suggested that the weak interfacial bonding between the glass veneer and the zirconia core could be protected by a thicker occlusal veneer. However, it becomes clear that more *in vitro* and *in vivo* studies are needed to support new guidelines and to better comprehend the findings due to the complex nature and multifactorial of delamination.

Furthermore, according to several clinical studies, high stability has been demonstrated by the Y-TZP core ceramic as a framework material. Sailer et al., (2006, 2007), and Raigrodski et al., (2006) reported that there were no fractures of the zirconia framework. Nonetheless, the most recurrent factor beyond the failures of zirconia FPDs has been found to be the smallest chip-off fracture or delamination of the veneering ceramics. The occurrence of veneer ceramic fractures in metal-ceramic FPD was considerably lower compared with those in zirconia FPD (Sailer et al., 2007). This leads to the conclusion that the bond among veneer and core or the veneer ceramic itself is one of the most noticeable limitations in multilayered zirconia-based dental crown restorations (Guazzato et al., 2004a, 2004b, 2004c; Chio et al., 2009).

In earlier studies, Al-Dohan et al., (2004), Dündar et al., (2005, 2007), Chio et al., (2009), and Özkurt et al., (2010) reported that the SBS in all-ceramic-veneer specimens in the range of 9.4 - 42 MPa. In this present work, the values of the SBS of veneering ceramics to alumina, zirconia, alumina- zirconia ceramic (with different compositions) core with or without infiltrated graded silica ranged from 19.06 to 25.43 MPa, supporting the outcomes of previous work. However, in contrast to Al-Dohan's study (2004), the results of this study indicate a significant difference in mean values of the SBS between the zirconia with or without infiltrated silica groups. The variations in the results could be related to several parameters, such as methodology, study design, experience and proficiency of the operator, and various properties of various types ceramic materials.

Moreover, in this study and for every specimen group, the veneering ceramics remained on the alumina and zirconia surfaces. Therefore, it could be concluded that the cohesive strength of the veneering ceramics was lesser than the bond strength between the veneering ceramics and zirconia cores. In other hands, the veneering ceramic itself was the weakest link and not the interface. Such a finding also noted that the applied test design analysed the SBS of the veneering ceramic adjacent to the interface and not the bond strength. These results come in agreement with the findings of Al-Dohan et al., (2005) and Fischer et al., (2008) who also utilized the SBS test. This failure outcome could be related to the generated stress, that peaked towards the interface, due to a variance in the CTE among both layers. This further led to a stress concentration along to the interface, avoiding crack propagation parallel the interface.

Lately, a modern production of ceramics has been developed for the veneering zirconia system taking on the pressing technology. The gains of this framework include defect-free structures, simplicity and swiftness. Furthermore, the extra tensile strength of these press on veneer ceramics, along with their increased bond strength with zirconia and

superior interface quality, makes them optimal biomaterials for the uses (Aboushelib et al., 2008a, 2008c).

Moreover, the performance of a SBS test in a dry condition represents one of the limitations of this study, whereas in the real oral condition, water would be continuously existent, thus repeated temperature and pH changes would be generated. Based on most the SBS studies, the real bond strength would be lower than anticipated since the bond strength would reduce further with artificial aging or thermo-cycling (Sobrinho et al., 1998). Therefore, subsequent studies should include thermo-cycling or artificial aging procedures.

As anticipated the CTE of the veneer and core is an essential factor in making an effective veneer-core combination. Delamination of the veneer and formation of large microcracks were showed whenever the CTE of the veneer materials was lesser than that of the core material. The conservation of a narrow positive of CTE mismatch among the veneer and core ceramics is compulsory for more successful of the veneered all-ceramic core restorations (Isgro et al., 2004; Aboushelib et al., 2005; Fischer et al., 2008).

Three main factors should be considered for the interpretation of the SBS data, which are: (1) the bonding of the veneering ceramics and cores materials, (2) the CTE of the veneers and cores, and (3) the geometry of the multilayered ceramic composite and cooling rate (Guess et al., 2008), as following;

- 1- The vastly deviating outcomes of the all-ceramic tested groups can be ascribed principally to the different adhesion mechanisms of zirconia core and alumina with or without infiltrated silica materials to veneering ceramics. Up till now, the bonding technique mechanisms of the veneering ceramic to synthesised Y-TZP surfaces are still unidentified. Based on the analyses of the veneering ceramics with

wettability of zirconia core, interactions of the micro-mechanical were simply estimated (Guess et al., 2008).

The surfaces of all the synthesised ceramic cores in this study were sandblasted and etched by HF acid before to Cercon Ceram veneering in order to raise a mechanical interlock according to manufacturers' recommendations. Correspondingly, surface roughening with 110 μm Al_2O_3 (3 bars) sandblasting and surface etching with 9.5% hydrofluoric acid were standardized for all the ceramic cores samples. However, it is recommended that more investigation is conducted to study the impacts of the different techniques of sandblasting with or without etching on the veneer-core shear bond strength.

2- The influence of the CTE mismatch on core and veneer bonding had been explained in the dental literature (De Kler et al., 2007). The bond strength can be compromised by residual stresses from core and veneer CTE mismatch (Aboushelib et al., 2005). In order to produce adequate degrees of residual stress within a multilayered all-ceramic composite, dental manufacturers have exerted efforts to produce low fusing veneering ceramics and ceramic cores with the similar CTEs. In the current work, the CTE mismatch varied from 0.75 to $1.7 \times 10^{-6} \times \text{K}^{-1}$ for the synthesised all-ceramic cores systems (Table 4.5), while there were no differences in the measured bond strengths. There are a couple of factors that should be taken into consideration when looking into the nonlinearity and variance related to the CTE of veneering ceramics, which include the size of particles, the time of heat soak at peak firing temperature and the temperature interval studied. Therefore, the question arises if the CTE measured between 25 °C and 500 °C is sufficient to describe the thermal compatibility of veneer and all-ceramic core frameworks. Further, dental all-ceramics display phase changes that

are related to thermal history (i.e. number of firings) (Mackert et al., 1986). It may also impact the thermal compatibility of the veneering and all-ceramic core materials (Isgro et al., 2005; Guess et al., 2008).

- 3- Zirconia and alumina ceramic core ceramics are thermal insulators. Based on the manufacturers' information, the core ceramics offer a thermal conductivity of 2-2.2 $\text{Wm}^{-1}\text{K}^{-1}$. The range of thermal conductivity for veneer ceramics (Cercon Ceram) is of 2.39 $\text{Wm}^{-1}\text{K}^{-1}$. The combined low thermal conductivities of veneering and ceramic cores significantly delay the veneer cooling rate at the interface as compared to the metal configuration, potentially changing the CTE and producing residual thermal stresses (Mora and O'Brien, 1994; Hermann et al., 2006; Guess et al., 2008). These residual interfacial stresses represent an imaginable justification for the cooling rate and could contribute to the lower values of shear bond for these systems. Based on clinical research, additional residual stresses may also be a product of place to place differences in thermal properties owing to the non-uniform thickness of veneering ceramic and the relative thickness ratio of the veneer-core layer (Hojjatie and Anusavice, 1993).

In this study, the failure mode observed for the Zr 100% and Al 100% with or without infiltrated silica all-ceramic frameworks was fundamentally combined as cohesive in the veneering ceramic and an adhesive at the interface. The described failure modes with delamination of the veneer from sound zirconia and alumina core structures were comparable to the outcomes of other experimental researches, where crack deflection has been identified at the veneer-core interface (Aboushelib et al., 2006; Studart et al., 2007; Kim et al., 2007a, 2007b). There are two possible interpretations for that. The first is that crack deflection could be a consequence of the exceptional ability of alumina and Y-TZP to withstand crack propagation. The second is that the interlaminar crack deflection could also correlate with the relatively poor bond of the veneering ceramic to the zirconia and

alumina cores. The clinical implication of this finding is that the evaluated all-ceramic systems could have a tendency to generate chip-off fractures or delamination of the veneering ceramic rather than a catastrophic failure of the core with/ without infiltrated graded silica structure (White et al., 2005). The accurate mechanism of apparent interfacial bond failure in the present study is unidentified and requires furthermore evaluation.

Moreover, the SEM and EDX evaluations in this study detected that the fracture generated in veneering ceramics in both the alumina and zirconia with/without infiltrated silica ceramic samples. The failure modes of the samples from the zirconia and alumina ceramic samples propose the significance of the veneering ceramics mechanical properties, since cracks started in the veneering ceramics. It is conceivable that internal defects and pores of veneer cause to the starting of fractures. Thus, there are critical steps to the production technique such as layering, surface polishing and finishing, and firing of veneering ceramics (Kelly et al., 1990; Chio et al., 2009). In addition, the level of structural and crystallinity order of the porcelain veneer, which is directly related to its strength is of paramount importance to the durability of the dental crown restorations (Quinn et al., 2003; Chio et al., 2009).

The microscopic observations of the ceramic core fractured samples observed that an edge of veneering ceramic stayed on the ceramic core of all samples and that the veneering ceramic adhered to the core. The mostly cohesive mode of failure of the control core ceramic groups is in accordance with previous studies (Albakry et al., 2003; Al-Dohan et al., 2004; Dündar et al., 2005; Dündar et al., 2007; Fischer et al., 2008; Guess et al., 2008; Chio et al., 2009; Özkurt et al., 2010; Komine et al., 2010; Moon et al., 2016).

In this study, the authors acknowledged that based on the porosities, CET, volumetric shrinkage (veneer and core ceramic), micro-gap formations at the interface and technical

proficiencies, especially needed for the advanced layering approach fabrication of all-ceramic multilayered composites could be noted in this current work and that these may be other factors that weaken the interfacial bond (Dunder et al., 2007; Luthardt et al., 1999; Aboushelib et al., 2006; Guess et al., 2008; Chio et al., 2009). Thus, multiple factors may influence the ceramic veneer-core bond failure. Many variables may have an impact on the veneer-zirconia core bond strength; such as the surface finish of the core, which can influence mechanical retention; residual stress produced by mismatch in CTE; development of structure defects and flaws at veneer-core interface; and volumetric shrinkage and wetting properties of the veneer (Isgro et al., 2003; Chio et al., 2009).

Advanced technical skills are required to build-up ceramic. Large flaws and porosities are also responsible for the mode failure, especially in crowns with decreased occlusal thickness. Another significant factor is the core ceramic thickness, whereas small differences can impact the strength of the restoration (Chai et al., 2000). Some clinical failures that are observed in the form of veneering ceramic cracks might be a result of these phenomena. It has been proposed that thicker ceramic cores lead to bulk fractures in veneer porcelains under fracture resistance tests (Wakabayashi and Anusavice, 2000; Dunder et al., 2007). The veneer-core ratio in this study was 2mm-3mm and when normal core ceramic thicknesses (0.5–1mm) in multilayered all-ceramic materials are considered in dental restorations, this may not exhibit clinically relevant (Dunder et al., 2007).

As a limitation of this study, the samples' geometry design was conducted in a manner that the multilayered all-ceramic evaluated samples do not represent clinical shape situations of dental crown restorations, but provide a geometry that allows measurement of SBS. Substantial improvements are needed to get quantitative assessments of interfacial stress in the multicomponent dental complex-designed restoration. Predictive

3D models such as FEA and evaluations on the influences of cooling rates and residual stresses might be most helpful (Guess et al., 2008).

Also, in this study, the FEA analysis was real complex geometry which represented clinical shape condition of dental crown all-ceramic restoration and discussed previously in details in chapter three section 3. The results of experimental shear bond strength with line agreement to the results were obtained from FEA models.

In comparison to the gold standard, sufficient values of SBS between Y-TZP and alumina ceramic core and their corresponding veneering ceramics evaluated could not be obtained. The low bond strength values of all Y-TZP ceramic frameworks evaluated can be considered as a possible explanation for the high fracture rates of the veneering ceramics observed in clinical studies. Further evaluations and refinement of the Y-TZP core and veneering ceramic interface are substantial for clinical long-term success (Guess et al., 2008).

Oral fluids are known to facilitate stress corrosion of ceramic materials, resulting in slow crack growth and finally leading to failure of ceramic restorations in the complex situation of the oral cavity (Peterson et al., 1998; Zhang et al., 2005). The *in vitro* aging sensitivity of the SBS of multilayered samples was therefore estimated by exposure to a standardised thermocycling test setup (Dunder et al., 2005). In the study by Guess et al., (2008), they reported that the application of 20,000 cycles of thermo-cycling had no effect on the SBS of all tested samples. Comparative researches on the bond strength of veneering ceramics and zirconia core after exposure to thermo-cycling are not available up to now (Guess et al., 2008).

In this study, it was not intended to investigate the effect of sandblasting, etching (HF), and abrasion by using alumina oxide on the interface between synthesised

zirconia/alumina and the veneering ceramic, and further investigations are needed. However, it had been reported there is no effect from sandblasting, abrasion and etching on the interface between the ceramic core and veneer (Borges et al., 2003; Atsu et al., 2006; Aboushelib et al., 2008c; Phark et al., 2009; Menezes et al., 2009; Ernst et al., 2009; Jevnikar et al., 2010; Yun et al., 2010; Thompson et al., 2011).

Recently, many researches have reported that high strength alumina- and zirconia-based dental ceramics cannot be etched with hydrofluoric acid because of their high crystalline phase content (Borges et al., 2003; Atsu et al., 2006; Aboushelib et al., 2008c; Phark et al., 2009; Menezes et al., 2009; Ernst et al., 2009; Jevnikar et al., 2010; Yun et al., 2010; Thompson et al., 2011). Further, a recent study by Sriomporn et al., (2014) concluded that the hydrofluoric acid can etch dental zirconia ceramics, creating micro-morphological changes on the zirconia surface. Zirconia surfaces etched with hydrofluoric acid presented the tetragonal-to-monoclinic phase transformation.

5.7 Conclusions

Under the limitations of this chapter, it can be concluded that:

There was a different significance between the zirconia group and alumina group with/without infiltrated graded silica in the SBS ($P < 0.05$). Surface analysis of failure modes results observed that there are combined failure modes; adhesive failures at the veneer core interface (unloaded side), and cohesive failures in the veneer (loaded side). SEM examination observed that the fractures generated in the veneering ceramic in both the alumina and zirconia groups with/without infiltrated graded silica and the fracture source in the veneering ceramic were mostly on the loaded surface. In the case of interfacial fractures, a thin layer of the silica or veneering ceramic layer stayed on the synthesised ceramic cores.

CHAPTER 6: CYTOTOXICITY EVALUATION OF NEW SYNTHESISED DENTAL BIO-CERAMIC CORES BY USING HUMAN GINGIVAL FIBROBLAST CELLS – AN IN VITRO STUDY

6.1 Introduction

According to Manicone et al., (2007) review on zirconia biocompatibility, the first proposed utilization of zirconium oxide ceramic for the medical applications was made in 1969 and involved orthopedic applications. ZrO_2 was suggested as a modern biomaterial for femoral head substitution as a substitute for titanium or alumina prostheses. The evaluation of the reaction was made by putting ZrO_2 bioceramic in the femur bone of a monkey and no adversely reactions were reported. The orthopedic studies centred on the mechanical behaviour of zirconia bioceramic, on its wear, and on its integration with the muscle and bone. Furthermore, these first researches were largely performed *in vivo* because some *in vitro* technologies were yet insufficiently advanced. Before 1990, several other research was carried out, in which zirconia ceramic was examined on the muscle and bone without any unfavourable outcomes. Since 1990, *in vitro* studies have also been carried out in order to get data about the cellular behaviour towards zirconia. *In vitro* investigation has shown that zirconia is not toxic (Dion et al., 1994; Torricelli et al., 2001; Lohmann et al., 2002; Grenade et al., 2016).

Equivocal outcomes were reported in depend to zirconia ceramic powders that produced an adverse reaction (Li et al., 1993; Catelas et al., 1999). This was possibly due to zirconium hydroxide, that is no longer existent after sintering process, so that solid specimens can permanently be considered as safe. Covacci et al., (1999) and Silva et al., (2002) evaluated the mutagenicity and both reported that the zirconia was not able to produce mutations of the cellular genome. Mutant fibroblasts cells found on zirconia

ceramic were fewer than those got with the lowest probable oncogenic dose suitable with the cells viability (Covacci et al., 1999; Manicone et al., 2007).

Biocompatible alumina (Al_2O_3) was first introduced as a reinforcing inclusion for dental porcelain for 50 years ago, However, the inherently low tensile strength of porcelain does not allow it to be used in areas of high stress. Zirconia (ZrO_2) has a remarkably dense, inert, and hard surface, and is highly biocompatible. ZrO_2 currently has multiple purposes, and is used as root canal posts, to reinforce non-vital teeth since the mid-1990s, as subgingival dental implant abutments, as orthodontic brackets, as subgingival dental implant fixtures, and as frameworks for all-ceramic fixed dental prostheses. To date, its contraindications are unknown, or at least unreported (Liu et al., 2012; Mallineni et al., 2013; Kilic et al., 2013; Tete et al., 2014; Grenade et al., 2016).

6.2 Aim of this Chapter

The purpose of this chapter was to evaluate and determine the cytotoxic influences of new micro- with/without nano-particles sized synthesised dental bioceramic (powders and discs) for dental crown restorations on human gingival fibroblast (HGF-1) cells using cell proliferation assay.

6.3 Objectives of this Chapter

- 1- To evaluate and determine the effect of synthesised ceramics discs on the survival rate of HGF-1 cells lines by using cell proliferation assay.
- 2- To evaluate and determine the effect of the synthesised ceramics powders with different concentrations on the survival rate of HGF-1 cells lines by using cell proliferation assay.

- 3- To evaluate and compare the influence of the physical form of synthesised ceramic (powders and dense ceramics) or (non-sintering and sintering ceramics) on the survival rate of HGF-1 cells lines by using cell proliferation assay.

6.4 Null Hypothesis of this Chapter

There are no cytotoxicity effects of new micro- with/without nano-particles sized synthesised dental bioceramic (powders and discs) for dental crown restorations on human gingival fibroblast (HGF-1) cells using cell proliferation assay.

6.5 MATERIALS AND METHODS

6.5.1 Materials

The bioceramic powders were previously used as described in the Chapter 4 Section 4.2.1, (Table 4.1 and Table 4.2) and the cell line and materials for testing biocompatibility are listed in Table 6.1.

Table 6.1: The cell line and materials used for testing biocompatibility of synthesised bioceramic.

Product	Supplier	Batch No.
HGF-1 cells	ATCC®, USA	CRL-2014
DMEM	Sigma aldrich, USA	D5648
FBS- Fetal Bovine Serum	Sigma aldrich, USA	F9665
Dimethyl Sulfoxide	Sigma aldrich, USA	D2650
Penicillin-streptomycin(Pen-strep)	Gibco, USA	15140122
Sodium Pyruvate	Sigma aldrich, USA	S8636
24 and 96-well cell culture plates	Costar, USA	LAB353047and LAB353072
Resazurin sodium salt	Sigma aldrich, USA	R7017

6.5.2 Methods

The biocompatibility of the synthesised bioceramic powders and discs were evaluated according to *in vitro* cytotoxicity tests methodology of the ISO 10993-5 (E) (ISO, 2009).

The starting ceramic powders were used as recorded in Table 4.1 and Table 4.2. Seven compositions were prepared with pure YZrO_2 , varying of Al_2O_3 contents (0, 20, 40 to 50 wt.%) in YZrO_2 matrix, pure alumina, and graded silica as listed in Table 6.2. The mixtured powders were prepared by an attrition milling machine for 7 h in pure isopropyl alcohol, ZrO_2 balls (5 mm in diameter) were used as a medium. After milling, the mixtured powders were dried at 120 °C for 24 h. Samples were obtained by uniaxial hydraulic pressing beneath 200 MPa. Cylindrical samples of 5 mm diameter and 3 mm high were sintered at 1500 °C with heating rate was 5 °C/min and the cooling rate was 3°C/min down to room temperature as described in Chapter 4. All sintered ceramic core discs were polished using rubber wheels with the medium-, fine-, ultra-fine-grit silicone polisher papers (Buehler, Binghamton, NY, USA) and the diamond polishing solutions (1 µm) in order to obtain a mirror-like surface. Sixty-three discs of the synthesised ceramic cores were fabricated. Before sterilisation in an autoclave for cytotoxicity testing, the disc specimens were washed twice in an absolute isopropyl alcohol and once in demineralised water in an ultrasonic machine.

Table 6.2: The synthesised bioceramic materials (powders and discs).

Groups	Materials and percentage (%)	Particle size
Control	Negative Control	No treatment (cell-line with growth media)
A	Y Zirconia (100%)	Micro/Nano
B	Y Zirconia (80%) + Mg Alumina (20%)	Micro/Nano
C	Y Zirconia (60%) + Mg Alumina (40%)	Micro/Nano
D	Y Zirconia (50%) + Mg Alumina (50%)	Micro/Nano
E	Silica Graded	Micro/Nano
F	Zirconia (100%)	Micro
G	Mg Alumina (100%)	Micro/Nano

6.5.2.1 Maintenance of Cell Lines

Human gingival fibroblast-1 cell lines (HGF-1) (ATCC[®] CRL-2014[™], Manassas, VA, USA) were preserved and grown in the medium containing of 10% Fetal Bovine Serum (FBS) + Dulbecco's Modified Eagle Medium (DMEM) + 1X Pen-strep + 1 mM sodium pyruvate. HGF-1 cell lines were used for the experiment after passage no. 6 in the culture. The maintenance and growth of HGF-1 cell line were carried out according to the protocol instructions of ATCC[®] CRL-2014[™] and ISO 10993-5 (2009).

6.5.2.2 Seeding HGF-1 Cells in a 24- and 96-Wells

1 ml of cell suspension was seeded at the density of 0.01 million cells/ml of complete medium in 24 well flat bottom plates (Costar[®], Cambridge, LAB353047, One Riverfront Plaza Corning, NY, USA) and 100 μ l of 0.025 million cells/ml in 96 well flat bottom plates (Costar[®], Cambridge, LAB353072, One Riverfront Plaza Corning, NY, USA) as shown in Figure 6.1. The plates were incubated for 24 h in an incubator (Thermo Electron HERAcell[®] 150 CO₂ Incubator w/Copper Chamber, Langenselbold, Germany) (Figure 6.2.) with 5% CO₂ must be strictly maintained at 37 °C, because of the used medium was buffered with sodium carbonic/bicarbonate acid and pH (7.0 to 7.6) (see Appendix C, Figure 1 and Table 1).



Figure 6.1: The well plate used.



Figure 6.2: Incubator used.

6.5.2.3 Synthesised Bioceramic Powders and Discs Addition

500 mg of ceramic powders were weighed into individual 15 ml falcon tubes (Figure 6.3). Both ceramic powder and disc were sterilized by autoclaving. The sterile ceramic powders were dissolved in complete medium as 166 mg/ml stock solution. The falcon tubes containing ceramic solution were shaken overnight in an incubator with 5% CO₂ at 37°C. The powder extract was then filtered through a 0.22 µm membrane filter and was serially diluted (1:2) in the complete medium by adding 1ml of stock solution in 1ml of complete medium. Five different concentrations of compound were prepared (See Appendix C). Media were removed from overnight culture plate and 200 µl of each concentration was added into wells in triplicates (Figure 6.4). Sterile ceramic discs were put in the middle of each well of 24 well-culture plates with the help of sterile forceps (Figure 6.5). Cells with growth medium without ceramic powder and disc served as a negative control. Well plates were also incubated for 72 h with 5% CO₂ at 37°C in an incubator.

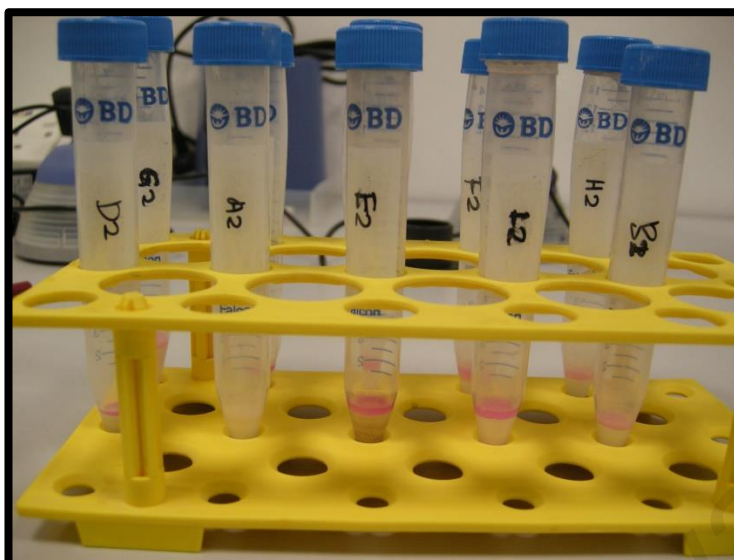


Figure 6.3: The falcon tubes used.



Figure 6.4: Ceramic powders with HGF-1 cell in 96 well plates.



Figure 6.5: Ceramic discs with HGF-1 cells in 24 well plates.

6.5.2.4 Preparation of Resazurin Reagent for Proliferation Assay

The resazurin reagent is a blue dye (7-Hydroxy-3H-phenoxazin-3-one-10-oxide sodium salt) (Sigma Aldrich, Louis, MO, USA) and utilized as an oxidation-reduction index for assessment of the viability of cells in mammalian cell cultures. The resazurin sodium salt powder was dissolved in 1X PBS (Phosphate Buffered Saline) to the stock concentration of 0.05 mg/ml.

6.5.2.5 HGF-1 Cell Proliferation Assay

After 72 h, treated and non-treated HGF-1 cells were eliminated from CO₂ incubator and equilibrated to room temperature. The old medium was replaced with fresh medium in both 96 well and 24 well-culture plates. 50 µl and 250 µl solutions of the resazurin reagents were added into each well of 96 and 24 well-plates respectively (Figure 6.6) and incubated with 5% CO₂ at 37°C for 4h. The light inverted microscope (Nikon T1-SM, Nikon corporation, Tokyo, Japan) was used to observe living cells and evaluate morphological alterations of HGF-1 cells (Figure 6.7). The well-plates were read on

Victor X5 spectrophotometer (VICTOR™ X5, PerkinElmer, Inc., Waltham, MA, USA)

(Figure 6.8) using fluorescence mode with Ex/Em of 531/595 nm.

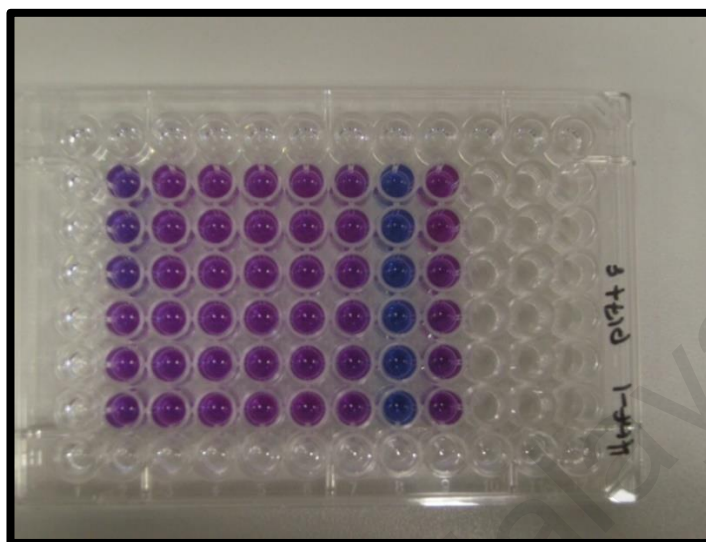


Figure 6.6: Resazurin reagent added into well plates.

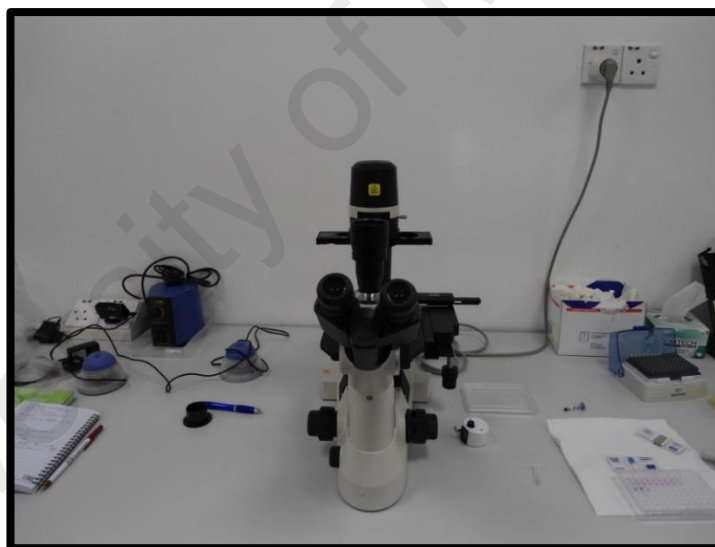


Figure 6.7: Inverted light microscope used.



Figure 6.8: Spectrophotometer used.

6.5.2.6 Raw Data Definition, Processing and Data Compiling

Raw data was obtained in the form of Excel sheet from Victor X5. Mean of blank (media alone) and mean of negative control (cell alone) were calculated. Mean blank was subtracted from fluorescence intensity of each experimental well and negative cell control. Blank subtracted values were used to calculate % survival. Percentage survival cell rate was calculated by using the formula,

$$\% \text{ survival} = (F_{\text{sample}} / F_{\text{cell control}}) \times 100\%$$

where F is fluorescence

Fluorescence values were normalized by subtracting blank values from each compound concentration values respectively. The value for each compound concentration was calculated as a percentage of the non-treated cell sample values. The obtained values reflect the percentage of survival of HGF-1 cells by each of ceramic compounds relative to non-treated cell control.

The data represented by the average mean values and the standard errors of means that obtained from the experiment which was carried out in triplicate. For ceramic discs, one-way analysis of variance (ANOVA) was utilized to determine statistical significant differences among the synthesised ceramic discs' groups, and also Dunnett's post hoc test was utilized for multiple comparisons. For powders ceramics, two-way analysis of variance (Two-way ANOVA) was employed to determine the interaction influence between synthesised ceramic powders with five different concentrations, also Dunnett's post hoc test was used for multiple comparisons. Also, parametric t-test was utilized to compare the mean between non-sintered and sintered synthesised ceramics. for all statistical tests, the significant level was set at 0.05.

6.6 Results:

6.6.1 Survival Cell Rate of HGF-1 (Cytotoxicity) of Ceramic Discs Groups

6.6.1.1 Mean of Survival Cell Rate of HGF-1 for Different Ceramic Discs Groups

As seen in Table 6.3, an examination was made of the mean survival cells rates (%), standard deviations, and standard error mean for seven different synthesised ceramic discs' groups. Generally, it was found that the mean of survival cells rate of HGF-1 of the control group was higher (100%) than other groups A (91.67%), B (94%), C (89.50%), D (88.67%), E (77.33%), F (82.33%), and G (72.33%), respectively. It was also noted that the mean of survival cell rate of group B was correspondingly higher than other groups (A, C, D, E, F, and G groups). The highest toxicity was found in those groups E and G respectively as shown in Figure 6.9.

Table 6.3: Mean of survival cell rate of different synthesised ceramic cores discs*.

Groups	N	Mean	SD ±	SE	95% Confidence Interval for Mean	
					Lower Bound	Upper Bound
Control	6	100.00	0.00	0.00	100.00	100.00
A	6	91.67	4.84	1.98	86.58	96.75
B	6	94.00	5.90	2.41	87.81	100.19
C	6	89.50	5.89	2.40	83.32	95.68
D	6	88.67	6.98	2.85	81.35	95.99
E	6	77.33	6.83	2.79	70.16	84.50
F	6	82.33	1.21	.49	81.11	83.60
G	6	72.33	6.22	2.54	65.81	78.86

*. Mean of survival cells rate expressed in percentage (%).

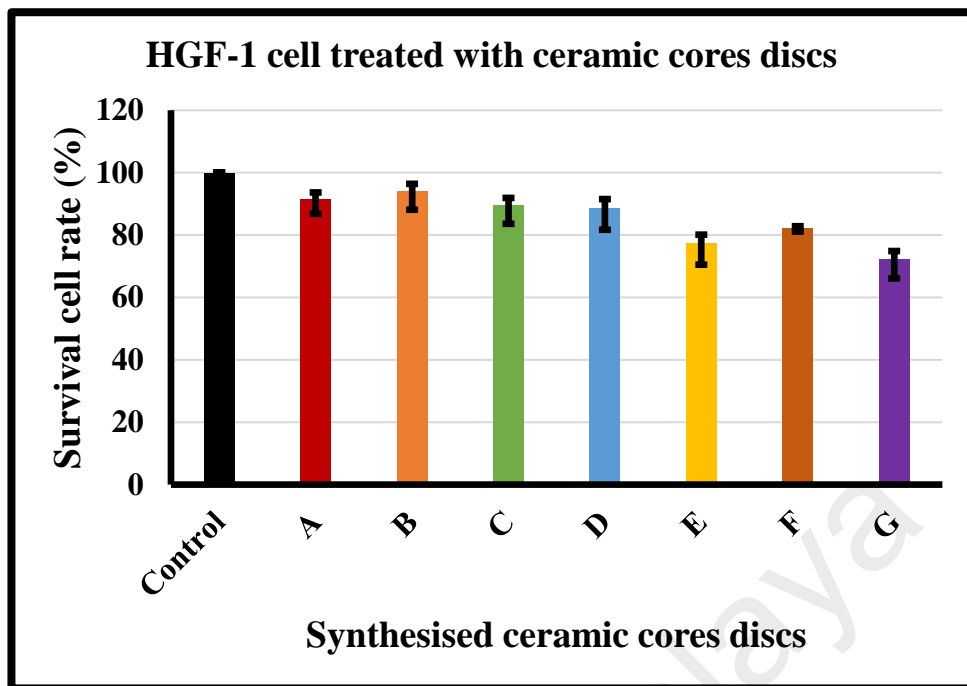


Figure 6.9: Mean of survival cell rate of different synthesised ceramic cores discs.

6.6.1.2 Effect of Different Synthesised Ceramic Discs on Survival Cell of HGF-1

One-way ANOVA was employed to determine the effects of different synthesised ceramic cores discs on survival cell rate of HGF-1. An assumption of one-way ANOVA was checked the normality test also checked for each factor. Each factor showed either it was normally distributed or slightly skewed positively which was in the accepted range of skewness (see Appendix C, Table 2 and Figure 2). Homogeneity equality of variance was checked using Levene's test ($P=0.211$) and found that the equality of variance assumption was met. Thus, it can be concluded that it had not violated the homogeneity of variance assumption for one-way ANOVA. Therefore, post hoc of an equal of variances it was used Dunnett t test. As seen in Table 6.4, the different ceramic cores discs show a highly significant influence on the survival cell rate of HGF-1 ($P=0.000$).

Also, the interaction effect within groups was checked, *post hoc* Dunnett t test (2-sided) was used for multiple comparisons between groups to control group. The results showed that the synthesised ceramic cores C, D, E, F, and G groups have a highly

significant effect on survival cell rate of HGF-1 when compared to the control group (P -values <0.000), having a different level of toxic effect on survival cell rate of HGF-1. But, there is no a different significance between A and B groups when compared to the control group (P -values >0.05) as shown in Table 6.5.

Table 6.4: The effect of different ceramic discs core on survival cell rate of HGF-1.

	Sum of Squares	Df	Mean Square	F	Sig.*
Between Groups	3474.813	7	496.402	17.385	.000
Within Groups	1142.167	40	28.554		
Total	4616.979	47			

*One-way ANOVA.

Table 6.5: Multiple comparisons of different ceramic discs Dunnett t (2-sided)^a.

(I)Groups	(J) Groups	Mean Difference (I-J)	Std. Error	Sig.
Group A	Group Control	-8.33333	3.08513	.054
Group B	Group Control	-6.00000	3.08513	.257
Group C	Group Control	-10.50000*	3.08513	.009
Group D	Group Control	-11.33333*	3.08513	.004
Group E	Group Control	-22.66667*	3.08513	.000
Group F	Group Control	-17.66667*	3.08513	.000
Group G	Group Control	-27.66667*	3.08513	.000

*. The mean difference is significant at the 0.05 level.

^a. Dunnett t-tests treat one group as a control, and compare all other groups against it.

6.6.2 Survival Cell Rate of HGF-1 (Cytotoxicity) of Powders Ceramics Groups

6.6.2.1 Mean of Survival Cell Rate of HGF-1 of Different Ceramic Powders Groups

As seen in Table 6.6., an examination of the mean survival cells rate (%) and standard error mean for seven different synthesised ceramic powders groups with five different concentrations compared to control group. Generally, it was found that the mean of survival cells rate of HGF-1 of the control group was higher survival cell rate (100%) than another groups tested. All the synthesised bioceramic powders extracted were not toxic to the cells at 10.38 mg/ml, 20.75 mg/ml, and 41.5 mg/ml concentrations. All the

synthesised bioceramic powders extracted were not toxic to the fibroblasts at a concentration less than 83 mg/ml except for powder E. Powder E group showed significantly lower cell survival rate at 83 mg/ml concentration. All the synthesised bioceramic powders extracted were toxic at 166mg/ml concentration except for powder B which was less toxic to the cell at higher concentrations. Groups C and E powders were very toxic to the cells at a high concentration as 100% cell was inhibited as shown in Figure 6.10.

Table 6.6: Mean of survival cell rate of different ceramic powders with different concentrations (%).

Groups	Concentration mg/ml of ceramic powders									
	10.38 mg/ml		20.75 mg/ml		41.50 mg/ml		83 mg/ml		166 mg/ml	
	Mean	SE	Mean	SE	Mean	SE	Mean	SE	Mean	SE
Control	100.00	.00	100.00	.00	100.00	.00	100.00	.00	100.00	.00
A	107.00	5.20	107.00	3.27	106.33	3.62	106.33	5.31	36.33	4.14
B	104.17	2.54	104.00	3.23	103.33	1.80	103.17	1.82	75.33	7.38
C	86.50	4.18	91.67	5.38	89.67	3.88	87.67	3.51	28.67	3.31
D	103.67	3.72	98.33	6.60	94.17	5.68	78.83	3.28	48.50	4.14
E	104.00	2.44	102.00	4.19	101.00	3.75	37.67	8.66	27.50	0.07
F	89.83	2.98	89.67	3.03	82.33	4.69	81.33	5.72	51.00	5.71
G	107.50	1.73	105.50	1.58	102.67	2.40	102.33	2.01	68.67	6.42

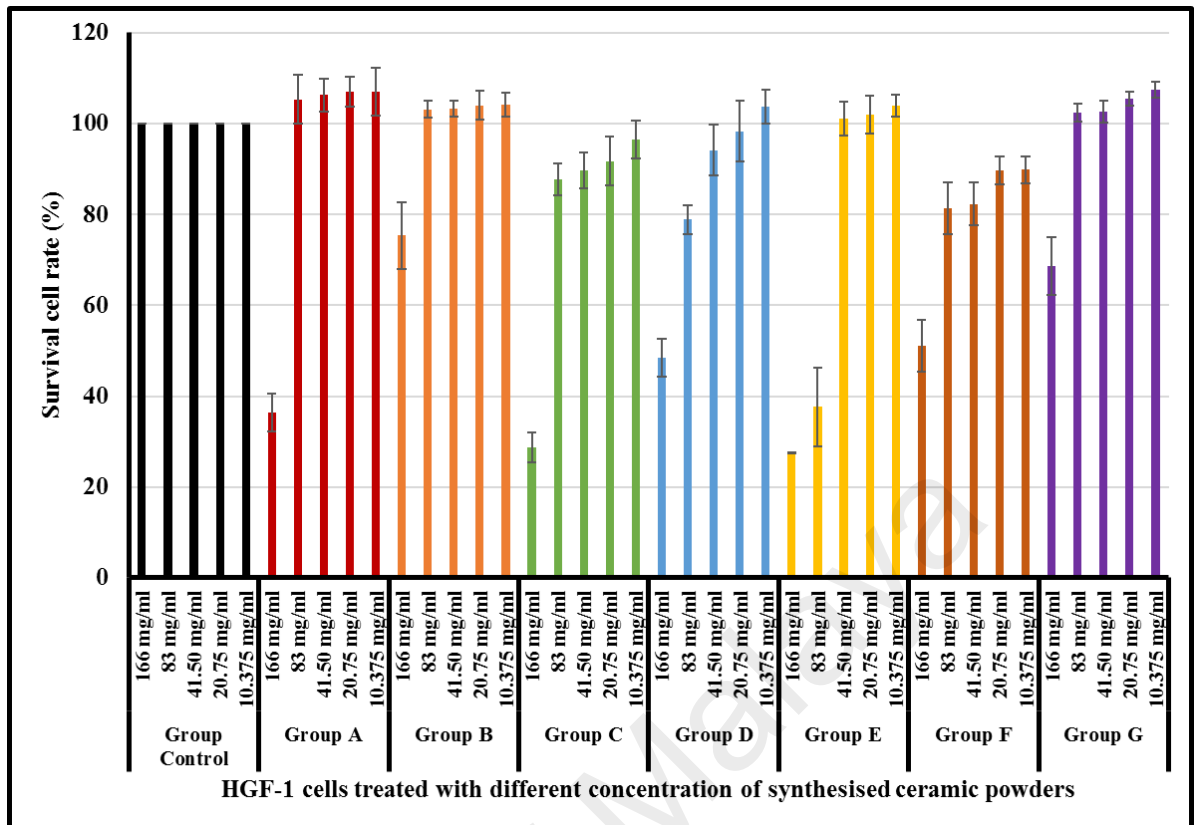


Figure 6.10: Mean of survival cell rate of different synthesised ceramic powders.

6.6.2.2 Effect of Different Ceramic Powders on Survival Cell Rate of HGC-1.

Two-way ANOVA was employed to determine the influences of different ceramic powders cores, different concentrations, and different times on survival cell rate of HGF-1. An assumption of two-way ANOVA has checked the normality test and also checked for each factor. Each factor showed either it was normally distributed or slightly skewed positively which was in the accepted range of skewness (see Appendix Table 3 and Figure 3). Homogeneity equality of variance was checked using Levene's test ($P=0.312$) and found that the equality of variance assumption was met. Thus, it can be concluded that it had not violated the homogeneity of variance assumption for two-way ANOVA.

As seen in Table 6.7., The interaction effect between each studied factor was checked, and found that there was a significant interaction effect between different ceramic powders and different concentrations on the mean survival cell rate of HGF-1 ($P=0.000$).

It indicated that there is an effect of different concentration and different ceramic powders on survival cell viability of HGF-1 ($P=0.000$). According to the two-way ANOVA, the most significant effect on the cell viability was produced by the different concentrations (F-value=307.319), whereas different ceramic powders had less effect (F-value=51.004) as shown in Table 6.7. Therefore, multiple comparisons analysis to control was done to locate the effect of different concentrations and different materials on survival cell rate. The results of Dunnett t test for multiple comparisons showed that the synthesised ceramic cores A, C, D, E, and F groups have highly significant effect on survival cell rate of HGF-1 when compared to the control group (P -values <0.000), it indicated that there are different levels of toxic effect on survival cell rate of HGF-1. But, there is no a different significance between B and G groups when compared to the control group (P -values >0.05) as shown in Table 6.8.

Table 6.7: The effect of different ceramic powders and different concentrations on survival cell rate of HGF-1.

Source	Type III Sum of Squares ^a	Df	Mean Square	F	Sig.
Groups	21403.067	7	3057.581	51.004	.000
Concentrations	73693.058	4	18423.265	307.319	.000
Groups * Concentration	32593.142	28	1164.041	19.417	.000

^a. R Squared = .914 (Adjusted R Squared = .897).

Table 6.8: The effect of different ceramic powders and different concentrations on survival cell of HGF-1.

(I)Groups	(J) Groups ^a	Mean Difference (I-J)	Std. Error	Sig.	95% Confid. Interval	
					Lower Bound	Upper Bound
Group A	Group Control	-7.6000*	1.99914	.001	-12.869	-2.330
Group B	Group Control	-2.0000	1.99914	.857	-7.269	3.269
Group C	Group Control	-21.1667*	1.99914	.000	-26.436	-15.897
Group D	Group Control	-15.3000*	1.99914	.000	-20.569	-10.030
Group E	Group Control	-25.5667*	1.99914	.000	-30.836	-20.297
Group F	Group Control	-21.1667*	1.99914	.000	-26.436	-15.897
Group G	Group Control	-2.6667	1.99914	.629	-7.936	2.603

*. The mean difference is significant at the .05 level.

^a. Dunnett t-tests treat one group as a control, and compare all other groups against it.

6.6.3 Comparison between the Effect of the Sintered and Non-Sintered Ceramic Groups on the Mean Survival Cell Rate of HGF-1.

Generally, it was found that the mean survival cells rate of HGF-1 of the all sintered groups was higher than the all non-sintered ceramic groups and the same between all the synthesised ceramics groups. It was also noted that the mean survival cell rate of group B was correspondingly higher than the other A, C, D, E, F, and G groups. In addition, the highest toxic was found in the groups E and C respectively as shown in Table 6.9 and Figure 6.11.

Table 6.9: Mean survival cell rate of HGF-1 of non-sintered and sintered synthesised ceramic groups.

Groups	Type	Mean	SD ±	SEM	N
Control	Non-sintering	100.00	.00	.00	6
	Sintering	100.00	.00	.00	6
Group A	Non-sintering	36.33	4.59	1.88	6
	Sintering	91.67	4.84	1.98	6
Group B	Non-sintering	75.33	6.15	2.51	6
	Sintering	94.00	5.90	2.41	6
Group C	Non-sintering	28.67	3.08	1.26	6
	Sintering	89.50	5.89	2.41	6
Group D	Non-sintering	48.50	4.85	1.98	6
	Sintering	88.67	6.98	2.85	6
Group E	Non-sintering	27.50	1.87	.76	6
	Sintering	77.33	6.83	2.79	6
Group F	Non-sintering	51.00	3.41	1.39	6
	Sintering	82.33	1.21	.49	6
Group G	Non-sintering	68.67	7.74	3.16	6
	Sintering	72.33	6.22	2.54	6

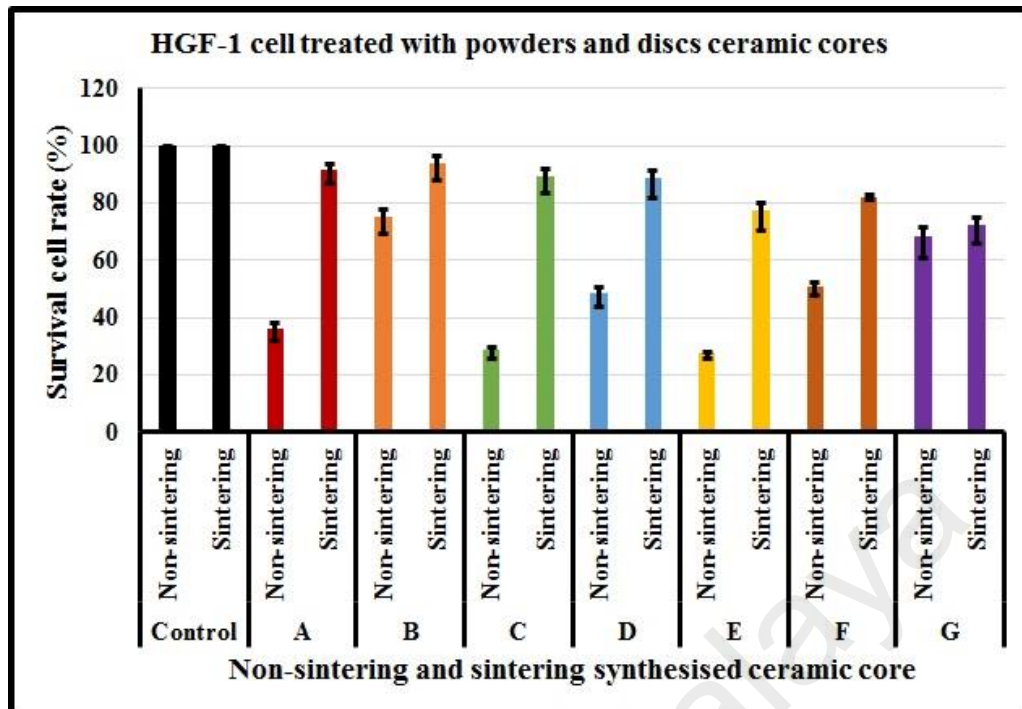


Figure 6.11: Mean survival cell rate of HGF-1 of non-sintered and sintered ceramic groups.

As seen in Table 6.10, the parametric t-test was employed to determine the effect of sintering and non-sintering ceramic on the survival cells rate of HGF-1. The normality was checked and it was found to be normally distributed (see Appendix C, Table 4 and 5, Figure 4 and 5). The results showed that there was a highly significant effect between sintering and non-sintering ceramic (P -value=0.000) in all groups tested as shown in Table 6.10. Also, there was a significant difference among the sintering ceramics groups were lesser toxic than non-sintering in each same ceramic material group (A, B, C, D, E, and F groups), but there was no significant difference between sintered and non-sintered ceramic materials in group G (P -value=0.387) as shown in Table 6.11.

Table 6.10: The effect of sintering and non-sintering ceramic on survival cell rate of HGF-1.

Variable: Cytotoxicity	N	Mean	SD	t-test for quality of Means		
				Mean differ (95% CI)	T statistic (df) ^a	P value
No-sintering	48	54.50	24.28	-32.479(-40.046, -24.913)	-8.580 (94) ^a	.000
Sintering	48	86.98	9.91			

^a Equality of variance not assume for cytotoxicity (Levene's test P -value= .000).

Table 6.11: The comparisons effect between sintering and non-sintering in each same ceramic material on survival cell rate of HGF-1.

Variable: Cytotoxicity		N	Mean	SD	t-test for quality of Means		
					Mean differ (95% CI)	T statistic (df) ^a	P value
Group A	No-sintering	6	36.33	4.59	-55.34 (-61.40, -49.26)	-20.31 (10) ^a	.000
	Sintering	6	91.67	4.84			
Group B	No-sintering	6	75.33	6.15	-18.67 (-26.41, -10.91)	-5.36 (10) ^a	.000
	Sintering	6	94.00	5.90			
Group C	No-sintering	6	28.67	3.08	-60.83 (-66.88, -54.79)	-22.42 (10) ^a	.000
	Sintering	6	89.50	5.89			
Group D	No-sintering	6	48.50	4.85	-40.17 (-47.89, -32.44)	-11.58 (10) ^a	.000
	Sintering	6	88.67	6.98			
Group E	No-sintering	6	27.50	1.87	-49.83 (-56.28, -43.39)	-17.23 (10) ^a	.000
	Sintering	6	77.33	6.83			
Group F	No-sintering	6	51.00	3.41	-31.33 (-34.62, -28.05)	-21.23 (10) ^a	.000
	Sintering	6	82.33	1.21			
Group G	No-sintering	6	68.67	7.74	-3.67 (-12.70, 5.36)	-0.91 (10) ^a	.387
	Sintering	6	72.33	6.22			

^a. Equality of variance assume for cytotoxicity of all groups (Levene's test P -value > .05).

6.7 Discussion

In the dental restorative field, research on the biological behaviour of human gingival fibroblasts (HGF-1) with regards to the dental biomaterials are considerable, as far as the gingival fibroblasts cells are concerned to evaluate the oral soft tissue reactions with to the biomaterials. Gingival fibroblasts in particular share in the integration method with ceramic biomaterials, being capable of merging or not with the materials (Simion et al., 1991; Rompen et al., 2006; Di Nisio et al., 2013; Cataldi et al., 2013; Tete et al., 2014).

In this current study, HGF cells were chosen to be used for the cytotoxicity evaluation of new synthesised ceramic powders and cores because they were in the close proximity to dental biomaterials restorations in the oral cavity and also considered to be clinically more relevant. Additionally, HGF-1 are susceptible cells which could be simply separated and cultured in the ordinary cultures media (Hensten-Pettersen and Helgeland, 1981; Moharamzadeh et al., 2007). HGF cells have been widely used to assess cytotoxic effects of various dental restorative materials (Pae et al., 2009; Santos et al., 2009b; Tete et al., 2014; Grenade et al., 2016).

The *in vivo* cytotoxicity tests are costly, time-consuming and often short of clear cut-end points for quantitative evaluation. The acute cytotoxicity testing, as a tissue culture-based alternative offers distinctive advantages in the initial screening programmes. These include the following: (1) experiments are allowing for the examination of many variables, short-term and the testing of more materials, (2) the experimental settings can be controlled to allow quantitative assessments of the cellular response, (3) more homogeneous cell populations *in vitro* culture provide for reduced biological variability; and (4) the system is more susceptible to toxic biomaterials than an *in vivo* implantation (Kasten et al., 1982).

Based upon detection of the metabolic activities of HGF cells, the resazurin assay integrates a colourimetric and fluorometric growth indicator. The method integrates an oxidation shorthand point which both changes colour and fluoresces in reaction to the chemical shorthand of the growth media produced from the cell growth (Nociari et al., 1998). It has two features up the MTT assay: first, its alteration in colour could be discovered both fluorometrically and spectrophotometrically, that awards the greatest ability for the detection; second, it is not cytotoxic to cells, it has potential to estimate the viability of cell on extra than one case (Fields and Lancaster, 1993). However, the Alamar Blue assay contains resazurin and additional compounds to prevent the over reduction of resazurin to a non-fluorescent product. These additives also slow the rate of generation of the fluorescent product. Consequently, the Alamar Blue requires longer incubation times than resazurin assay (Czekanska, 2011).

The resazurin assay was employed in this study to evaluate the cytotoxicity of synthesised bioceramic powders and cores as it supplies an accurate guide of the proliferation and the cell viability. That is in addition to the fact that its alteration in colour could be calculated fluorometrically as has been stated above. The results of this study also show that the resazurin screening could be distinguish susceptibility of the HGF-1 cultures of the different concentrations.

Exposure time is considered a significant parameter in the toxicity evaluation. The cell lines are affected after 12 to 24 h exposure to the toxic substance (Hanks et al., 1996). In this current study, HGF-1 cells were exposed to five different concentrations of ceramic powders and discs for 24 h, because it has been shown that degradation of ions released from ceramics is complete in 24 h (Kasten et al., 1982; Lawson, 1995). Therefore, the most toxic effects from ceramic powders happen during the first 24 h at high concentrations. Otherwise, the transformation also can be induced by an environmental

stress, leading to the so-called ageing phenomenon (Lawson, 1995). The degradation producing from this phenomenon is identified by micro-cracking at the surface, surface roughening and particle release in the body (Deville et al., 2006).

Bagambisa et al., (1994), reported that the bioceramics reduced the outgrowth of the osteoblasts cells and the cytotoxicity was depended to the structure surface rather than to the dissolution substances. The observed cytotoxicity might be explained by the fact that the cells were cultured by direct connection to the ceramics, compared with the results obtained in this current study. However, other studies have reported that the many of the ions observed in bioceramics are not cytotoxic (Schuster et al., 1996; Sjögren et al., 2000).

Moreover, the influence of the physical form (of both sintered and non-sintered) of the synthesized bioceramic materials on the *in vitro* biocompatibility was analysed and the results of this study were similar to the findings of Li et al., (1993); Santos et al., (2009b); and Kilic et al., (2013) who demonstrated that the powder bioceramics were more toxic than disc bioceramics using direct contact tests with HGF.

The results in this study also revealed that the effect of sintered synthesised ceramic cores have higher survival cell rates (cell viability) than those of the non-sintered ceramic cores, which exhibited a less toxic effect in solid form than powder form. Thus, it could be concluded that the ceramic material in a solid form is more stable than the powder form. This comes in agreement with the results revealed in the *in vitro* study of Li et al., (1993).

It has also been concluded through the experimentations in this study that the graded silica powder has a higher toxic effect on cell viability of HGF-1 than that of zirconia, alumina, and ATZ tested with different ceramic powder compositions. However, Tate et al., (2014) reported that the zirconia observed a higher gingival fibroblasts cytotoxicity

than lithium disilicate glass-ceramic, while other studies showed cytotoxic influences (Messer et al., 2003; Brackett et al., 2008; Pabst et al., 2014). Thus, lithium disilicate glass-ceramic could be considered a second-grade bioceramic material in terms of biocompatibility as compared to the zirconia (Grenade et al., 2016). The findings of this study in these regards are in concert with other studies, such as Messer et al., (2003); Brackett et al., (2008); Kilic et al., (2013); Pabst et al., (2014); and Grenade et al., (2016).

Several *in vitro* studies have reported that the indirect dental ceramic restorative materials have not biological responses, except for the wear on the opposing teeth and/or restorations. The relative incidence of biological adversely from dental bioceramics compared with others dental biomaterials restorations has been observed to be very little (Matinlinna and Vallittu, 2007; Ho and Matinlinna, 2011; Mallineni et al., 2013). Nevertheless, Roulet et al., (1995) reported that there were no long-term effects with the dental bioceramics.

Many *in vitro* studies have also suggested that the chemical composition and surface roughness have been able to change proliferation and cell adhesion, that represent the first procedures in the biomaterial-host tissue integration processes (Tate et al., 2014; Grenade et al., 2016). However, the effect of the surface roughness of synthesised ceramic cores has not been sufficiently assessed in this study. Therefore, it is recommended that future works focus on the systematic analysis of the biomaterial effect on the cellular behaviour for each parameter such as the chemical compositions of materials in addition to surface roughness properties and aging; and in an independent manner.

A previous study by Pae et al., (2009), found that the presence of grooves on the surface of zirconia ceramics can a little improve the proliferation and cellular attachment of HGF, compared with smooth surfaces. The study further suggested that more evaluation is needed to determine the ideal surface for the build-up of the zirconia

abutments for dental implants. Once again, further investigation is required to identify the effect of the thickness and depth of the notches on the surface of zirconia ceramic. Generally, zirconia ceramic may be appropriate for the implant abutments, but more mechanical and clinical experiments would be useful in order to obtain the best understanding of the zirconia ceramic abutments for long period of time (Pae et al., 2009).

Earlier studies have also clearly shown that the all-ceramic dental materials are not equals in their *in vitro* biological behaviour, whether in their first state of the production, after disorder with polishing procedures or with aging. This variation in biological response with regards to ceramics is reverse to the prevailing confirmed that the bioceramic materials are biocompatible and inert (Deany, 1996; Messer et al., 2003) and validates notices of the various amounts of the masses loss from the various bioceramics (Milleding et al., 2002). Moreover, the contrasting outcomes of the lithium disilicate biomaterials the required to abolish assuming a favourable biological reaction to any single kind of biomaterial (Hanks et al., 1996).

Nevertheless, it becomes hard to explain why the different biomaterials offered the various biologic behaviour (Messer et al., 2003). Then could be linked to the limitations associated with the commercial dental ceramic materials used in those studies, especially if proper preparation methods for the adequate control of microstructures were not applied as minor variations in the chemical composition and purity of the powder can have profound effects. However, the microstructures in this study have been carefully formulated with detailed knowledge of physical, thermal and mechanical to avoid such variations. The results observed that the overall biological reactions of HGF cells to zirconia, alumina, alumina toughened zirconia (with different compositions), and graded silica were comparable to one another.

Moreover, the results exhibited that the synthesised ceramics were equivalent in their biological behaviour considering that the materials used were physically, thermally and mechanically characterised microstructures and as discussed in chapter four. However, it is imperative to note that further evaluation is required to detect the effect of the thickness and depth of notches on the synthesised ceramic cores surfaces in addition to chemical characterisation, including the release of the substances as a manner to predict and understand the biologic response of all-ceramic biomaterials over a long period of time.

Different studies have been conducted to examine local toxicity of bioceramics. Cobb et al., (1988) indicated that the porous opaque porcelain is biocompatible to HGF cells. Thereafter, Josset et al., (1999) found that no toxic influence was shown because wither alumina or zirconia ceramics altered the growth rate of the human osteoblasts cells in similarity with the absence of any stimulating influence on proliferation or DNA synthesis. Additionally, Sjögren et al., (2000) and Uo et al., (2003) reported that all dental bioceramics studied were estimated non-cytotoxic. However, the results of study done by Messer et al., (2003) revealed that the dental bioceramics were not equal in their *in vitro* biologic influence, even with the similar grade of biomaterial and the most bioceramics resulted in only mild *in vitro* inhibition of the functions HGF cell to degrees that would be agreeable on the basis of standards used to evaluate composites and alloys. Also, the results of study were done by Pera et al., (2005) revealed that not all tested ceramics materials were free from toxicity.

Another *in vitro* study conducted by Elshahawy et al., (2009a), showed that the transient exposure of tested material to an acidic environment for one week is possible to significantly increase ions release from it (potassium and aluminium elements). However, the amount of the released ions were found insufficient to show high guide of cytotoxicity against HGF cells cultured using the trypan blue assay. Regardless of the dental

biomaterial used for the fixed prosthodontic restorations, it is becoming hard to predict the clinical behaviour of a material from *in vitro* studies since the oral factors such as variations in the quality and quantity of oral hygiene, diet, saliva, distribution and amount of the occlusal forces, polishing of the material surface, or brushing with toothpaste, can all effect corrosion to differ in stages. From a biocompatibility viewpoint, the corrosion of a material indicates that some of the ions are available to influence the tissues around it (Elshahawy et al., 2009b).

A recent study was done by Elshahawy et al., (2013), revealed that the ions of aluminium and silicon were released after three months in service. However, amounts of the released ions from CAD/CAM leucite-reinforced glass-ceramic dental crowns into the saliva of the fixed prosthodontic patients were not sufficient to produce strong cytotoxicity effects against HGF cells.

According to the results of this study, various biological responses to all synthesised bioceramic materials used in dental restorations contradict the widespread belief that dental bioceramic materials are always biocompatible, inert, and they substantiate reports indicating that the different ceramics lead to the different amounts of mass loss (Li et al., 1993; Milleding et al., 2002; Kilic et al., 2013). Since the powders substrate materials in this study were obtained from the manufacturers specifically for use in the study with being characterized physically or chemically in a detailed manner, it was easy to determine why the various materials exhibited different biologic effects.

In this study, the analysis obtained for the ceramic discs sintered at 1500 °C showed promising results, because of the cell viability of 90% of the ATZ composite ceramic materials is visibly up the 80% cell viability limit, that indicates superior biocompatibility of the synthesised ceramic composites materials. Therefore, it can be affirmed that the synthesised $\text{Al}_2\text{O}_3\text{-ZrO}_2$ ceramic composite material used in this study can be categorized

as non-cytotoxic, hence having great powerful for possible usage as dental crown restorations and implants. These findings were confirmed and come in agreement with the *in vitro* studies conducted by Li et al., (1993) and Santos et al., (2009b).

Furthermore, the findings of this study confirmed that the effect of micron alumina has lower effect on cell viability than that of nano alumina, but the mechanical properties were less than the nano. A less harmful effect of nano-particles in comparison with the micron alumina on the functions of osteoblast has been demonstrated by previous study (Gutwein and Webster, 2004), while, the nano-particles of alumina may be decreased of functions macrophage on nano-phase in comparison with the micro-particles alumina (Khang et al., 2009).

6.8 Conclusions

In this sixth chapter, it can be concluded that:

1. From the different synthesised ceramic discs, compound B (Zr80%-Al20%) showed the least level of toxicity and compound E (graded silica) and G (MgAl_2O_4) were most toxic to HGF-1 cells viability.
2. Out of the five different concentrations of ceramic powder, ceramic powder B (Zr80%-Al20%) was shown to be the most promising compound that is not toxic to the cells viability of HGF-1. This is followed by ceramic powders A (YZrO_2) and F (ZrO_2). Most of the ceramic powder compositions exhibited higher cytotoxicity rates at a higher concentration of 166 mg/ml in HGF-1 cells.
3. Ceramic discs exhibited minimal cytotoxicity in HGF-1 cells compared to ceramic powders with regards to the comparison made between non-sintered and sintered synthesised ceramics.

4. Moreover, the introductory testing of the cytotoxicity exhibited that the Al_2O_3 - ZrO_2 ceramic composite can be considered and categorized as nontoxic, thus having a possible usage as dental implants. It has been noted in this *in vitro* study that the Al_2O_3 - ZrO_2 ceramic composites may be used as bioceramic materials in dental applications such as all-ceramic crown restorations due to its superior biocompatibility, mechanical properties, and besides being more aesthetic in appearance.

University of Malaya

CHAPTER 7: CONCLUSIONS AND FUTURE STUDIES

7.1 Conclusions

- 1- An FEA model was used to develop a system to analyze stresses on the tooth, to support the jawbone, and to restore a tooth using the dental crown system (veneer-core-cement) during simulated mastication load based on FEM. The described method can produce detailed and valid 3D FE models of the maxillary premolar tooth with single layer and multilayered dental crown restorations. The 3D FE model constructed from CT images can be used for different mechanical simulations. A novel mechanical clinical diagnostic criterion could also be clinically applied based on this study to understand the stress analysis of the dental ceramic crown system.
- 2- Dense $\text{ZrO}_2\text{-Al}_2\text{O}_3$ synthesised ceramic graded composites were developed when sintered at $1500\text{ }^\circ\text{C}$ by using pressureless sintering. In all sintered ceramic cores materials, only the tetragonal ZrO_2 phase with α -alumina phase were observed, also, the m- ZrO_2 phase content in the starting powder was observed, indicating the complete stabilization of the tetragonal phase during cooling. Also, the graded silica was developed and the microstructures were characterized by SEM, EDX, and XRD to show the phase type of synthesised graded ceramic.
- 3- There was a significant difference between the zirconia group and alumina group with/without infiltrated graded silica in the shear bond strength ($P < 0.05$). Also, surface analysis of failure modes showed that the following combined failure modes: cohesive failures in the veneer (loaded side) and adhesive failures at the core veneer interface (unloaded side). SEM evaluation showed that the fractures originated in the veneering porcelain in both the zirconia and alumina groups with/without infiltrated graded silica and the fracture origin in the veneering

porcelain were mostly on the loaded surface. In the case of interfacial fractures, a thin layer of the veneering ceramic or silica layer remained on the core materials.

- 4- The biocompatibility evaluation of synthesised graded ceramics by using proliferation cell assay, showed that the composite material $ZrO_2-Al_2O_3$ graded ceramic sintered at $1500\text{ }^\circ\text{C}$ can be classified as noncytotoxic, therefore having great potential for use such as a dental crown restoration and/or as implant components due to its excellent mechanical properties and biocompatibility, as well as being aesthetic.

7.2 Recommendations for Future Studies

- 1- Further investigations are needed to compare the models constructed from CT scan and analysed by FEA with different thickness of cement material and combined with strain gauge test. Also, a study of the effect of thermomechanical stress is needed.
- 2- Hot isostatic press sintering should be conducted to get more densification than pressureless sintering, and fracture toughness and flexural strength should be investigated following aging. Also, reliable compressive strength test methods for ceramic materials which will be used in dental ceramic crown applications are needed prior to giving design recommendations.
- 3- Further long-term evaluations of zirconia behaviour are needed to determine the long-term stability of the material.
- 4- Further studies on shear bond strength tests are needed to compare different veneering techniques, such as the conventional layering technique and pressed-on veneering technique to synthesised ceramic composite with/without coated graded silica under aging and thermocycling. Also, more investigations are required to

study the effect of different techniques of sandblasting with/without etching on core-veneer shear bond strength.

- 5- In biocompatibility evaluation for ceramic, future studies should include characterization of the ceramic materials before and after aging to attempt to understand the causes of the changes in cytotoxicity observed and the relevance of these changes to clinical practice. Chemical surface analysis techniques, as well as measurement of release elements and physical surface characterization, may all improve understanding of the biologic behavior of these and other ceramic materials. Such an understanding may ultimately lead to the development of dental ceramics with more biocompatibility.

University of Malaya

REFERENCES

- ABAQUS, (2010). Manual Abaqus/CAE Professional version 6.10.1, Abaqus Inc., Simulia, Valley, St. Providence, USA.
- Abden, M. J., Islam, M. K., & Afroze, J. D. (2014). Microstructure and mechanical properties of 3YSZ ceramics reinforced with Al₂O₃ particles. *Int J Mater Eng*, 4: 129-135.
- Abduo, J., & Lyons, K. (2013). Rationale for the use of CAD/CAM technology in implant prosthodontics. *Int J Dent*, 768121: 1-8.
- Abduo, J., Lyons, K., & Bennamoun, M. (2014). Trends in computer-aided manufacturing in prosthodontics: A review of the available streams. *Int J Dent*, 783948: 1-15.
- Aboushelib, M. N., de Jager, N., Kleverlaan, C. J., & Feilzer, A. J. (2005). Microtensile bond strength of different components of core veneered all-ceramic restorations. *Dent Mater*, 21: 984-991.
- Aboushelib, M. N., de Jager, N., Kleverlaan, C. J., & Feilzer, A. J. (2007). Effect of loading method on the fracture mechanics of two layered all-ceramic restorative systems. *Dent Mater*, 23: 952-959.
- Aboushelib, M. N., Kleverlaan, C. J., & Feilzer, A. J. (2006). Microtensile bond strength of different components of core veneered all-ceramic restorations. Part II: Zirconia veneering ceramics. *Dent Mater*, 22: 857-863.
- Aboushelib, M. N., Kleverlaan, C. J., & Feilzer, A. J. (2008a). Microtensile bond strength of different components of core veneered all-ceramic restorations. Part 3: double veneer technique. *J Prosthodont*, 17: 9-13.
- Aboushelib, M. N., Kleverlaan, C. J., & Feilzer, A. J. (2008b). Effect of zirconia type on its bond strength with different veneer ceramics. *J Prosthodont*, 17: 401-408.
- Aboushelib, M. N., Matinlinna, J. P., Salameh, Z., & Ounsi, H. (2008c). Innovations in bonding to zirconia-based materials: Part I. *Dent Mater*, 24: 1268-1272.
- Akgungor, G., Sen, D., & Aydin, M. (2008). Influence of different surface treatments on the short-term bond strength and durability between a zirconia post and a composite resin core material. *J Prost Dent*, 99: 388-399.
- Al-Amleh, B., Lyons, K., & Swain, M. (2010). Clinical trials in zirconia: a systematic review. *J Oral Rehabil*, 37: 641-652.
- Al-Amleh, B., Waddell, J. N., Lyons, K., & Swain, M. V. (2014). Influence of veneering porcelain thickness and cooling rate on residual stresses in zirconia molar crowns. *Dent Mater*, 30: 271-280.
- Albakry, M., Guazzato, M., & Swain, M. V. (2003). Fracture toughness and hardness evaluation of three pressable all-ceramic dental materials. *J Dent*, 31: 181-188.

- Albakry, M., Guazzato, M., & Swain, M. V. (2004). Effect of sandblasting, grinding, polishing and glazing on the flexural strength of two pressable all-ceramic dental materials. *J Dent*, 32: 91-99.
- Al-Dohan, H. M., Yaman, P., Dennison, J. B., Razzoog, M. E., & Lang, B. R. (2004). Shear strength of core-veneer interface in bi-layered ceramics. *J Prosthet Dent*, 91: 349-355.
- Alexander, K. B., Becher, P. F., Waters, S. B., & Bleier, A. (1994). Grain growth kinetics in alumina-zirconia (CeZTA) composites. *J Am Ceram Soc*, 77: 939-946.
- Al-Harbi, F. A., Ayad, N. M., Khan, Z. A., Mahrous, A. A., & Morgano, S. M. (2016). In vitro shear bond strength of Y-TZP ceramics to different core materials with the use of three primer/resin cement systems. *J Prosthet Dent*, 115: 84-89.
- Al-Omiri, M. K., Rayyan, M. R., & Abu-Hammad, O. (2011). Stress analysis of endodontically treated teeth restored with post-retained crowns: A finite element analysis study. *J Am Dent Assoc*, 142: 289-300.
- Annamaria, C., Antonella, T., Leonardo, E., & Carlo, P. (2003). Fractal analysis of cracks in alumina-zirconia composites. *J Eur Ceram Soc*, 23: 469-479.
- Anstis, G. R., Chantikul, P., Lawn, B. R., & Marshall, D. B. (1981). A critical evaluation of indentation techniques for measuring fracture toughness: I. Direct crack measurements. *J Am Ceram Soc*, 64: 533-538.
- Anusavice, K. J. (2003). Phillip's science of dental materials. 11th ed. St. Louis: WB Saunders. p. 655-681.
- Anusavice, K. J. (2012). Standardizing failure, success, and survival decisions in clinical studies of ceramic and metal-ceramic fixed dental prostheses. *Dent Mater*, 28: 102-111.
- Anusavice, K. J., & Hojjatie, B. (1992). Tensile stress in glass-ceramic crowns: effect of flaws and cement voids. *Int J Prosthodont*, 5: 351-358.
- Anusavice, K. J., Zhang, N. Z., & Moorhead, J. E. (1994). Influence of colorants on the crystallization and mechanical properties of lithia-based glass-ceramics. *Dent Mater*, 10: 141-146.
- Ashkanani, H. M., Raigrodski, A. J., Flinn, B. D., Heindl, H., & Mancl, L. A. (2008). Flexural and shear strengths of zro2 and a high-noble alloy bonded to their corresponding porcelains. *J Prosthet Dent*, 100: 274-284.
- ASTM C 773-88 (1999). Standard test method for compressive (crushing) strength of fired whiteware materials. in: Annual Book of ASTM Standards, vol. 03.03, American Society for Testing and Materials, West Conshohocken, PA, USA.
- ASTM C 1327 (2001). Standard test method for Vickers indentation hardness of advanced ceramics. in: Annual Book of ASTM Standards, vol. 15.01, American Society for Testing and Materials, West Conshohocken, PA, USA.

- ASTM F 1873-98 (1998). Standard specification for high-purity dense yttria tetragonal zirconium oxide polycrystal (Y-TZP) for surgical implant applications. p: 1349-1351.
- ASTM F 603-00 (2000). Standard specification for high-purity aluminium oxide for medical application, p: 103-105.
- Atsu, S. S., Kilicarslan, M. A., Kucukesmen, H. C., & Aka, P. A. (2006). Effect of zirconium-oxide ceramic surface treatments on the bond strength to adhesive resin. *J Prosthet Dent*, 95: 430-436.
- Ausiello, P., Apicellab, A., Davidsonc, C. L., & Rengo, S. (2001). 3D-finite element analyses of cusp movements in a human upper premolar, restored with adhesive resin-based composites. *J Biomech*, 34: 1269–1277.
- Aykul, H., Toparli, M., & Dalkiz, M. (2002). A calculation of stress distribution in metal-porcelain crowns by using three-dimensional finite element method. *J Oral Rehabil*, 29: 381-386.
- Babu, P. J., Alla, R. K., Alluri, V. R., Datla, S. R., & Konakanchi, A. (2015). Dental ceramics: Part I – An overview of composition, structure and properties. *Am J Mater Eng Techn*, 3: 13-18.
- Bagambisa, F. B., Kappert, H. F., & Schilli, W. (1994). Interfacial reactions of osteoblasts to dental and implant materials. *J Oral Maxillofac Surg*, 52: 52-56.
- Bamba, N., Choa, Y. H., Sekino, T., & Niihara, K. (2003). Mechanical properties and microstructure for 3 mol% yttria doped zirconia/silicon carbide nano-composites. *J Eur Ceram Soc*, 23: 773–780.
- Basso, G. R., Moraes, R. R., Borba, M., Griggs, J. A., & Della Bona, A. (2015). Flexural strength and reliability of monolithic and trilayer ceramic structures obtained by the CAD-on technique. *Dent Mater*, 31: 1453-1459.
- Bayne, S. C. (2005). Dental biomaterials: Where are we and where are we going?. *J Dent Edu*, 69: 571-585.
- Becher, P. F., Alexander, K. B., & Warmick, W. (1993). Influence of ZrO₂ grain size and content on the transformation response in the Al₂O₃- ZrO₂ (12% mol CeO₂) system. *J Am Ceram Soc*, 76: 657-663.
- Benzaid, R., Chevalier, J., Saadaoui, M., Fantozzi, G., Nawa, M., Antonio Diaz, L., & Ramon Torrecillas, R. (2008). Fracture toughness, strength and slow crack growth in a ceria stabilized zirconia–alumina nanocomposite for medical applications. *Biomaterials*, 29: 3636–3641.
- Best, S. M., Porter, A. E., Thian, E. S., & Huang, J. (2008). Bioceramics: Past, present and for the future. *J Eur Ceram Soc*, 28: 1319–1327.
- Beuer, F., Schweiger, J., Eichberger, M., Kappert, H. F., Gernet, W., & Edelhoff, D. (2009). High-strength CAD/CAM-fabricated veneering material sintered to zirconia copings — A new fabrication mode for all-ceramic restorations. *Dent Mater*, 25: 121-128.

- Bindl, A., & Mormann, W. H. (2002). An up to 5-year clinical evaluation of posterior in-ceram CAD/CAM core crowns. *Int J Prosthodont*, 15: 451–456.
- Blatz, M. B., Sadan, A., & Kern, M. (2003). Resin–ceramic bonding: a review of the literature. *J Prosthet Dent*, 89: 268–274.
- Blatz, M. B., Richter, C., Sadan, A., & Chiche, G. J. (2004). Resin bond to dental ceramics, part ii: high-strength ceramics. *J Esthetic Rest Dent*, 16: 324–328.
- Borges, G. A., Sophr, A. M., de Goes, M. F., Sobrinho, L. C., & Chan, D. C. (2003). Effect of etching and airborne particle abrasion on the microstructure of different dental ceramics. *J Prosthet Dent*, 89: 479-488.
- Bottino, M. A., Valandro, L. F., Scotti, R., & Buso, L. (2005). Effect of surface treatments on the resin bond to zirconium-based ceramic. *Int J Prosthodont*, 18: 60–65.
- Brackett, M. G., Lockwood, P. E., Messer, R. L., Lewis, J. B., Bouillaguet, S., & Wataha, J. C. (2008). In vitro cytotoxic response to lithium disilicate dental ceramics. *Dent Mater*, 24: 450-456.
- Bravo-Leon, A., Morikawa, Y., Kawahara, M., & Mayo, M. J. (2002). Fracture toughness of nanocrystalline tetragonal zirconia with low yttria content. *Acta Mater*, 50: 4555–4562.
- Burger, W., Richter, H. G., Piconi, C., Vatteroni, R., Cittadini, A., & Boccalari M. (1997). New Y-TZP powders for medical grade zirconia. *J Mater Sci Mater Med*, 8: 113–118.
- Burak, T., Jason, A. G., John, J. M. J., & Jia-Hua, Y. (2008). Analysis of subcritical crack growth in dental ceramics using fracture mechanics and fractography. *Dent Mater*, 24: 700–707.
- Burke, F. J. (1996). Fracture resistance of teeth restored with dentin-bonded crowns: effect of increased tooth preparation. *Quint Int*, 27: 115-121.
- Burke, F. J., Fleming, G. J., Nathanson, D., & Marquis, P. M. (2002). Are adhesive technologies needed to support ceramics? An assessment of the current evidence. *J Adhes Dent*, 4: 7-22.
- Burstome, C. J., & Pryputniewicz, R. J. (1980). Holographic determination of centers of rotation produced by orthodontic forces. *Am J Orthod*, 77: 396-409.
- Cales, B., & Stefani, Y. (1994). Mechanical properties and surface analysis of retrieved zirconia femoral hip joint heads after an implantation time of two to three years. *J Mater*, 5: 376–380.
- Campbell, S. D. (1989). A comparative strength study of metal ceramic and all-ceramic esthetic materials: modulus of rupture. *J Prosthet Dent*, 62: 476-479.
- Canneto, J. J., Cattani-Lorente, M., Durual, S., Wiskott, A. H., & Scherrer, S. S. (2016). Grinding damage assessment on four high-strength ceramics. *Dent Mater*, 32: 171-182.

- Carinci, F., Pezzetti, F., Volinia, S., Francioso, F., Arcelli, D., Farina, E., & Piattelli, A. (2004). Zirconium oxide: analysis of MG63 osteoblast-like cell response by means of a microarray technology. *Biomater*, 25: 215–228.
- Casellas, D., Ràfols, I., Llanes, L., & Anglada, M. (1999). Fracture toughness of zirconia-alumina composites. *Int J Refractory Metals & Hard Materials*, 17: 11-20.
- Cataldi, A., Zara, S., Rapino, M., Patruno, A., & Di Giacomo, V. (2013). Human gingival fibroblasts stress response to HEMA: A role for protein kinase C α . *J Biomed Mater Res A*, 101: 378-384.
- Catelas, I., Petit, A., Zukor, D. J., Marchand, R., Yahia, L., & Huk, O. L. (1999). Induction of macrophage apoptosis by ceramic and polyethylene particles in vitro. *Biomaterials*, 20: 625–630.
- Cattani-Lorente, M., Durual, S., Amez-Droz, M., Wiskott, H. W., & Scherrer, S. S. (2016). Hydrothermal degradation of a 3Y-TZP translucent dental ceramic: A comparison of numerical predictions with experimental data after 2 years of aging. *Dent Mater*, 32: 394-402.
- Cattani-Lorente, M., Scherrer, S. S., Ammann, P., Jobin, M., & Wiskott, H. W. (2011). Low temperature degradation of a Y-TZP dental ceramic. *Acta Biomater*, 7: 858-865.
- Cavalcanti, A. N., Foxton, R. M., Watson, T. F., Oliveira, M. T., Giannini, M., & Marchi, G. M. (2009). Y-TZP ceramics: key concepts for clinical application. *Oper Dent*, 34: 344-351.
- Celli, A., Tucci, A., Esposito, L., & Palmonari, C. (2003). Fractal analysis of cracks in alumina-zirconia composites. *J Eur Ceram Soc*, 23: 469-479.
- Cesaria, F., Esposito, L., Furgiuele, F. M., Maletta, C., & Tucci, A. (2006). Fracture toughness of alumina zirconia composites. *Ceram Int*, 32: 249–255.
- Chai, H., & Lawn, B. R. (2002). Cracking in brittle laminates from concentrated loads. *Acta Mater*, 50: 2613–2625.
- Chai, H., Lawn, B. R., & Wuttiphan, S. (1999). Fracture modes in brittle coatings with large interlayer modulus mismatch. *J Mater Res*, 14: 3805–3817.
- Chai, J., Tkahashi, Y., Sulaiman, F., Chong, K., & Lautenschlager, E. P. (2000). Probability of fracture of all-ceramic crowns. *Int J Prosthodont*, 13: 420–424.
- Chaiyabutr, Y., McGowan, S., Phillips, K. M., Kois, J. C., & Giordano, R. L. (2008). The effect of hydrofluoric acid surface treatment and bond strength of a zirconia veneering ceramic. *J Prosthet Dent*, 100: 194-202.
- Chantikul, P., Anstis, G. R., Lawn, B. R., & Marshall, D. B. (1981). A critical evaluation of indentation techniques for measuring fracture toughness: II. Strength method. *J Am Ceram Soc*, 64: 539-543.
- Chartier, T., & Rouxel, T. (1997). Tape-cast alumina-zirconia laminates: processing and mechanical properties. *J Eur Ceram Soc*, 15: 299–308.

- Chen, D. Y., Jordan, E. H., Gell, M., & Ma, X. Q. (2008). Dense alumina-zirconia coating using the solution precursor plasma spray process. *J Am Ceram Soc*, 91: 359-365.
- Chevalier, J. (2006). What future for zirconia as a biomaterial? *Biomater*, 27: 534-543.
- Chevalier, J., Cales, B., & Drouin, J. M. (1999). Low-temperature aging of Y-TZP ceramics. *J Am Ceram Soc*, 82: 2150-2154.
- Chevalier, J., & Gremillard, L. (2009). Ceramics for medical applications: A picture for the next 20 years. *J Eur Ceram Soc*, 29: 1245-1255.
- Chevalier, J., Deville, S., Munch, E., Jullian, R., & Lair, F. (2004). Critical effect of cubic phase on aging in 3 mol% yttria-stabilized zirconia Ceramics for hip replacement prosthesis. *J Biomater*, 25: 5539-5545.
- Choa, Y. H., Nakahira, A., & Nihara, K. (1998). Effect of second phase dispersions on microstructure and mechanical properties in MgO/SiC nanocomposites. *Sci Eng Compos Mater*, 7: 249-258.
- Choi, S. R., & Bansal, N. P. (2005). Mechanical behavior of zirconia/alumina composites. *Ceram Int*, 31: 39-46.
- Choi, E-K., Han, J-S., Yang, J-H., Lee, J-B., & Kim, S-H. (2009). Shear bond strength of veneering porcelain to zirconia and metal cores. *J Adv Prosthodont*, 1: 129-135.
- Claussen, N. J. (1976). Fracture toughness of Al₂O₃ with an unstable ZrO₂ dispersed second phase. *J Am Ceram Soc*, 61: 49-51.
- Cobb, C. M., White, C. L., Gillahan, D. R., & Tira, D. E. (1988). In vitro compatibility of air-fired opaque porcelain with human gingival fibroblasts. *J Prosthet Dent*, 59: 187-194.
- Coelho, P. G., Bonfante, E. A., Silva, N. R., Rekow, E. D., & Thompson, V. P. (2009a). Laboratory simulation of Y-TZP all-ceramic crown clinical failures. *J Dent Res*, 88: 382-386.
- Coelho, P. G., Silva, N. R., Thompson, V. P., Rekow, D., & Zhang, G. (2009b). Effect of proximal wall height on all-ceramic crown core stress distribution: a finite element analysis study. *Int J Prosthodont*, 22: 78-86.
- Conrad, H. J., Seong, W. J., & Pseun, I. J. (2007). Current ceramic materials and systems with clinical recommendations: A systematic review. *J Prosthet Dent*, 98: 389-404.
- Cotton, B. A., & Mayo, M. J. (1996). Fracture toughness of nanocrystalline ZrO₂-3mol% Y₂O₃ determined by Vickers indentation. *Scripta Mater*, 34: 809-814.
- Covacci, V., Bruzzese, N., Maccauro, G., Andreassi, C., Ricci, G. A., Piconi, C., Marmo, E., Burger, W., & Cittadini, A. (1999). In vitro evaluation of the mutagenic and carcinogenic power of high purity zirconia ceramic. *Biomater*, 20: 371-376.
- Couegnat, G., Fok, S. L., Cooper, J. E., & Qualtrough, A. J. E. (2006). Structural optimization of dental restorations using the principle of adaptive growth. *Dent Mater*, 22: 3-12.

- Curtis, A. R., Wright, A. J., & Fleming, G. J. (2006). The influence of surface modification techniques on the performance of a Y-TZP dental ceramic. *J Dent*, 34: 195-206.
- Cuy, J. L., Mann, A. B., Livi, K. J., Teaford, M. F., & Weihs, T. P. (2002). Nanoindentation mapping of the mechanical properties of human molar tooth enamel. *Arch Oral Biol*, 47: 281-291.
- Czekanska, E. M. (2011). Assessment of cell proliferation with resazurin-based fluorescent dye. *Methods Mol Biol*, 740: 27-32.
- Daguano, J. K. M. F., Santos, C., Souza, R. C., Balestra, R. M., Strecker, K. & Elias, C. N. (2007). Properties of ZrO₂- Al₂O₃ composite as a function of isothermal holding time. *Int J Refract Met Hard Mater*, 25: 374-379.
- Daou, E. E. (2014). The zirconia ceramic: strengths and weaknesses. *Open Dent J*, 8: 33-42.
- Darendeliler, S., Darendeliler, H., & Kınoglu T. (1992). Analysis of central maxillary incisor by using a three-dimensional finite element method. *J Oral Rehabil*, 19: 371-373.
- De Aza, A. H., Chevalier, J., Fantozzi, G., Schehl, M., & Torrecillas, R. (2002). Crack growth resistance of alumina, zirconia and zirconia toughened alumina ceramics for joint prostheses. *Biomaterials*, 23: 937-945.
- Deany, I. L. (1996). Recent advances in ceramics for dentistry. *Crit Rev Oral Biol Med*, 7: 134-143.
- DeHoff, P. H., Anusavice, K. J., & Hojjatie, B. (1998). Thermal incompatibility analysis of metal-ceramic systems based on flexural displacement data. *J Biomed Mater Res*, 41: 614-623.
- De Jager, N., de Kler, M., & van Zel, J. (2006). The influence of different core material on the FEA-determined stress distribution in dental crowns. *Dent Mater*, 22: 234-242.
- Dejak, B., Młotkowski, A., & Langot, C. (2012). Three-dimensional finite element analysis of molars with thin-walled prosthetic crowns made of various materials. *Dent Mater*, 28: 433-441.
- De Kler, M., De Jager, N., Meegdes, M., & Van Der Zel, J. M. (2007). Influence of thermal expansion mismatch and fatigue loading on phase changes in porcelain veneered Y-TZP zirconia discs. *J Oral Rehabil*, 34: 841-847.
- Della Bona, A. (2005). Characterization ceramics and the interfacial adhesion to resin: I- The relationship of microstructure, composition, properties and fractography. *Appl Oral Sci*, 13: 1-9.
- Della Bona, A., & Anusavice, K. J. (2002). Microstructure, composition, and etching topography of dental ceramics. *Int J Prosthodont*, 15: 159-167.

- Della Bona, A., Donassollo, T. A., Demarco, F. F., Barrett, A. A., & Mecholsky, J. J. (2007). Characterization and surface treatment effects on topography of a glass-infiltrated alumina/zirconia-reinforced ceramic. *Dent Mater*, 23: 769–775.
- Della Bona, A., Mecholsky, Jr. G., Barrett, A. A., & Griggs, J. A. (2008). Characterization of glass-infiltrated alumina-based ceramics. *Dent Mater*, 24: 1568–1574.
- Della Bona, I., Borba, M., Benetti, P., Duan, Y., & Griggs, J. A. (2013). Three-dimensional finite element modelling of all-ceramic restorations based on micro-CT. *J Dent*, 41: 412-419.
- DeLong, R., & Douglas, W. H. (1983). Development of an artificial oral environment for the testing of dental restoratives: Bi-axial force and movement control. *J Dent Res*, 62: 32-36.
- Deng, Y., Lawn, B. R., & Lloyd, I. K. (2002a). Characterization of damage modes in dental ceramic bilayer structures. *J Biomed Mater Res*, 63: 137–145.
- Deng, Y., Lawn, B. R., & Lloyd, I. K. (2002b). Damage characterization of brittle materials in ceramic-based crown-like layer structures. *Key Eng Mater*, 224–226: 453–458.
- Denisova, L. A., Maev, R. G., Poyurovskaya, I. Y., Grineva, T. V., Denisov, A. F., Maeva, E. Y., & Bakulin, E. Y. (2004). The use of acoustic microscopy to study the mechanical properties of glass ionomer cement. *Dent Mater*, 20: 358-363.
- Denry I. (2013). How and when does fabrication damage adversely affect the clinical performance of ceramic restorations? *Dent Mater*, 29: 85-96.
- Denry, I., & Kelly, J. R. (2008). State of the art of zirconia for dental applications. *Dent Mater*, 24: 299-307.
- Derand, P., & Derand T. (2000). Bond strength of luting cements to zirconium oxide ceramics. *Int J Prosthodont*, 13: 131-135.
- Derand, T. (1974). Effect of variation of the shape of the core on stresses in loaded model of a porcelain crown. *Odontol Revy*, 25: 11-26.
- Derand, T., Molin, M., & Kvam, K. (2005). Bond strength of composite luting cement to zirconia ceramic surfaces *Dental Mater*, 21: 1158-1162.
- Deville, S., Chevalier, J., & Gremillard, L. (2006). Influence of surface finish and residual stresses on the ageing sensitivity of biomedical grade zirconia. *Biomaterials*, 27: 2186–2192.
- Diego, A. A., dos Santos, C., Landim, K. T., & Elias, C. N. (2007). Characterization of ceramic powders used in the in ceram systems to fixed dental prosthesis. *Mater Res*, 10: 47-51.
- Di Nisio, C., Zara, S., Cataldi, A., & Di Giacomo V. (2013). 2-Hydroxyethyl methacrylate inflammatory effects in human gingival fibroblasts. *Int Endod J*, 46: 466-476.
- Dion, I., Bordenave, L., & Levebre, F. (1994). Physico-chemistry and cytotoxicity of ceramics. *J Mater Sci Mater Med*, 5:18–24.

- Dittmer, M. P., Kohorst, P., Borchers, L., & Stiesch-Scholz, M. (2009). Finite element analysis of a four-unit all-ceramic fixed partial denture. *Acta Biomater*; 5: 1349-1355.
- Doyle, M. G., Goodacre, C. J., Munoz, C. A., & Andres, C. J. (1990). The effect of tooth preparation design on the breaking strength of Dicor crowns. *Int J Prosthodont*, 3: 327-340.
- Drummond, J. L. (2003). Ceramic behavior under different environmental and loading conditions. In: Eliades, G., editor. *Dental materials in vivo: aging and related phenomena*. Chicago; London: Quintessence Pub. Co.; p.35-45.
- Duan, Y., & Griggs J. A. (2015). Effect of elasticity on stress distribution in CAD/CAM dental crowns: Glass ceramic vs. polymer-matrix composite. *J Dent*, 43: 742-749.
- Dudnik, E. V., Shevchenko, A. V., Ruban, A. K., Red'ko, V. P., & Lopato, L. M. (2011). Microstructural design of ZrO_2 - Y_2O_3 - CeO_2 - Al_2O_3 materials. *Powder Metall Metal Ceram*, 49: 528-536.
- Dündar, M., Ozcan, M., Cömlekoglu, E., Güngör, M. A., & Artunc, C. (2005). Bond strengths of veneering ceramics to reinforced ceramic core materials. *Int J Prosthodont*, 18:71-72.
- Dündar, M., Ozcan, M., Gökce, B., Cömlekoglu, E., Leite, F., & Valandro, L. F. (2007). Comparison of two bond strength testing methodologies for bilayered all-ceramics. *Dent Mater*, 23: 630-636.
- Eichler, A. (2001). Tetragonal Y-doped zirconia: structure and ion conductivity. *Phys Rev B*, 64: 174103-8.
- Elshahawy, W., Ajlouni, R., James, W., Abdellatif, H., & Watanabe, I. (2013). Elemental ion release from fixed restorative materials into patient saliva. *J Oral Rehabil*, 40: 381-388.
- Elshahawy, W., Watanabe, I., & Koike, M. (2009a). Elemental ion release from four different fixed prosthodontic materials. *Dent Mater*, 25: 976-981.
- Elshahawy, W., Watanabe, I., & Kramer, P. (2009b). In vitro cytotoxicity evaluation of elemental ions released from different prosthodontic materials. *Dent Mater*, 25: 1551-1555.
- EL-Wazery, M. S., & EL-Desouky, A. R. (2015). A review on functionally graded ceramic-metal materials. *Mater Environ Sci*, 6: 1369-1376.
- Ender, A., Bienz, S., Mörmann, W., Mehl, A., Attin, T., & Stawarczyk, B. (2016). Marginal adaptation, fracture load and macroscopic failure mode of adhesively luted PMMA-based CAD/CAM inlays. *Dent Mater*, 32: e22-e29.
- Er, O., Yaman, S. D., & Hasan, M. (2007). Finite element analysis of the effects of thermal obturation in maxillary canine teeth. *Oral Surg Oral Med Oral Pathol Oral Radiol Endod*, 104: 277-286.

- Ernst, C. P., Aksoy, E., Stender, E., & Willershausen, B. (2009). Influence of different luting concepts on long term retentive strength of zirconia crowns. *Am J Dent*, 22: 122-128.
- Ernst, C. P., Cohnen, U., Stender, E., & Willershausen, B. (2005). In vitro retentive strength of zirconium oxide ceramic crowns using different luting agents. *J Prosthet Dent*, 93: 551-558.
- Eskitascioglu, G., Usumez, A., Sevimay, S., Soykan, E., & Unsal, E. (2004). The influence of occlusal loading location on stresses transferred to implant-supported prostheses and supporting bone: A three-dimensional finite element study. *J Prosthet Dent*, 91: 144-150.
- Evans, A. G. (1974). Slow crack growth in brittle materials under dynamic loading conditions. *Int J Fract*, 10: 214-222.
- Evans, A. G. (1990). Perspectives on the development of high-toughness ceramics. *J Am Ceram Soc*, 73: 187-206.
- Fabris, S., Paxton, A. T., & Finnis, M. W. (2002). A stabilization mechanism of zirconia based on oxygen vacancies only. *Acta Mater*, 50: 5171-8.
- Fantozzi, G., & Orange, G. (1986). Thermomechanical properties of zirconia toughened alumina materials, In: eds. Moya, J.S.; De Aza, S. editors, Processing of advanced ceramics, Soc. Esp. Ceram. Vidr. Arganda Del Rey Madrid, Spain:187-215.
- Farah, J. W., Craig, R. G., & Meroueh, K. A. (1989). Finite element analysis of three- and four-unit bridges. *J Oral Rehabil*, 16: 603-611.
- Feng, X., Chen, A., Zhang, Y., Wang, J., Shao, L., & Wei, L. (2015). Application of dental nanomaterials: potential toxicity to the central nervous system. *Int J Nanomedicine*, 10: 3547-3565.
- Fennis, W. M., Kuijs, R. H., Barink, M., Kreulen, C. M., Verdonschot, N., & Creugers, N. H. (2005). Can internal stresses explain the fracture resistance of cusp-replacing composite restorations? *Eur J Oral Sci*, 113: 443-448.
- Ferraris, M., Verne, E., Appendino, P., Moisescu, C., Krajewski, A., Ravaglioli, A. & Piancastelli, A. (2000). Coatings on zirconia for medical applications. *Biomaterials*, 21: 765-773.
- Fields, R. D., & Lancaster, M. V. (1993). Dual-attribute continuous monitoring of cell proliferation/cytotoxicity. *Am Biotechnol Lab*, 11: 48-50.
- Filser, F., Kocher, P., & Gauckler, L. J. (2003). Net-shaping of ceramic components by direct ceramic machining. *Assembly Autom*, 23: 382-390.
- Fischer, H., Niedhart, C., Kaltenborn, N., Prange, A., Marx, R., Niethard, F. U., & Telle, R. (2005). Bioactivation of inert alumina ceramics by hydroxylation. *Biomaterials*, 26: 6151-6157.
- Fischer, H., Weber, M., & Marx, R. (2003). Lifetime prediction of all-ceramic bridges by computational methods. *J Dent Res*, 82: 238-242.

- Fischer, J., Grohmann, P., & Stawarczyk, B. (2008). Effect of zirconia surface treatments on the shear strength of zirconia/veneering ceramic composites. *Dent Mater J*, 27: 448-454.
- Fischer, J., Stawarczyk, B., & Haemmerle, C. H. F. (2010). Shear bond strength between veneering ceramics and ceria-stabilized zirconia/alumina. *J Prosthet Dent*, 103: 267-274.
- Frank, K., & Rainer, G. (2012). Alumina toughened zirconia from yttria coated powders. *J Eur Ceram Soc*, 15: 3911-3918.
- Frohlich, E., & Roblegg, E. (2012). Models for oral uptake of nanoparticles in consumer products. *Toxicology*, 291: 10-17.
- Galoppini, E. (2004). Linkers for anchoring sensitizers to semiconductor nanoparticles. *Coord Chem Rev*, 248: 1283-1297.
- García, D. E., & Hotza, D. (2012). Effect of the particulate size on mechanical properties of alumina-zirconia composites. *Mater Lett*, 82: 88-90.
- Garive, R., C., Hannink, R., H., & Pascoe, R., T. (1975). Ceramic steel?. *Nature*, 258: 703-704.
- Garvie, R. C., & Nicholson, P. S. (1972). Phase analysis in zirconia systems. *J Am Ceram Soc*, 55: 303-305.
- Gatti, A., & Knowles, J. (2002). Biocompatibility and biological tests, In: *Integrated Biomaterials Science*, R. Barbucci, 793-813, Kluwer Academic/Plenum Publishers, ISBN 0-306-46678-3, New York, USA.
- Geramy, A., & Sharafoddin, F. (2003). Abfraction: 3D analysis by means of the finite element methods. *Quintessence Int*, 34: 526-533.
- Geng, J. P., Tan, K. B., & Liu, G. R. (2001). Application of finite element analysis in implant dentistry: a review of the literature. *J Prosthet Dent*, 85: 585-598.
- Ghosh, S., Teweldebrhan, D., Morales, J., Garay, J., & Balandin, A. (2009). Thermal properties of the optically transparent pore-free nanostructured yttria-stabilized zirconia. *J Appl Phy*, 106: 113504-113507.
- Gibbs, C. H., Anusavice, K. J., Young, H. M., Jones, J. S., Esquivel-Upshaw, J. F. (2002). Maximum clenching force of patients with moderate loss of posterior tooth support: a pilot study. *J Prosthet Dent*, 88: 498-502.
- Giordano, R. A. (2002). CAD/CAM: overview of machines and materials. *J Mass Dent Soc*, 51: 12-15.
- Goodacre, C. J., Bernal, G., Rungcharassaeng, K., & Kan, J. Y. (2003). Clinical complications in fixed prosthodontics. *J Prosthet Dent*, 90: 31-41.
- Gregori, G., Burger, W., & Sergio, V. (1999). Piezo-spectroscopic analysis of the residual stress in zirconia-toughened alumina ceramics: the influence of the tetragonal-to-monoclinic transformation. *Mater Sci Eng A*, 271: 401-406.

- Gremillard, L., Chevalier, J., Epicier, T., Deville, S., & Fantozzi, G. (2004). Modeling the aging kinetics of zirconia. *J Eur Ceram Soc*, 24: 3483–3489.
- Grenade, C., De Pauw-Gillet, M. C., Gailly, P., Vanheusden, A., & Mainjot, A. (2016). Biocompatibility of polymer-infiltrated-ceramic-network (PICN) materials with human gingival fibroblasts (HGFs). *Dent Mater*, 32: 1152-1164.
- Griggs, J. A. (2007). Recent advances in materials for all-ceramic restorations. *Dent Clin North Am*, 51: 713-727.
- Guazzato, M., Quach, L., Albakry, M., & Swain, M. V. (2005). Influence of surface and heat treatments on the flexural strength of Y-TZP dental ceramic. *J Dent*, 33: 9-18.
- Guazzato, M., Albakry, M., Ringer, S. P., & Swain, M. V. (2004a). Strength, fracture toughness and microstructure of a selection of all-ceramic materials. Part I. Pressable and alumina glass-infiltrated ceramics. *Dent Mater*, 20: 441-448.
- Guazzato, M., Albakry, M., Ringer, S. P., & Swain, M. V. (2004b). Strength, fracture toughness and microstructure of a selection of all-ceramic materials. Part II. Zirconia-based dental ceramics. *Dent Mater*, 20: 449-456.
- Guazzato, M., Proos, K., Sara, G., & Swain, M. V. (2004c). Strength, reliability, and mode of fracture of bilayered porcelain/core ceramics. *Int J Prosthodont*, 17: 142-149.
- Guess, P. C., Kulis, A., Witkowski, S., Wolkewitz, M., Zhang, Y., & Strub, J. R. (2008). Shear bond strengths between different zirconia cores and veneering ceramics and their susceptibility to thermocycling. *Dent Mater*, 24: 1556-1567.
- Gupta, T. K., Lange, F. F., & Bechtold, J. H. (1978). Effect of stress induced phase transformation on properties of polycrystalline zirconia containing metastable tetragonal phase. *J Mater Sci*, 13: 1464-1470.
- Gutknecht, D., Chevalier, J., Garnier, V., & Fantozzi, G. (2007). Key role of processing to avoid low temperature ageing in alumina zirconia composites for orthopedic application. *J Eur Ceram Soc*, 27: 1547–1552.
- Gutwein, L. G., & Webster, T. J. (2004). Increased viable osteoblast cell density in the presence of nanophase compared to conventional alumina and titania particles. *Biomaterials*, 25: 4175–4183.
- Ha, S. R., Kim, S. H., Han, J. S., Yoo, S. H., Jeong, S. C., Lee, J. B., & Yeo, I. S. (2013). The influence of various core designs on stress distribution in the veneered zirconia crown: a finite element analysis study. *J Adv Prosthodont*, 5: 187–197.
- Ha, S. R., Kim, S. H., Lee, J. B., Han, J. S., Yeo, I. S., Yoo, S. H., & Kim, H. K. (2016). Biomechanical three-dimensional finite element analysis of monolithic zirconia crown with different cement thickness. *Ceram Int*, 42: 14928–14936.
- Haijiang, Y., Yihong, G., Julin, W., & Kaiming, L. (1999). The preparation of laminated ceramic composites by sedimentation and sieving. *J Mat Sci*, 34: 2855–2857.

- Hamza, T. A., Attia, M. A., El-Hossary, M. M., Mosleh, I. E., Shokry, T. E., & Wee, A. G. (2016). Flexural strength of small connector designs of zirconia-based partial fixed dental prostheses. *J Prosthet Dent*, 115: 224-229.
- Hankinson, J. A., & Cappetta, E. G. (1994). Five-year clinical experience with a leucite-reinforced porcelain crown system. *Int J Periodont Restor Dent*, 14: 138–153.
- Hanks, C. T., Wataha, J. C., & Sun, Z. (1996). In vitro models of biocompatibility: A review. *Dent Mater*, 12: 186-196.
- Hannink, R. H. J., Howard, C. J., Kisi, E. H., & Swain, M. V. (1994). Relationship between fracture toughness and phase assemblage in Mg-PSZ. *J Am Ceram Soc*, 77: 571–579.
- Hannink, R. H. J., Kelly, P. M., & Muddle, B. C. (2000). Transformation toughening in zirconia-containing ceramics. *J Am Ceram Soc*, 83: 461–487.
- Hansen, S. (2000). Preparations for Cerec 3: Where are the limits. *Int J Comput Dent*, 3: 197–205.
- Harada, K., Shinya, A., Gomi, H., Hatano, Y., Shinya, A., & Raigrodski, A. J. (2016). Effect of accelerated aging on the fracture toughness of zirconias. *J Prosthet Dent*, 115: 215-223.
- Hasegawa, A., Shinya, A., Nakasone, Y., Lassila, L. V. J., Vallittu, P. K., & Shinya, A. (2010). Development of 3D CAD/FEM analysis system for natural teeth and jaw bone constructed from x-ray CT images. *Int J Biomat*, 2010: 1-7.
- Hbaieb, K., McMeeking, R. M., & Lange, F. F. (2007). Crack bifurcation in laminar ceramics having large compressive stress. *Int J Solids Struct*, 44: 3328–3343.
- He, L. F., Bao, Y. W., & Zhou, Y. C. (2009). Zirconium aluminum carbides: New precursors for synthesizing $ZrO_2-Al_2O_3$ composites. *J Am Ceram Soc*, 89: 2751-2758.
- Hedia, H. S., & Mahmoud, N. A. (2004). Design optimization of functionally graded dental implant. *Biomed Mater Eng*, 14: 133-143.
- Hench, L. L. (1991). Bioceramics: from concept to clinic. *J Am Ceram Soc*, 74: 1487-1510.
- Hench, L. L. (1998). Bioceramics. *J Am Ceram Soc*, 8: 1705-1728.
- Hench, L. L., & Wilson, J. (1993). An Introduction to Bioceramics. Advanced Series in Ceramics-Vol.1, World Scientific Publishing.
- Hensten-Pettersen, A., & Helgeland, K. (1981). Sensitivity of different human cell line in the biologic evaluation of dental resin-based restorative materials. *Scand J Dent Res*, 89: 102–107.
- Hermann, I., Bhowmick, S., Zhang, Y., & Lawn, B. R. (2006). Competing fracture modes in brittle materials subject to concentrated cyclic loading in liquid environments: Trilayer structures. *J Mater Res*, 21: 512–521

- Heuer, A. H. (1987). Transformation toughening in ZrO₂-containing ceramics. *J Am Ceram Soc*, 70: 689–698.
- Heuer, A. H., Claussen, N., Kriven, W.M., & Ruhle, M. (1982). Stability of tetragonal ZrO₂ particles in ceramic matrices. *J Am Ceram Soc*, 65: 642–650.
- Heuer, A. H., Lange, F. F., Swain, M. V., & Evans, A. G. (1986). Transformation toughening: an overview. *J Am Ceram Soc*, 69: i–iv.
- Hillam, D. G. (1973). Stress in the periodontal ligament. *J Periodont*, 8: 51:56.
- Ho, G. W., & Matinlinna, J. P. (2011). Insights on ceramics as dental materials. Part I: Ceramic material types in dentistry. *Silicon*, 3: 109–115.
- Hojjat, B., & Anusavice, K. J. (1990). Three-dimensional finite element analysis of glass ceramic dental crowns. *J Biomech*, 23: 1157–1166.
- Hojjat, B., & Anusavice, K. J. (1993). Effects of initial temperature and tempering medium on thermal tempering of dental porcelains. *J Dent Res*, 72: 566–571.
- Holland, W., Schweiger, M., Frank, M., & Rheinberger, V. (2000). A comparison of the microstructure and properties of the IPS Empress 2 and the IPS Empress glass-ceramics. *J Biomed Mater Res*, 53: 297–303.
- Hondo, T., Kato, Z., Yasuda, K., Wakai, F., & Tanaka, S. (2016). Coarse pore evolution in dry-pressed alumina ceramics during sintering. *Adv Powd Tech*, 27:1006–1012.
- Hori, S., Yoshimura, M., & Somiya, S. (1986). Strength-toughness relation in sintered and isostatically hot-pressed ZrO₂- toughened Al₂O₃. *J Am Ceram Soc*, 69: 169–172.
- Hoshida, T., Hayashi, K., Saito, T., Katsuki, K., & Inoue, T. (1996). Mechanical properties of borosilicate glass coated with alumina by sputtering process. *Mat Sci Res Int*, 2: 33–38.
- Hsueh, C. H., Thompson, G. A., Jadaan, O. M., Wereszczak, A. A., & Becher, P. F. (2008). Analyses of layer-thickness effects in bilayered dental ceramics subjected to thermal stresses and ring-on-ring tests. *Dent Mater*; 24: 9–17.
- Huang, M., Niu, X., & Soboyejo, W. O. (2007a). Creep induced rate effects on radial cracks in multilayered structure. *J Mater Sci: Mater Med*, 18: 65–69.
- Huang, M., Rahbar, N., Wang, R., Thompson, V., Rekow, D., & Soboyejo, W. O. (2007b). Bioinspired design of dental multilayers. *Mater Sci Eng A*, 464: 315–320.
- Huang, X. W., Wang, S. W., & Huang, X. X. (2003). Microstructure and mechanical properties of ZTA fabricated by liquid phase sintering. *Ceram Int*, 29: 765–769.
- Hvizdos, P., Jonsson, D., Anglada, M., Anne, G., & Van Der Biest, O. (2007). Mechanical properties and thermal shock behaviour of an alumina/zirconia functionally graded material prepared by electrophoretic deposition. *J Eur Ceram Soc*, 27: 1365–1371.
- Imanishi, A., Nakamura, T., Ohyama, T., & Nakamura, T. (2003). 3-D Finite element analysis of all-ceramic posterior crowns. *J Oral Rehabil*, 30: 818–822.

- Inokoshi, M., De Munck, J., Minakuchi, S., & Van Meerbeek, B. (2014). Meta-analysis of bonding effectiveness to zirconia ceramics. *J Dent Res*, 93: 329-334.
- Ironside, J. G., & Swain, M. V. (1998). Ceramics in dental restorations-A review and critical issues. *J Austral Ceram Soc*, 34: 78–91.
- International Organization for Standardization, BS ISO-6872 (E) TC 106/SC 2. (2008). Dentistry-Ceramic materials. British Standard. Third edition.
- International Organization for Standardization (ISO-9693) (1999). Metal-ceramic bond characterization (Schwickerath crack initiation test). Geneva, Switzerland.
- International Organization for Standardization, ISO-10993-5 (2009). Biological Evaluation of Medical Device. Part 5. Tests for in vitro cytotoxicity. Geneva. Switzerland.
- Isgrò, G., Kleverlaan, C. J., Wang, H., & Feilzer, A. J. (2004). Thermal dimensional behavior of dental ceramics. *J Biomat*, 25: 2447–2453.
- Isgrò, G., Pallav, P., van der Zel J. M., & Feilzer, A. J. (2003). The influence of the veneering porcelain and different surface treatments on the biaxial flexural strength of a heat-pressed ceramic. *J Prosthet Dent*, 90: 465-473.
- Isgrò, G., Wang, H., Kleverlaan, C. J., & Feilzer, A. J. (2005). The effects of thermal mismatch and fabrication procedures on the deflection of layered all-ceramic discs. *Dent Mater*, 21: 649–655.
- Ivosevic, M., Knight, R., Kalidindi, S. R., Palmese, G. R., & Sutter, J. K. (2005). Solid particle erosion resistance of thermally sprayed functionally graded coatings for polymer matrix composites. *Surface Coat Tech*, 200: 5145-5151.
- Jackson, A. (1988). The mechanical design of nacre. *Proc R Soc Lond*, B234: 415-425.
- Jakovac, M., Zivko-Babic, J., Curkovic, L., & Aurer, A. (2006). Measurement of ion elution from dental ceramics. *J Eur Ceram Soci*, 26: 1695–1700.
- Jalali, S. K., Reza Yarmohammadi, R., & Maghsoudi, F. (2016). Finite element stress analysis of functionally graded dental implant of a premolar tooth. *J Mech Sci Tech*, 30: 4919–4923.
- Javidi, M., Zarei, M., Naghavi, N., Mortazavi, M., & Nejat, A. H. (2014). Zinc oxide nano-particles as sealer in endodontics and its sealing ability. *Contemp Clin Dent*, 5: 20–24.
- Jevnikar, P., Krnel, K., Kocjan, A., Funduk, N., & Kosmac, T. (2010). The effect of nano-structured alumina coating on resin-bond strength to zirconia ceramics. *Dent Mater*, 26: 688-696.
- Jeon, P. D., Turley, P. K., Moon, H. B., & Ting, K. (1999). Analysis of stress in the periodontium of the maxillary first molar with a three-dimensional finite element model. *Am J Orthodont Dentofacial Orthoped*, 115: 267–274.
- Jin, X., Homaei, E., Matinlinna, J.P. & Tsoi, K. H. (2016). A new concept and finite-element study on dental bond strength tests. *Dent Mater*, 32: e238-e250.

- Josset, Y., Oum'Hamed, Z., Zarrinpour, A., Lorenzato, M., Adnet, J. J., & Laurent-Maquin, D. (1999). In vitro reactions of human osteoblasts in culture with zirconia and alumina ceramics. *J Biomed Mater Res*, 47: 481-493.
- Julien, K. C., Buschang, P. H., Throckmorton, G. S., & Dechow, P. C. (1996). Normal masticatory performance in young adults and children. *Arch Oral Biol*, 41: 69-75.
- Jung, Y-G., Peterson, I. M., Kim, D. K., & Lawn, B. R. (2000). Lifetime-limiting strength degradation from contact fatigue in dental ceramics. *J Dent Res*, 79: 722-731.
- Jung, Y-G., Wuttiphan, S., Peterson, I. M., & Lawn, B. R. (1999). Damage modes in dental layer structures. *J Dent Res*, 78: 887-897.
- Kaizer, M. R., Gonçalves, A. P., Soares, P. B., Zhang, Y., Cesar, P. F., Cava, S. S., & Moraes, R. R. (2016). Mono or polycrystalline alumina-modified hybrid ceramics. *Dent Mater*, 32: 450-460.
- Karihaloo, B. L. (1991). Contributions of t-m phase transformation to the toughening of ZTA. *J Am Ceram Soc*, 74: 1703-1706.
- Kasraei, S., Sami, L., Hendi, S., Alikhani, M. Y., Rezaei-Soufi, L., & Khamverdi, Z. (2014). Antibacterial properties of composite resins incorporating silver and zinc oxide nanoparticles on Streptococcus mutans and Lactobacillus. *Restor Dent Endod*, 39: 109-114.
- Kasten, F. H., Felder, S. M., Gettleman, L., & Alchediak, T. (1982). A model culture system with human gingival fibroblast for evaluating the cytotoxicity of dental materials. *In vitro Cellular & Developmental Biology - Plant*, 18: 650-660.
- Katayama, T., Sukenaga, S., Saito, N., Kagata, H., & Nakashima, K. (2011). Fabrication of Al₂O₃-W functionally graded materials by slip casting method. *IOP Conf. Series: Mater Sci Eng*, 18.
- Kellett, B., & Lange, F. F. (1984). Stresses induced by differential sintering in powder compacts. *J Am Ceram Soc*, 67: 369-371.
- Kelly, J. R. (2004). Dental ceramics: current thinking and trends. *Dent Clin North Am*, 48: 513-530.
- Kelly, J. R. (1997). Ceramics in restorative and prosthetic dentistry. *Annu Rev Mater Sci*, 27: 443-468.
- Kelly, J. R., & Denry, I. (2008). Stabilized zirconia as a structural ceramic: an overview. *Dent Mater*, 24: 289-298.
- Kelly, J. R., Giordano, R., Pober, R., & Cima, M. J. (1990). Fracture surface analysis of dental ceramics: clinically failed restorations. *Int J Prosthodont*, 3: 430-440.
- Kelly, J. R., Tesk, J. A., & Sorensen, J. A. (1995). Failure of all-ceramic fixed partial dentures in vitro and in vivo: analysis and modeling. *J Dent Res*, 74: 1253-1258.
- Kern, M., & Wegner, S. M. (1998). Bonding to zirconia ceramic: adhesion methods and their durability. *Dent Mater*, 14: 64-71.

- Khang, D., Liu-Snyder, P., Pareta, R., Lu, J., & Webster, T. J. (2009). Reduced responses of macrophages on nanometer surface features of altered alumina crystalline phases. *Acta Biomater*, 5: 1425-1432.
- Khera, S. C., Goel, V. K., Chen, R. C. S., & Gurusami, S. A. (1988). A three-dimensional finite element mode. *Oper Dent*, 13: 128-137.
- Kibbel, B., & Heuer, A. H. (1986). Exaggerated grain growth in ZrO₂-toughened Al₂O₃. *J Am Ceram Soc*, 69: 231-236.
- Kieback, B., Neubrand, A., & Riedel, H. (2003). Processing techniques for functionally graded materials. *Mater Sci Eng*, A362: 81-105.
- Kilic, K., Bulent Kesim, B., Sumer, Z., Polat, Z., & Kesim, S. (2013). In vitro cytotoxicity of all-ceramic substructural materials after aging. *J Dent Sci*, 8: 231-238.
- Kim, J. H., Miranda, P., Kim, D. K., & Lawn, B. R. (2003). Effect of an adhesive interlayer on the fracture of a brittle coating on a supporting substrate. *J Mater Res*, 18: 222-227.
- Kim, J. H. & Paulino, G. H. (2003). An accurate scheme for mixed-mod fracture analysis of functionally graded materials using the interaction integral and micromechanics models. *Int J Numer Meth Engr*, 58: 1457-1497.
- Kim, S. W. & Khalil, K. A. R. (2006). High-frequency induction heat sintering of mechanically alloyed alumina-Yttria stabilized nano-bioceramics. *J Am Ceram Soc*, 89: 1280-1285.
- Kim, B., Zhang, Y., Pines, M., & Thompson, V. P. (2007a). Fracture of porcelain-veneered structures in fatigue. *J Dent Res*, 86: 142-146.
- Kim, J. W., Bhowmick, S., Chai, H., & Lawn, B. R. (2007b). Role of substrate material in failure of crown-like layer structures. *J Biomed Mater Res B Appl Biomater*, 81: 305-311.
- Koehler, J. S. (1970). Attempt to design a strong solid. *Phys Rev B*, 2: 547-551.
- Kohal, R. J., Bächle, M., Renz, A., & Butz, F. (2016). Evaluation of alumina toughened zirconia implants with a sintered, moderately rough surface: An experiment in the rat. *Dent Mater*, 32: 65-72.
- Kohorst, P., Herzog, T. J., Borchers, L., & Stiesch-Scholz, M. (2007). Load-bearing capacity of all-ceramic posterior four-unit fixed partial dentures with different zirconia frameworks. *Eur J Oral Sci*, 115: 161-166.
- Kokoti, M., Sivropoulou, A., Koidis, P., & Garefis, P. (2001). Comparison of cell proliferation on modified dental ceramics. *J Oral Rehabil*; 28: 880-887.
- Komine, F., Saito, A., Kobayashi, K., Koizuka, M., Koizumi, H., & Matsumura, H. (2010). Effect of cooling rate on shear bond strength of veneering porcelain to a zirconia ceramic material. *J Oral Sci*, 52: 647-652.

- Kosmac, T., Oblak, C., Jevnikar, P., Funduk, N., & Marion, L. (1999). The effect of surface grinding and sandblasting on flexural strength and reliability of Y-TZP zirconia ceramic. *Dent Mater*, 15: 426-433.
- Kosmac, T., Oblak, C., Jevnikar, P., Funduk, N., & Marion, L. (2000). Strength and reliability of surface treated Y-TZP dental ceramics. *J Biomed Mater Res*, 53: 304-313.
- Koyama, T., Nishiyama, A., & Niihara, K. (1993). Effect of a small amount of liquid-forming additives on the microstructure of Al₂O₃ ceramics. *J Mater Sci*, 28: 5953-5956.
- Krell, A. (1995). Load dependence of hardness in sintered submicrometer Al₂O₃-ZrO₂. *J Am Ceram Soc*, 78: 1417-1419.
- Kunes, K., Havrda, J., Hronikova, K., Gregorova, E., & Pabst, W. (2000). Stabilization of Bioceramic suspensions prepared from alumina-containing zirconia powders. *Ceramics*, 44: 1-8.
- Kunzelmann, K. H., & Hickel, R. (1993). Machinability of different dental materials for CAD/CAM systems. *NIST Special Publication*, 847: 479-487.
- Lange, F. F. (1982). Transformation toughening: Part 4 – Fabrication fracture toughness and strength of Al₂O₃- ZrO₂ composites. *J Mat Sci*, 17: 247-254.
- Lange, F. F., & Hirlinger, M. M. (1984). Hindrance of grain growth in Al₂O₃ by ZrO₂ inclusions. *J Am Ceram Soc*, 67: 164-168.
- Lange, F. F., Yamaguchi, T., Davis, B. I., & Morgan, P. E. D. (1988). Effect of ZrO₂ inclusions on the sinterability of Al₂O₃. *J Am Ceram Soc*, 71: 446-448.
- Larsson, C., Vult von Steyern, P., Sunzel, B., & Nilner, K. (2006). All-ceramic two- to five-unit implant-supported reconstructions. A randomized, prospective clinical trial. *Swed Dent J*, 30: 45-53.
- Lawn, B. R., Deng, Y., Lloyd, I. K., Janal, M. N., Rekow, E. D., & Thompson, V. P. (2002a). Materials design of ceramic-based layer structures for crowns. *J Dent Res*, 81: 433-438.
- Lawn, B. R., Deng, Y., Miranda, P., Pajares, A., Chai, H., & Kim, D. K. (2002b). Overview: Damage in brittle layer structures from concentrated loads. *J Mater Res*, 17: 3019-3036.
- Lawson, S. (1995). Environmental degradation of zirconia ceramics. *J Eur Ceram Soc*, 15: 485-502.
- Lazar, R. R., Bottino, M. C., Özcan, M., Valandro, L. F., Amaral, R., Ussui, V., & Bressiani, A. H. A. (2008). Y-TZP ceramic processing from coprecipitated powders: A comparative study with three commercial dental ceramics. *Dent Mater*, 24: 1676-1685.
- Leach, C. A. (1987). Sintering of magnesium partially-stabilized zirconia—behavior of an impurity silicate phase. *Mater Sci Tech*, 3: 321-324.

- Lee, H. E., Lin, C. L., Wang, C. H., Cheng, C. H., & Chang, C. H. (2002). Stresses at the cervical lesion of maxillary premolar—a finite element investigation. *J Dent*, 30: 283-290.
- Li, J., Liu, Y., Hermansson L., & Soremark, R. (1993). Evaluation of biocompatibility of various ceramic powders with human fibroblasts in vitro. *Clin Mater*, 12: 197-201.
- Li, Q., Ichim, I., Loughran, J., Li, W., Swain, M., & Kieser, J. (2006). Numerical simulation of crack formation in all ceramic dental bridge. *Key Eng Mater*, 312: 293-298.
- Li, R. W., Chow, T. W., & Matinlinna, J. P. (2014). Ceramic dental biomaterials and CAD/CAM technology: state of the art. *J Prosthodont Res*, 58: 208-216.
- Li, L. F., & Watanabe, R. (1997). Influence of a small amount of Al₂O₃ addition on the transformation of Y₂O₃-partially stabilized ZrO₂ during annealing. *J Mater Sci*, 32: 1149–1153.
- Li, J., & Watanabe, R. (1998). Phase transformation in Y₂O₃-partially-stabilized ZrO₂ polycrystals of various grain sizes during low-temperature aging in water. *J Am Ceram Soc*, 81: 2687–2691.
- Lin, C. L., Chang, C. H., & Ko, C. C. (2001). Multifactorial analysis of an MOD restored human premolar using auto-mesh finite element approach. *J Oral Rehabil*, 28: 576-585.
- Liu, P. R. (2005). A panorama of dental CAD/CAM restorative systems. *Compend*, 26: 507-513.
- Liu, D., Matinlinna, J. P., & Pow, E. H. N. (2012). Insights into porcelain zirconia bonding. *J Adhes Sci Tech*, 26: 1249–1265.
- Lohbauer, U., von der Horst, T., Frankenberger, R., Kramer, N., & Petschelt, A. (2003). Flexural fatigue behavior of resin composite dental restoratives. *Dent Mater*, 19: 435-440.
- Lohbauer, U., Petschelt, A., & Greil P. (2002). Lifetime prediction of CAD/CAM dental ceramics. *J Biomed Mater Res*, 63: 780–785.
- Lohmann, C. H., Dean, D. D., Koster, G., Casasola, D., Buchhorn, G. H., Fink, U. Schwartz, Z., & Boyan, B. D. (2002). Ceramic and PMMA particles differentially affect osteoblast phenotype. *Biomaterials*, 23: 1855–1863.
- Lorenzoni, F. C., Martins, L. M., Silva, N. R., Coelho, P. G., Guess, P. C., Bonfante, E. A., Thompson, V. P., & Bonfante, G. (2010). Fatigue life and failure modes of crowns systems with a modified framework design. *J Dent*, 38: 626–634.
- Luthardt, R. G., Holzhuter, M., Sandkuhl, O., Herold, V., Schnapp, J. D., Kuhlisch, E., & Walter, M. (2002). Reliability and properties of ground Y-TZP-zirconia ceramics. *J Dent Res*, 81: 487-491.
- Luthardt, R.G., Sandkuhl, O., & Reitz, B. (1999). Zirconia-TZP and alumina-advanced technologies for the manufacturing of single crowns. *Eur J Prosthodont Restor Dent*, 7: 113–119.

- Luthra, R., & Kaur, P. (2016). An insight into current concepts and techniques in resin bonding to high strength ceramics. *Aust Dent J*, 61: 163-173.
- Lüthy, H., Filser, F., Loffel, O., Schumacher, M., Gauckler, L. J., & Hammerle, C. H. (2005). Strength and reliability of four-unit all-ceramic posterior bridges. *Dent Mater*, 21: 930-937.
- Lüthy, H., Loeffel, O., & Hammerle, C. H. (2006). Effect of thermocycling on bond strength of luting cements to zirconia ceramic *Dent Mater*, 22: 195-200.
- Mackert, Jr. J. R., Butts, M. B., & Fairhurst, C. W. (1986). The effect of the leucite transformation on dental porcelain expansion. *Dent Mater*, 2: 32–36.
- Magne, P. (2007). Efficient 3D finite element analysis of dental restorative procedures using micro-CT data. *Dent Mater*, 23: 539-548.
- Magne, P., & Belser, U. C. (2003). Porcelain versus composite inlays/onlays: effects of mechanical loads on stress distribution, adhesion, and crown flexure. *Int J Periodont Restor Dent*, 23: 543-555.
- Magne, P., Schlichting, L. H., Maia, H. P., & Baratieri, L. N. (2010). In vitro fatigue resistance of CAD/CAM composite resin and ceramic posterior occlusal veneers. *J Prosthet Dent*, 104: 149–157.
- Mahamood, R. S., Akinlabi, E. T., Shukla, M., & Pityana, S. (2012). Functionally Graded Material: An Overview. Proceedings of the World Congress on Engineering 2012 Vol III: WCE 2012, London, U.K. ISSN: 2078-0958 (Print); ISSN: 2078-0966 (Online).
- Mallineni, S. A., Nuvvula, S., Matinlinna, J. P., Yiu, C. K., & King, N. M. (2013). Biocompatibility of various dental materials in contemporary dentistry: a narrative insight. *J Invest Clin Dent*, 4: 9–19.
- Manicone, P. F., Rossi Iommetti, P., & Raffaelli, L. (2007). An overview of zirconia ceramics: Basic properties and clinical applications. *J Dent*, 35: 819-826.
- Marchack, B. W., Futatsuki, Y., Marchack, C. B., & White, S. N. (2008). Customization of milled zirconia copings for all-ceramic crowns: A clinical report. *J Prosthet Dent*, 99: 169-173.
- Matinlinna, J. P., & Vallittu, P. K. (2007). Bonding of resin composites to etchable ceramic surfaces—an insight review to the chemical aspects on surface conditioning. *J Oral Rehabil*, 34: 622–630.
- Marple, B. R., & Green, D. J. (1993). Graded compositions and microstructure by infiltration processing. *J Mat Sci*, 28: 4637–4643.
- Mazurat, R. D., & Pesun, S. (1998). Resin–metal bonding systems: a review of the silicoating and kevloc systems. *J Can Dent Assoc*, 64: 503–507.
- Mecholsky, J. (1995). Fractography: Determining the sites of fracture initiation. *Dent Mater*, 11: 113-116.

- Mehta, N. R., Roeber, F. W., Gaddad, A. W., Glickman, I., & Goodman, J. B. (1996). Stresses created by occlusal prematurities in a new photoelastic model system. *JADA*, 93: 334-341.
- Memarzadeh, K., Sharili, A. S., Huang, J., Rawlinson, S. C., & Allaker, R. P. (2015). Nanoparticulate zinc oxide as a coating material for orthopedic and dental implants. *J Biomed Mater Res A*, 103: 981–989.
- Menezes, F. C. H., Borges, G. A., Valentino, T. A., Oliveira, M. A. H. M., Turssi, C. P., & Correr-sobrinho, L. (2009). Effect of surface treatment and storage on the bond strength of different ceramic systems. *Braz J Oral Sci*, 8: 119-123.
- Messer, R. L. W., Lockwood, P. E., Wataha, J. C., Lewis, J. B., Norris, S., & Bouillaguet, S. (2003). In vitro cytotoxicity of traditional versus contemporary dental ceramics. *J Prosthet Dent*, 90: 452-458.
- Milleding, P., Haraldsson, C., & Karlsson, S. (2002). Ion leaching from dental ceramics during static in vitro corrosion testing. *J Biomed Mater Res*, 61: 541-550.
- Mishina, H., Inumaru, Y., & Kaitoku, K., (2008). Fabrication of ZrO₂/AISI316L functionally graded materials for joint prostheses. *Mat Sci Eng, A* 475: 141–147.
- Miyazaki, T., Nakamura, T., Matsumura, H., Ban, S., & Kobayashi, T. (2013). Review: Current status of zirconia restoration. *J Prosthodont Res*, 57: 236-261.
- Moharamzadeh, K., Van Noort, R., Brook, I. M., & Scutt, A. M. (2007). Cytotoxicity of resin monomers on human gingival fibroblasts and HaCaT keratinocytes. *Dent Mater*, 23: 40–44.
- Molin, M. K., & Karlsson, S. L. (2008). Five-year clinical prospective evaluation of zirconia-based Denzir 3-unit FPDs. *Int J Prosthodont*, 21: 223-227.
- Moon, J-E., Kim, S-H., Lee, J-B., Han, J-S., Yeo, I-S., & Ha, S-R. (2016). Effects of airborne-particle abrasion protocol choice on the surface characteristics of monolithic zirconia materials and the shear bond strength of resin cement. *Ceram Int*, 42: 1552–1562.
- Mora, G. P., & O'Brien, W. J. (1994). Thermal shock resistance of core reinforced all-ceramic crown systems. *J Biomed Mater Res*, 28: 189–194.
- Moraes, M. C. C. S., Nelson, E. C., Duailibi, F. J., & Gulmaraes de Oliveira, L. (2004). Mechanical properties of alumina–zirconia composites for ceramic abutments. *Mater Res*, 7: 643–649.
- Motta, A., B., Pereira, L. C., & da Cunha, A. R. C. C. (2006). Finite element analysis in 2D and 3D models for sound and restored teeth. *ABAQUS Users' Conference*: 329-343.
- Mukherjee, A., Maiti, B., Shara, A. D., Basu, R. N., & Maiti, H. S. (2001). Correlation between slurry. rheology. Green density and sintered density of tape cast yttria stabilized zirconia. *Ceram Int*, 27: 731-739.
- Musil, R., & Tiller, H. J. (1984). The adhesion of dental resin to metal surfaces. The kulzer silicoater technique. Gmb: Wehrbeim: Kulzer and Co; P: 9–53.

- Nawa, M. (2005). ZrO₂–Al₂O₃ ceramic material. *Eur Patent*, EP 1 508 554 A2.
- Nevarez-Rascon, A., Aguilar-Elguezabal, A., Orrantia, E., & Bocanegra-Bernal, M. H. (2009). On the wide range of mechanical properties of ZTA and ATZ based dental ceramic composites by varying the Al₂O₃ and ZrO₂ content. *Int J Refrac Metals & Hard Mater*, 27: 962–970.
- Nevarez-Rascon, A., Aguilar-Elguezabal, A., Orrantia, E., & Bocanegra-Bernal, M. H. (2010). Al₂O_{3(w)}–Al₂O_{3(n)}–ZrO₂ (TZ-3Y)_n multi-scale nanocomposite: An alternative for different dental applications?. *Acta Biomater*, 6: 563–570.
- Nevarez-Rascon, A., Aguilar-Elguezabal, A., Orrantia, E., & Bocanegra-Bernal, M. H. (2011). Compressive strength, hardness and fracture toughness of Al₂O₃ whiskers reinforced ZTA and ATZ nanocomposites: Weibull analysis. *Int J Refrac Metals Hard Mater*, 29: 333–340.
- Niu, L. N., Fang, M., Jiao, K., Tang, L. H., Xiao, Y. H., Shen, L. J., & Chen, J. H. (2010). Tetrapod-like zinc oxide whisker enhancement of resin composite. *J Dent Res*, 89: 746–750.
- Niu, X., Yang, Y., & Soboyejo, W. (2008). Contact deformation and cracking of zirconia/cement/foundation dental multilayers. *Mater Sci Eng A*, 485: 517–523.
- Nkamgoue, E. M., Adnet, J. J., Bernard, J., Zierold, K., Kilian, L., Jallot, E., Benhayoune, H., & Bonhomme, P. (2000). In vitro effects of zirconia and alumina particles on human blood monocyte-derived macrophages: X-ray microanalysis and flow cytometric studies. *J Biomed Mater Res*, 52: 587-594.
- Nociari, M. M., Shalev, A., Benias, P., & Russo, C. (1998). A novel one-step, highly sensitive fluorometric assay to evaluate cell-mediated cytotoxicity. *J Immunol Methods*, 213: 157–167.
- Oelgardt, C., Anderson, J., Heinrich, J. G., & Messing, G. L. (2010). Sintering, microstructure and mechanical properties of Al₂O₃–Y₂O₃–ZrO₂ (AYZ) eutectic composition ceramic microcomposites. *J Eur Ceram Soc*, 30: 649–656.
- Olsson, K. G., Fürst, B., Andersson, B., & Carlsson, G. E. (2003). A long-term retrospective and clinical follow-up study of In-Ceram Alumina FPDs. *Int J Prosthodont*, 16: 150–156.
- Otto, T., & De Nisco, S. (2002). Computer-aided direct ceramic restorations: A 10-year prospective clinical study of Cerec CAD/CAM inlays and onlays. *Int J Prosthodont*, 15: 122–128.
- Ozawa, M., & Hasegawa, H. (1991). Transformation characteristics of 3 mol% Y₂O₃-ZrO₂ thin foils with different grain sizes. *J Mater Sci*, 10: 1359-1361.
- Özcan M., & Bernasconi, M. (2015). Adhesion to zirconia used for dental restorations: a systematic review and meta-analysis. *J Adhes Dent*, 17: 7-26.
- Özcan, M., Kerkdijk, S., & Valandro, L. F. (2008). Comparison of resin cement adhesion to Y-TZP ceramic following manufacturers' instructions of the cements only. *Clin Oral Invest*, 12: 279–282.

- Ozen, J., Caglar, A., Beydemir, B., Aydin, C., & Dalkiz, M. (2007). Three-dimensional finite element stress analysis of different core materials in maxillary implant-supported fixed partial dentures. *Quintessence Int*, 38: e355-363.
- Özkurt, Z., Kazazoglu, E., & Unal, A. (2010). In vitro evaluation of shear bond strength of veneering ceramics to zirconia. *Dent Mater J*, 29: 138-146.
- Pabst, A. M., Walter, C., Grassmann, L., Weyhrauch, M., Brüllmann, D. D., Ziebart, T., Scheller, H., & Lehmann, K. M. (2014). Influence of CAD/CAM all-ceramic materials on cell viability, migration ability and adenylylate kinase release of human gingival fibroblasts and oral keratinocytes. *Clin Oral Investig*, 18: 1111–1118.
- Pae, A., Lee, H., Kim, H. S., Kwon, Y. D., & Woo, Y. H. (2009). Attachment and growth behaviour of human gingival fibroblasts on titanium and zirconia ceramic surfaces. *Biomed Mater*, 4: 025005.
- Palamara, J. E., Palamara, D., & Messer, H. H. (2002). Strains in the marginal ridge during occlusal loading. *Aust Dent J*, 47: 218-222.
- Park, J. B., & Bronzino, J. D. (2003). *Biomaterials: Principles and Applications*. p.6. This material was originally published in Vol. 1 of *The Biomedical Engineering Handbook*, 2nd ed. Bronzino, J. D. (2000). CRC Press, Boca Raton, FL.
- Park, S., Quinn, J. B., Romberg, E., & Arola, D. (2008). On the brittleness of enamel and selected dental materials. *Dent Mater*, 24: 1477–1485.
- Paulino, G. H., Jin, Z. H., & Dodds, R. H. (2003). Failure of functionally graded materials. In: *comprehensive structure integrity*. 607-644 Elsevier Science.
- Pera, P., Conserva, E., Pin, D., Acquaviva, A., Riboldi, A., & Mariottini, G. L., (2005). Cytotoxicity in vitro analysis of ceramic materials for “metal free” prosthetic substructures. *Minerva Stomatol*, 54: 363-371.
- Pereira, G. K., Fraga, S., Montagner, A. F., Soares, F. Z., Kleverlaan, C. J., & Valandro, L. F. (2016). The effect of grinding on the mechanical behavior of Y-TZP ceramics: A systematic review and meta-analyses. *J Mech Behav Biomed Mater*, 63: 417-442.
- Peterson, I. M., Wuttiphan, S., Lawn, B. R., & Chyung, K. (1998). Role of microstructure on contact damage and strength degradation of micaceous glass-ceramics. *Dent Mater*, 14: 80–89.
- Phark, J. H., Duarte, S. Jr., Blatz, M., & Sadan, A. (2009). An in vitro evaluation of the long-term resin bond to a new densely sintered high-purity zirconium-oxide ceramic surface. *J Prosthet Dent*, 101: 29-38.
- Piasek, J. R., Thompson, J. Y., Bower, C. A., & Stoner, B. R. (2006). Stress evolution as a function of substrate bias in RF magnetron sputtered yttria-stabilized zirconia films. *J Vac Sci Technol A*, 24: 1091–1095.
- Piasek, J. R., Thompson, J. Y., Swift, E. J., Grego, S., & Stoner, B. R. (2009). Surface modification for enhanced silanation of high strength ceramics. *Dent Mater*, 25: 1116–1121.

- Piconi, C., & Maccauro, G. (1999). Zirconia as ceramic biomaterial. *Biomaterials*, 20: 1-25.
- Pilathadka, S., Vahalova, D., & Vosahlo, T. (2007). The zirconia: a new dental ceramic material. An overview. *Prague Med Rep*, 108: 5-12.
- Pinckney, L. R., & Beall, G. H. (2008). Microstructural evolution in some silicate glass-ceramics: A Review. *J Am Ceram Soc*, 91: 773-779.
- Piwowarczyk, A., Lauer, H. C., & Sorensen, J. A. (2005). The shear bond strength between luting cements and zirconia ceramics after two pre-treatments. *Oper Dent*, 30: 382-388.
- Proos, K. A., Swain, M. V., Ironside, J., & Steven, G. P. (2003). Influence of cement on a restored crown of a first premolar using finite element analysis. *Int J Prosthodont*, 16: 82-90.
- Qasim, T., Ford, C., Bush, M. B., Hu, X., Malament, K. A., & Lawn, B. R. (2007). Margin failures in brittle dome structures: relevance to failure of dental crowns. *J Biomed Mater Res B Appl Biomater*, 80: 78-85.
- Quinn, J. B., Sundar, V., & Lloyd, I. K. (2003). Influence of microstructure and chemistry on the fracture toughness of dental ceramics. *Dent Mater*, 19: 603-611.
- Quinn, J. B., Sundar, V., Parry, E. E., & Quinn, G. D. (2010). Comparison of edge chipping resistance of PFM and veneered zirconia specimens. *Dent Mater*, 26: 13-20.
- Radovic, M., Lara-Curzio, E., & Riester, L. (2004). Comparison of different experimental techniques for determination of elastic properties of solids. *Mater Sci Eng A Struct Mater Prop Microstruct Process*, 368: 56-70.
- Raffaelli, L., Rossi Iommetti, P., Piccioni, E., Toesca, A., Serini, S., Resci, F., Missori, M., De Spirito, M., Manicone, P. F., & Calviello, G. (2008). Growth, viability, adhesion potential, and fibronectin expression in fibroblasts cultured on zirconia or feldspatic ceramics in vitro. *J Biomed Mater Res A*, 86: 959-968.
- Rafferty, B. T., Janal, M. N., Zavanelli, R. A., Silva, N. R., Rekow, E. D., Thompson, V. P., & Coelho, P. G. (2010). Design features of a three-dimensional molar crown and related maximum principal stress. A finite element model study. *Dent Mater*, 26: 156-163.
- Rahaman, M. N. (1995). Ceramic processing and sintering. 2nd Edition. New York: Marcel Dekker, Inc. p. 200-210.
- Raigrodski, A. J. (2004). Contemporary materials and technologies for all-ceramic fixed partial dentures: a review of the literature. *J Prosthet Dent*, 92: 557-562.
- Raigrodski, A. J., Chiche, G. J., & Potiket, N. (2006). The efficacy of posterior three-unit zirconium-oxide-based ceramic fixed partial denture prostheses: a prospective clinical pilot study. *J Prosthet Dent*, 96: 237-244.

- Rees, J. S. (2001). An investigation into the importance of the periodontal ligament and alveolar bone as supporting structures in finite element studies. *J Oral Rehabil*, 28: 425–432.
- Rees, J. S., & Jacobsen, P. H. (1997). Elastic modulus of the peiodental ligament. *Biomaterials*, 18: 995-999.
- Rees, J. S., Jacobsen, P. H., & Hickman, J. (1994). The elastic modulus of dentine determined by static and dynamic methods. *Clin Mater*, 17: 11-15.
- Rekow, E. D., Erdman, A. G., Riley, D. R., & Klamecki, B. (1991). CAD/CAM for dental restorations—some of the current challenges. *IEEE Trans, Biomed Eng*, 38: 318–414.
- Rekow, E. D., Harsono, M., Janal, M., Thompson, V. P., & Zhang, G. (2006). Factorial analysis of variables influencing stress in all-ceramic crowns. *Dent Mater*, 22: 125–132.
- Rekow, E. D., & Thompson, V. P. (2007). Engineering long term clinical success of advanced ceramic prostheses. *J Mater Sci Mater Med*, 18: 47-56.
- Reich, S., Petschelt, A., & Lohbaure, U. (2008). The effect of finish line preparation and layer thickness on the failure load and fractography of ZrO₂ copings. *J Prosthet Dent*, 99: 369-376.
- Requena, J., Moreno, R., & Moya, J. S. (1989). Alumina and alumina/zirconia multilayer composites obtained by slip casting. *J Am Ceram Soc*, 72: 1511–1513.
- Reuter, J. E., & Brose, M. O. (1984). Failures in full crown retained dental bridges. *Br Dent J*, 157: 61–63.
- Rompen, E., Domken, O., Degidi, M., Pontes, A. E., & Piattelli, A. (2006). The effect of material characteristics, of surface topography and of implant components and connections on soft tissue integration: a literature review. *Clin Oral Implants Res*, 17 (Suppl 2): 55-67.
- Rong, S. H., Ji, Z. S., Zhu, Y. C., & Zhang, J. Q. (2008). Effect of rod-like grain on properties and toughening mechanism of 3Y-TZP/Al₂O₃ ceramics. *Trans Nonferrous Met Soc China*, 18: 1388–1392.
- Rosenblum, M., & Schulman, A. (1997). A review of all-ceramic restorations. *J Am Dent Assoc*, 128: 297–307.
- Rosenstiel, S. F., Land, M. F., & Fujimoto, J. (2001). Contemporary Fixed Prosthodontic. Mosby. 3rd ed. Ch. 19, 24.
- Rosentritt, M., Behr, M., Lang, R., & Handel, G. (2004). Influence of cement type on the marginal adaptation of all-ceramic MOD inlays. *Dent Mater*, 20: 463-469.
- Rosentritt, M., Behr, M., Thaller, C., Rudolph, H., & Feilzer, A. (2009). Fracture performance of computer-aided manufactured zirconia and alloy crowns. *Quintessence Int*, 40: 655–662.

- Ross, I. M., Rainforth, W. M., McComb, D. W., Scott, A. J., & Brydson, R. (2001). The role of trace additions of alumina to yttria-tetragonal zirconia polycrystal (Y-TZP). *Scripta Mater*, 45: 653–660.
- Rousseau, C. E. and Tippur, H. V. (2001). Dynamic fracture of compositionally graded materials with cracks along the elastic gradient: Experiments and analysis. *Mech Mater*, 33: 403-421.
- Roulet, J. F., Söderholm, K. J., & Longmate, J. (1995). Effects of treatment and storage conditions on ceramic/composite bond strength. *J Dent Res*, 74: 381–387.
- Rubin, C., Krishnamurthy, N., Capilouto, E. & Yi, H. (1983) Stress analysis of the human tooth using a three-dimensional finite element model. *J Dent Res*, 62: 82-86.
- Ruddell, D. E., Thompson, J. Y., & Stoner, B. R. (2000). Mechanical properties of a dental ceramic coated by RF magnetron sputtering. *J Mater Res*, 51: 316-320.
- Ruiz, L., and Readey, M. J. (1996). Effect of heat-treatment on grain size, phase assemblage, and mechanical properties of 3mol% Y-TZP. *J Am Ceram Soc*, 79: 2331–2340.
- Sailer, I., Fehér, A., Filser, F., Lüthy, H., Gauckler, L. J., & Schärer, P. (2006). Prospective clinical study of zirconia posterior fixed partial dentures: 3-year follow-up. *Quintessence Int*, 37: 685-693.
- Sailer, I., Pjetursson, B. E., Zwahlen, M., & Hammerle, C. H. F. (2007). A systematic review of the survival and complication rates of all-ceramic and metal-ceramic reconstructions after an observation period of at least 3 years. Part II: Fixed partial prostheses. *Clin Oral Implants Res*, 18: 86-96.
- Sarkar, P., Haung, X., & Nicholson, P. S. (1993). Electrophoretic deposition and its use to synthesize YSZ/Al₂O₃ macro-laminate ceramic/ceramic composites. *Ceram Eng Sci Proc*, 14: 707–716.
- Santos, A. F., Tanaka, C. B., Lima, R. G., Espósito, C. O., Ballester, R. Y., Braga, R. R., & Meira, J. B. (2009a). Vertical root fracture in upper premolars with endodontic posts: finite element analysis. *J Endod*, 35: 117-120.
- Santos, C., Teixeira, L. H. P., Daguano, J. K. M. F., Rogero, S. O., Strecker, K., & Elias, C. N. (2009b). Mechanical properties and cytotoxicity of 3Y-TZP bioceramics reinforced with Al₂O₃ particles. *Ceram Int*, 35: 709–718.
- Sasaki, K., Terai, T., Suzuki, A., & Akasaka, N. (2010). Effect of the Y₂O₃ concentration in YSZ on the thermophysical property as a thermal shielding material. *Int J Appl Ceram Tech*, 7: 518-527.
- Sato, T., & Shimada, M. (1985). Control of the tetragonal to monoclinic phase transformation of yttria partially stabilized zirconia in hot water. *J Mater Sci*, 20: 3988–3992.
- Schehl, M., Díaz, L. A., & Torrecillas, R., (2002). Alumina nano-composites from powder-alcoxide mixtures. *Acta Mater*, 50: 1125–1139.

- Scherrer, S. S., & de Rijk, W. G. (1992). The effect of crown length on the fracture resistance of posterior porcelain and glass-ceramic crowns. *Int J Prosthodont*, 5: 550-557.
- Scherrer, S. S., & de Rijk, W. G. (1993). The fracture resistance of all-ceramic crowns on supporting structures with different elastic moduli. *Int J Prosthodont*, 6: 462-467.
- Scherrer, S. S., Kelly, J. R., Quinn, G. D., & Xu, K. (1999). Fracture toughness (K_{IC}) of a dental porcelain determined by fractographic analysis. *Dent Mater*, 15: 342-348.
- Schuster, G. S., Lefebvre, C. A., Wataha, J. C., & White, S. N. (1996). Biocompatibility of posterior restorative materials. *J Calif Dent Assoc*, 24: 17-31.
- Scott, H. G. (1975). Phase relationships in the zirconia–yttria system. *J Mater Sci*, 10: 1527–1535.
- Şeker, E., Ozcelik, T. B., Rathi, N., & Yilmaz, B. (2016). Evaluation of marginal fit of CAD/CAM restorations fabricated through cone beam computerized tomography and laboratory scanner data. *J Prosthet Dent*, 115: 47-51.
- Selna, L. G., Shillingburg, H. T., & Kerr, P. A. (1975). Finite element analysis of dental structures-Axisymmetric and plane stress idealizations. *J Biomed Mater Res*, 9: 237-252.
- Shahmoradi, M., & Swain, M. V. (2016). Quantitative characterization and micro-CT mineral mapping of natural fissural enamel lesions. *J Dent*, 46: 23-29.
- She, J., Scheppokat, S., Janssen, R., & Claussen, N. (1998). Reaction-bonded three-layer alumina-based composites with improved damage resistance. *J Am Ceram Soc*, 81: 1374–1376.
- Shevchenko, A. V., Dudnik, E. V., Ruban, A. K., Zaitseva, Z. A. & Lopato, L. M. (2003). Functional graded materials based on ZrO_2 and Al_2O_3 . Production methods. Powder Metallurgy and Metal Ceramics. *Mater Sci Eng A*, 42: 145-153
- Shrotriya, P., Wang, R., Katsube, N., Seghi, R., & Soboyejo, W. O. (2003). Contact damage in model dental multilayers: An investigation of the influence of indenter size. *J Mater Sci: Mater Med*, 14: 17–26.
- Shi, J. L., Li, B. S., & Yen, T. S. (1993). Mechanical properties of Al_2O_3 particle-YTZP matrix composite and its toughening mechanism. *J Mater Sci*, 28: 4019–4022.
- Silva, N. R. F. A., Bonfante, E. A., Rafferty, B. T., Zavanelli, R. A., Rekow, E. D., Thompson, V. P., & Coelho, P. G. (2011). Modified Y-TZP core design improves all-ceramic crown reliability. *J Dent Res*, 90: 104-108.
- Silva, N. R. F. A., Bonfante, E. A., Rafferty, B. T., Zavanelli, R. A., Martins, L. L., Rekow, E. D., Thompson, V. P., & Coelho, P. G. (2012). Conventional and modified veneered zirconia vs. metal ceramic: Fatigue and finite element analysis. *J Prosthodontics*, 21: 433–439.
- Silva, V. V., Lameiras, F. S., & Lobato, Z. I. (2002). Biological reactivity of zirconia-hydroxyapatite composites. *J Biomed Mater Res*, 63: 583–590.

- Simion, M., Baldoni, M., & Rossi, P. (1991). A study on the attachment of human gingival cell structures to oral implant materials. *Int J Prosthodont*, 4: 543-547.
- Sindel, J., Petschelt, A., Grellner, F., Dierken, C., & Greil, P. (1998). Evaluation of subsurface damage in CAD/CAM machined dental ceramics. *J Mater Sci: Mater in Medi*, 9: 291-295.
- Sjögren, G., Sletten, G., & Dahl, J. E. (2000). Cytotoxicity of dental alloys, metals, and ceramics assessed by Millipore filter, agar overlay, and MTT tests. *J Prosthet Dent*, 84: 229-236.
- Soares, F. Z., Follak, A., da Rosa, L. S., Montagner, A. F., Lenzi, T. L., & Rocha, R. O. (2016). Bovine tooth is a substitute for human tooth on bond strength studies: A systematic review and meta-analysis of in vitro studies. *Dent Mater*, 32: 1385-1393.
- Soares, P. V., Santos-Filho, P. C. F., Martins, L. R. M., & Soares, C. J. (2008a). Influence of restorative technique on the biomechanical behavior of endodontically treated maxillary premolars. Part I: fracture resistance and fracture mode. *J Prosthet Dent*, 99: 30-37.
- Soares, P. V., Santos-Filho, P. C. F., Gomide, H., A., Araujo, C. A., Martins, L. R. M., & Soares, C. J. (2008b). Influence of restorative technique on the biomechanical behavior of endodontically treated maxillary premolars. Part II: Strain measurement and stress distribution. *J Prosthet Dent*, 99: 114-122.
- Soboyejo, W. O., Wang, R., Katsube, N., Seghi, R., Pagedas, C., Skraba, P., Mumm, D. R., & Evans, A. G. (2001). Contact damage of model dental multilayers: experiments and finite element simulations. *Key Eng Mater*, 198-199: 135-178.
- Sobrinho, L. C., Cattell, M. J., Glover, R. H., & Knowles, J. C. (1998). Investigation of the dry and wet fatigue properties of three all-ceramic crown systems. *Int J Prosthodont*, 11: 255-262.
- Song, X., Xie, M., Zhou, F., Jia, G., Hao, X., & An, S. (2011). High-temperature thermal properties of yttria fully stabilized zirconia ceramics. *J Rare Earths*, 29: 155-159.
- Sonza, Q. N., Della Bona, A., & Borba, M. (2014). Effect of the infrastructure material on the failure behavior of prosthetic crowns. *Dent Mater*, 30: 578-585.
- Srdić, V. V., Winterer, M., & Hahn, H. (2000). Sintering behavior of nanocrystalline zirconia doped with alumina prepared by chemical vapor synthesis. *J Am Ceram Soc*, 83: 1853-1860.
- Srikanth, R., Tomaz Kosmac, T., Della Bona, A., Yin, L., & Zhang, Y. (2015). Effects of cementation surface modifications on fracture resistance of zirconia. *Dent Mater*, 31: 435-442.
- Sriamporn, T., Thamronganansku, N., Busabok, C., Poolthong, S., Uo, M., & Tagami, J. (2014). Dental zirconia can be etched by hydrofluoric acid. *Dent Mater J*, 33: 79-85.
- Stevens, R. (1981). Zirconia: second phase particle transformation toughening of ceramics. *Trans Br Ceram Soc*, 80: 81-85.

- Stuart, A. R., Filser, F., Kocher, P., Luthy, H., & Gauckler, L. J. (2007). Mechanical and fracture behavior of veneer-framework composites for all-ceramic dental bridges. *Dent Mater*, 23: 115–123.
- Sudre, O., & Lange, F. F. (1992). Effect of inclusions on densification: I, Microstructure development in an Al₂O₃ matrix containing a high volume fraction of ZrO₂ inclusions. *J Am Ceram Soc*, 75: 519–524.
- Sun, R., Suansuwan, N., Kilpatrick, N., & Swain, M. (2000). Characterisation of tribochemically assisted bonding of composite resin to porcelain and metal. *J Dent*, 28: 441–445.
- Sundah, A., & Göran, S. (2006). Fracture resistance of all-ceramic zirconia bridges with differing phase stabilizers and quality of sintering. *Dent Mater*, 22: 778-784.
- Sundah, A., & Göran, S. (2008). A study of the bending resistance of implant-supported reinforced alumina and machined zirconia abutments and copies. *Dent Mater*, 24: 611-617.
- Suresh, S. (2001). Graded materials for resistance to contact deformation and damage. *Sci*, 292: 2447-2451.
- Swab, J. J. (1991). Low temperature degradation of Y-TZP materials. *J Mater Sci*, 26: 6706–6714.
- Snyder, M. D., & Hogg, K. D. (2005). Load-to-fracture value of different all-ceramic crown systems. *J Contemp Dent Pract*, 6: 54-63.
- Takayuki, N., & Fumihito, W. (1993). Fabrication of zirconia-alumina functionally gradient materials by superplastic diffusion bonding. *J Mat Sci*, 28: 5793–5799.
- Tang, X., Luo, H., Bai, Y., Tang, H., Nakamura, T., & Yatani, H. (2015). Influences of multiple firings and aging on surface roughness, strength and hardness of veneering ceramics for zirconia frameworks. *J Dent*, 43: 1148-1153.
- Tanne, K., Hiraga, J., Kakiuchi, K., Yamagata, Y., & Sakuda, M. (1989). Biomechanical effect of anteriorly directed extraoral forces on the craniofacial complex: a study using the finite element method. *Am Orthodont Dentofacial Orthoped*, 95: 200–207
- Teixeira, E. C., Piascik, J. R., BStoner, B. R., & Thompson, J. Y. (2008). Dynamic fatigue behavior of dental porcelain modified by surface deposition of a YSZ thin film. *J Prosthodont*, 17: 527–531.
- Tekeli, S. (2005). Fracture toughness (K_{IC}), hardness, sintering and grain growth behavior of 8YSCZ/Al₂O₃ composites produced by colloidal processing. *J Alloys Compd*, 391: 217-224.
- Tete, S., Zizzari, V. L., Borelli, B., De Colli, M., Zara, S., Sorrentino, R., Scarano, A., Gherlone, E., Cataldi, A., & Zarone, F. (2014). Proliferation and adhesion capability of human gingival fibroblasts onto zirconia, lithium disilicate and feldspathic veneering ceramic in vitro. *Dent Mater J*, 33: 7–15.

- Thompson, G. A. (2000). Influence of relative layer height and testing method on the failure mode and origin in a bilayered dental ceramic composite. *Dent Mater*, 16: 235- 243.
- Thompson, J. Y., Anusavice, K. J., Naman, A., & Morris, H. F. (1994). Fracture surface characterization of clinically failed all-ceramic crowns. *J Dent Res*, 73: 1824-32.
- Thompson, J. Y., Stoner, B. R., & Piascik, J. R. (2007). Ceramics for restorative dentistry: Critical aspects for fracture and fatigue resistance. *Mater Sci Eng C*, 27: 565–569.
- Thompson, J. Y., Stoner, B. R., Piascik, J. R., & Smith, R. (2011). Adhesion/ cementation to zirconia and other non-silicate ceramics: where are we now?. *Dent Mater*, 27: 71-82.
- Tinschert, J., Zwez, D., Marx, R., & Anusavice, K. J. (2000). Structural reliability of alumina-, feldspar-, leucite-, mica- and zirconia- based ceramics. *J Dent*, 28: 529–535.
- Tjong, S. C., & Chen, H. (2004). Nanocrystalline materials and coatings. *Mater Sci Eng: R*, 45: 1-88.
- Tomaszewski, H. (1999). Residual stresses in layered ceramic composites. *J Euro Ceram Soc*, 19: 1329-1331.
- Toparli, M., Aykul, H., & Aksoy, T. (2002). Stress distribution associated with loaded acrylic-metal-cement crowns by using finite element method. *J Oral Rehabil*, 29: 1108-1114.
- Toparli, M., Aykul, H., & Sasaki, S. (2003). Temperature and thermal stress analysis of a crowned maxillary second premolar tooth using three-dimensional finite element method. *J Oral Rehabil*, 30: 99-105.
- Toparli, M., Gokay, N., & Aksoy, T. (1999). Analysis of a restored maxillary second premolar tooth by using three-dimensional finite element method. *J Oral Rehabil*, 26: 157-164.
- Toricelli, P., Verne, E., Brovarone, C. V., Appendino, P., Rustichelli, F., Krajewski, A., Ravaglioli, A., Pierini, G., Fini, M., Giavaresi, G., & Giardino, R. (2001). Biological glass coating on ceramic materials: in vitro evaluation using primary osteoblast cultures from healthy and osteopenic rat bone. *Biomaterials*, 22: 2535–2543.
- Touzi, H., Chevalier, Y., Kalfat, R., Quada, H. B., Zarrouk, H., Chapel, J. P., & Jaffrezic-Renault, N. (2006). Elaboration and electrical characterization of silicone-based anion-exchange materials. *Mater Sci Eng C*, 48: 1347–1354.
- Tsalouchou, E., Cattell, M. J., Knowles, J. C., Pittayachawan, P., & McDonald, A. (2008). Fatigue and fracture properties of yttria partially stabilized zirconia crown systems. *Dent Mater*, 24: 308-318.
- Tsubakino, H., Nozato, R., & Hamamoto, M. (1991). Effect of alumina addition on the tetragonal-to-monoclinic phase transformation in zirconia–3 mol% yttria. *J Am Ceram Soc*, 74: 440–443.

- Tsukada, G., Sueyoshi, H., Kamibayashi, H., Tokuda, M., & Torii, M. (2014). Bending strength of zirconia/porcelain functionally graded materials prepared using spark plasma sintering. *J Dent*, 42: 1569-1576.
- Tuan, W. H., & Brook, R. J. (1989). Sintering of heterogeneous ceramic compacts: part 2: $ZrO_2-Al_2O_3$. *J Mater Sci*, 24: 1953-1958.
- Tzanakakis, E. G., Tzoutzas, I. G., & Koidis, P. T. (2016). Is there a potential for durable adhesion to zirconia restorations? A systematic review. *J Prosthet Dent*, 115: 9-19.
- Uchida, M., Kim, H. M., Kokubo, T., Nawa, M., Asano, T., Tanaka, K., & Nakamura, T. (2002). Apatite-forming ability of a zirconia/alumina nano-composite induced by chemical treatment. *J Biomed Mater Res B Appl Biomater*, 60: 277-282.
- Uddanwadiker, R. (2012). Study of various molar crown designs and their assessment. *J Biomed Sci Eng*, 5: 629-633.
- Uno, M., Kurachi, M., Wakamatsu, N., & Doi, Y. (2013). Effects of adding silver nanoparticles on the toughening of dental porcelain. *J Prosthet Dent*, 109: 241-247.
- Uo, M., Sjoren, G., Sundh, A., Watari, F., Bergman, M., & Lerner, U. (2003). Cytotoxicity and bonding property of dental ceramics. *Dent Mater*, 19: 487-492.
- Valandro, L. F., Della Bona, A., Bottino, M. A., & Neisser, M. P. (2005). The effect of ceramic surface treatment on bonding to densely sintered alumina ceramic. *J Prosthet Dent*, 93: 253-259.
- Van Noort, R. (2002). Dental ceramics. In: van Noort R, editor. Introduction to Dental Materials, 2nd ed. Oxford: Elsevier; p. 231-246.
- Vanoorbeek, S., Vandamme, K., Lijnen, I., & Naert, I. (2010). Computer-aided designed/computer-assisted manufactured composite resin versus ceramic single-tooth restorations: a 3-year clinical study. *Int J Prosthodont*, 23: 223-30.
- Vasiliev, V. V., & Morozov, E. V. (2001). Mechanics and Analysis of Composite Materials. Elsevier Science Ltd. First Edition, Oxford, UK. Chapter 4. p. 121-222.
- Vitale Brovarone, C., Verne, E., Krajewski, A., & Ravaglioli, A. (2001). Graded coatings on ceramic substrates for biomedical applications. *J Eur Ceram Soc*, 21: 2855-2862.
- Vult von Steyern, P., Carlson, P., & Nilner, K. (2005). All-ceramic fixed partial dentures designed according to the DC-Zircon technique. A 2-year clinical study. *J Oral Rehabil*, 32: 180-187.
- Vult von Steyern, P., Jönsson, O., & Nilner, K. (2001). Five-year evaluation of posterior all-ceramic three-unit (In-Ceram) FPDs. *Int J Prosthodont*, 14: 379-384.
- Wakabayashi, N., & Anusavice, K. J. (2000). Crack initiation modes in bilayered alumina/porcelain disks as a function of core/veneer thickness ratio and supporting substrate stiffness. *J Dent Res*, 79: 1398-1404.
- Walker, F. J., & Anderson, A. (1984). Low-energy excitations in yttria-stabilized zirconia. *Phys Rev B*, 29: 5881-5890.

- Walters, M. C., Paulino, G. H., & Dodds, R. H. Jr. (2004). Stress-intensity factors for surface cracks in functionally graded materials under Mode-I thermomechanical loading. *Inte J Sol Struct*, 41: 1081-1118.
- Wang, F., Lee, H. P., & Lu, C. (2007). Thermal-mechanical study of functionally graded dental implants with the finite element method. *J Biomed Mater Res A*, 80: 146-158.
- Wang, J., & Stevens, R. (1989). Review zirconia-toughened alumina (ZTA) ceramics. *J Mater Sci*, 24: 3421-3440.
- Wang, S. W., Chen, L. D., Hirai, T., & Guo, J. (2001). Formation of Al₂O₃ grains with different sizes and morphologies during the pulse electric current sintering process. *J Mater Res*, 16: 3514–3517.
- Watanabe, Y., Kawamoto, A., & Matsuda, K. (2002). Particle size distributions in functionally graded materials fabricated by the centrifugal solid-particle method. *Comp Sci Tech*, 62: 881-888.
- Watari, F., Yokoyama, A., Matsuno, H., Miyao, R., Uo, M., Kawasaki, T., Omori, M., & Hirai, T. (2001). “Fabrication of functionally graded implant and its biocompatibility,” functionally graded materials in the 21st century: a workshop on trends and forecasts. Boston, Kluwer Academic, pp. 187–190.
- Watari, F., Yokoyama, A., Omori, M., Hirai, T., Kondo, H., Uo, M., & Kawasaki, T. (2004). Biocompatibility of materials and development to functionally graded implant for bio-medical application. *Comp Sci Tech*, 64: 893-908.
- Weimin, M., Lie, W., Renguo, G., Xudong, S., & Xikun, L. (2008). Sintering densification, microstructure and transformation behavior of Al₂O₃/ZrO₂(Y₂O₃) composites. *Mater Sci & Eng A*, 477: 100–106.
- Wendler, M., Belli, R., Petschelt, A., & Lohbauer, U. (2015). Characterization of residual stresses in zirconia veneered bilayers assessed via sharp and blunt indentation. *Dent Mater*, 31: 948-957.
- Wiederho, S. M. (1968). Moisture assisted crack in ceramics. *Int J Fract*, 4:171-177.
- White, S. N., Miklus, V. G., McLaren, E. A., Lang, L. A., & Caputo, A. A. (2005). Flexural strength of a layered zirconia and porcelain dental all-ceramic system. *J Prosthet Dent*, 94: 125–131.
- Williams, D. F. (1990). Biocompatibility: an overview. p:52. In Williams D. F. (ed.) Concise Encyclopedia of Medical and Dental Materials. Pergamon Press: Oxford and The MIT Press; p: xvii–xx.
- Wiskott, H. W., Nicholls, J. I., & Belser, U. C. (1995). Stress fatigue: basic principles and prosthodontic implications. *Int J Prosthodont*, 8: 105-116.
- Wolfart, M., Lehmann, F., Wolfart, S., & Kern, M. (2007). Durability of the resin bond strength to zirconia ceramic after using different surface conditioning methods. *Dent Mater*, 23: 45–50.
- Xhohga, F. A. (1977). Bruxism and its effect on the teeth. *J Oral Rehabil*, 4: 65–76.

- Xiao-ping, L., Jie-mo, T., Yun-long, Z., & Ling, W. (2002). Strength and fracture toughness of MgO-modified glass infiltrated alumina for CAD/CAM. *Dent Mater*, 18: 216-220.
- Xie, H., Li, Q., Zhang, F., Lu, Y., Tay, F. R., Qian, M., & Chen, C. (2016). Comparison of resin bonding improvements to zirconia between one-bottle universal adhesives and tribochemical silica coating, which is better?. *Dent Mater*, 32: 403-411.
- Xu H. H., Smith, D. T., Jahanmir, S., Romberg, E., Kelly, J. R., Thompson, V. P., & Rekow, E. D. (1998). Indentation damage and mechanical properties of human enamel and dentin. *J Dent Res*, 77: 472-480.
- Yaman, D. S., Alaçam, T., & Yaman, Y. (1995). Analysis of stress distribution in a vertically condensed maxillary central incisor root canal. *J Endod*, 21: 321-325.
- Yaman, D. S., Alaçam, T., & Yaman, Y. (1998). Analysis of stress distribution in a maxillary central incisor subjected to various post and core applications. *J Endod*, 24: 107-111.
- Yaman, D. S., Karacaer, O., & Sahin, M. (2004). Stress distribution of post-core applications in maxillary central incisor. *J Biomater App*, 118: 163-177.
- Yanga, J., & Xiang, H-J. (2007). Three-dimensional finite element study on the biomechanical behavior of an FGBM dental implant in surrounding bone. *J Biomech*, 40 :2377-2385.
- Ye, Y., Li, J., Zhou, H., & Chen, J. (2008). Microstructure and mechanical properties of yttria-stabilized ZrO₂/Al₂O₃ nanocomposite ceramics. *Ceram Int*, 34: 1797-1803.
- Yin, L., Song, X. F., Song, Y. L., T. Huang, T., & Li, J. (2006). An overview of in vitro abrasive finishing and CAD/CAM of bioceramics in restorative dentistry. *Int J Machine Tools Manufacture*, 46: 1013–1026.
- Yi, Y. J., & Kelly, J. R. (2008). Effect of occlusal contact size on interfacial stresses and failure of a bonded ceramic: FEA and monotonic loading analyses. *Dent Mater*, 24: 403–409.
- Yoshida, K., Tsuo, Y., & Atsuta, M. (2006). Bonding of dual-cured resin cement to zirconia ceramic using phosphate acid ester monomer and zirconate coupler. *J Biomed Mater Res B: Appl Biomater*, 77: 28-33.
- Yoshida, K., Yamashita, M., & Atsuta, M. (2004). Zirconate coupling agent for bonding resin luting cement to pure zirconium. *Am J Dent*, 17: 249-252.
- Yun, J. Y., Ha, S. R., Lee, J. B., & Kim, S. H. (2010). Effect of sandblasting and various metal primers on the shear bond strength of resin cement to Y-TZP ceramic. *Dent Mater*, 26: 650-658.
- Zhang, D., Song, D., Liao, Y., Chen, X., & Wang, M. (2014). Effect of alumina addition on mechanical behavior and fracture properties of all-ceramic zirconia dental materials. *J Mech Med Biol*, 14: 1450015/1-1450015/16.
- Zhang, F., Lin, L-F., & Wang, E-Z. (2015). Effect micro-alumina content on mechanical properties of Al₂O₃/3Y-TZP composites. *Ceram Int*, 41: 12417-12425.

- Zhang, J., Wang, Y-Q., Zhou, B-L., & Wu, X-Q. (1998). Functionally graded Al/Mg₂Si in-situ composites prepared by centrifugal casting. *J Mater Sci Lett*, 17: 1677–1679.
- Zhang, Y. (2014). Making yttria-stabilized tetragonal zirconia translucent. *Dent Mater*, 30: 1195-1203.
- Zhang, Y., Allahkarami, M., & Hanan, J. C. (2012). Measuring residual stress in ceramic zirconia–porcelain dental crowns by nanoindentation. *J Mech Behav Biom Mater*, 6: 120–127.
- Zhang, Y., Chai, H., & Lawn, B. R. (2010). Graded structures for all-ceramic restorations. *J Dent Res*, 89: 417–421.
- Zhang, Y., Chen, J., Hu, L., & Liu, W. (2006a). Pressureless-sintering behavior of nanocrystalline ZrO₂-Y₂O₃- Al₂O₃ system. *Mater Lett*, 60: 2302-2305.
- Zhang, Y., & Kim, J. W. (2009). Graded structures for damage resistant and aesthetic all-ceramic restorations. *Dent Mater*, 25: 781-790.
- Zhang, Y., & Kim, J. W. (2010). Graded zirconia glass for resistance to veneer fracture. *J Dent Res*, 89: 1057–1062.
- Zhang, Y., & Lawn, B. (2005). Fatigue sensitivity of Y-TZP to microscale sharp-contact flaws. *J Biomed Mater Res: Appl Biomater*, 72B: 388–392.
- Zhang, Y., Lawn, B. R., Malament, K. A., Thompson, V. P., & Rekow, E. D. (2006b). Damage accumulation and fatigue life of sandblasted dental ceramics. *Int J Prosthodont*, 19: 442–448.
- Zhang, Y., Lawn, B. R., Rekow, E. D., & Thompson, V. P. (2004a). Effect of sandblasting on the long-term performance of dental ceramics. *J Biomed Mater Res B: Appl Biomater*, 71: 381-386.
- Zhang, Y., & Ma, L. (2009). Optimization of ceramic strength using elastic gradients. *Acta Materialia*, 57: 2721–2729.
- Zhang, Y., Mai, Z., Barani, A., Bush, M., & Lawn B. (2016a). Fracture-resistant monolithic dental crowns. *Dent Mater*, 32: 442-449.
- Zhang, Y., Pajares, A., & Lawn, B. R. (2004b). Fatigue and damage tolerance of Y-TZP ceramics in layered biomechanical systems. *J Biomed Mater Res B: Appl Biomater*, 71: 166–171.
- Zhang, Y., Rao, P., Lü, M., & Wu, J. (2008). Mechanical properties of dental porcelain with different leucite particle sizes. *J Am Ceram Soc*, 91: 527–534.
- Zhang, Y., Song, J. K., & Lawn, B. R. (2005). Deep-penetrating conical cracks in brittle layers from hydraulic cyclic contact. *J Biomed Mater Res B Appl Biomater*, 73: 186–193.
- Zhang, Y., Sun, M. J., & Zhang, D. (2012). Designing functionally graded materials with superior load-bearing properties. *Acta Biomaterialia*, 8: 1101–1118.

- Zhang, Y., Won Kim, J. W., Bhowmick, S., Thompson, V. P., & Rekow, E. D. (2009). Competition of fracture mechanisms in monolithic dental ceramics: Flat model systems. *J Biomed Mater Res B Appl Biomater*, 88: 402–411.
- Zhang, Z., Sornsuwan, T., Rungsiyakull, C., Li, W., Li, Q., & Swain, M. V. (2016b). Effects of design parameters on fracture resistance of glass simulated dental crowns. *Dent Mater*, 32: 373-384.
- Zheng, Z., Lin, J., Shinya, A., Matinlinna, J. P., Botelho, M. G., & Shinya, A. (2012). Finite element analysis to compare stress distribution of gold alloy, lithium-disilicate reinforced glass ceramic and zirconia based fixed partial denture. *J Invest Clin Dent*, 3: 291–297.
- Zhou, J., Mah, J., Shrotriya, P., Mercer, C., & Soboyejo, W. O. (2007). Contact damage in an yttria stabilized zirconia: Implications for biomedical applications. *J Mater Sci: Mater Med*, 18: 71–78.
- Zmudzki, J., Chladek, G., & Kasperski, J. (2006). Single implant-retained dentures: Loading of various attachment types under oblique occlusal forces. *J Mech Med Biol*, 12: 1250087.

LIST OF PUBLICATIONS AND PAPERS PRESENTED

1. Participated in the International 3RD Borneo Dental Congress, Scientific Convention and Trade Exhibitions Cum 4th Malaysian Dental Association Eastern Zone, Sabah, Malaysia. (25-27-2-2013).” 3D-FE Analysis of Graded Multilayered Structured Dental Ceramic Cores.” Al-Maqtari, A. A., Razak, A.A.A. and Hamdi, M.
2. Participated in the International 35th Asia Pacific Dental Congress, Malaysian Dental Association, Kuala Lumpur, Malaysia. (7-12-5-2013). “Stress-Strain Distributions of Graded Multilayered Structured Dental Bioceramic Cores.” Al-Maqtari, A. A., Razak, A.A.A. and Hamdi, M.
3. Paper in titled “3D-FE Analysis of Functional Graded Multilayered Dental Ceramic Cores”. Al-Maqtari, A.A., Razak A.A.A. Hamdi, M. on Dental Materials Journal (ISI, Q2); 33(4):458-465. (Published 1-8-2014).
4. Patent in titled “A Multilayered Dental Ceramic Crown”. New International PCT (Publication number: WO2014158012 A8, Publication date: Sep 17-2015) Application Based on Malaysian Patent Application No. PI 2013001087 (Accepted:28-3-2014). www.google.com/patents/WO2014158012A8?cl=en
5. Paper in titled “Development and improvement of Functional Graded Multilayered Dental Ceramic Cores” Al-Maqtari, A.A., Razak A.A.A. Hamdi, M. (In progress).
6. Paper in titled “Shear Bond Strength between Synthesised Bioceramic Cores Infiltrated with Graded Silica and Veneer” Al-Maqtari, A.A., Razak A.A.A. Hamdi, M. (In progress).
7. Paper in titled “Cytotoxicity Evaluation of New Synthesised Dental Bioceramic Cores by using human gingival fibroblast cells – In Vitro Study” Al-Maqtari, A.A., Razak A.A.A. Hamdi, M. (In progress).